Study and simulation of model fluids and of pigment colours during paper coating by curtain coater

Philippe Martinez

UNIVERSITÉ DE GRENOBLE

THÈSE

Pour obtenir le grade de

DOCTEUR DE L'UNIVERSITÉ DE GRENOBLE

Spécialité : **Mécanique des fluides, Procédés, Energétique**

Arrêté ministériel : 7 août 2006

Présentée par

Philippe MARTINEZ

Thèse dirigée par **Véronique MORIN** et
codirigée par **Martine RUEFF et David GUERIN**

préparée au sein du **Laboratoire de Génie des Procédés Papetiers**
dans **l'École Doctorale Ingénierie – Matériaux Mécanique Energétique Environnement Procédés Production**

Etude expérimentale et simulation d'écoulements de fluides modèles et de dispersions pigmentaires dans une coucheuse rideau

Experimental study and CFD simulation of the flow of model fluids and coating colours in a slide die curtain coater

Thèse soutenue publiquement le **23 Juin 2011,**
devant le jury composé de :

M. Didier CHAUSSY
Professeur à Grenoble INP-Pagora, Président
M. Raj CHHABRA
Professeur à l'Indian Institute of Technology of Kanpur, Rapporteur
M. Samuel SCHABEL
Professeur à l'Université technologique de Darmstadt, Rapporteur
M. Yann COUILLAUD
Chargé d'affaires chez Allimand S.A., Examinateur
Mme Véronique MORIN
Directrice de la recherche au CTP, Examinateur
Mme Martine RUEFF
Ingénieur de recherche, Examinateur
M. David GUERIN
Manageur de l'UST 8 au CTP

UNIVERSITÉ DE GRENOBLE

THÈSE

Pour obtenir le grade de

DOCTEUR DE L'UNIVERSITÉ DE GRENOBLE

Spécialité : **Mécanique des fluides, Procédés, Energétique**

Arrêté ministériel : 7 août 2006

Présentée par

Philippe MARTINEZ

Thèse dirigée par **Véronique MORIN** et
codirigée par **Martine RUEFF et David GUÉRIN**

préparée au sein du **Laboratoire de Génie des Procédés Papetiers**
dans **l'École Doctorale Ingénierie – Matériaux Mécanique Energétique Environnement Procédés Production**

Etude expérimentale et simulation d'écoulements de fluides modèles et de dispersions pigmentaires dans une coucheuse rideau

Experimental study and CFD simulation of the flow of model fluids and coating colours in a slide die curtain coater

Thèse soutenue publiquement le **23 Juin 2011,**
devant le jury composé de :

M. Didier CHAUSSY
Professeur à Grenoble INP-Pagora, Président
M. Raj CHHABRA
Professeur à l'Indian Institute of Technology of Kanpur, Rapporteur
M. Samuel SCHABEL
Professeur à l'Université technologique de Darmstadt, Rapporteur
M. Yann COUILLAUD
Chargé d'affaires chez Allimand S.A., Examinateur
Mme Véronique MORIN
Directrice de la recherche au CTP, Examinateur
Mme Martine RUEFF
Ingénieur de recherche, Examinateur
M. David GUERIN
Manageur de l'UST 8 au CTP

AKNOWLEDGEMENT

First of all, I would like to thank Prof. Raj CHHABRA and Samuel SCHABEL for reading and reviewing my thesis manuscript and for their interesting exchanges during my defence. I would also like to thank Prof. Didier CHAUSSY and Dr. Yann COUILLAUD who accepted to evaluate the quality of my work.

It is with pleasure that I acknowledge Martine Rueff who, with her precious scientific advices and insights, made possible the work presented here.

I deeply thank Dr David GUERIN for his guidance, support and comments. Thank you for your continuous friendship and encouragement (on my thesis and my tennis results).

I express my gratitude to Dr. Véronique MORIN for supervising me.

This work is the results of a synergy between the CTP and the LGP2. That is why I would like to thanks all the members of both CTP and LGP2.

My project was part of the CURTAIN II research programme at CTP. I would like to thank all the partners for their support and interesting discussions on this work.

Finally, I would also like to thank the French National Agency for Research and Technology (ANRT) for their financial support.

REMERCIEMENTS

Aux personnes qui ont contribué à faire avancer ce projet, à savoir les membres de l'UST 8 qui m'ont accueilli les bras grands ouverts, à savoir Bernard, Franck, Flo, Lolo et David ainsi que le service technique (principalement Patrick et Philippe). Je tiens à remercier chaleureusement Salah pour tous les conseils au niveau rhéologique et pour avoir passé du temps avec moi pour me permettre de faire des mesures avec la PIV.

Aux anciens de papet pour tous les bons moments que l'on a passé ensemble : Les lulus, Alex, Romain, Bishop et son épaule en carton, Mat et son magnifique pays d'adoption sans oublier Kat et Oscar ? ;).

Aux thésards de Papet et du CTP à savoir mes anciens cobureaux Felipe et Delphine, Deb, Aurore, Chloé, Base et sa mauvaise foi, mon chômeur préféré Zizou, Céline, Robin et sa frappe légendaire, Oliv et ses arrêts tout aussi légendaires.

Aux copines de thé Dallal et Priss, merci pour votre accueil, vos ragots et de m'avoir écouté me plaindre pour arriver au bout de cette rédaction.

A tous ceux qui ont croisé la frappe du Taiwo blanc les jeudis midi.

Aux pines-co Pout, Mini moule, V pour les crémaillères et autres sorties, et pour avoir détendu ma chérie.

Aux potos du tennis Ju, Rom, La rate pour notre superbe amitié et pour m'avoir permis de me défouler.

Au Hasard qui m'a permis d'y voir plus clair certains soirs.

Au ricain Beng beng qui m'a permis de bien m'intégrer et pour toutes ces moments de déconne.

Aux gros, ivrognes et autres alcooliques Mouki, Gogo, Croustibat, Mon ancien colloc Maxou, Lio, Manu, et j'en oublie qui m'ont justement fait oublié les moments un peu tendus.

A ma famille, mes parents qui m'ont toujours soutenu et poussé dans mes études et Mum pour avoir enlevé toutes ces vilaines fautes d'anglais (surtout de grammaire…), ma sœur qui n'en rate pas une quand on est ensemble.

Et enfin à mon Ptich pour ton soutien, j'espère être aussi bon pendant ta rédaction, tu m'as permis de devenir qui je suis aujourd'hui…

Table of contents

Introduction

In order to improve the visual aspect and the printability of papers, a coating is necessary. It permits to modify the surface properties of the substrate. Among all the existing coating processes, curtain coating, which is a non-contact technique, represents a promising alternative to conventional technologies such as blade and metering size-press coating for the production of a wide range of paper and board grades. The curtain coating process has been used for years in food and photographic industries. Nowadays in papermaking, about 30 industrial machines are running worldwide and producing specialty papers such as thermal and inkjet papers. Its advantages are mainly a reduction of web breaks, good coverage and coating colour savings since it is a pre-metered technique. Moreover, the slide die curtain technique enables several coating layers to be applied simultaneously, which gives rise to new engineering possibilities for customized coating characteristics. Because of all these advantages, research in curtain coating is exploring how to apply this technology to graphic paper grades and boards.

Nevertheless this process requires a perfect stable curtain to obtain a good quality of coating. And this quality is linked to the rheological behaviour of the fluids used, their surface tension, the geometry of the coater and the operating conditions. Many experimental works revealed some differences between stability theory and results observed on the curtain. That is why it is essential to increase fundamental knowledge of key parameters governing the curtain coating process which is the aim of this thesis. Faced with the extent of this subject, we will focus here on the internal flow in a pilot curtain coater at the CTP and the flow down the inclined plane. Indeed many published papers deal with problems linked to the dynamic contact line and ways to obtain a uniform and stable film on paper and with the stability of the curtain itself. But problems may originate from the internal flow when the fluid goes through cavities and slots or when liquids flow down the inclined plane. These defects can be transferred onto the substrate and lead to coating defects.

This thesis forms part of an international research programme at the CTP (CURTAIN II) dealing with the development of curtain coating for Wood Free Coated paper which shall provide the basis for controlled engineering of coating formulations, both for the specific needs to the curtain coating process and for the product quality target. The main objective of this thesis is to help understand the main criteria for a successful multi-layer curtain application on a pilot curtain coater and subsequently permit to develop coating colours adapted to the curtain coating process for WFC papers thanks to their rheological parameters. It is based on Computational Fluid Dynamics with an experimental part in order to validate results from simulations.

This thesis is composed of three chapters. The first one is a literature review dealing with coating defects that can occur in curtain coating, the internal flow and finally the flow of liquid films down an inclined plane. The second chapter focuses on the types of fluids used, their composition and their rheological properties in relation with the coating process. Three coating colours classically used in multilayer coating for Wood Free Coated paper were tested in addition with Newtonian fluids and model shear-thinning fluids. Then we describe the experimental device, which is a transparent replica of the CTP pilot curtain coater made of Plexiglas that was designed and manufactured in order to visualize the flow inside the manifold and validate CFD results. Two methods of measurements for experimental validations are used, the tracer method and 2D Particle Imaging Velocimetry.

The last chapter is devoted to the analysis of the flow in the pilot curtain coater. We first performed CFD simulations of the internal flow both for Newtonian and Non-Newtonian fluids by dividing the problem into two parts. The flow in the manifold of the laboratory curtain

coater was simulated in three dimensions in order to analyse the phenomena taking place in the first cavity, find parameters that spark off defects and propose some solutions. A 2D simulation of the flow in the second cavity was also carried out in order to analyse the usefulness or not of this adding cavity on the flow uniformity for the range of fluids and operating conditions used. In addition, an experimental study has been performed to validate the results using a flow visualization technique with tracers and 2D-PIV in a laboratory setup with transparent parts. Finally 2D CFD simulations on the inclined plane were carried out in order to understand the conditions of the development of waves for three layers with several operating conditions for the range of those used on the pilot curtain coater.

After the general conclusion, some future perspectives will be proposed.

Literature review

1. Introduction

The objective of coating is to modify surface properties in order to, for instance, improve the aspect and printability of the paper or obtain barrier properties. The curtain coating process has been used for years in food and photographic industries. In papermaking, it is nowadays used for specialty papers such as thermal and inkjet papers and it has been commercially used for relatively wide web manufacturing of carbonless papers and paperboard [1]. There are about 30 industrial machines in the world; the locations and specifications of the most recent ones are gathered in Table 1.

Table 1: Firms that recently set up curtain coaters with their main products.

Firm	Country City	Products	Date of setting up	Machine speed	Machine width
Mayr-Melnhof	Austria Frohnleiten	Coated Cartonboard	2010	550 m/min	4m
Dong il	South Corea Ansan	Paperboard White Liner	2006	800 m/min	4.1 m
Jujo Thermal	Finland	Thermal paper	2006	1500 m/min	2.5 m
Mitsubishi paper mills	Japan Takasago	Photo paper Inkjet paper Colour paper Carbonless paper	2000	1050-1250 m/min	1.7 to 2.6 m
August Koehler group	Germany Oberkirch Kehl	Thermal paper Inkjet paper Thin paper	2001	1500 m/min	4.2 m

This contactless technology has many potential advantages compared to traditional methods for printing and writing coated paper grades such as blade coating or metering size press coating [2]. Indeed, this pre-metered technology is expected to allow increase in productivity, and gave the highest uniformity in coating thickness and the highest coating coverage as it was explained by Endres and Tietz, 2007 [3]. Moreover, it allows multilayer coating for slide dies. Indeed, two kinds of die are used in papermaking: the slot die which is usually used with one layer and the slide die which is used in multilayer curtain coating as shown on Figure 1.

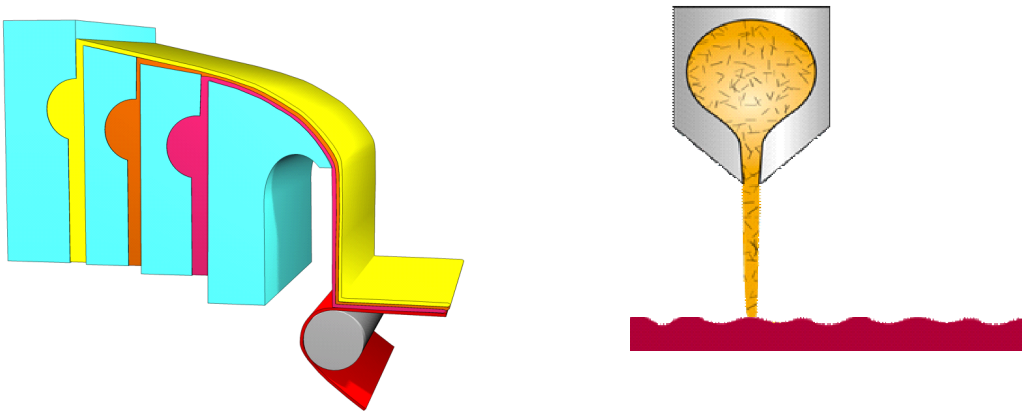

Figure 1: Scheme of a multilayer curtain coater pilot (left) and a slot die curtain coater (right).

It means that several layers with different properties can be deposited onto paper all at once whereas, with other systems, several successive coating and drying operations must be performed. Nevertheless, this process is demanding and its requirements differ from the conventional self-metered processes concerning the composition and preparation of coating colour. Weinstein and Ruschak in 2004 reviewed the flow elements of self-metered and pre-metered coating processes with physical insights [4]. They noted “Although some flow elements are well studied and understood, others require additional investigation. Genuinely predictive modeling of complex coating processes is not yet possible and coating practice remains largely empirical. Nonetheless, coating science is sufficiently advanced that physical insights and mathematical models greatly benefit design and practice”. Different types of fluids are used depending on the objectives; for example, to improve printability, pigment-based colours will be used and to obtain barrier properties (grease, moisture, oxygen…), polymer-based colours such as PVOH or starch will be applied. These fluids have different rheological behaviours which is important for the study of the flow. Some fluids are Newtonian, which means that their viscosities are the same whatever the shear rate and others are shear-thinning (their viscosities decrease when the shear rate increases) which means that their viscosities are not constant along the process where the shear stress significantly varies.

In curtain coating operation, a perfect stable curtain is required, which is hardly achieved in a large range of operating conditions [5-6]. We must solve the difficult equation to obtain a fixed geometry, which must be versatile enough for such a wide range of fluids. In the literature, there are many articles dealing with problems linked to the dynamic contact line to obtain a uniform and stable film on the paper, for instance those by Black *et al.*, 1994 and Shikhmurzaev, 1996 [7-8]. Other papers studied the stability of the curtain itself and found variables to optimize a high speed curtain coater [5, 9]. Many aspects of curtain coating were the focus of the 3rd European Coating Symposium in 1999 [10].

Nevertheless, we may wonder if uniformity problems can also come from upstream, and more particularly from the internal flow, when the fluid goes through the inlet manifold (first cavity), slots and a possible second cavity (Figure 2), and the flow down the inclined plane, where individual layers can be stacked on top of another one in order to be simultaneously deposited on a moving substrate downstream of the coater. The flow down the inclined plane can be very unstable; waves may develop on fluid interfaces – these waves can be transferred onto the substrate which leads to coating defects. That is why we will focus in this chapter on a literature survey about first, coating defects that can occur in curtain coating, then about the internal flow and finally about liquid films flowing down an inclined plane.

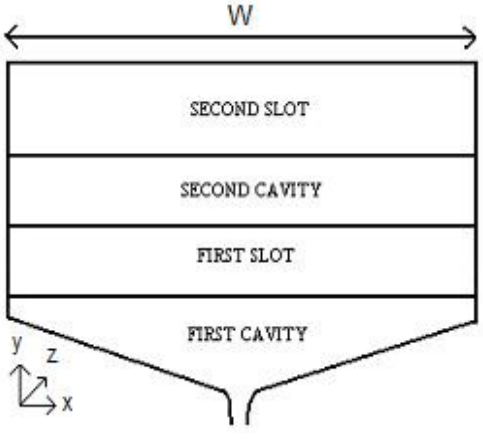

Figure 2: Design of the internal parts of a curtain coater.

2. Coating defects

Curtain coating is a pre-metered coating system. It means that all the material metered to the coating die gets coated onto the web. Thus, knowing the web speed, the coating width and the desired wet coverage, it is simple to determine the necessary flow rate. This assumes, of course, that all the material gets applied to the web to give a uniform, smooth coating. This is not always the case and, in this section, potential problems are exposed.

The wet coverage is controlled by the coating operation. If the dissolved or dispersed solids are uniformly distributed in the coating liquid and there is no flow or instability of the coating on the web, the dry coverage will be as uniform as the wet coverage.

2.1. The window of coatability

In curtain coating there are not only the limits of coatability on the coating, but there are also limits on the curtain. A certain flow rate is needed in order to form and maintain the falling curtain. By fixing the minimum flow rate for the curtain, the minimum coverage will decrease as the speed of the paper web increases. This means that for thin coatings, high coating speeds have to be used. Curtain coating is inherently a high-speed coating operation. The surface tension of all the layers is also very important. It should be below 40 mN/m, with the surface tension of the middle layer slightly higher than that of the two others; thus, the top and bottom layers spread on it.

In curtain coating, different phenomena limit a successful coating: the curtain stability as explained above, the air entrainment, the heel formation and the pulled film.

A liquid curtain is said to be stable if ever present disturbances will not lead to a rupture of the curtain. The mechanism of curtain rupture is related to the evolution and propagation of a free edge in a liquid sheet. If the propagation velocity of the free edge is smaller than the main velocity of the falling curtain, the free edge will be swept downstream and the curtain is said to be stable, otherwise the free edge will move upstream in the curtain and reach the die lip causing the curtain disintegration. There is a coating speed limit above which air bubbles start entering the coating film from V-shaped air pockets formed at the moving contact line (air entrainment). As a result craters appear in the formed film and in the extreme case, skip coating can occur. The heel formation is due to the fact that when the flow rate is increased, the dynamic contact line migrates upstream in proportion to the increase of the distance needed for the boundary layer to develop. The mechanism involves eddies, which are encapsulated inside the formed heel, that trap air bubbles and also retain agglomerated particles. This leads to an uneven contact line, which can cause various non-uniformities of the coating in the machine line direction as shown by Kistler [11]. At low flow rates and low coating speed, the viscous drag imparted by the substrate shifts the dynamic contact line downstream, the capillary pressure dominates over the inertia force and a highly bent curtain without a freely falling part tends to form. A pulled film is close to instability and a slight reduction of flow rate causes the curtain to break up.

All these phenomena limiting successful curtain coating operation define an operating window presented on Figure 3that is often drawn according to dimensionless numbers which govern the flow field in the impingement region, as presented on the paper by Miyamoto and Katagari, 1997 [12].

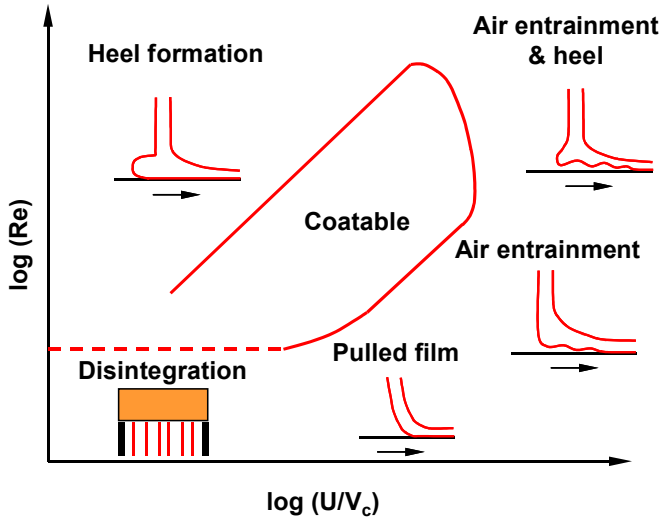

Figure 3: Operating window in curtain coating, from [12].
(U : web speed, V_c : curtain speed at impact, Re : curtain Reynolds number).

The lower limit of flow is given by the need to maintain a stable curtain, which requires a flow over 3.5 L/min per meter width. The highest coating speeds are given by the need to avoid air entrainment. With increasing flow rates the coating speeds can be increased while still avoiding air entrainment. At high flow rate both air entrainment and heel formation occur. The low-speed limit is due to heel formation.

2.2. Defects due to instabilities in curtain coating

Curtain coating and slide coating are subject to perturbations due to fluid mechanical instabilities that could lead to defects on the final coated paper. Some of these defects and failures have been identified by authors such as Christodoulou [13] and validated experimentally by Tjiptowidjojo [14] as shown on Figure 4.

Most of the instabilities encountered in curtain coating are either barring, ribbing or streaks and were well described in “Coating and drying defects” [15]. These defects set the operability limits of the coating process. Knowing operating conditions at which each defect or failure occurs is essential in producing defect-free coating:

- Barring is the appearance of bars at regular intervals in the coating on the paper in machine direction and creates periodic coverage variations. Most of the time it results from mechanical causes such as vibrations, speed or vacuum fluctuations. Fluctuations in flow rate can occur from pump pulsations that remain undamped. Finally, the hydrodynamics of the system could be a cause of this defect.
- Another type of flow instability that can occur is the ribbing that creates non-uniformity along the cross-web direction, just as if a comb was run down the wet coating. It arises from the hydrodynamics of the coating system and is increased with high speed coating or low flows. A too high viscoelasticity coming from the addition of some surfactant above the critical micelle concentration can also cause ribbing. However, surfactants are needed in a certain amount to decrease the surface tension of fluids in the curtain in order to have a stable curtain.
    - Waves can exist in liquid films flowing down the inclined plane. In multilayer slide or curtain coating, both surface and interfacial waves can exist. Thanks to surfactant,

surface waves are rarely seen in slide or curtain coating. However, in multilayer curtain coating, there are interfaces between adjacent layers and interfacial waves can be found and grow up on the inclined plane.

- In some extreme conditions, alternating wet and dry stripes can be observed, which are called rivulets but most of the time streaks can be encountered. They are lines running in the coating direction and appear in many forms. Bands are due to incorrect tension in the web when coating is against unsupported web or to the hydrodynamic system. Eddies and vortices in dies can also cause these defects. Particles of dirt carried along by the web and caught in the gap between the coating die and the web can lead to streaks such as nicks in coating dies. Indeed coating dies are very delicate to handle even if they are often made of stainless steel.

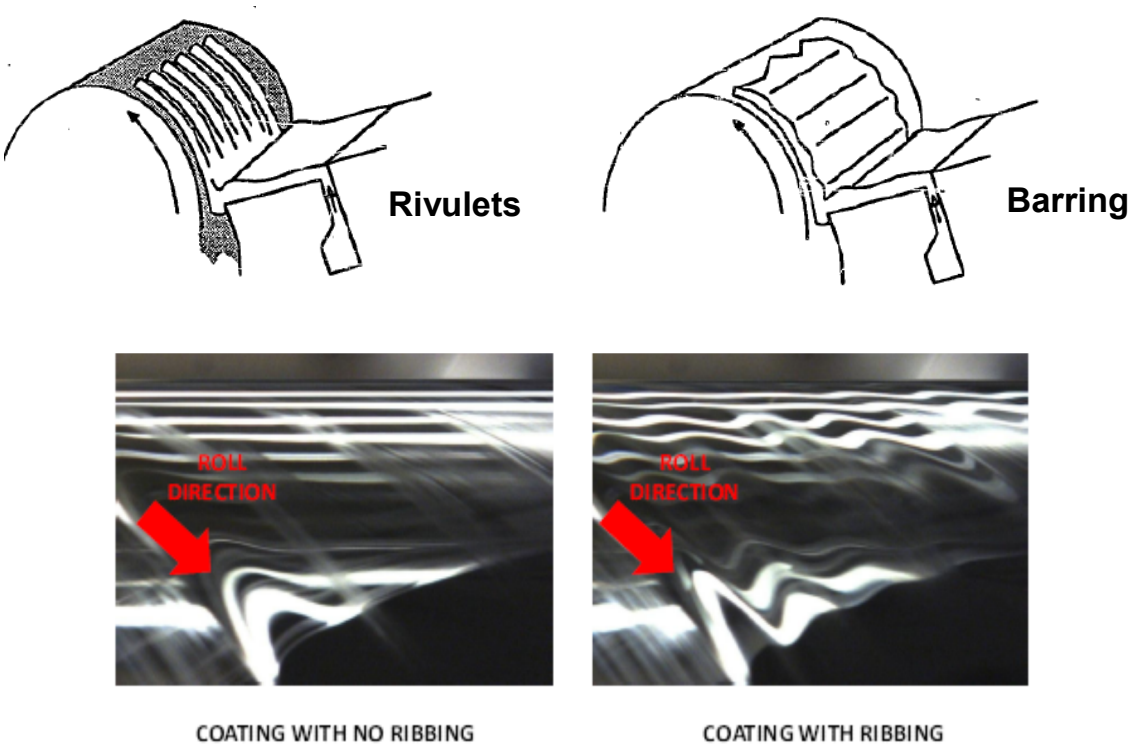

Figure 4: Some coating defects, from [*13-14*].

3. The internal flow

The purpose of the internal cavities of coating dies of all types is to distribute the coating liquid in a manner which, in conjunction with the rest of the coating process, produces a liquid film with uniform dimensions and properties. Indeed, flow distribution has the biggest impact on the cross-web uniformity of the coated liquid.

The distribution chambers of most coating dies have a common general shape. They consist of a cavity (also referred to as a distribution chamber or channel) which is oriented substantially in the cross-web direction which is connected to a slot (or slit). The combination of the cavity and slot is referred to as the "distribution manifold". The resistance to flow in the cavity is minimized by choosing a relatively large cross-sectional area, while the slot is designed in such a way that its resistance to flow is high. In this way, the fluid entering the distribution chamber tends to distribute widthwise (in the x-direction) before entering the slot, where the flow is oriented primarily toward the slot exit (in the y direction). Two particular types of distribution manifold are often distinguished as mentioned by Kistler and Schweizer, 1997 [16], the T-manifold and the coat-hanger manifold.

- The T-manifold, also referred to as an 'infinite cavity' manifold (*cf*. Figure 5):

  It has a uniform cross-section across the width of the die, and then an equal flow resistance through the die manifold. The idea is to minimise film thickness variance by having a low pressure loss in the cavity compared to the one in the slot. In the limiting case of low viscosity the distribution uniformity is determined without knowing the rheological behaviour of the fluid. That is why this manifold is attractive. In fact many fluids with different rheological behaviours can be used here such as Newtonian, shear-thinning with or without yield stress, viscoelastic fluids. Two types of manifold exist here, one with the inlet in the centre of the cavity and one in the side.

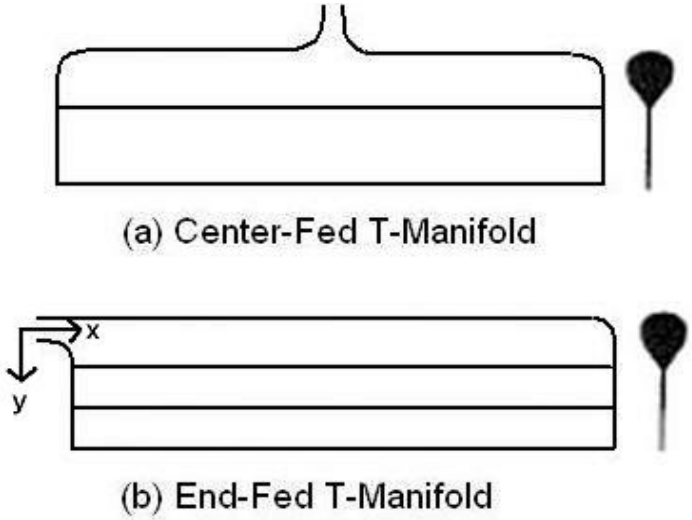

Figure 5: T-manifold design.

- The coat-hanger manifold sometimes referred as fishtail manifold (*cf*. Figure 6):

  The coat-hanger manifold features decreasing slot length and cavity size with cross-web distance from the feed location in order to reduce the liquid residence time. The idea is to maintain a constant pressure gradient at the inlet of the slot and so to have a constant flow in the length at the outlet. Whereas a circular cavity of constant size is easily

fabricated, a circular cavity of decreasing radius is difficult to machine. Here again, two types of coat-hanger manifolds are distinguished, the linearly tapered coat-hanger which has a linear taper in both the slot length and the cavity size and the curvilinearly tapered coat-hanger as shown in Figure 6.

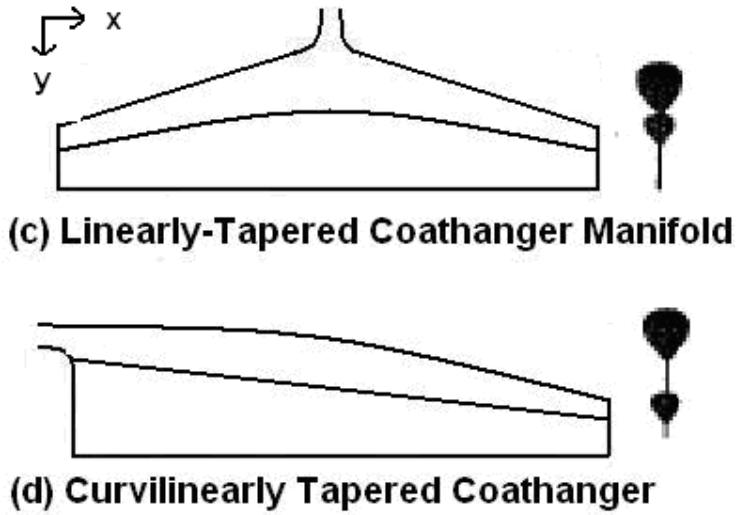

Figure 6: Coat-hanger manifold design.

- The case of the pilot curtain coater at CTP (Figure 7):

  In this PhD work, we used a laboratory pilot coater at CTP facilities. It has a hybrid manifold because there is an increase of the radius along the section but the length of the slot is constant. In literature, there is no mention of such a shape.

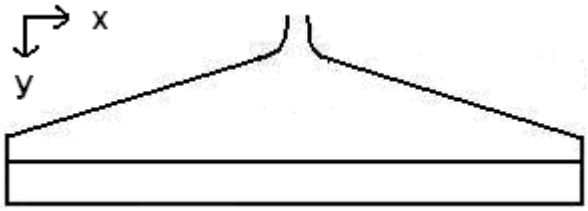

Figure 7: The first cavity of the CTP pilot curtain coater.

The cross-sectional shape of the manifold cavities also comes in various shapes which are depicted in Figure 8.Circular shapes are very popular for analysis but no so common in practice. The teardrop, triangular and rectangular shapes are more common. Concerning the studied case, CTP pilot cavities are a half circle for the biggest cavity and again a hybrid which is triangular with round ends as shown in Figure 9.

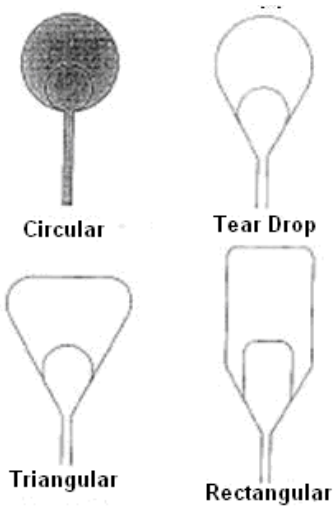

Figure 8: Cross sectional shapes of manifolds.

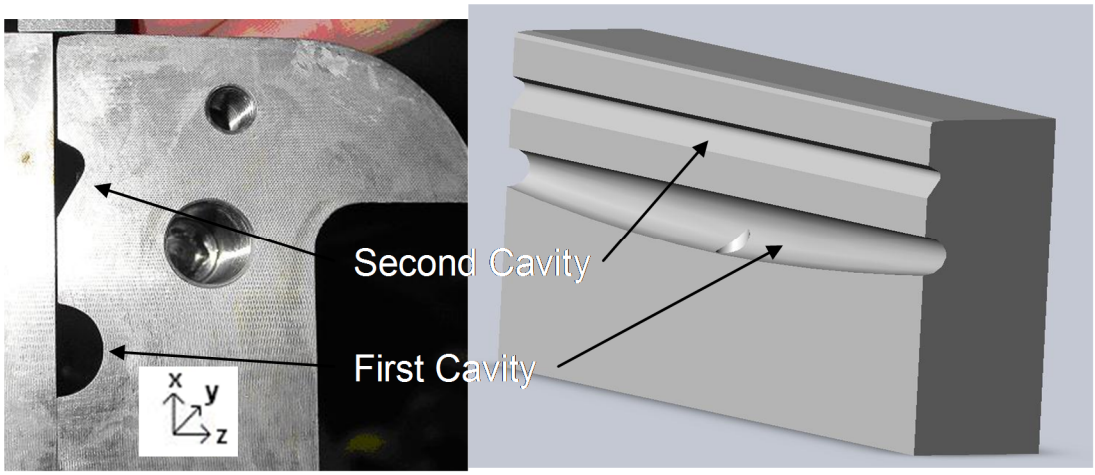

Figure 9: Shapes of the CTP pilot cavities.

In the literature, the flow analysis of die manifolds principally uses a combination of a one-dimensional flow model of viscous effects in the cavity and the slot to determine flow uniformity [17-18]. In addition a number of papers specifically address the problem of using one-dimensional cavity flow models for the noncircular shapes often encountered [19-20]. Gravity and inertial forces are neglected in several studies [21-22], but these forces can have a strong influence on the flow as we will see later. Leonard in 1985 [23] was one of the first to consider these effects. Gravitational forces affect the pressure distribution in the die cavity and the slot flow distribution when the die is not oriented in a perfectly horizontal position. Inertial forces will also have an impact on the flow in the slot.

3.1. Equations describing the internal die flows

We consider the steady state, laminar (Reynolds number $<2\cdot10^3$, which an acceptable approximation to assume that laminar flow ceases to prevail for both Newtonian and power-law fluids) in a duct of any shape (Figure 10). The fluid is in isotherm and incompressible conditions. The duct axis is in the positive x-direction.

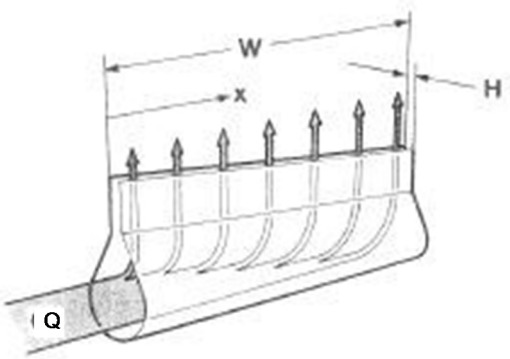

Figure 10: End-fed coater geometry.

The mathematical equations that describe the flow in cavity and slot are based on the momentum conservation and the continuity equation applied to the case we are concerned with, with specific simplifications permitted by the geometry.

- Cavity flow:

  Flow equations are based on momentum conservation and continuity. The momentum conservation equation for steady flow of liquid in cavity is:

$$\rho\left(u\frac{\partial u}{\partial x}+\upsilon\frac{\partial u}{\partial y}+w\frac{\partial u}{\partial z}\right)=-\frac{\mathrm{d}P}{\mathrm{d}x}+\frac{\partial\tau_{xy}}{\partial y}+\frac{\partial\tau_{xz}}{\partial z}+\rho g_x \qquad (1)$$

  where u, υ and w are the Cartesian components of the liquid velocity vector, τ is the stress tensor, P the hydrodynamic pressure, ρ the liquid density and g_x the x-component of the gravitational force vector. The variation of the hydrodynamic pressure down the axis of the manifold cavity is of primary interest here because it is mostly this that influences the flow in the slot.

  The stress tensor is defined as follows:

$$\tau=\begin{bmatrix}\tau_{xx} & \tau_{xy} & \tau_{xz}\\ \tau_{yx} & \tau_{yy} & \tau_{yz}\\ \tau_{zx} & \tau_{zy} & \tau_{zz}\end{bmatrix}$$

  with: $\tau_{xx}=\mu\frac{\partial u}{\partial x}$, $\tau_{xy}=\mu\frac{\partial u}{\partial y}$ and $\tau_{xz}=\mu\frac{\partial u}{\partial z}$

  where μ is the viscosity of the fluid. In the general case, the stress tensor is symmetrical.

  Here only the x-component is considered because the axial variation is usually dominant for flow in the cavity.

  There is also the continuity equation:

$$\frac{\partial u}{\partial x}+\frac{\partial\upsilon}{\partial y}+\frac{\partial w}{\partial z}=0 \qquad (2)$$

  Combining these two equations and integrating them over the cross-sectional area, A, we get:

$$\rho\int\left(\frac{\partial u^2}{\partial x}+\frac{\partial u\upsilon}{\partial y}+\frac{\partial uw}{\partial z}\right)dA=\int\left(-\frac{dP}{dx}+\frac{\partial\tau_{xy}}{\partial y}+\frac{\partial\tau_{xz}}{\partial z}+\rho g_x\right)dA \qquad (3)$$

Applying the divergence theorem, yields:

$$\int\left(\frac{\partial u\upsilon}{\partial y}+\frac{\partial u\upsilon}{\partial z}\right)dA=0 \tag{4}$$

and the average wall shear stress $\bar{\tau}$ is as follows:

$$\bar{\tau}=\frac{1}{Pe}\cdot\int\left(\frac{\partial \tau_{xy}}{\partial y}+\frac{\partial \tau_{xz}}{\partial z}\right)dA \tag{5}$$

where Pe is the wetted perimeter.

So we have now:

$$\frac{\rho}{A}\int\frac{\partial u^2}{\partial x}\,dA=-\frac{dP}{dx}+\frac{\bar{\tau}\cdot Pe}{A}+\rho g_x \tag{6}$$

The left-hand side term of this equation represents the contribution of the inertial forces for the momentum conservation equation. This term can be simplified as:

$$\frac{\rho}{A}\int\frac{\partial u^2}{\partial x}\,dA=\rho\frac{\partial}{\partial x}\left(\frac{\chi Q^2}{A^2}\right) \tag{7}$$

with Q the volumetric rate of flow and χ the inertia shape parameter.

$$\chi=\frac{1}{A}\int\frac{u^2}{(Q/A)^2}\,dA \tag{8}$$

Equation (6) can be rearranged as:

$$\frac{dP}{dx}=-\rho\frac{\partial}{\partial x}\left(\frac{\chi Q^2}{A^2}\right)-\frac{\bar{\tau}\cdot Pe}{A}+\rho g_x \tag{9}$$

Equation (9) stipulates that the change in the hydrodynamic pressure in the cavity results from a combination of viscous losses, inertial acceleration and gravitational forces.

Lee and Liu [24] presented values of χ for power-law fluids as a function of the cavity shape. Their results are gathered in Table 2.

Table 2: Inertia shape factor for power-law fluids and various cavity shapes, from [24].

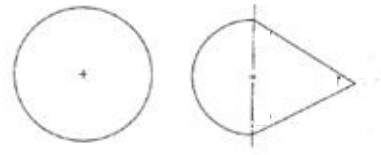

Circular cavity

60° Tear dropped cavity

Semi-circular cavity

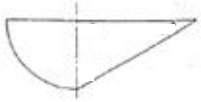

Semi 60° Tear dropped cavity

Power-law index	Cavity shape			
	Circular	60° Tear-Dropped	Semi-Circular	Semi-60° Tear-Dropped
1	1.3333	1.3709	1.3614	1.4270
0.8	1.3077	1.3469	1.3415	1.4189
0.6	1.2727	1.3138	1.3130	1.3964
0.4	1.2222	1.2655	1.2700	1.3507
0.2	1.1429	1.1931	1.2060	1.3067

Miller [19] proposed a model to determine the viscous losses with the wall shear stress for a laminar flow of an incompressible fluid in duct where $\bar{\tau}$ depends strictly on the average wall shear rate $\bar{\dot{\gamma}}$. For a Newtonian fluid, this expression may be written in the form:

$$\bar{\tau} = \mu \bar{\dot{\gamma}} = \mu \frac{Q f}{2 A D_h} \tag{10}$$

where D_h is the hydraulic diameter of the conduit and f is a shape factor which depends only on duct cross-sectional geometry but it is constant for geometrically similar channels. Values of the shape factor for several geometries are presented in Table 3.

Table 3: Values of the shape factor for various cross-sectional geometries, from [19].

Geometry	Parameter		Shape factor
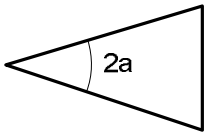	2a	10°	12.50
		20°	12.80
		30°	13.10
		40°	13.15
		50°	13.25
		60°	13.33
		70°	13.25
		80°	13.20
		90°	13.15
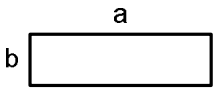	b/a	0	24.0
		0.5	15.7
		1	14.3
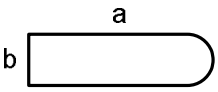	b/a	0	24.0
		0.5	16.4
		1	14.9
		2	14.8

Finally a mass balance gives the change in cavity flow rate as a function of the slot outflow:

$$\frac{dQ}{dx} = q \tag{11}$$

q is the flow out of the slot per unit width. It is given by equation (12):

$$q = \frac{PH^3}{12 L \mu \dot{\gamma}} \tag{12}$$

where P denotes the cavity pressure, H the gap in the slot channel and L the length of the slot.

Equations (9) to (12) form a system of algebraic and ordinary differential equations that may be solved for the pressure profile in the cavity and the flow distribution in the die.

The effects of inertia and die orientation with respect to gravity are included. For the case of non-Newtonian fluid, the equation 10 must be changed with the appropriated rheological model. Solutions of these equations can easily be programmed on computers.

- Slot flow:

The flow of the coating liquid in the slots of coating dies is considered to be rectilinear because of the large aspect ratio of coating die slot; the length is indeed 10 to 100 times larger than the height. The width of the die slot may in addition be 10 to 100 times the length of the slot. As a result, the analysis of the flow in the slot can be done with the lubrication approximation which applies under the following conditions:

$$\left(\frac{H}{L}\right)^2 \ll 1, \quad Re \cdot \left(\frac{H}{L}\right)^2 \ll 1 \tag{13}$$

When a fluid is confined between two surfaces, it is possible to simplify the Navier-Stokes equation. Simplifications are:

- ✓ The component of the velocity parallel to the wall is much bigger than the perpendicular component which is thus neglected.
- ✓ The velocity essentially varies in the perpendicular direction to the wall: velocity gradient in relation to the coordinates parallel to the wall can be neglected compared to those in relation to perpendicular coordinates.
- ✓ The liquid pressure is constant across the thickness of the flow channel.

In steady state and with the simplifications just described, the components of the momentum equation are given in dimensional form as:

$$\frac{\partial \tau_{yz}}{\partial z} = \frac{\partial P}{\partial y} - \rho g_y \tag{14}$$

$$\frac{\partial P}{\partial z} = 0 \tag{15}$$

$$\frac{\partial \tau_{xz}}{\partial z} = 0 \tag{16}$$

The continuity equation *(2)* is unaffected in form by this approximation.

- Cavity-Slot transition

In the literature, only few articles deal with flow problems in the transition zones. Most investigators assume that the cavity pressure is identical to the pressure at the beginning of the slot. More recently, others such as Secor, 1997 [25], think that these pressures will differ by an entrance pressure loss which characterises the viscous losses, inertial forces, extensional viscosity effects and elastic effects in the cavity-slot transitional flow:

$$P_{cavity} = \Delta P_{slot\ entrance} + \Delta P_{slot} \tag{17}$$

where P_{cavity} is the relative pressure in the cavity (the reference is the pressure at slot exit), ΔP_{slot} the pressure drop in the slot.

For Newtonian liquids in a circular contraction, Boger, 1987 [26] reports the following for the role of inertial forces and viscous losses in the entrance pressure loss:

$$\frac{\Delta P_{entrance}}{2\tau} = 0.0725Re + 0.69 \tag{18}$$

where τ denotes the wall shear stress and Re is the Reynolds number.

Because the viscous contribution to the dimensionless entrance pressure loss in (18) is of the order of unity, the viscous loss is not expected to be significant as long as the aspect ratio is large (*i.e.* L/H >10).

3.2. Dimensional Analysis

In order to better assess the regimes where viscous, inertial and gravitational forces play an important role, dimensional analysis is employed. It allows a quick approach in order to have a better idea of the predominant forces in the coater. The procedure was used by Leonard, 1985 [23], and modified by Secor, 1997 [25].

- Definition of dimensionless numbers:

  These authors defined three dimensionless numbers which are the Viscous Number, N_v, for the viscous forces, the Momentum Number, N_m, which reflects the inertial forces and finally the Gravity Number, N_g, for the gravitational forces.

  Before describing and calculating these dimensionless numbers, the pressure drop due to the flow through the slot downstream of the cavity has to be defined. It is given by equation (19):

$$\Delta P_{slot} = \frac{2L\mu_s\dot{\gamma}_s}{H} \tag{19}$$

  with

$$\dot{\gamma}_s = \frac{6Q}{W H^2} \tag{20}$$

  where H is the slot gap, W the width of the die, Q the volumetric flow rate of liquid entering the die, μ_s the viscosity in the slot and $\dot{\gamma}_s$ the shear rate in the slot.

  Then, the viscous number N_v can be defined. It is the ratio of viscous pressure in the cavity to the pressure drop in the slot:

$$N_v = \frac{W\mu_c\dot{\gamma}_c}{R_h\Delta P_{slot}} \tag{21}$$

  with

$$\dot{\gamma}_c = \frac{2Q}{R_h A} \tag{22}$$

  Here R_h is the hydraulic radius of the cavity cross-section, μ_c the viscosity in the cavity and $\dot{\gamma}_c$ the shear rate in the cavity.

  It should be noted that as long as the rheological behaviour of the fluid in the slot and the cavity is the same, the viscous number, N_v, and so the relative flow resistance in the

cavity and the slot are independent of the flow rate in the die; it depends only on the die geometry. This is no longer the case if inertial forces are significant, which is measured by the Momentum Number, N_m , *i.e*. the ratio of the inertial pressure gradient in the cavity to the pressure drop in the slot:

$$N_m = \frac{\rho Q^2}{A^2 \Delta P_{slot}} \tag{23}$$

The phenomena taking place in the presence of significant inertial forces were described by Acrivos *et al.*, 1959 [27].

The influence of gravitational forces on the die flow is materialised by the Gravity Number, N_g , which is the ratio of the gravitational force in the cavity to the viscous forces in the slot:

$$N_g = \frac{\rho g_x W}{\Delta P_{slot}} \tag{24}$$

In order to see if gravitational and inertial forces must be considered compared to viscous forces, ratios of these dimensionless numbers have to be checked.

- Influence of inertial forces:

  The ratio of the momentum to viscous numbers reflects the relative importance of inertial and viscous forces in the cavity; it is closely associated to the Reynolds Number.

$$\frac{N_m}{N_v} = \frac{Re}{8\, W/R_h} \tag{25}$$

- Influence of gravitational forces:

  The ratio of the gravity to viscous numbers reflects the role of gravitational forces in the cavity and it is closely associated with the Stokes Number, St , which is the ratio of the solid particle inertia divided by the viscous forces:

$$\frac{N_g}{N_v} = \frac{St}{32} \tag{26}$$

- Uniformity evolution of flow rate with no gravitational or inertia effects, $N_g \simeq 0,\ N_m \simeq 0$:

  As the ratios N_m / N_v and N_g / N_v are very low, we observe here the uniformity evolution of flow rate with only viscous effects, which is close to the studied case. A uniformity index, Δ , is defined as the difference between the maximum and minimum slot flow rates per unit width divided by the slot flow rate in the inlet. The lower this index, the more uniform the distribution:

$$\Delta = \frac{Q_{s\max} - Q_{s\min}}{Q} \tag{27}$$

Gravity and inertia are here negligible; so equations to have the pressure profile are simplified and an analytical solution can be found. Figure 11 presents exact solutions for the uniformity index and the dimensionless pressure as a function the power-law index for several values of the viscous number. They are for any cavity cross-sectional shape. The dimensionless pressure, $\overline{P}$, was defined by Leonard [23] as follows:

$$\overline{P} = \frac{\Delta P_{slot} H^{2n+1}}{2LK} \left(\frac{W}{6Q} \right)^n \tag{28}$$

Figure 11 shows that a small viscous number leads to better uniformity.

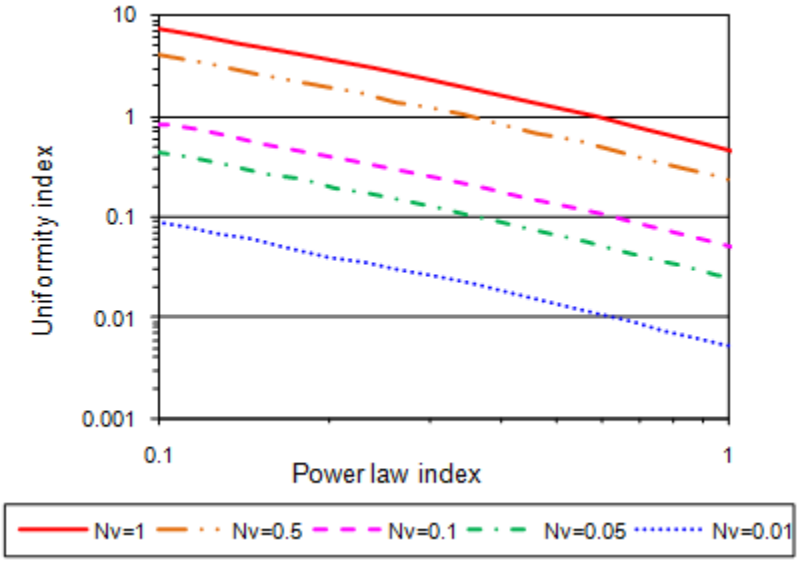

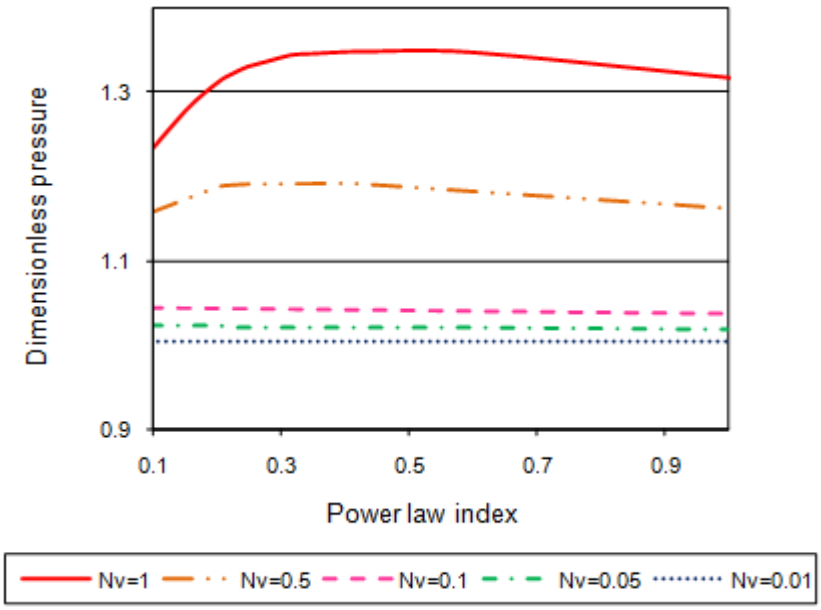

Figure 11: Uniformity index and dimensionless pressure for a constant geometry, for power-law fluids, from [23].

3.3. Analysis of fluid flow in the manifold by computational simulation

Many authors simulated the flow in the cavity in order to find conditions of non-uniformity for several fluids and geometrical conditions. These non-uniformities came from vortex creation in the manifold. Most of the numerical approaches were carried out in two dimensions and their models are based on a one-dimensional model, such as Booy, 1982, Lee *et al.*, 1990 or Vrahopoulou, 1991, [21, 28-29]. Nevertheless, the internal flow in curtain coating is a three-dimensional problem and a two-dimensional analysis may not be sufficient to get precise and detailed description of the flow fields. It will not take into account the geometrical features of the inlet die and of the manifold.

Little information about 3D simulations in the manifold is available in the literature. Some authors studied the flow uniformity on three dimensional simulations for extrusion dies but they neglected the inertial force since the viscosity of polymers is very high, which is not the case in curtain coating where the inertial force has a significant influence on the flow [30-31]. One of the initial experiments and simulations in three dimensions with the finite element method was done by Dooley in 1990 [30] where he simulated the flow into two different coat-hanger geometries with two sizes of slots and evaluated the uniformity of the distribution by measuring the flow rate out of the die lips at several points. He was not interested in the evolution of the streamlines into the manifold and only observed the result of the uniformity of the fluid at the exit, similar to Na and Kim [31] in 1995. They modelled a power-law fluid and provided basic results concerning a coat-hanger die. They focused on the effect of design parameters such as the slot thickness, manifold angle or die inlet and power-law index on flow rate distribution and residence time and found that the power-law index greatly affects the uniformity in the manifold (Figure 12). Moreover, since they neglected the inertial effect, they did not find any recirculation in the cavity.

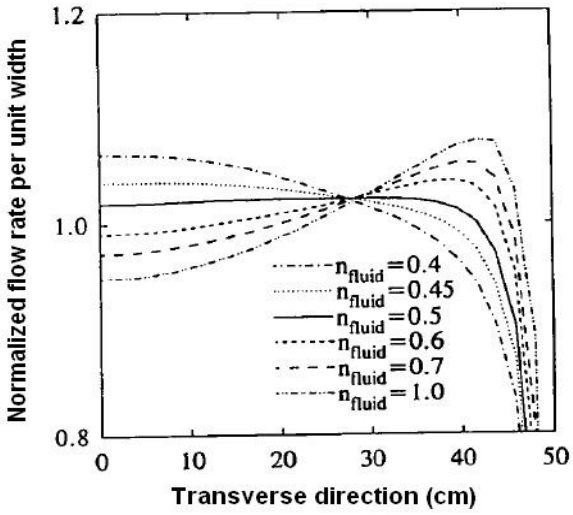

Figure 12: Effect of the power-law index of the fluid on the flow rate uniformity, from [*31*].

On Figure 12, we can notice that the fluid power-law index greatly affects the flow rate distribution and more precisely that using a polymer with a power-law index different from the design value can deteriorate the flow rate uniformity.

The inertia force was taken into account for the first time by Wen and Liu, 1994 [32], and then by Chang *et al.*, 1996 [33] when they analysed and simulated polymeric fluid flow in an extrusion die and made a comparison with experimental observations. A three-dimensional flow field of power-law fluids with the effects of the inertial force, power-law index and the geometry of the manifold (end-fed and centre fed manifold) on flow uniformity and vortex formation were studied. In order to validate the accuracy of the three-dimensional finite element simulation, a flow visualization technique was chosen in order to observe the streamlines in the different manifolds. This classical technique had already been used in manifold by Lee *et al.*, 1990 [28], when they observed vortex formation in a dual cavity coat-hanger die.

An extrusion die was made with transparent polymethyl methacrylate (PMMA) so that a direct visual observation is possible. A small amount of highly reflective aluminium particles was added to the tested fluids as tracers and a light sheet coming from a He-Ne laser passed through any plane of the die. As a result continuous streamlines appeared on photographic films. The experimental setup is displayed in Figure 13.

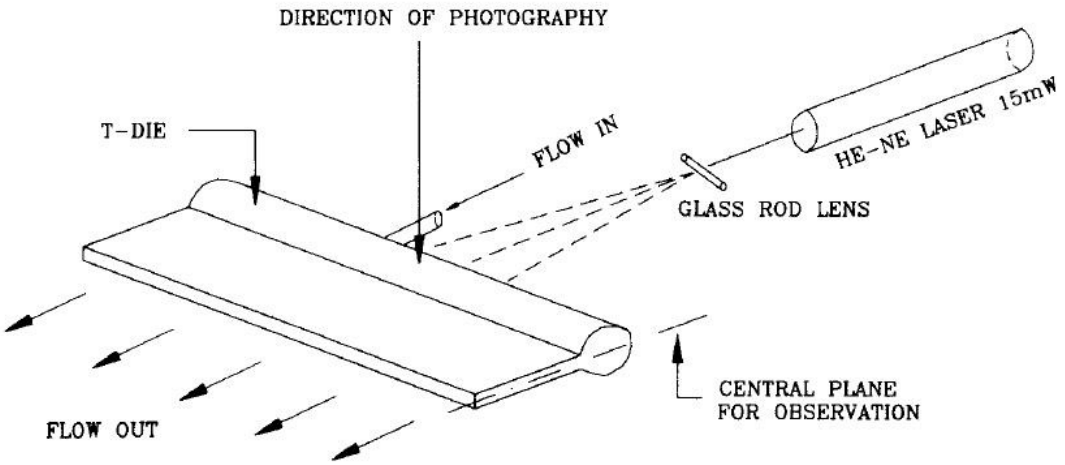

Figure 13: Experimental setup for flow visualization, from [32].

The influence of the inertial effect is studied as represented by the Reynolds number. Computed velocity fields at several Reynolds and photographs of the streamlines at this same Reynolds number are compared on Figure 14 on a centre-fed T die. Figure 14 permitted to conclude that, even if the Reynolds number is low, vortices could appear in the entrance region and, increasing the Reynolds number leads to an increase of the size of the vortex.

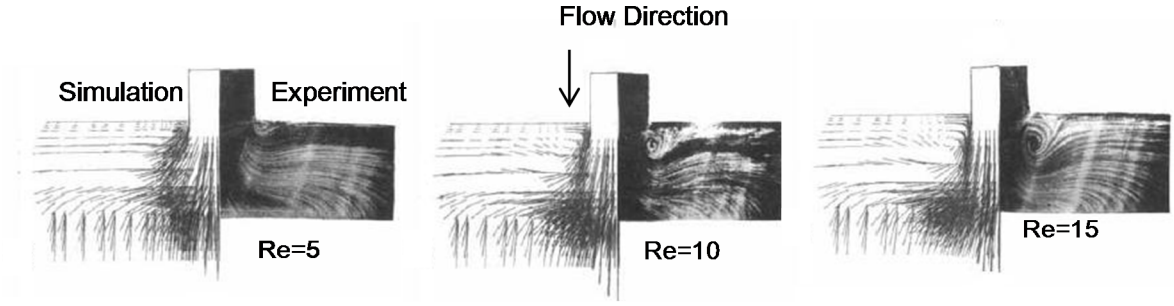

Figure 14: Influence of Reynolds number and comparison of experimental observations with simulations for a Newtonian fluid, from [32].

A quantitative comparison is difficult, even if experiments and modelling seem to be in quite good agreement. The effect of shear-thinning is displayed on Figure 15 and it can be noticed that, as the power-law index decreases, the flow uniformity deteriorates and the maximum flow rate is located in the central region.

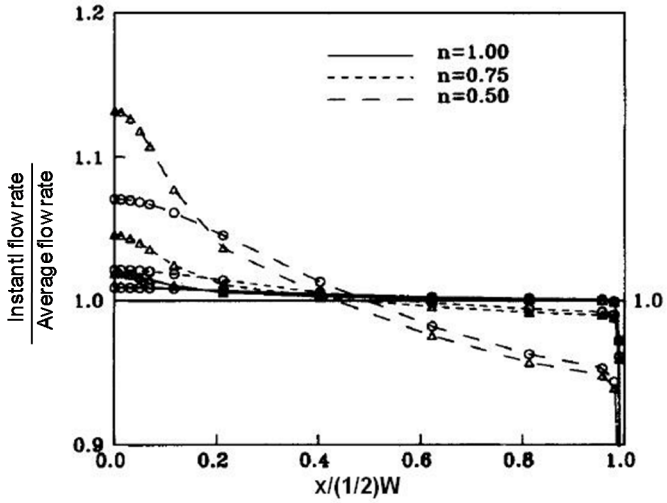

Figure 15: Effect of the power-law index on flow distributions in a centre-fed die O: Re≈0, ▲: Re=25, from [32].

Two different configurations of centre-fed and end-fed curtain coaters were examined. Their geometries are presented on Figure 16. The flow distributions were checked for each geometry and it was found that two vortices are created at the entrance region for the geometry (a) as depicted on Figure 17 on the left whereas there is no vortex with the geometry (b). Concerning the centre-fed geometry, the region of instabilities (vortices) is confined only to the central region (Figure 17, right). The diameter of the inlet tube should not be small compared to the manifold in order to avoid vortex creation in an end-fed curtain-coater. It should be noted that the Reynolds number was calculated in the inlet pipe.

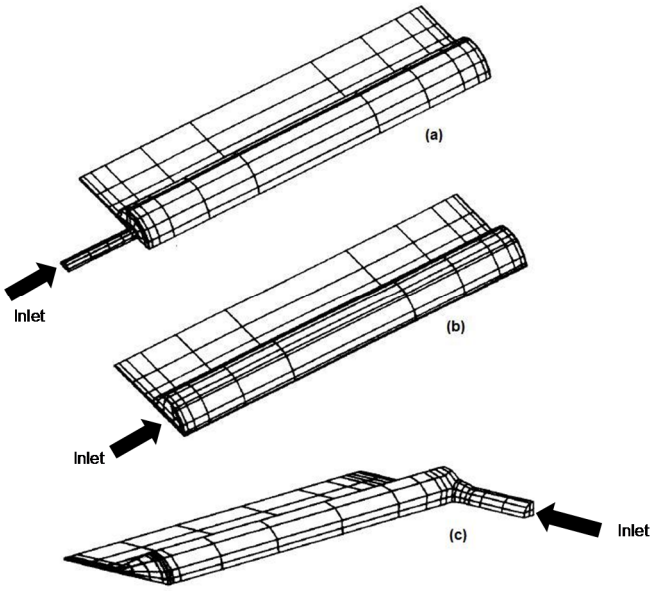

Figure 16: Die geometries and finite element discretization for two end-fed dies (a,b) and a centre-fed die (c).

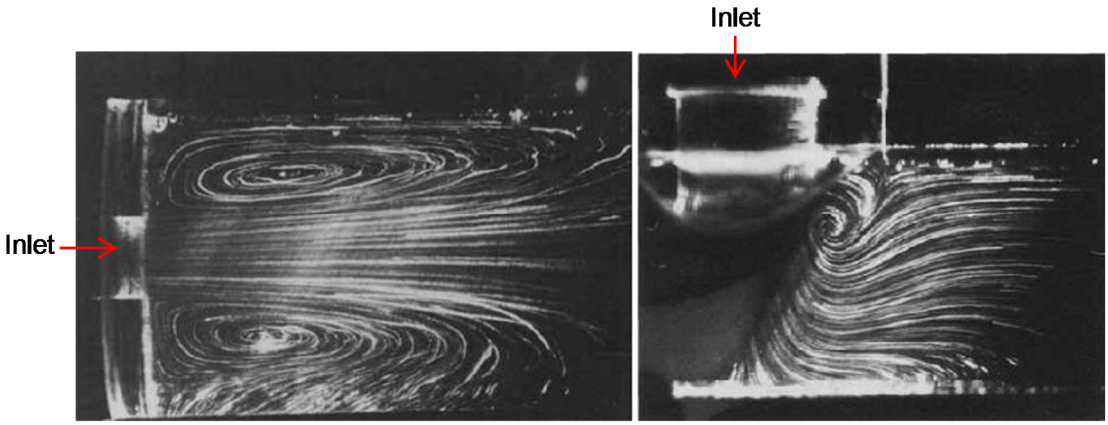

Figure 17: Visualization of vortices for a Newtonian fluid in an end-fed curtain coater at Re=22 (left) and in a centre-fed curtain coater at Re=32, from [33].

3.4. Design considerations: secondary cavities

One option in the design of flow distribution manifolds is the inclusion of additional cavities in the slot region which is the case on the CTP pilot curtain coater. It provides another chance for flow across the die if a non-uniform distribution resulted from the flow out of the original cavity.

- Flow model for a dual-cavity slot die

  Leonard, 1985 [34], developed a model with two cavities using a similar analysis to the one made above with one cavity. Equations found earlier are still available provided all the usual single cavity model assumptions are made; the only difference is that here the second cavity has a constant cross-sectional area A and the mass balance is:

$$\frac{dQ_2}{dx} = q_1 - q_2 \tag{29}$$

  Here the flow between the cavities in the connecting slots is assumed to be unidirectional with no flow in the x-direction. It is produced by the pressure gradient through the slot. With equations (9) to (12) and (29), it is possible to have the pressure profiles in the cavities and the flow distribution from the slots.

- Uniformity improvement with secondary cavities

  The aim of the second cavity is to improve uniformity flow. Figure 18 shows how uniformity is improved by the presence of secondary cavity, I is the improvement ratio, defined as the difference between the die outflow uniformity index with one cavity and the one with 2 cavities divided by the uniformity index with one cavity (Eq. (30)). Thus if the improvement ratio is equal to 0.4, this means that the non-uniformity will be reduced to 40% of its original value. For Newtonian fluids, improvement can stretch up to 60 %.

$$I = \frac{\Delta_{1\,\text{cavity}} - \Delta_{2\,\text{cavities}}}{\Delta_{1\,\text{cavity}}} \tag{30}$$

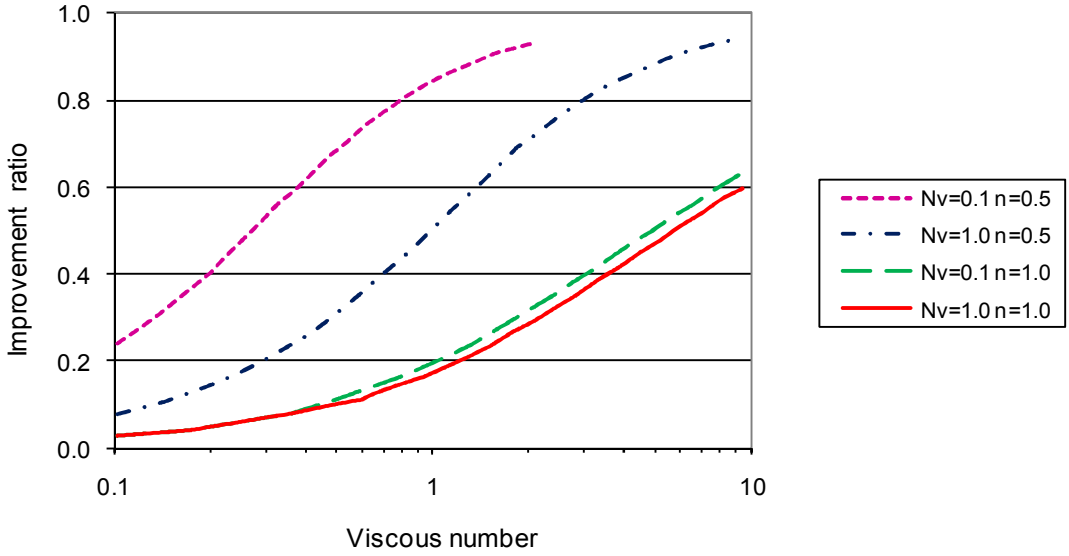

Figure 18: Uniformity improvement with two cavities as function of the viscous number (Nv) and power-law index (n), from [34].

Another way of viewing the potential benefit of secondary cavities is to examine whether it is better to add area to the primary cavity or add a secondary cavity. In almost any die, the uniformity will be improved by reducing the viscous flow resistance of the cavity while maintaining constant the slot flow resistance. This reduces N_v by definition. It may be accomplished by increasing the cross-sectional area.

Nevertheless, if the area is increased by 10% in terms of surface, when is it better to add this area in the form of a secondary cavity instead of just adding it to the primary? If the fluid is either time dependant or very viscous, it is quite important to minimize the internal volume in order to reduce the residence time.

For a constant geometry, Leonard, 1985 [34] determined the break-even point as a function of power-law index for 10, 50 and 100% additional cavity area (Figure 19). For any value above the curve, it is more beneficial to add area to the primary cavity instead of introducing the addition area in the form of a secondary cavity. Below the curve a secondary cavity is more efficient. These curves are calculated for circular cavities. For other shapes the relationship between area and hydraulic radius are different. Therefore, the curves would be shifted.

Adding a secondary cavity depends on the Viscous Number and on the rheological behaviour of the fluid. It could be summarised as follows:

- ✓ For a Newtonian fluid and a small viscous number: a secondary cavity is useful
- ✓ For a shear-thinning fluid and a high viscous number: a secondary cavity is useless.

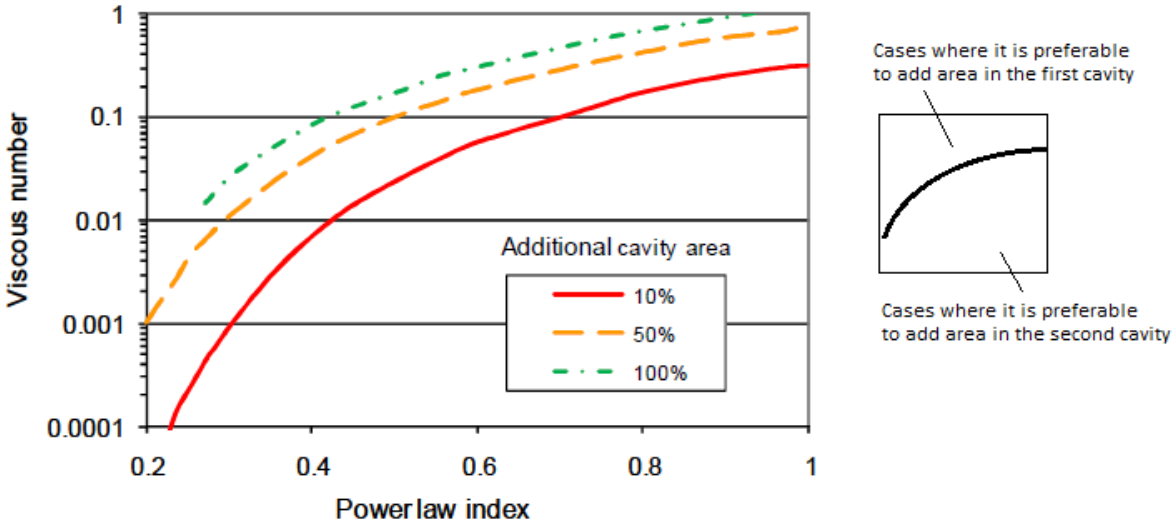

Figure 19: One versus two cavity breakeven curves for adding cavity area, from [34].

- Major problem with the addition of a secondary cavity

  As shown above, adding a secondary cavity could improve flow uniformity especially for small viscous number values, which will be the CTP pilot case. Nevertheless Lee and Liu [24, 28] showed that it could lead to the formation of a vortex which can cause polymer degradation, deteriorate product quality and generate sedimentation, notably when the Reynolds number increases. The mainstream of liquid in the first cavity is in the x-direction. However, as the fluid moves toward the second cavity, it gradually reduces to nearly two-dimensional flow (*i.e.* the x-component of the fluid velocity is small). Therefore the flow field in the outer cavity can be approximated by a two-dimensional flow model as shown on Figure 20. It should be noted that, even if the x-component of the fluid velocity is weak, only this velocity component will contribute to flow non-uniformities and consequently, equation 9 cannot be excluded from our analysis for flow distributions.

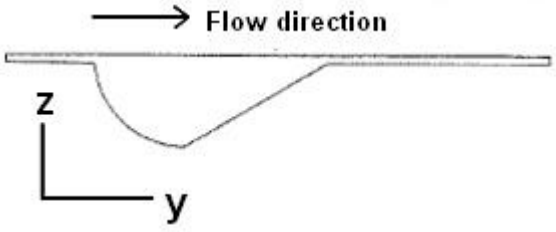

Figure 20: Flow system for an outer cavity.

Several assumptions were made by Lee and Liu to simplify the flow model:

- ✓ Isothermal and steady state flow
- ✓ The fluid is incompressible
- ✓ The flow is 2-dimensional
- ✓ The flow in the inner and outer slots has fully-developed profiles
- ✓ No-slip boundary condition

The governing equations for the two-dimensional flow are as follows:

$$\frac{\partial \upsilon}{\partial y}+\frac{\partial w}{\partial z}=0 \tag{31}$$

$$\rho\left(\upsilon\frac{\partial \upsilon}{\partial y}+w\frac{\partial \upsilon}{\partial z}\right)=-\frac{dP}{dy}+\frac{\partial \tau_{yy}}{\partial y}+\frac{\partial \tau_{yz}}{\partial z}+\rho g_y \tag{32}$$

$$\rho\left(\upsilon\frac{\partial w}{\partial y}+w\frac{\partial w}{\partial z}\right)=-\frac{dP}{dy}+\frac{\partial \tau_{yz}}{\partial y}+\frac{\partial \tau_{zz}}{\partial z}+\rho g_z \tag{33}$$

with the stress tensor components: $\tau_{yy}=2\mu\frac{\partial \upsilon}{\partial y}$, $\tau_{zz}=2\mu\frac{\partial w}{\partial z}$ and $\tau_{yz}=\mu\left(\frac{\partial \upsilon}{\partial z}+\frac{\partial w}{\partial y}\right)$.

The finite element method is then employed for the solution of discretized set of equations with υ, w and P as independent variables. The domain is subdivided into complete quadratic elements. The solutions process starts from a very small value of the Reynolds number ($Re\sim 0$). Successive solutions are obtained by incrementing the Reynolds number. The streamlines are obtained *a posteriori* from the velocity field by solving Poisson's equation. The results presented here are with a semi 60° tear-drop and a semi-circular cavity, the first one has nearly the same geometry as CTP pilot second cavity. The meshing is presented on Figure 21 for the two cases. The downstream slot length was selected long enough to ensure that the fluid flow had fully developed profiles. It should be noted that the authors calculated the Reynolds number in the slot for a power-law fluid as follows:

$$Re=\frac{\rho V^{2-n}H^n}{K} \tag{34}$$

where ρ is the density of the fluid (kg/m^3), V the flow velocity (m/s), H the slot gap (m), K the consistency index of the fluid (Pa.s^n) and n the power-law index.

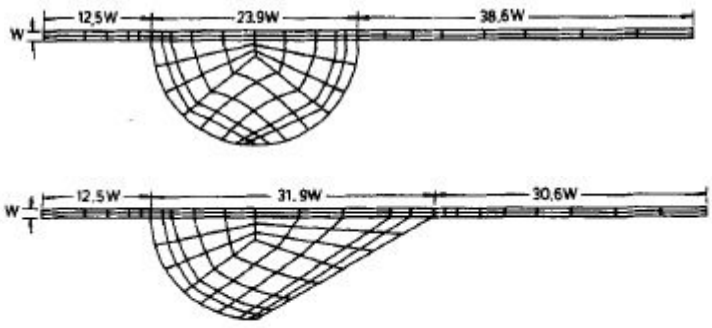

Figure 21: Meshing of the tear-drop and semi-circular cavities, from [24].

The flow patterns for a Newtonian fluid in a semi 60° tear-dropped and a semi-circular cavity are shown in Figure 22. As the Reynolds number increases, a vortex that is indicated by closed streamlines appears and then grows in size.

The effect of the power-law index n on vortex formation for a power-law fluid passing a semi-circular cavity are shown in Figure 23 with a constant Reynolds number ($Re=20$). It is interesting to note that as n decreases, the size and intensity of the vortex will

decrease. In these two figures, the numerical values are the ones of the of the stream function.

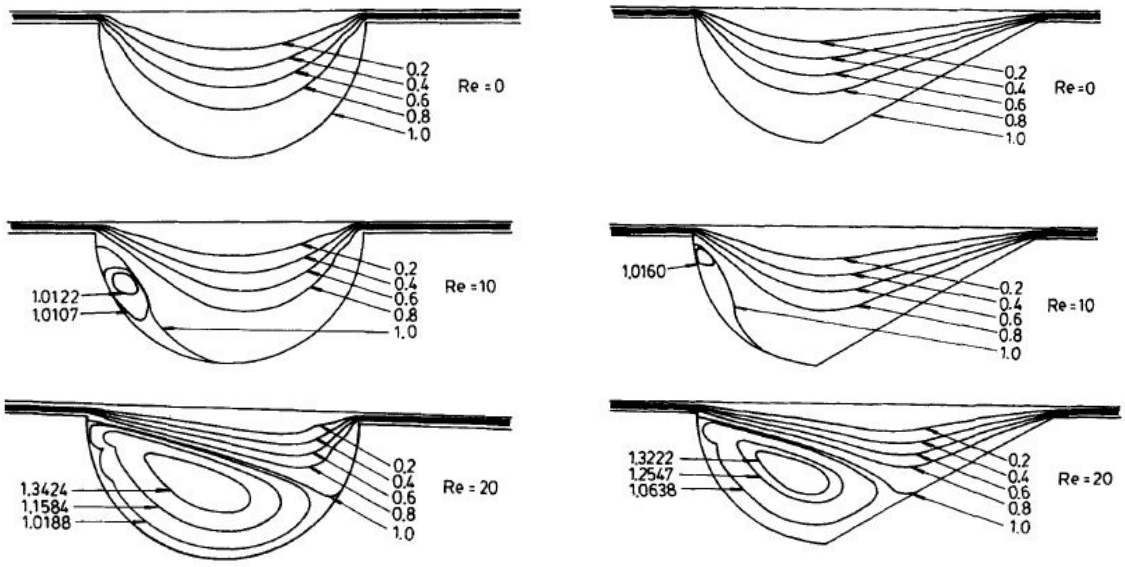

Figure 22: The streamlines for Newtonian fluid in different cavities, from [24].

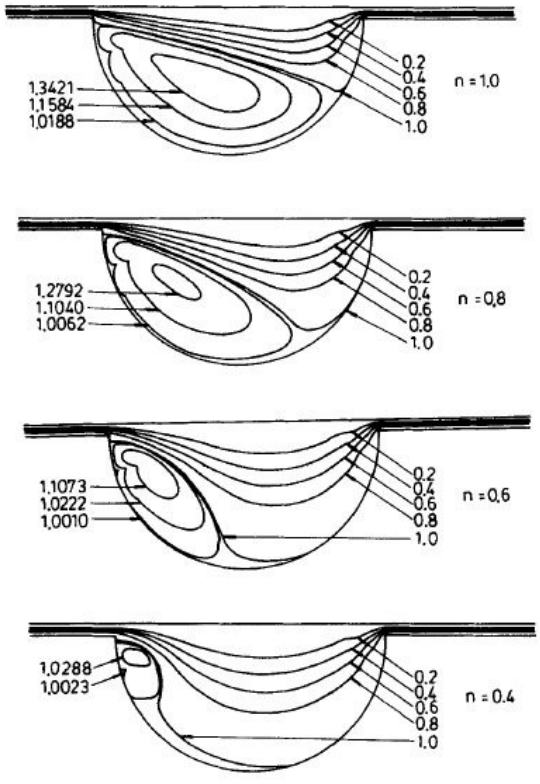

Figure 23: Influence of power-law fluid index on vortex formation at constant Reynolds number ($Re = 20$), from [24].

Therefore a critical value of the Reynolds number can be found, above which a vortex will appear in the outer cavity for different power-law fluids. Figure 24 presents the values of the critical Reynolds number as a function of n for the 2 cavity shapes. Lee and Liu found that as long as the cavity size is large enough compared with the slot gap, the critical Reynolds number is independent of the slot gap. The shape of the cavity has no influence on this critical Reynolds Number.

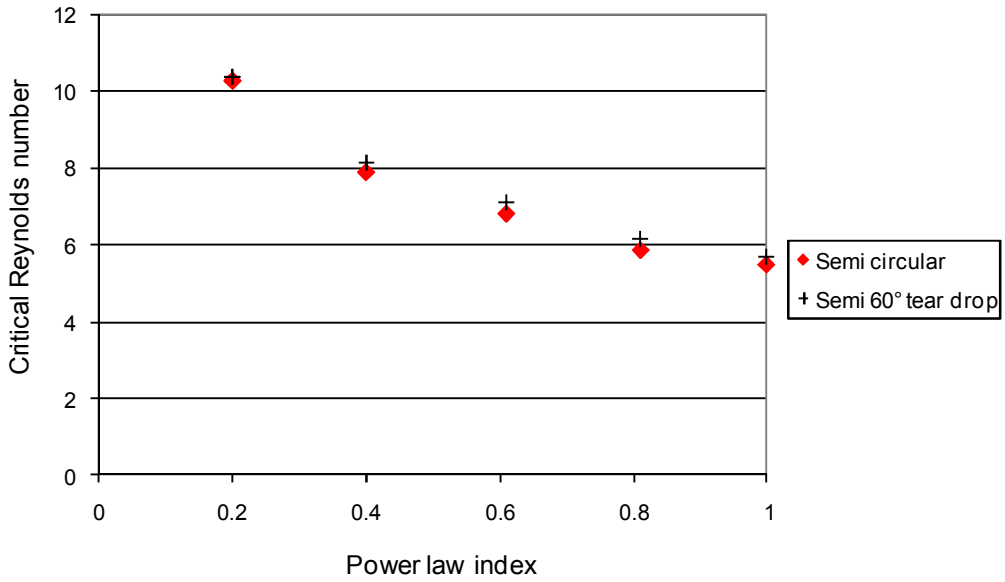

Figure 24: The critical Reynolds Numbers for power-law fluids, from [24].

Finally Lee, Wen and Liu [28] have demonstrated that reducing the entry angle of the secondary cavity with the same operating conditions eliminated the eddy (Figure 25), which seems to be considered in the fabrication of the CTP pilot curtain coater since the divergent angle of the second cavity is 30°.

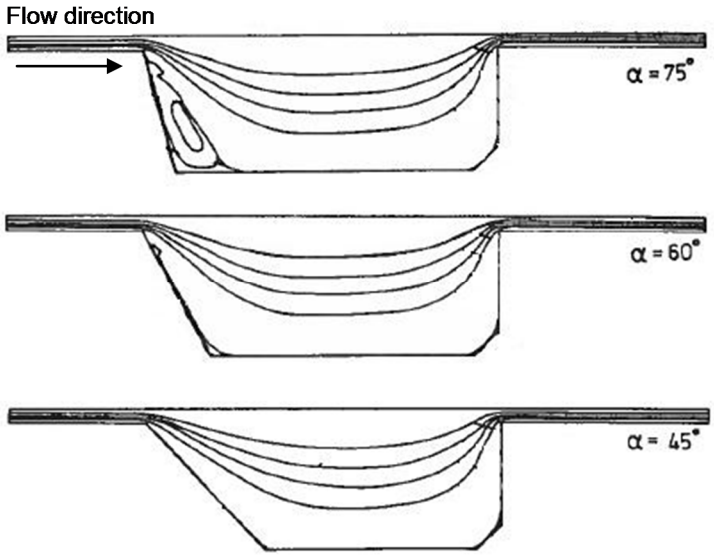

Figure 25: The effect of the divergent angle on vortex formation for a Newtonian fluid ($Re = 10$)*, from* [28].

3.5. Conclusion

The flow distribution through the internal cavities of a coating die is a result of the interaction between the geometry of the die, viscous, inertial and gravitational forces of the liquid observed. In the cavity, the viscous, inertial and gravitational forces dominate. In the slot, only viscous forces are dominant. Concerning the transition zone, there is a certain blur. In order to better understand these flows, we must have the combined mass and momentum equations conservation principles and the associated boundary conditions.

In order to have a view of the importance of each force, it is interesting to calculate the values of dimensionless numbers such as the momentum, viscous and gravity numbers. These numbers reflect the importance of the inertial, viscous and gravitational forces in the manifold cavity to the viscous forces in the slot.

The design strategies of coating die manifolds vary depending on the intended die application. T-manifold designs are suited for a wide range of fluids with different material properties but may result in excessive fluid residence time, which can lead to sedimentation. Coat-hanger designs feature lower residence time and lower cavity pressures. Nevertheless, the flow uniformity is more sensitive to liquid material properties.

There is little information about three-dimensional flow in the manifold and most of the papers dealing with this issue neglected the inertial force since they concerned extrusion dies. Nevertheless, the initial work on simulations in three-dimensions with the finite element analysis was carried out; the simulation results showed that the power-law index and the Reynolds number greatly affect the flow rate distribution. The end-fed manifold could be an alternative to the centre-fed manifold if the diameter of the inlet tube has the same size as the manifold, otherwise two big vortices could be created. Moreover, a flow visualization technique using reflective aluminium particles was used to observe the streamlines and validate the accuracy of the simulations.

The influence of a dual-cavity coat-hanger die has also been studied and it can effectively reduce the flow perturbations caused by fluid inertia and viscosity variations. The usefulness of a secondary cavity depends on the viscous number and on the rheological behaviour of the fluid. A second cavity could lead to better uniformity in the CTP pilot case. Nevertheless, an undesirable vortex may appear in the outer cavity as the Reynolds number increases. It could lead to sedimentation. Below a critical value of the Reynolds number, this vortex is avoided.

4. Liquid film flow down an inclined plane

The flow of liquid film down a solid wall may often be observed in everyday life, as when rainwater runs in a sheet down a window plane or when paint drains from some solid object that has been dipped in the liquid. Co-current flow of multiple viscous fluids occurs in many industrial processes such as coating processes, but also in many geophysical phenomena (glaciers, mud and lava flows). Concerning the curtain coating process, the inclined plane itself provides a means by which individual layers can be stacked on top of another one; at the end of the plane and after the curtain, these layers are deposited simultaneously on a moving substrate. However, it is well known that the flow down the inclined plane can be very unstable. It creates waves on fluid interfaces that can be translated onto the substrate and leads to coating defects. That is why the knowledge of the conditions under which these waves can develop is an important point in industrial research. Indeed, it is essential to understand how these instabilities occur and propagate before trying to control them to avoid a spoiling of the final product. Many cases of interest to us were well summarised by Millet in 2007 [35].

In this part, we will examine first cases of Newtonian fluids, which are less complicated, in order to understand the role of physical parameters related to the fluid such as density, viscosity, thickness and geometrical parameters of the coater such as the inclination of the plane. We will consider cases with one and several layers because their behaviours are different. Then we will examine cases with non-Newtonian fluids such as power-law fluids and more particularly shear-thinning fluids that are usually used in curtain coating.

4.1. Flow of Newtonian fluids down an inclined plane

4.1.1. One-layer flow down an inclined plane

The stability of a laminar liquid layer flowing down an inclined plane (Figure 26) was first rigorously investigated by Benjamin [36] and Yih [37] who solved the Orr-Sommerfeld equation (Eq. 35). This equation represents the basis equation for the study of hydrodynamic stability in the case of plane laminar flow. In fact, the linear stability problem for thin liquid films flowing down a plane is formulated in terms of disturbances that are harmonic in space and time and grow or decay spatially. Solutions of the Orr-Sommerfeld equation can predict the wavelengths and the growths of the disturbances in such a case.

$$(u-c)\left(\varphi''-\alpha^2\varphi\right)-u''\varphi=-\frac{1}{\alpha\, Re}\left(\varphi^{(4)}-2\alpha^2\varphi''+\alpha^4\varphi\right) \qquad (35)$$

where u is the velocity in the direction of the main flow, $c=c_r+i\,c_i$ is the complex wave velocity where c_r is the real wave velocity and c_i is the degree of damping. If the degree of damping is negative, there is amplification. $\varphi(y)$ is the amplitude of the perturbation and φ'' and $\varphi^{(4)}$ are the second and fourth order derivatives of φ with respect to y, α is the wavenumber with $2\pi d/\lambda$ where λ is the wavelength, d the thickness of the film and Re is the Reynolds number.

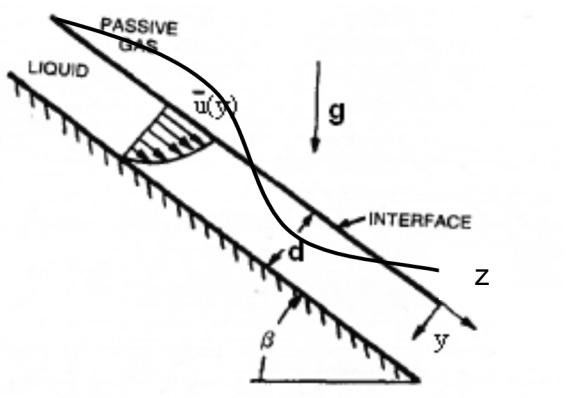

Figure 26: Sketch of a one-layer flow on an inclined plane.

There are some differences between authors [36-55], which come from the methods used to solve this equation and approximations done to resolve it. All analyses were restricted to two-dimensional wave disturbances in the vertical plane since it was pointed out that each three-dimensional disturbance is governed by the same equations of a two-dimensional disturbance in a similar flow at low Reynolds number. Therefore, this simplification is completely adequate only if the stability of the flow is questioned.

Benjamin [36] and Yih [37] studied the hydrodynamic stability of a film for small values of the Reynolds number (less than 10) and they found a critical Reynolds number for long waves compared with the thickness d , *i.e*. about 10 times d (which gives about 0.2<α <1) above which some disturbances could appear and be amplified. This critical Reynolds number is a function of the angle of inclination of the plane, β . It is given by Equation (36):

$$Re_c = \frac{5}{6}\cot(\beta) \tag{36}$$

These authors also found that the long wave disturbances are propagated downstream with a velocity equal to twice the average velocity of the film. To solve this equation they both neglected terms in α^2 and α^4 and used a power series expansion. Benjamin performed a calculation of the neutral stability curves analytically. Benjamin's calculation is based on the assumption that the wavenumber is small whereas Yih studied also cases where the wavenumber is very large, which means that the length of waves is very short. He found that these waves are damped by surface tension and that increasing the viscosity leads to reducing the rate of damping for short waves, which is unexpected.

Falling films on an inclined plane display another instability mode that is important at small angle of inclination β , the shear mode. DeBruin [38] pointed out this phenomenon and it was completed later by Floryan *et al.* [39]. They found that these shear modes have lower critical Reynolds numbers than those with the surface modes when β is very small as shown in Figure 27 (a) and (b) (under 0.5' which is obviously not the case in the CTP laboratory). These modes have wavelengths comparable to the mean depth of the liquid and spread more slowly than the mean speed of the liquid at the interface. The authors used a dimensionless surface tension parameter that is independent of d and β and is calculated as follows:

$$\zeta = \left(\frac{3\rho\sigma^3}{g\mu^4}\right)^{1/3} \tag{37}$$

where ρ is the density (kg/m^3), σ is the surface tension (N/m), g is the gravitational acceleration (m/s^2) and μ is the viscosity (Pa·s). A layer of pure water has a surface tension parameter value equal to 4850.

These authors also studied the surface mode with long waves and the influence of surface tension and the angle of inclination. Figure 27 (b) shows the narrowness of the instability regions and the sensitivity to the surface tension (Equation (37)) especially for angles higher than 4°. The increase of surface tension or the decrease of the inclination angle is stabilizing the flow, which means that the critical Reynolds number is higher for a fluid with a high surface tension and on an inclined plane with a small angle.

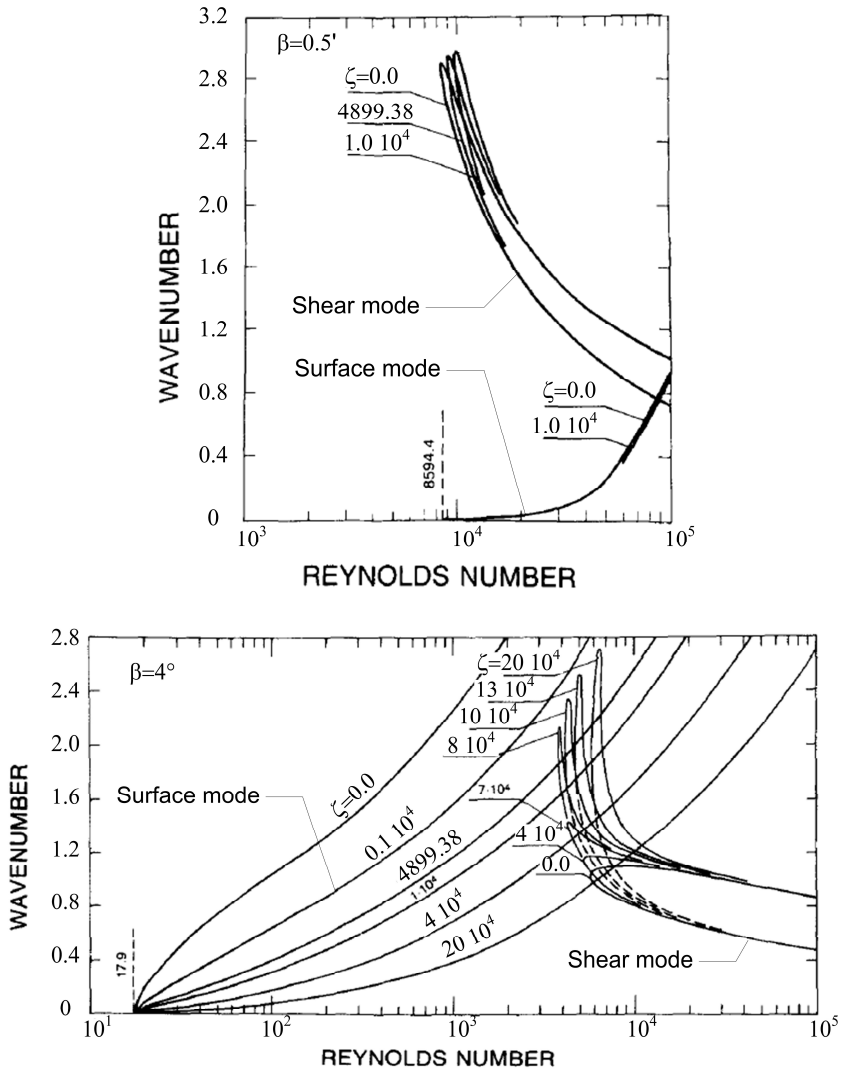

Figure 27: Neutral curves for β =0.5' (a), β =4° (b) and various values of surface tension parameter ζ for the shear and surface modes, from [39].

4.1.2. Two-layer flow down an inclined plane

In this case, authors treated the stability of a two-layer flow down an inclined plane as shown on Figure 28, where each layer has its own rheological properties. They considered two modes of disturbances that can appear either for the interface air/fluid, called the free-surface mode, or for the interface fluid/fluid, called the interface mode.

They highlighted the influence of the depth of the film, physical parameters such as density, viscosity and surface tension. The last parameter is the most studied because it has a really significant impact on wave formation and there is a wide range of viscosity in curtain coating, so the difference between two layers can be significant.

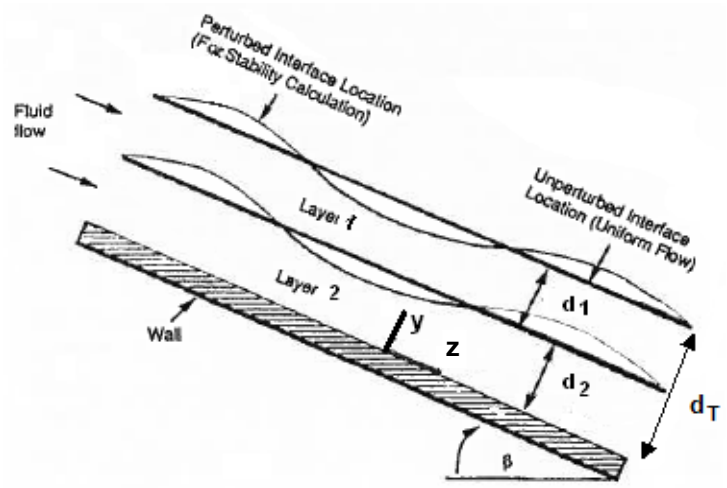

Figure 28: Sketch of two-layer flow down an inclined plane.

4.1.2.1. Influence of density and depth ratios on flow stability

Kao, [40] and [41], is the first author who studied the influence of density and thickness of layers for flow down an inclined plane. He neglected the surface tension and assumed that the two layers had the same viscosity. He showed that for two layers with different densities, the two modes exist and compete to govern the stability on the system depending on which one has the highest density. To do that, he plotted the ratio of amplitudes of the free surface and interface as a function of depth ratio, for various values of density ratios (Figure 29).

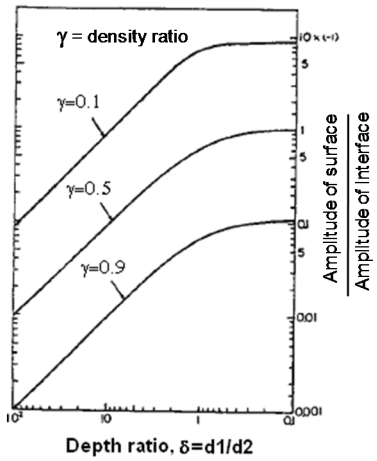

Figure 29: Ratio of the amplitudes of the free-surface and interface as function of the depth ratio for various values of density ratio, from [40].

It is clear here that the interface disturbances have much higher amplitude than the surface disturbances when densities are similar or just somewhat smaller for the upper layer. In this case, the interface mode governs the stability. Moreover, it is obvious that the interface mode is predominant when the depth of the upper layer is higher or equal to the depth of the lower one but its impact is lower than density. The competition between these two modes only exists when the difference of densities is very strong as shown on Figure 30. It is all the more true as the depth ratio is lower than 0.5 in this case.

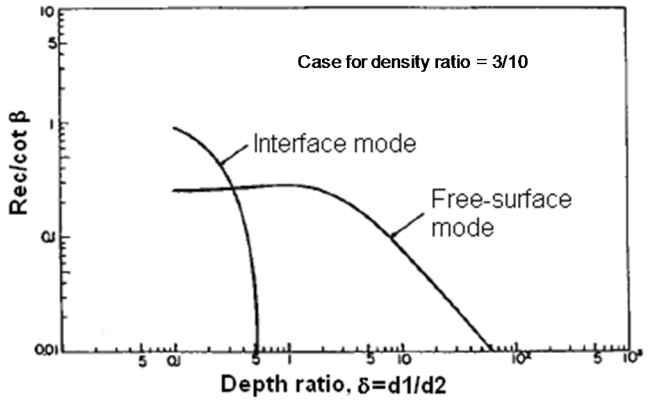

Figure 30: Ratio of the critical Reynolds number to the cotangent of inclination angle for the two modes from [40].

Loewenherz and Lawrence [42] studied the deformation of rock glaciers. They evaluated the stability of a low Reynolds number (Re=10^{-18}) free surface flow consisting of two layers of fluid having the same density and viscosity, different depth ratios and negligible surface tension. They found that inertia is required to create instabilities on the free surface. They also evaluated the flow stability at all wavenumbers for different depth ratios in order to identify the fastest growing mode (Figure 31).

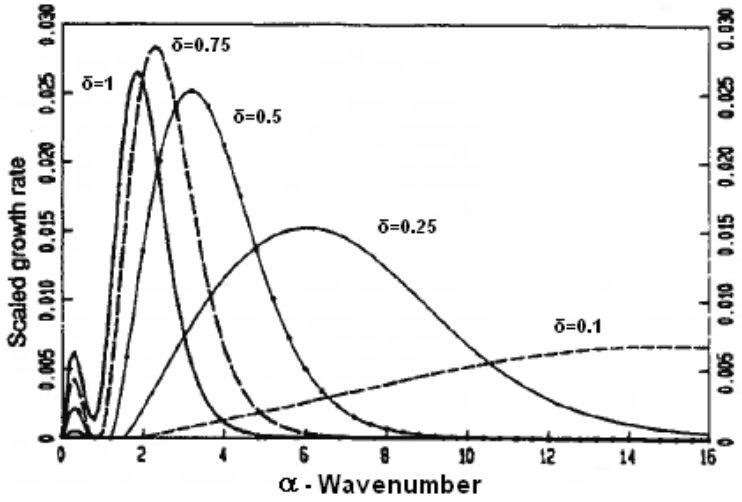

Figure 31: Dependence on wavenumber of the scaled growth rate with β =0.2°, γ =0.4 and different depth ratios from [42].

It is shown that there are two peaks of growth rate, one for the long waves (small wavenumber) and one for the small waves:

- The first peak is for a small wavenumber, which corresponds to instabilities for long waves, instabilities already observed by Kao [40]. The location of this peak does not

depend on the depth ratio, and the higher growth rate is reached when the upper layer is thicker.

- The second peak is located in the region of finite wavenumbers, which corresponds to instabilities for small waves and shows significant variation with respect to the thickness of the upper layer. As the thickness of the upper layer decreases, the value of the wavenumber exhibiting the maximum growth rate increases whereas the scale growth rate decreases.

We will see in Chapter 3 that for the operating conditions on the CTP pilot, the wavenumber is about 0.1. Therefore, we are more interested in the discussion for instabilities at long waves. Figure 31 permits to conclude on the influence of depth ratio, and, for long waves, it is useful to have a thin top layer and a thick bottom layer in order to reduce instability growth. This result will be important for the analysis of the flow in the pilot coater at CTP.

4.1.2.2. Influence of viscosity ratios and surface tension on flow stability

Many articles focus on the viscosity difference between two fluids, which can cause instability. The pioneering work was done by Yih [43], 1967, with a plane Couette-Poiseuille flow of two superposed layers of fluids of different viscosities between two horizontal planes for small Reynolds number. In this case, the author only studied the interface mode with the long wavelength. He assumed that the density was the same for the two layers and showed that a higher viscosity of the lower fluid led to instabilities for any Reynolds number.

Hooper and Boyd [44] considered the Couette flow of two superposed fluids of different viscosities where the depth of the upper fluid is infinite. That is why it is close to the case examined by Yih. The major difference is that they considered the instabilities at all wavelengths. They found that a free-surface mode is stable at low Reynolds numbers, and the most dangerous mode is the interface mode owing to the presence of the fluid-fluid interface. They validated results of Yih when the lower layer has a higher viscosity, and the growth rate is proportional to $(1-m)$ where m is the ratio of the viscosity of the top layer to the viscosity of the bottom layer, and so the flow is stable if the lower fluid is the least viscous fluid and unstable otherwise. However, it was found earlier by Hooper [45] that, if the less viscous component is next to the solid wall and the thickness of such a lubricating layer is thin, then the flow is stable to long waves. It is called the “thin-layer effect”. Nevertheless, there is short wave instability for large wavenumbers at low Reynolds numbers in the absence of interfacial tension as shown on Figure 32. Hooper and Boyd also discovered that surface tension effects stabilize the flow at small Reynolds numbers.

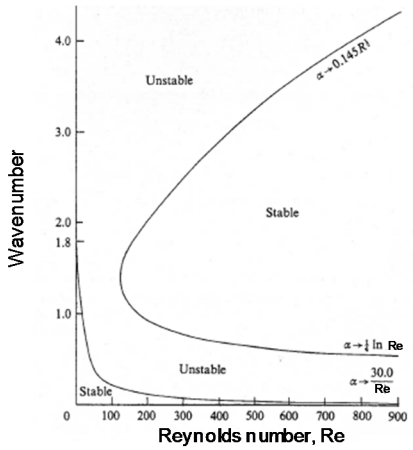

Figure 32: Neutral stability curve when the viscosity ratio is equal to two, from [44].

The configuration with two solid walls had been the focus of many articles. Then, authors paid more attention to the configuration in which one of the fluid layers is exposed to the ambient air, forming a fluid-air interface, which is the case with the CTP laboratory coater. It is one of the most studied free-surface problems with one or two layers and the article by Kao [40] is a very pertinent study for the two-layer case. Here again he considered long waves only and considered the case where the coefficient of dynamic viscosity of the upper fluid is different from that of the lower fluid in addition to the differences in density (we are not concerned by this case) and depth ratio δ. He concluded that the two modes competed for instability start. Figure 33 shows the ratio of the critical Reynolds number to the cotangent of inclination angle ($\cot(\beta)=1.73$ in the CTP pilot case) for the first and second modes respectively, as a function of the viscosity ratio *m* for various values of δ.

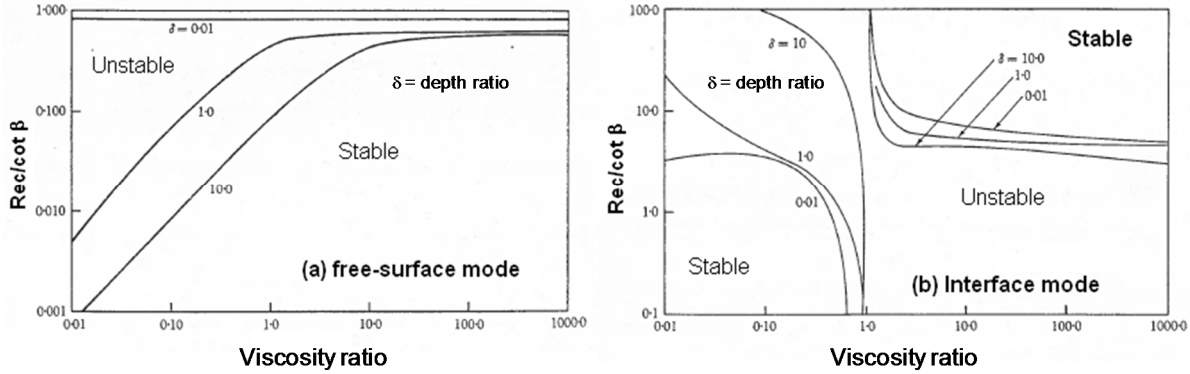

Figure 33: Ratio of the critical Reynolds number to the cotangent of inclination angle for the two modes with the ratio density equal to 0.9, from [41].

- It should be noted that when the less viscous fluid is adjacent to the inclined wall (viscosity ratio over unity), the two-layer flow is unstable at low Reynolds numbers whatever the depth ratio, due to the instability of the interface mode. This is in contrast to the thin-layer effect for the situation in which the fluid/air free surface is absent. This is called the “antilubrication effect”. Nevertheless, when the upper layer thickness increases, the value of the critical Reynolds number decreases and we could imagine that, in the limit of infinite upper layer thickness, we have the Hooper and Boyd configuration and the interface mode should be stable.
- It is clearly observed that the interface mode is unstable and governs the problem at $m=1$ but, for smaller values of m (*i.e.* when the high viscous fluid is next to the solid wall), this mode is all the more stabilized when the upper layer has a higher thickness. So, the free-surface mode governs this case.

Finally, Kao compared the stability of the two-layer flow relative to that of a homogeneous fluid of the same depth. He defined a relative stability index, which is the critical depth for a two-layer flow for a given angle divided by the critical depth for homogeneous flow for the same angle. The critical depths are function of the critical Reynolds number. It means that the lower the relative stability index value, the worse the stability. Figure 34 shows that the viscosity ratio is smaller than unity, so the presence of an upper layer is always destabilizing compared to the one with a homogeneous fluid of the same total depth.

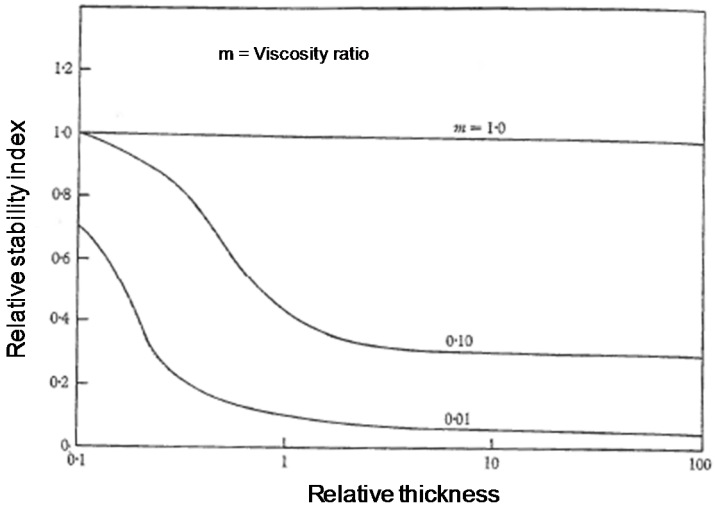

Figure 34: Relative stability index for the free-surface mode for a viscosity ratio <1, with a density ratio equal to 0.9, from [41].

Chen [46] focused a large part of his work on the case where the upper layer is thicker and then compared his results to those of Hooper and Boyd. He assumed that the two layers had the same density.

He studied first the inertialess interfacial stability (we will not focus on that) and then the inertial effect. He found that inertia has a significant influence on stability of the two-layer flow (Figure 35). Whether inertia is stabilizing or destabilizing the interface mode depends on the wavelength of disturbances. Indeed, Figure 35 shows the inertia contribution to the growth rate, and for a quite small Reynolds number, inertia is clearly stabilizing the long waves and slightly destabilizing the short waves. It confirms that with the less viscous fluid next to the solid wall, there is a stabilizing thin-layer effect for long wave disturbances. In the absence of interfacial tension and with the same viscosity, the interface mode is stable and then he concluded that the inertia contribution to the growth rate is proportional to the viscosity difference between the two fluids.

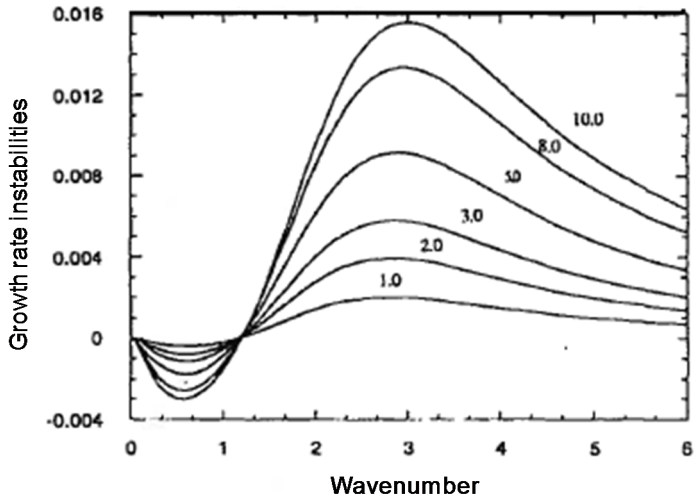

Figure 35: The inertia contribution to the growth rate, for a viscosity ratio equal to 2.5, the angle of inclination equal to 0.2° and various values of Reynolds number, from [*46*].

Then he explored the influence of viscosity stratification for different values of depth ratio by constructing the neutral stability curves for the two modes as a function of the Reynolds number and the wavenumber.

Case where the upper layer is lubricated by a less viscous layer (in the studied case, the viscosity ratio equal to 2.5, i.e. greater than unity):

- For the free-surface mode (Figure 36 *a*)

  Results are similar to those with one layer for which the unstable region is restricted to long waves. It can also be noticed that as the thickness ratio decreases (when the depth of the lower layer increases), the critical Reynolds number increases and, as the thickness ratio tends to zero, the value of the critical Reynolds number tends to the well-known result of $5/6 \cdot \cot\beta$ for a single layer.

- For the interface mode (Figure 36 *b, c and d*)

  Without surface tension, it is clear that there are two unstable zones, one for a very low wavelength and the other for a high wavelength. In the latter case, increasing the thickness of the upper layer leads to a higher area of stability. So, there is a window in the Reynolds number bounded below by the Reynolds number of the long wave and above by the critical Reynolds number of the short wave. For the Reynolds number falling within this region, the interface mode is stable to disturbances of all wavelengths. The upper limit can be raised by increasing the interfacial tension (Figure 36 *d)*. Thus, when the interfacial tension is high, the critical Reynolds number for the longest waves gives the minimum critical Reynolds number for interfacial stability.

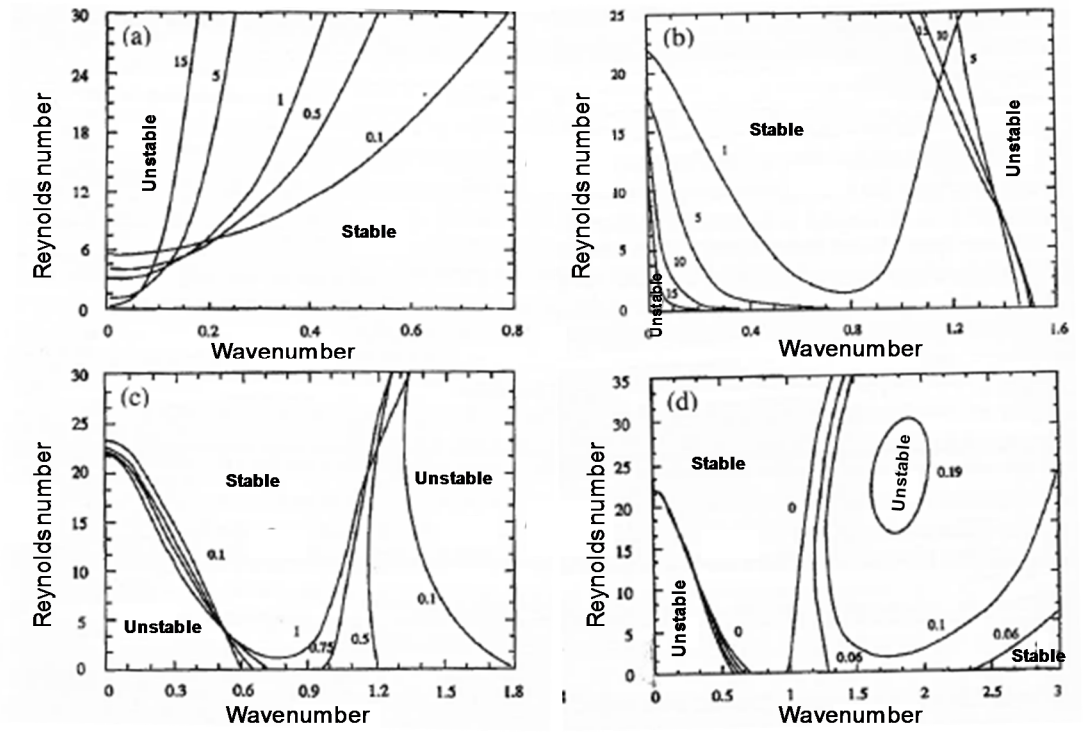

Figure 36: The neutral stability curves for the surface mode (a) and interface mode (b,c,d) for a viscosity ratio equal to 2.5, an inclination angle of the plane equal to 0.2° and various thickness ratios (a,b,c) and various interfacial tensions(d) (where the thickness ratio is 0.75), from [*46*].

To conclude, although the interface mode can be stabilized by an interfacial tension for a rather high Reynolds number ($Re > 22$), it is clear that in this case the surface mode is always destabilizing the fluid (maximum critical Reynolds number is equal to 5). Thus, it is impossible to stabilize both the interface and the free-surface mode simultaneously and wave motion will always appear in this configuration (lubricated configuration).

Case where the liquid layer adjacent to the solid wall is more viscous (in the studied case, the viscosity ratio is equal to 0.4, i.e. lower than unity):

- For the free-surface mode *(*Figure 37 *a)*

  Results are similar to those with the other viscosity configuration, for which the unstable region is restricted to long waves

- For the interface mode (Figure 37 *b* and *c*)

  Without surface tension, when the upper layer is of infinite thickness, the interface mode is always instable for any Reynolds number otherwise it is stable for long waves as mentioned by Kao but it becomes instable for very short waves. As the upper layer becomes thinner, there is an expansion of the stable region. Adding an interfacial tension will drastically stabilize the short waves whereas it will not affect the long waves. The lowest critical Reynolds number occurs at a wavenumber approximation of 0.5.

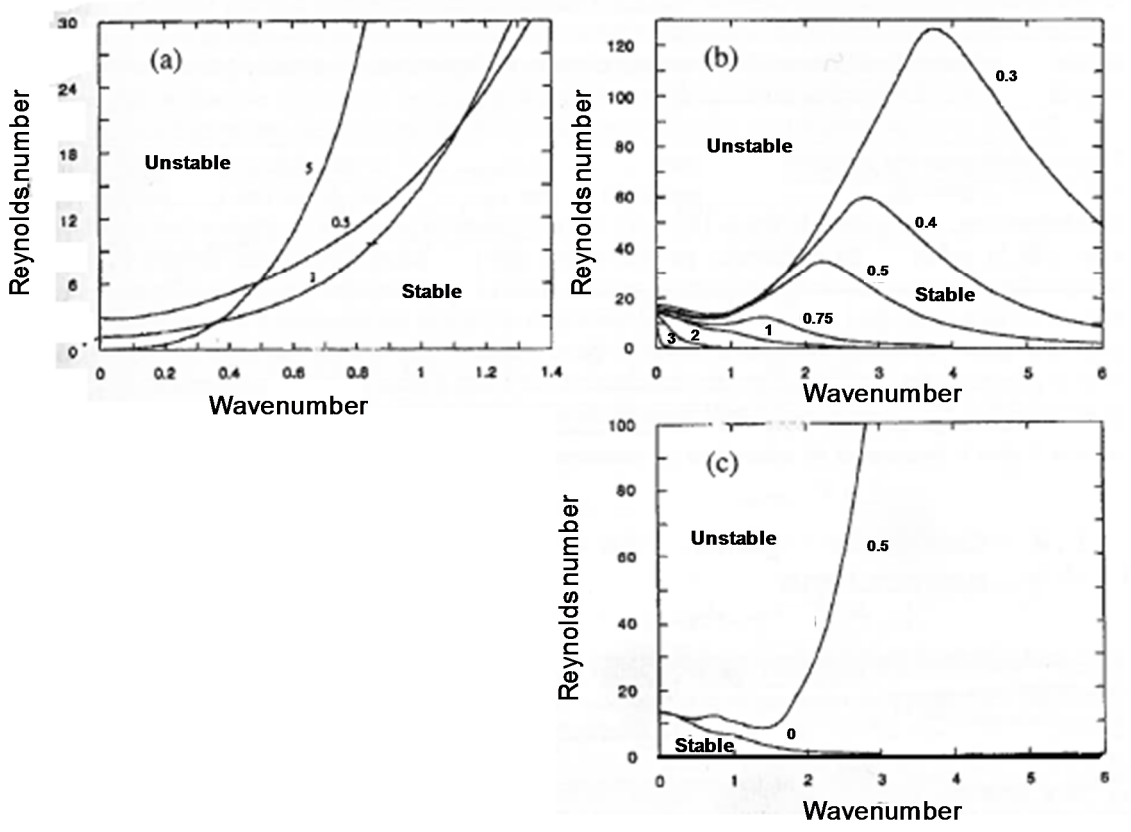

Figure 37: The neutral stability curves for the surface mode (a) and interface mode (b,c) for the viscosity ratio equal to 0.4, an inclination angle of the plane equal to 0.2° and various thickness ratios (a,b) and various interfacial tensions(c) (where the thickness ratio is 1), from [*46*].

To conclude, it is possible to find the critical condition for the onset of instability for a two-layer flow, so whether the wave is an interfacial or a surface one. On each case, you can compare the lowest critical Reynolds number for the interface mode and the surface mode and find an appropriate range of values for the Reynolds number. Most of the time, the critical Reynolds number is obtained for short waves, which had rarely been studied except by Kao.

Finally, we can summarize all these results as follows:

For the lubricated configuration, it is impossible to stabilize the interface and the free-surface mode simultaneously, wavy motion due to the linear instability can occur.

For the opposite arrangement, if a non-zero interfacial tension is present to stabilize the short wave instability, linear stability can be achieved to disturbances of all wavelengths at a low-Reynolds number.

The increase of interfacial tension does not seem to have an impact on disturbances

For small wavenumbers, increasing the depth ratio will lead to higher growth rates of instabilities.

4.1.3. Three-layer flow down an inclined plane

The stability of three-layer or more flow down an inclined plane has been studied by several authors with a small angle of inclination without inertia and with negligible surface and interfacial tensions as shown on Figure 38.

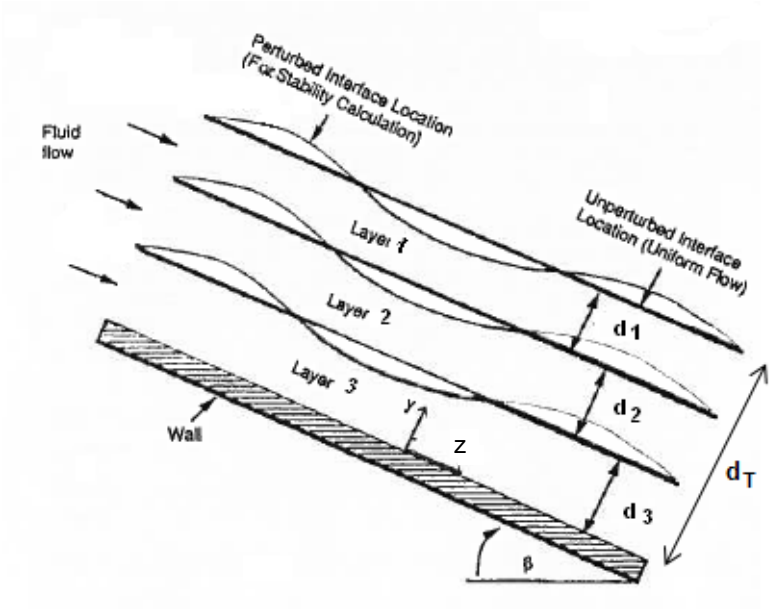

Figure 38: The geometry of the uniform flow and stability problems, from [*48*].

Wang *et al.* [47] examined the stability of an n -layered film flowing steadily down an inclined plane using linear theory. They obtained neutral curves for various ratios of viscosity, density and thickness but their graphs are quite complex. Their conclusion concerning the influence of density stratification is that, when the bottom heavy density stratification is considered, the film is stable for the interfacial mode but may be unstable for the free surface mode. The interfacial instabilities occur only in top-heavy system and the flow could be stable if α tended towards 0 as pointed out by Kao. The authors also found that the angle of inclination β does not change the character of the film instability of the different modes except that a reduction of this angle leads to stabilization of the free surface mode.

Weinstein and Kurz [48] considered long-wavelength instability for a three-layer surface flow down an inclined plane. They identified instability in the zeroth-order asymptotic solution in wavenumber which means that neither inertia nor infinite wavelengths are necessary to induce instabilities in a three-layer system. They presented an effect of viscosity stratification, density stratification and layer thickness. They examined first the influence of a middle layer of constant thickness and density for different cases of viscosity stratifications and bottom layer thickness as shown on Figure 38.

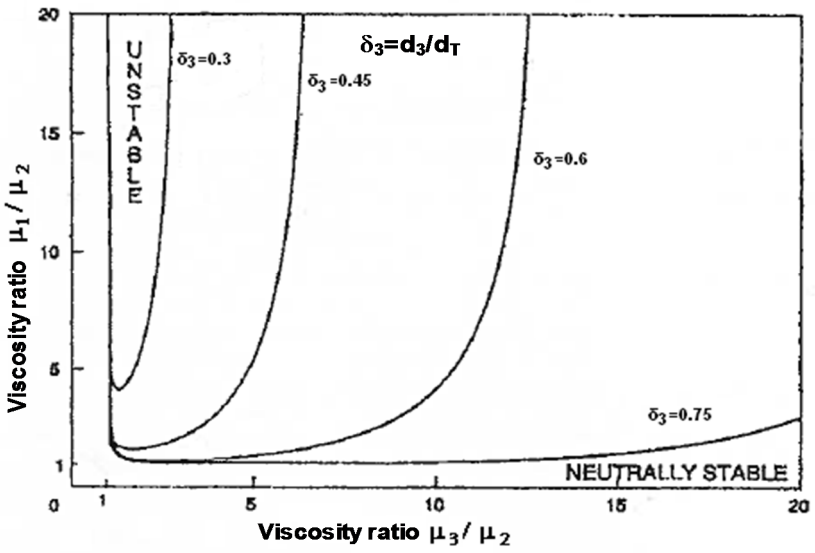

Figure 39: The effect of middle-layer viscosity and bottom-layer thickness on instability regions, with the ratio of the second layer to the total thickness equal to 0.1, from [48].

It is apparent that instabilities can only arise if the middle layer viscosity is smaller than those of the two adjacent layers. Moreover, it is seen that, as the bottom layer becomes thinner, the region of instability decreases in size. Indeed, when the bottom layer thickness is lower than 0.22 of the total thickness, which is not plotted on this figure, no region of instability exists for the viscosity ratios considered (between 0 and 20). The effect of density stratification was also considered and the same results as for viscosity were found which means that destabilization occurs where the middle-layer density (for equal density of each layer) is smaller than those of the adjacent layers. Then the authors demonstrated the effect of viscosity ratios while increasing the thickness of the middle layer and reducing that of the others, which are equal (Figure 40).

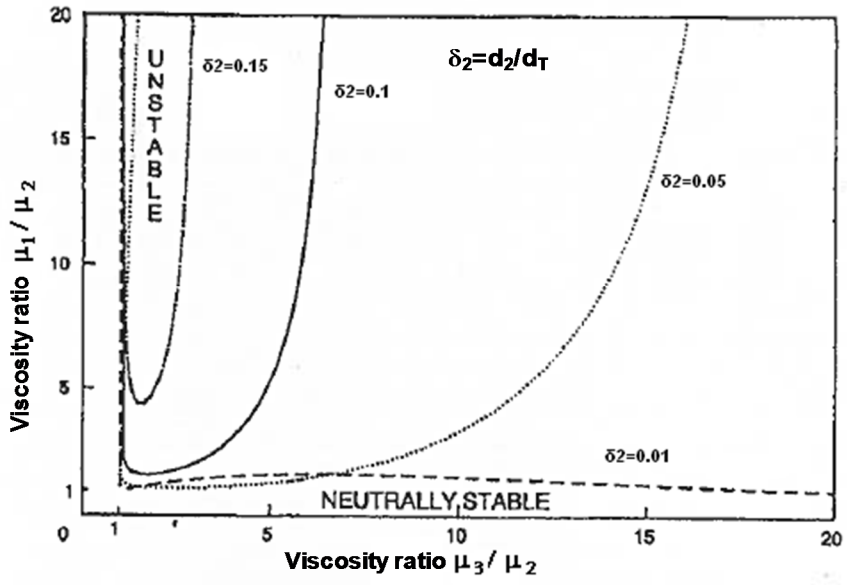

Figure 40: The effect of the middle-layer thickness on instability regions for various viscosity ratios, when the upper and bottom layer have the same thickness, from [48].

It is clear on this figure that, as the middle layer increases in thickness, the region of instability diminishes in size. Indeed, for values of thickness greater than 18% of the total thickness, no region of instability can be found for these viscosity ratios.

So, to avoid instability, the thickness of the bottom layer should be below 22% of the total thickness and the thickness of the middle layer above 18% of the total thickness.

Weinstein and Chen [48] examined the effect of viscosity stratification on wave propagation in a three-layer flow down an inclined plane at small Reynolds numbers and at finite wavelengths, which is the difference between this work and the one by Weinstein and Kurz. Their study is an extension of the work by Weinstein and Kurz and here again the authors neglected the effect of interfacial tensions. They found that the inertialess instability occurring into the finite wavelength mode, already described by these authors, persists into the finite wavelength domain in form of complex conjugate wave speed pairs. They presented three combinations of viscosity stratification in a three-layer system: monotonically increasing from the bottom to the top, high-viscosity and low-viscosity middle layer on Figure 41. To do that, they presented wave growth results as a function of the dimensionless wavelength ($\bar{\lambda} = \lambda / d_T$). When the wave growth coefficient is positive, wave amplitudes will grow, for negative wave growth coefficient, wave amplitudes will decay, and zero value corresponds to neutral stability.

On Figure 41, it is clear that whatever the combination of viscosities, the surface mode is stable at finite wavelength and neutrally stable in the long wavelength limit. Thus, the surface mode is neutrally stable in the zero Reynolds number limit, which is in agreement with what is stated in other studies.

- In the case of the high-viscosity middle-layer configuration (Figure 41 *a*), one of the interface modes is unstable to both short and long waves with a neutrally stable band of wavelength in between. Moreover, the largest growth occurs at the short waves and in this case, the two interface modes are nearly complex conjugates. The first regime of instabilities is characterized by relatively long but finite wavelengths ($\bar{\lambda} = 30$) and the second has wavelengths comparable to the thickness of the film ($\bar{\lambda} = 0.4$). The growth rate associated with the longer wavelength instabilities is similar to the results obtained in two-layer configurations with a high viscosity top layer, but the short wavelength growth rates are several orders of magnitude larger.
- In the case of the low-viscosity middle-layer configuration (Figure 41 *b*), one of the interface modes is unstable once the dimensionless wavelength exceeds 2. Moreover, the two interface modes are nearly complex conjugates. The growth of the disturbances extends all the way to infinitely long waves, without a neutrally stable band of wavelengths as seen in the high-viscosity middle-layer configuration. The authors also noticed that this result could be viewed as the finite wavelength extension of the work done by Weinstein and Kurz who found instabilities when there were low-viscosity middle-layers.
- In the case of the monotonically increasing viscosity configuration (Figure 41 *c*), one of the interface modes is unstable to long wavelength disturbances but the growth rate is very small.

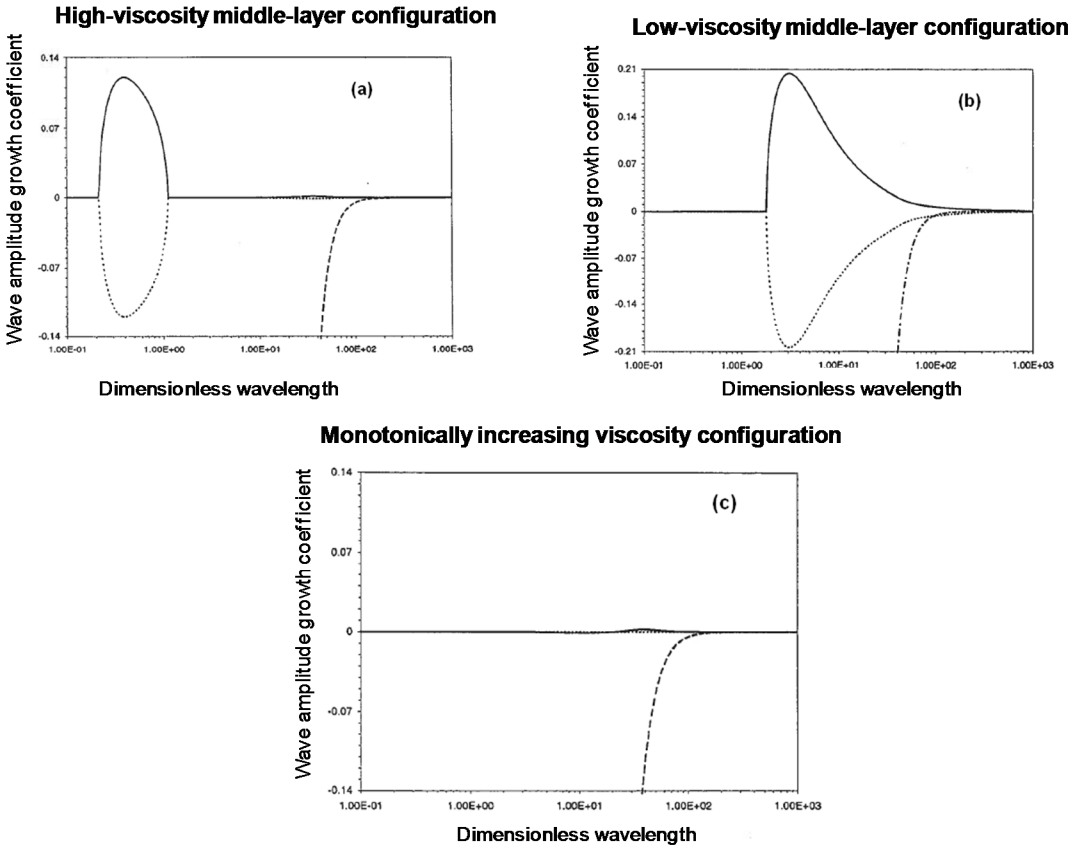

Figure 41: Growth rate vs. wavelengths for different viscosity configurations, from [*49*].

To conclude with this work, these authors compared values of the growth rate of instabilities with those found by Loewenherz and Lawrence [42] on the case of interface mode instability in the two-layer system. They demonstrated that the two-layer flow is unstable only when the bottom layer is less viscous. Values found for the three-layer configurations are ten times higher than the one found with two layers and the wavelength is about the total thickness of the system.

4.1.4. Conclusions

All these results found in literature show that instabilities can develop. Literature provides us with some practical parameters to reduce or avoid instabilities for Newtonian fluids in multi-layers. The best configuration is an increase of depth and viscosity from the bottom to the upper layer. A low viscosity middle-layer configuration has to be avoided because it is the worst configuration. Concerning the depth ratio, it is better to have a very thin bottom-layer (under 22% of the total thickness) and a thick middle-layer (over 18% of the total thickness).

Different configurations of coating colour viscosities are possible on the inclined plane as shown in Table 4. The expected effect of these arrangements on flow stability on the inclined plane is reported in the table and we can see that the best solution should be to use a low viscosity pre-coat and a high viscosity top-coat.

Table 4: Influence of viscosity configurations on flow stability on an inclined plane.

Case	Viscosity configuration (not on scale) Pre-coat	Middle-Coat	Top-Coat	Effect on stability	Comment
# 1				++	Best solution
# 2	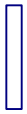			+	Little information
# 3				--	Worst solution
# 4	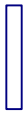			--	Worst solution
# 5				+	Very high growth rate in case of instability
# 6				+	Very high growth rate in case of instability

4.2. Flow of non-Newtonian down an inclined plane

There is an extensive literature on the stability of Newtonian flow down an inclined plane for single and multi-layer systems. The non-Newtonian film flows down an incline has been much less studied but recently authors focused on it, for instance Yih [50] for a triply nonlinear constitutive equation, Hwang *et al.* [51] for a power-law liquid and Rousset *et al.* [52] for a Carreau fluid. Indeed, in many processes, the rheological behaviour of the fluid cannot be properly described by the Newtonian model. For example mud and coating colours are shear-thinning and polymers generally exhibit a large elastic component. This second part focuses on the behaviour of inelastic non-Newtonian fluids for one and several layers.

4.2.1. One-layer flow down an inclined plane

a) Power-law fluid

The stability of a laminar liquid layer flowing down an inclined plane was investigated by Hwang *et al.* [50]. In the equation of such a model, when the power-law exponent n is equal to unity, the fluid becomes Newtonian, if it is lower than unity, the fluid is said “shear-thinning” and if it is higher than unity, the fluid is called “shear-thickening”. The authors used the integral method to derive non-linear evolution equations about the flow rate and the film thickness. They studied first the stability of the flow in terms of Reynolds number and Weber

number (which is related to the surface tension) fixing the power-law index, n. The Reynolds number is calculated for a power-law fluid on the inclined plane as follows:

$$Re = \frac{\rho V^{2-n} d^n}{K} \tag{38}$$

- Concerning the Weber number:

  The authors plotted the neutral curve in the wavenumber as function of Reynolds number for different values of Weber number (Figure 42) which is defined as:

$$We = \frac{\rho V^2 d}{\sigma} \tag{39}$$

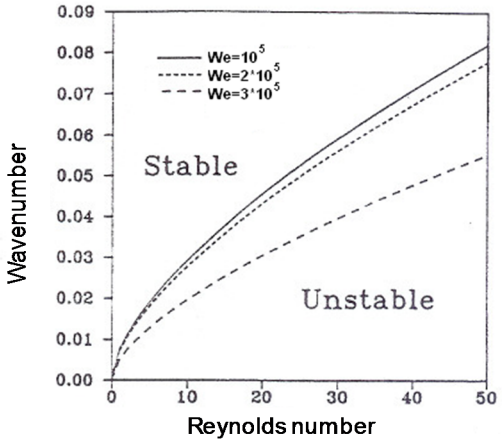

Figure 42: Neutral stability curve for wavenumber as a function of Reynolds number for different values of Weber number at a power-law index of 0.85 and an angle of inclination of the plane of 60°, from [*51*].

The authors found that when the Weber number is increased, the stable region is extended. It means that increasing the surface tension will lead to more stable films.

- Concerning the Reynolds number:

  Figure 43 displays the growth rate against the wavenumber for low values of the wavenumber and different values of the Reynolds number. The other parameters are the same as on Figure 42. It shows that the growth rate will increase if one enlarges the value of the Reynolds number.

  To conclude with these results, they reveal that while fixing the power-law index, the stability in terms of Reynolds and Weber numbers are identical to those of Newtonian fluids, *i.e*. increasing the Reynolds number or decreasing the Weber number will destabilize the film flow system.

  Then the authors studied the influence of the power-law index. They demonstrated, as shown on Figure 44, that reducing the power-law index will enlarge the growth rate value because the effective value of viscosity of the fluid will be reduced. Moreover the dimensional wave speed will be larger while the power-law index will decrease but it is not presented here. Therefore it is obvious that the film flow will be destabilized when the power-law exponent will decrease.

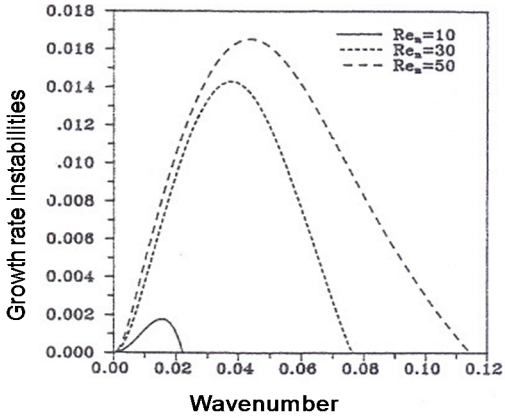

Figure 43: Temporal growth rate versus wavenumber for different values of Reynolds number at a power-law index of 0.85 and an angle of inclination of the plane of 60, from [*51*].

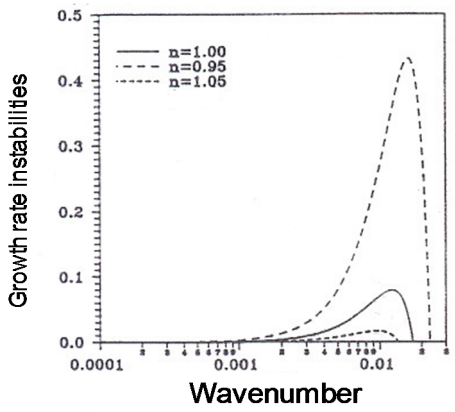

Figure 44: Growth rate against wavenumber for different values of the power-law index and an angle of inclination of the plane of 90°, from [*51*].

b) Carreau fluid

Among the studies of the stability of non-Newtonian film flows, some authors prefer to use the Carreau model instead of the power-law model. Indeed, it predicts a region in which a linear relation between viscosity and shear rate is observed when plotted on log/log coordinates. Moreover, the viscosity remains finite as the shear rate approaches zero.

Rousset *et al.* [52] used this model for a one-layer flow down an inclined plane in the limit of very long waves. They studied the influence of shear dependant rheology on the temporal stability of a liquid flow down an inclined plane. They carried out a stability analysis based first on analytical expressions with the asymptotic approach and then on numerical approach.

- Asymptotic approach

  Their study was done analytically and they obtained an expression for the first-order in α of the critical Reynolds number. They found that for the shear-thinning case, the critical Reynolds number is lower than for the Newtonian case as mentioned by Hwang but although it remains proportional to the cotangent of the inclination angle. Benjamin and Yih showed that the velocity is twice the free surface velocity for a Newtonian fluid but here the ratio is all the more important as the fluid is shear-thinning.

- Numerical approach

  The numerical part of this work consisted in solving the Orr-Sommerfeld generalized eigenvalue problem and compared results to those with the asymptotic approach when it is possible. They first compared cases between Newtonian and shear-thinning fluids. They evaluated the influence of the angle of inclination on the critical Reynolds number for both Newtonian and non-Newtonian fluids (Figure 45).

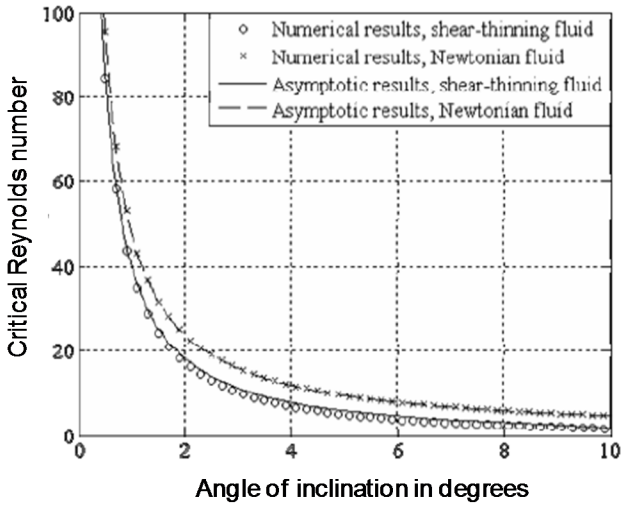

Figure 45: Critical Reynolds number as a function of the inclination of the plane with n *=0.5. Parameter δ is set to 0 for Newtonian case and equal to 0.1 otherwise, from* [52].

From Figure 45, it clearly appears that the asymptotic approach gives results which quantitatively validate those of numerical approach. Increasing the inclination angle leads to reducing the critical Reynolds number. Concerning the difference between Newtonian and non-Newtonian fluids, it is clear that for a fixed angle, the critical Reynolds number is higher for a Newtonian fluid, so shear-thinning properties will destabilize the flow.

4.2.2. Multi-layer flow down an inclined plane

Many articles about a multiple-layer flow down an inclined plane concern Newtonian systems. Nevertheless, the fluids we are interested in are non-Newtonian and this topic will focus on a multi-layer flow for non-Newtonian fluids.

Weinstein [53] was one of the first authors who focused on that. In his article, the flow rate in each layer is specified and the film thickness plays a passive role. He compared first the stability of the flow for one layer with specific Newtonian cases, which are Newtonian fluids with the highest and the lowest viscosity found in the layer for the shear-thinning fluid (reached at the free surface and the wall respectively). He found that all the curves for the shear-thinning fluids are between those of these two specific Newtonian cases except for very low wavenumbers. So he could conclude that, for one layer, the effect of shear-thinning is to provide an averaging effect of the viscosities across the layer. Then he considered two-layer systems with the assumptions that there is no surface tension and the densities in each layer are equal.

- Case where the bottom layer is the shear-thinning fluid and the top layer is the Newtonian fluid:

There are two solutions that arise upon solving the two-layer non-Newtonian system which are the surface and the interface mode. First Weinstein used shear-thinning fluid with the maximum viscosity equal to the viscosity of the Newtonian fluid on the top layer. Concerning the surface mode, results are similar to those with one layer, which means that all the curves are located between the two extreme Newtonian cases (Figure 46).

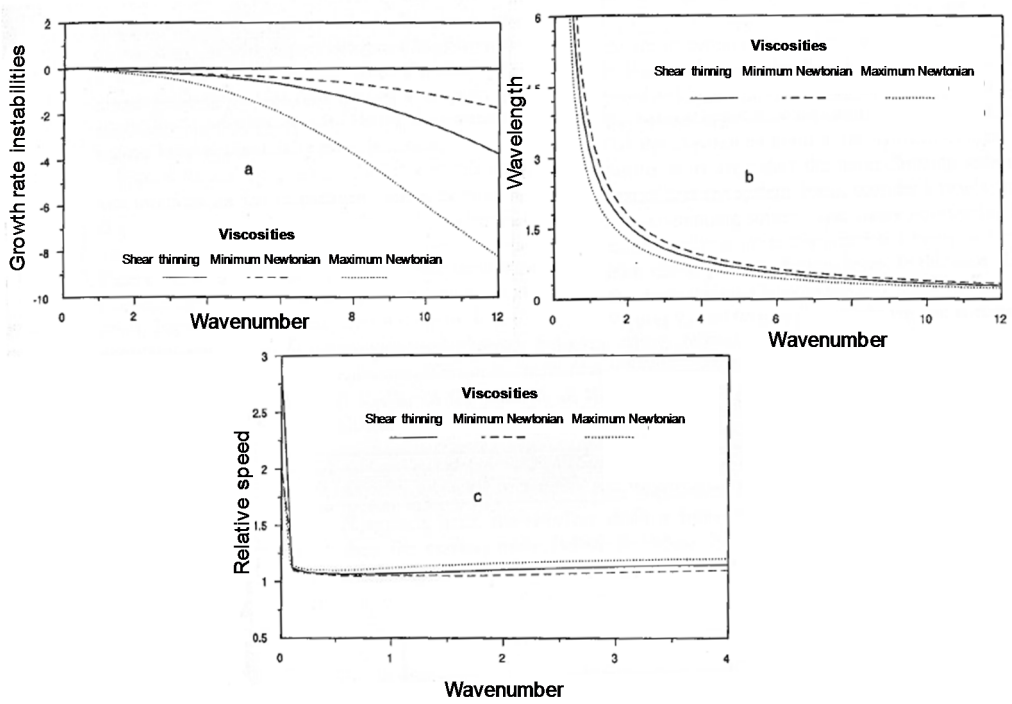

Figure 46: Effect of the shear-thinning bottom layer on the surface mode waves in a two-layer slide flow for growth factors (a), wavelengths (b) and wave speeds (c), from [*53*].

Figure 47 describes the effect of the shear-thinning bottom layer on the interface mode and results are totally different from the case with one layer. Indeed, in the limit of an infinite wavenumber, the relative wave speed of the interface mode against the interface uniform velocity appears to asymptote to unity whereas, in the surface mode results, the speed was always greater than the one of the free surface (c). Concerning the growth rate (a), it is shown that the non-Newtonian curve no longer lies between the curves corresponding to the maximum and minimum Newtonian viscosities in the bottom layer. Thus, the shear-thinning effect leads to a maximum growth factor which is smaller than the one associated with the corresponding Newtonian cases. It can also be noticed that, at high wavenumber, the growth factor associated with the maximum Newtonian case follows quite closely the one for the shear-thinning case.

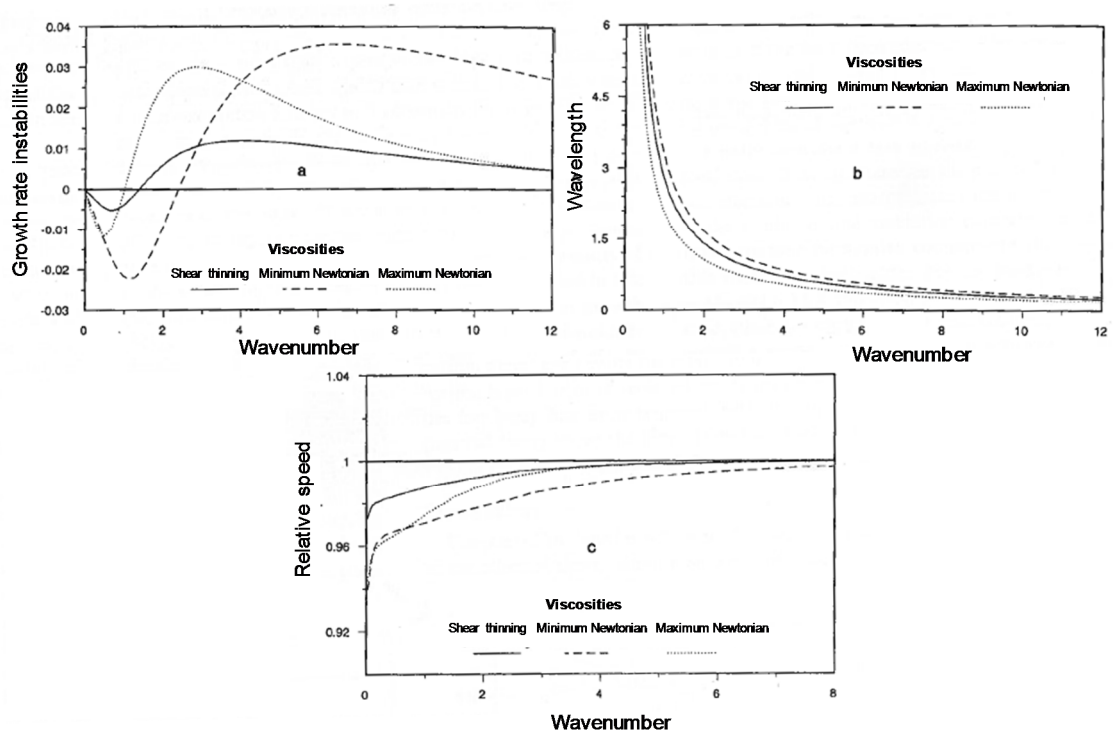

Figure 47: Effect of the shear-thinning bottom layer on the interface mode waves in a two-layer slide flow for growth factors (a), wavelengths (b) and wave speeds (c), from [*53*].

Then, Weinstein made some tests with more moderate shear-thinning in the bottom layer (the viscosity varies by a factor 2). He superimposed on Figure 48 the wave growth as a function of the wavenumber for the case where the bottom layer does not shear thin at all (called the Newtonian limit), so the two layers have the same viscosity.

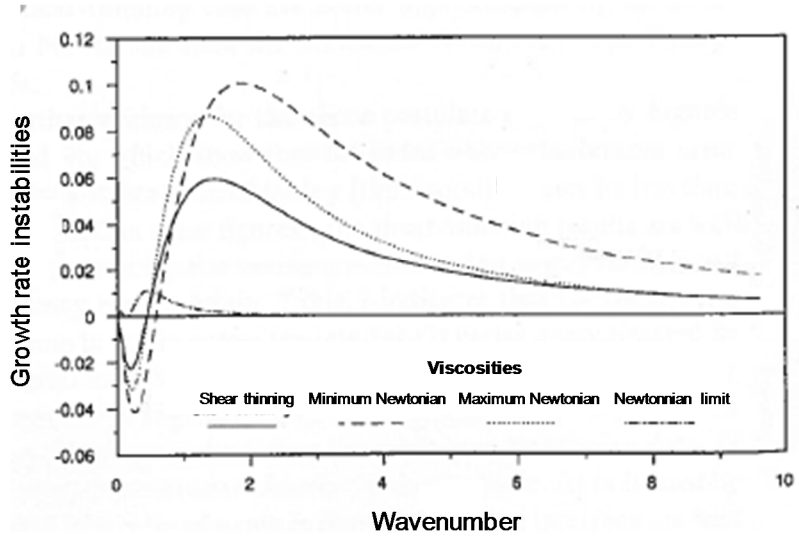

Figure 48: Effect of the shear-thinning bottom layer in a two-layer slide flow for the interface mode growth factors, from [*53*].

Here again the growth factor associated with the shear-thinning case follows quite closely the one for the maximum Newtonian case at a high wavenumber. By comparing results from the Newtonian limit and the shear-thinning fluid, we can conclude that the presence of the shear-thinning fluid greatly destabilizes the system.

Finally, some tests were conducted with a shear-thinning bottom layer where the top layer Newtonian viscosity is lower than the low-strain rate limiting Newtonian viscosity for the bottom layer in order to see if shear-thinning fluids always destabilize the system. Figure 49 (*a*) and (*b*) gives plots of the interface mode for the growth factors. It can be observed that the shear-thinning wave growth behaviour closely follows that of the maximum Newtonian curve over a broad wavenumber range. Figure 49 (*b*) indicates that in contrast to the previous case, the shear-thinning behaviour stabilizes the interface mode compared with the case where no shear-thinning occurs at all.

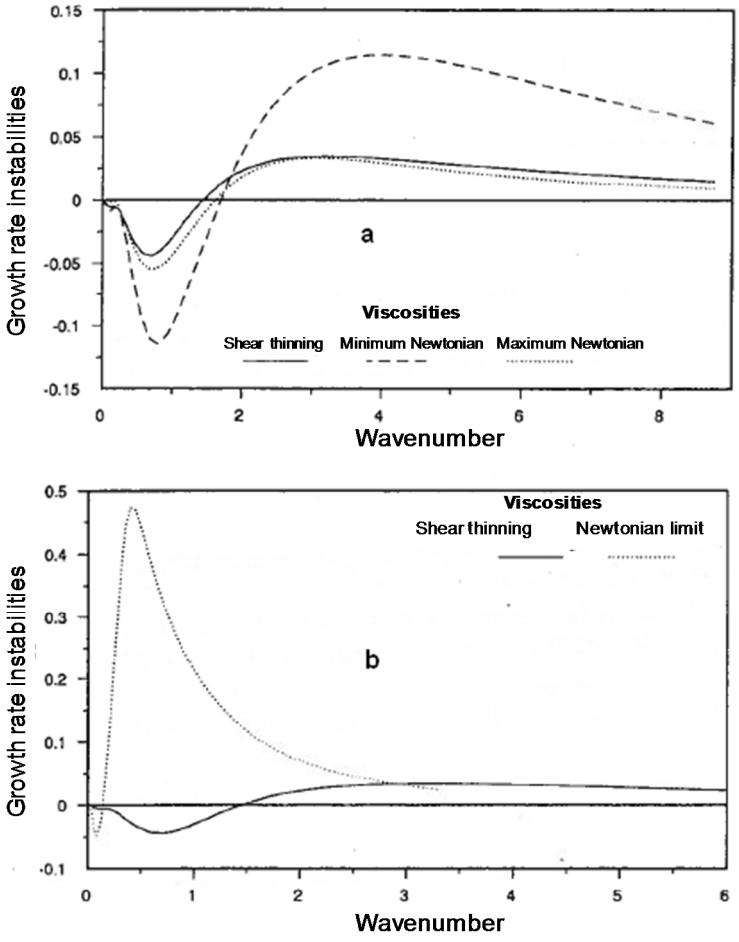

Figure 49: Effect of the shear-thinning bottom layer in a two-layer slide flow for the interface mode growth factors, from [*53*].

- Case where the bottom layer is the Newtonian fluid and the top layer is the shear-thinning fluid

  Weinstein plotted the growth factors for surface and interface modes. Concerning the surface mode he showed that there is the same trend as in the case where there is a shear-thinning bottom layer, the surface mode lies between those for the minimum and maximum top layer. Concerning the interface mode, results are in contrast to previous

cases because the shear-thinning interface mode growth factors follow the curve of the minimum Newtonian viscosity in the top layer (Figure 50).

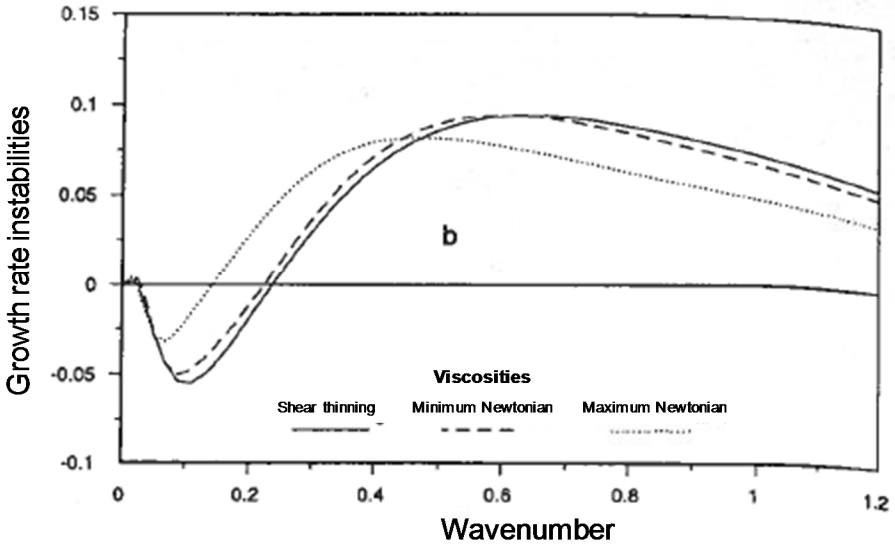

Figure 50: Effect of the shear-thinning top layer in a two-layer slide flow for the interface mode growth factors, from [*53*].

- Case where both layers are shear-thinning fluids

  Finally the author considered a case where both fluids are shear-thinning. Based on the previous arguments, there are two viscosities that characterize each shear-thinning layer, that is the minimum and maximum viscosities in each layer. He presented results of interface mode growth factors along with results for a Newtonian system in which the bottom layer has been replaced by its maximum viscosity and the top layer has been replaced by its minimum viscosity (called Interface on Figure 51). In this case the shear-thinning behaviour stabilizes the interface mode compared with the case with Newtonian fluids.

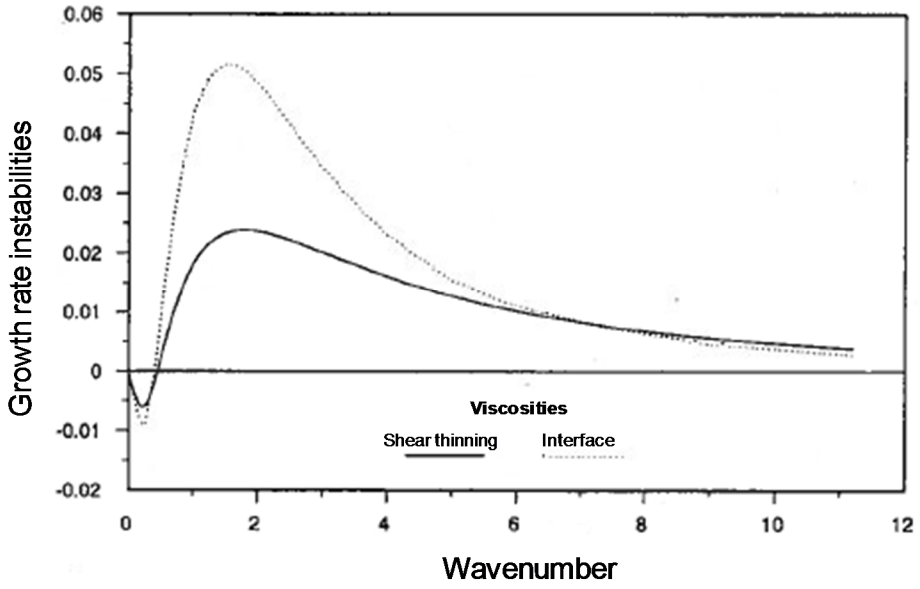

Figure 51: Effect of shear-thinning top and bottom layers on interface mode growth factors in a two-layer slide flow, from [*53*].

To conclude, it is clear that the shear-thinning behaviour affects the interface and surface mode waves in different ways.

- ✓ When there is shear-thinning, the single-layer and the surface mode wave results indicate that the wave propagates as if it is interacting with an average viscosity of the layer. This is indicated by the fact that the shear-thinning curve lies between the Newtonian results associated with the maximum and the minimum viscosities found in the shear-thinning layer.
- ✓ In case of double layer, the interface mode results are very different from the surface mode results since it is not interacting as an average viscosity of the layer. Indeed the interface mode does not have values that lie between those associated with the maximum and the minimum viscosities Newtonian results found in the shear-thinning layer. For cases where the bottom layer is shear-thinning, the shear-thinning results are well approximated by the maximum Newtonian case over a broad wavenumber range whereas they are approximated by the minimum Newtonian case when the top layer is shear-thinning. This provides evidence for the role of local viscosity effects in the vicinity of the interface.
- ✓ Finally it was pointed out that shear-thinning behaviour occurring on the inclined plane can either stabilize or destabilize compared to a case where no shear-thinning occurs, it depends on the rheological behaviour of fluids, the depth of the layers and their position.

Millet *et al*. recently studied the effects of density stratification and the position of the Carreau fluid layer on interfacial stability [54-55]. The effect of density stratification is studied in the case of a less viscous layer adjacent to the wall, which is favourable to interfacial instabilities. Millet [54] presented results for cases where the upper layer has a lower density.

Figure 52 (a) represents the growth rate of the interfacial instability as a function of the wavenumber for different densities for two Newtonians layers. We can notice that there are two different instabilities: one is for long wavelengths that are always unstable and the other one for short wavelengths that have a higher growth rate when the density ratio is over 0.947. These results validate those of Loewenherz and Lawrence [42] and Chen [46]. Moreover it shows that the growth rate of the long wavelength is not influenced by the density ratio.

Figure 52 (*b*) and (*c*) represent cases where the upper layer is Newtonian and the lower is shear-thinning (*b*) and the opposite for the (*c*). The shapes of these curves are similar to those of two Newtonians layers. However, the limiting values of density ratios where the change of instability takes place is lower when the lower layer is shear-thinning. Moderate wavelengths are destabilized by the shear-thinning properties when the non-Newtonian layer is at the bottom whereas they are stabilized when the non-Newtonian layer is upper layer. Finally it can also be noticed that there is a reduction of the growth rate for the long wavelengths when the lower fluid is shear-thinning, it means a stabilizing effect on the flow.

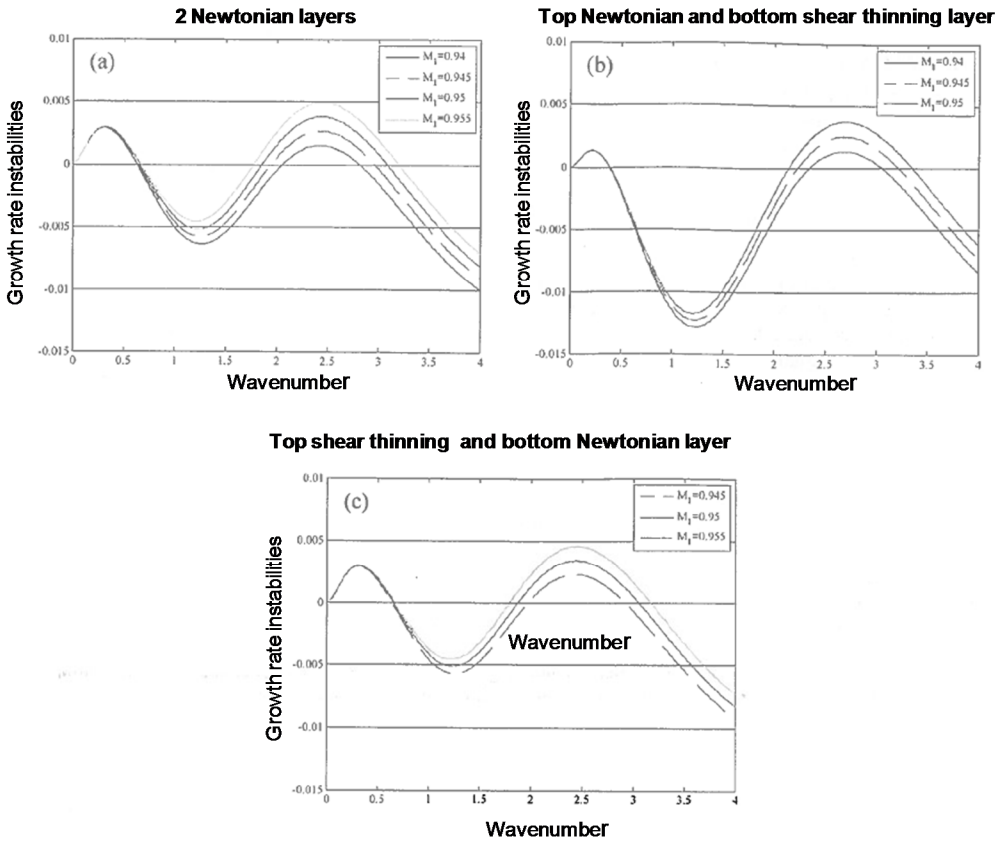

Figure 52: Growth rate as a function of wavenumber for different density ratios and several configurations where the power-law index is 0.2, the inclination angle is 0.2°, the Reynolds number is 1, and a viscosity ratio of 2.5, from [55].

4.3. Conclusion

This literature review enabled to better understand the influence of geometrical and rheological parameters on the flow on an inclined plane for one or several layers whether Newtonian or not. We found an extensive literature on the stability of Newtonian flow down an inclined plane for single and multi-layer systems but there is still a lack of knowledge on non-Newtonian stability, especially for multi-layer systems of only shear-thinning fluids.

In order to summarize the effect of all these parameters on the inclined plane of the curtain coating stability, Table 5 gathers all the results. Literature shows us that the influence of several parameters changes depending on long or short wavelength conditions or in interface or surface mode. So we below focus only on cases of interest to us, namely long wavelength and both interface and surface mode for Newtonian and non-Newtonian fluids since single or multi-layer curtain coatings are used.

Table 5: Summary of the influence of geometrical and physical parameters on flow stability on an inclined plane.

Fluid behaviour	Number of layers	Influence of an increase of					
		Surface tension parameter	Angle of inclination	Reynolds number	Density ratio	Viscosity ratio	Depth ratio
Newtonian	1	**+**	**--**	**--**			
	2	**+**	**--**	**--**	**-**	**-**	**-**
	3	**+**	**--**	**--**	**-**	**++**	**++**
Non-Newtonian	1	**+**	**--**	**--**			
	2 or 3	**+**	**--**	**--**	**=**	**++**	

++ High stabilisation + Low stabilisation = Negligible effect - Low destabilisation -- High destabilisation

Nomenclature:

A	Cross-sectional area of cavity
c	Complex wave velocity
c_r	Real wave velocity
c_i	Degree of damping
A	Thickness of the film
D_h	Hydraulic diameter of conduit
f	Shape factor
g	Gravitational acceleration
g_x	x-component of the gravitational force vector.
H	Slot gap
I	Improvement ratio
K	Consistency index of the fluid
L	Length of the slot
m	Viscosity ratio
n	Power-law index
N_g	Gravitational number
N_m	Momentum number
N_v	Viscous number
P	Hydrodynamic pressure
Pe	Wetted perimeter
Q	Average volumetric flow rate
q	Flow rate per unit die width in the slot
Re	Reynolds number
R_h	Hydraulic radius
S	Relative stability index of 2 layers / 1 layer of the same depth
u, υ, w	Cartesian components of the velocity vector
x, y, z	Cartesian coordinates
W	Width of die

Greek symbols

α	Wavenumber
β	Angle of inclination of the plane
γ	Density ratio
$\dot{\gamma}$	Shear rate

$\bar{\dot{\gamma}}$	Average wall shear rate
δ	Depth ratio
Δ	Uniformity index
ς	Surface tension parameter
λ	Wavelength
$\bar{\lambda}$	Dimensionless wavelength
μ	Viscosity
ρ	Density
σ	Surface tension
τ	Stress tensor
$\bar{\tau}$	Average wall shear stress
φ	Amplitude of the perturbation
χ	Inertia shape parameter
ω	Growth rate of instability

Subscripts

c	Cavity or critical
s	Slot

Materials and methods

1. Introduction

Our study aims at getting a better understanding of the flow of fluids that could be used for printing grades or barrier properties in curtain coating. It is based on computational simulation of the flow and experimental validation. In chapter 1, we made a literature review. In this chapter we will first present the types of fluids used, their composition and their rheological properties in relation with the coating process. The rheological study was limited to the shear rates encountered in the die and on the inclined plane. Then, we will present the experimental techniques used. We will describe the experimental device and the two methods of measurements for experimental validations, *i.e*. the use of tracers and 2D Particle Imaging Velocimetry (2D-PIV). Finally, we will briefly present the CFD software used.

2. Composition of the test fluids

In curtain coating, different types of fluids are used depending on the objectives. For example, to improve printability and surface aspect, pigment-based colours will be used and, to obtain barrier properties (grease, moisture, oxygen…), polymer-based colours such as PVOH or starch will be applied. These fluids have different rheological behaviours, which is important for the study of the flow.

Several test fluids have been used either Newtonian or not. In addition to the real fluids, model fluids were used in simulation.

A PVOH solution at different concentrations was used as a Newtonian liquid for the experimental and simulation studies. It is a well-known synthetic binder in paper-making and its distinctive characteristic is a wide range of viscosity adjustable with the concentration.

Three coating colours classically used in multilayer coating for Wood Free Coated paper (pre-coat, middle-coat and top-coat colours) were simulated. The pre-coat, middle coat and top-coat formulations and solid contents are gathered in Table 1 and the references with their suppliers are given in Annexe. They are shear-thinning and exhibit a yield stress.

Table 1: Colour compositions and solid contents for trials and simulations.

Reference	Pre-coating	Middle-coating	Top-coating
SB Latex 1	6 pph	8 pph	
Coarse GCC	100 pph	100 pph	
SB Latex 2			11 pph
Fine GCC			100 pph
PVOH			0.6 pph
Optical Brightening Agent			0.6 pph
Native Starch	10 pph	6 pph	
Surfactant (%/water)	0.6 %	-	0.8 %
Solids (%)	62 %	66 %	64 %

Concerning coating colours, there is a problem due to the opacity of such fluids with the experimental validation studies. It is indeed very difficult to clearly see streamlines inside the flow or measure velocity fields. Triantafillopoulos and Farrington Jr. used X-Ray radiography to visualize coating flows [56] but this is a heavy method to implement. In order to solve this problem, we used Carbopol solutions at different concentrations. It is a transparent Non-

Newtonian fluid that is classically used for studies on rheology. With this kind of fluid, we can easily study the influence of the yield stress. The Carbopol solution was used at a very low concentration because, over 0.2 % concentration, the dynamic viscosity is over 2000 mPa.s and we know that, in curtain coating, the maximum acceptable viscosity is about 800 mPa.s.

"Model" fluids were created for the CFD simulations, based on the rheological characterisation results. Three of them follow the power-law model and the others follow the Herschel-Bulkley model in order to analyse the influence of the power-law index and the yield shear stress. It should be noted that their properties were chosen in order to have the Newtonian case and cases close to those of coating colours without yield shear stress.

3. Rheological characterisation of the fluids

In order to study the flow in curtain coating, we must describe the rheological behaviour of the coating colours during the process, from the storage tank, to the pump, flowing to the curtain die, dwelling into cavities, flowing on the inclined plane, falling onto the paper and then settling at the surface of paper before drying. All these events have characteristic times and associated shear rates which are presented in Figure 1. Our study focused on the flow inside the coater and on the inclined plane. We therefore analysed the behaviour of the fluids in the shear rate range corresponding to these parts of the process. The shear rates into the slots and the cavities were approximated using the equations presented in Chapter 1:

$$\dot{\gamma}_s = \frac{6Q_0}{WH^2} \quad \text{and} \quad \dot{\gamma}_c = \frac{2Q_0}{R_h A}$$

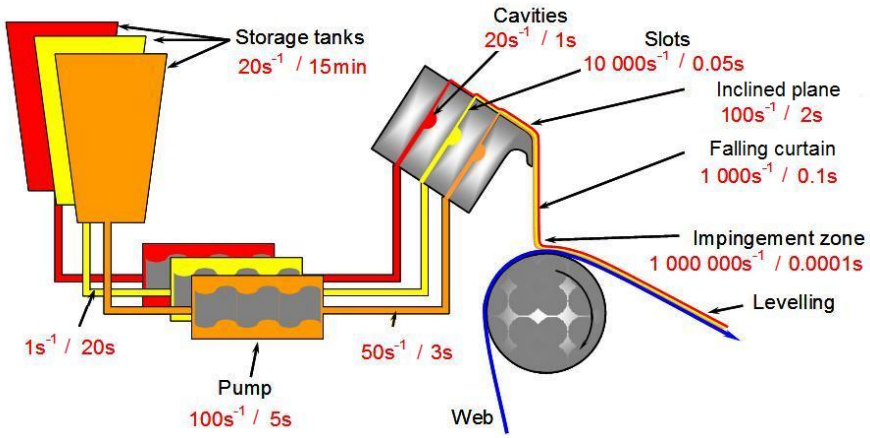

Figure 1 : Shear stress and residence time in curtain coating.

All "real fluids" were characterized in the laboratory at constant temperature with an AR-1000 cone-plate controlled stress rheometer from TA Instruments. The maximum shear rate tested with the AR 1000 was about 1 000s^{-1} which is close to the maximum shear rate available with this device. We know that the maximum shear rate in the slots is greater but there is less risk to have problems there than in the cavities where the shear rate is smaller.

A flow procedure was defined to study the coating colours and to describe the shear behaviour.

3.1. Test procedure used for characterising the rheological behaviour of the coating colours

A 60 mm in-diameter, 2° steel cone was selected for the measurements. A solvent trap cover (Figure 2) was used to prevent the colour from drying as some measurements took more than 15 minutes.

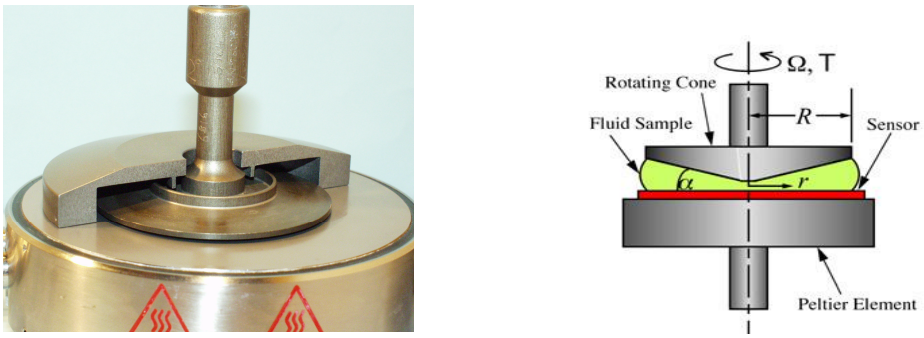

Figure 2: Features of the rheometer.

3.1.1. Procedure

We set up the following procedure in order to fully describe the rheological behaviour of coating colours under moderate shear stresses:

- The coating colours were prepared and let under a moderate stirring during all the tests.
- During the cone-plate measurements, the sample under the cone was maintained in a moist atmosphere to prevent the colours from drying on the edge.
- Measurements for five samples were performed for each coating colour.
- The flow procedure is made of:
    1. A conditioning step (20 °C, shear rate 100 s^{-1} for 20 seconds followed by an equilibrium step 20 °C for 30 seconds)
    2. A continuous shear ramp (20 °C, 1 s^{-1} to 1000 s^{-1} for 60 seconds).
    3. A continuous shear ramp (20 °C, 1000 s^{-1} down to 1 s^{-1} for 60 seconds).

Figure 3 is an example of result obtained with a Hydrocarb 90 top coating colour. The shear thinning behaviour of the colour associated with a thixotropy is shown on this graph. Since the studied coating colours are quasi no thixotropic, there is no use making several continuous shear ramps to obtain a stable behaviour profile.

3.1.2. Reproducibility

Tests were dedicated to the reproducibility analysis. Four samples of the same batch of pre-coating and top-coating colours were analysed according to the defined procedure. The shear responses of selected samples are given on Figure 4.

The results on Figure 4 show that the measurements are very reproducible. This comes from an accurate calibration of the rheometer and the geometry, the use of a graduated micro-syringe for the colour delivery and a dampening system to prevent the colour from drying.

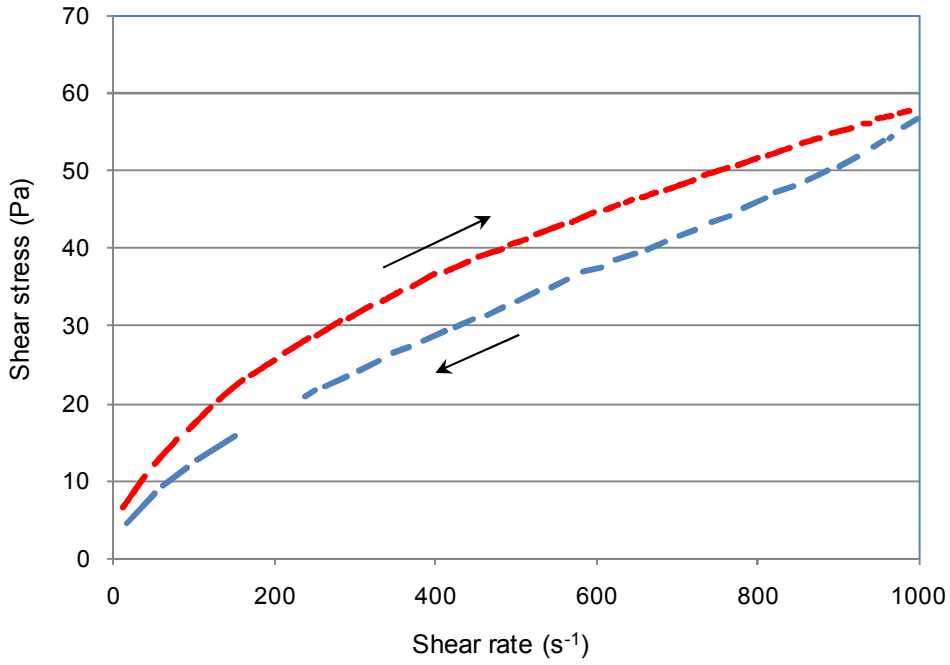

Figure 3 : Example of rheogram with a thixotropic fluid (coating colour)
Each segment is composed of 5 to 10 measurement points.

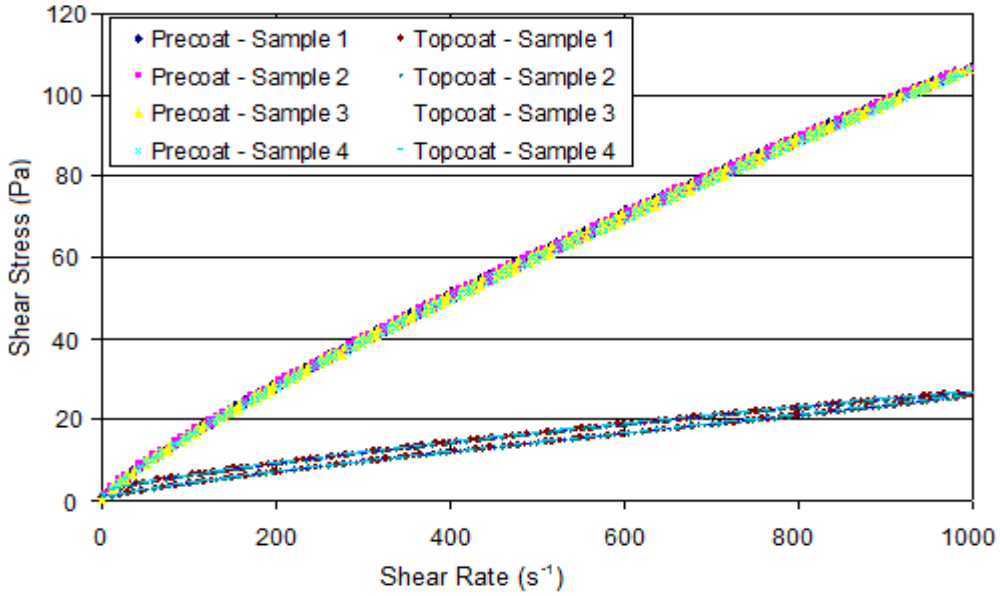

Figure 4: Shear response of five different samples of pre-coating and top-coating colours.

3.1.3. Analysis of time dependence

Coating colours are slightly thixotropic fluids. In order to validate the results obtained with a continuous shear ramp, we performed several trials for a given shear rate (low and high shear rate) and observed the evolution of the shear stress as a function of time as shown on Figure 5. We compared the stress average value in steady state and the stress value with the continuous ramp at the same shear rates (5 and 155 s^{-1}) and it was found that the difference was less than 0.2 %. Thus, we will take the values of the rheological parameters obtained with the continuous shear ramp studies for the simulations.

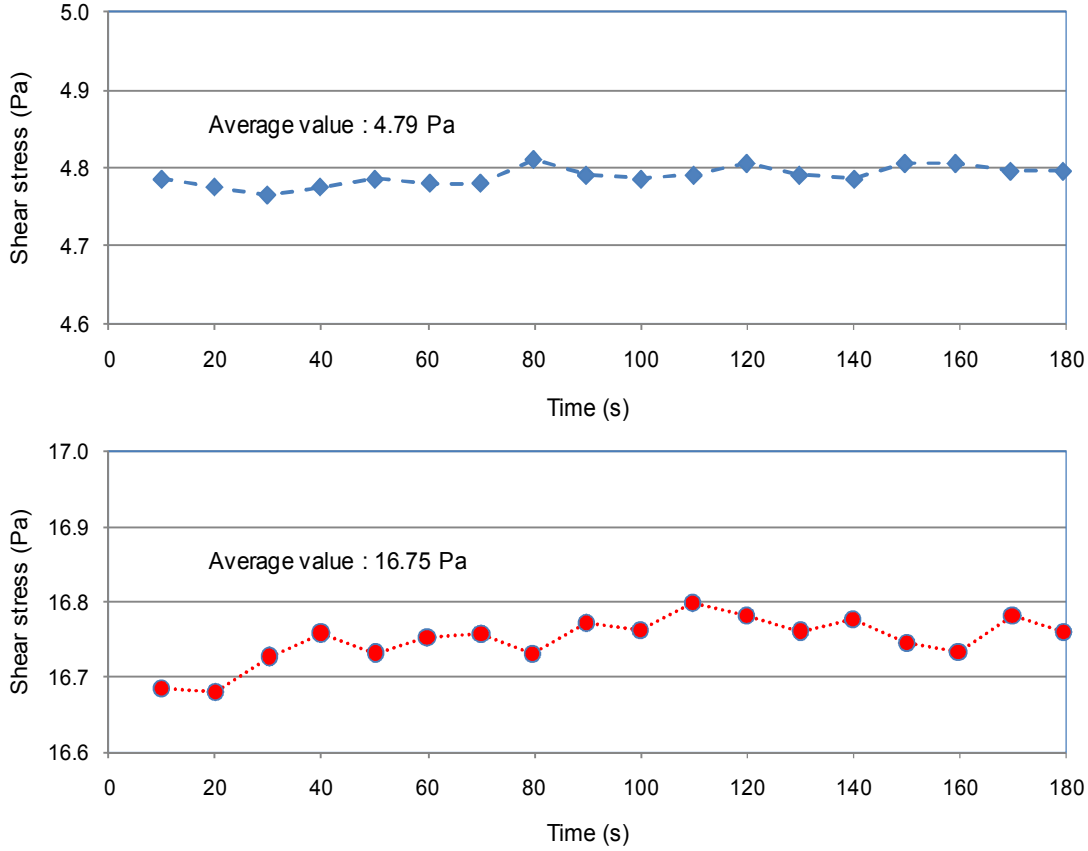

Figure 5 : Evolution of the shear stress with time for a given shear rate ($\dot{\gamma} = 5\,s^{-1}$ and $\dot{\gamma} = 155\,s^{-1}$ respectively).

3.2. Rheological characterisation results and application to the definition of the “Model” fluids

The flow behaviour of the real fluids was analysed using conventional rheology tools and models used in shear rheology (shear thinning or shear thickening behaviour, thixotropy…) [58, 59].

Results are presented on Figures 6 and 7 where the dots represent the experimental points and the lines represent the best fitting models.

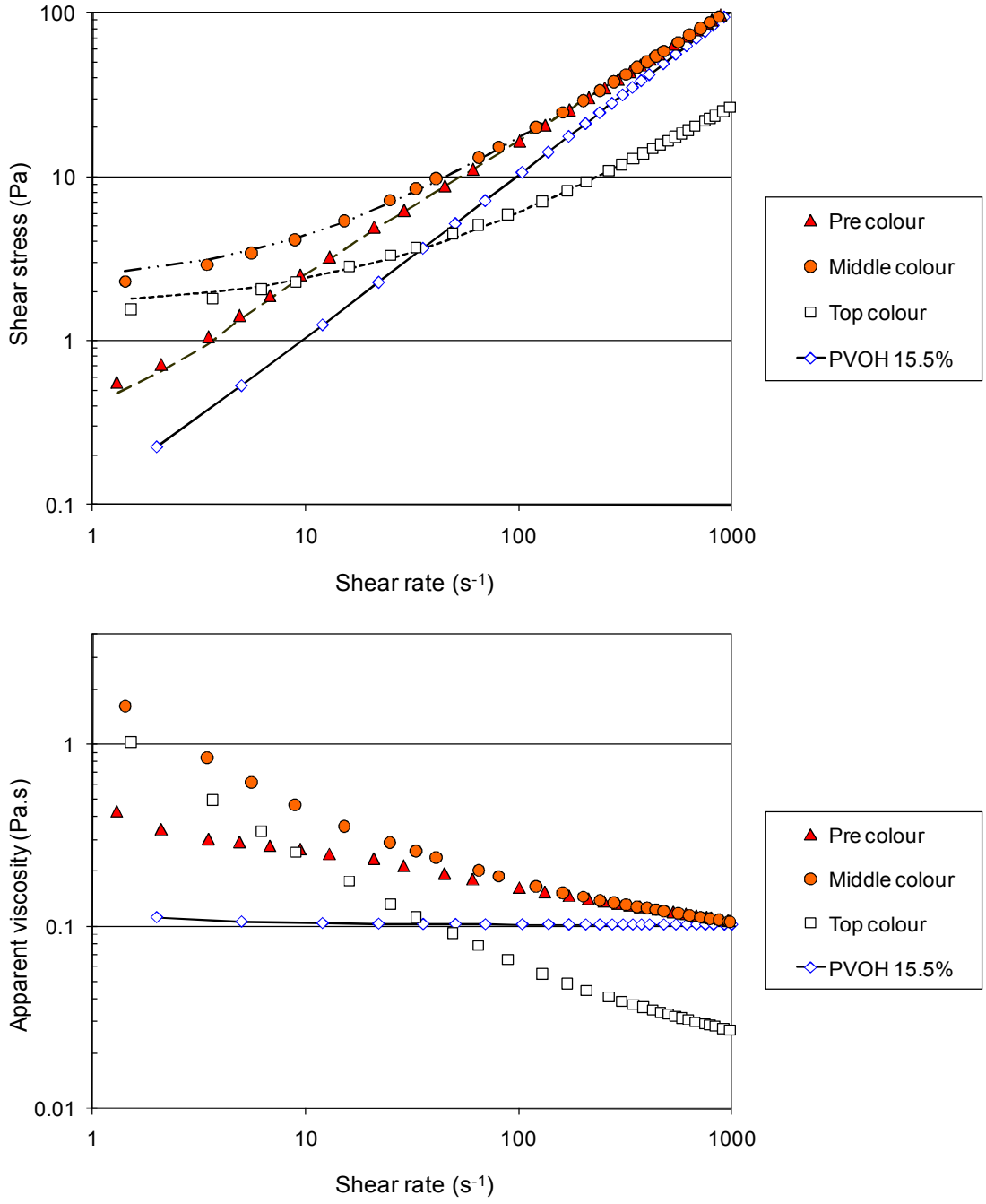

Figure 6: Rheological behaviour of the coating colours and a PVOH solution with the cone-plate controlled stress rheometer.

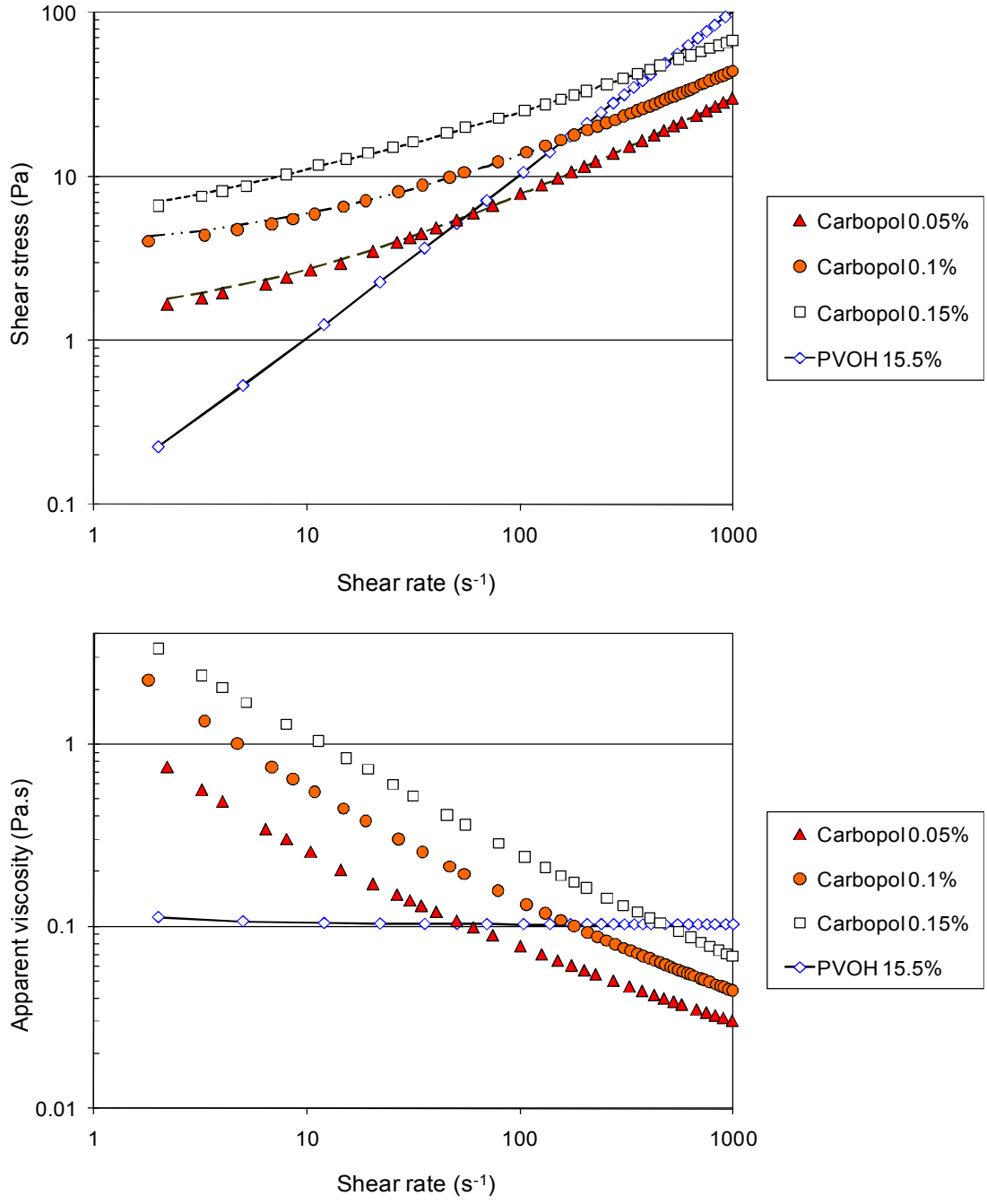

Figure 7: Rheological behaviour of the Carbopol solutions and a PVOH solution with the cone-plate controlled stress rheometer.

Concerning the rheological properties, it should be noticed that the Pre-coating and Middle-coating colours are quite identical because they almost have the same composition. The only difference is a slightly higher yield shear stress for the middle-coating colour. Moreover, Carbopol solutions at 0.05 % and 0.1 % have a rheological behaviour close to the one of the coating colours. Thus, it will be possible to validate the flow behaviour of coating colours in the manifold with these Carbopol solutions.

Taking into account the approximate assessment of the shear rates in the cavities and slots in the coater in relation with the behaviour found with the rheometer, it is possible to have some first results based on the analysis of Figure 8:

- In the slots, the pre and middle colours will have a similar flow behaviour.
- In the cavities, the flow behaviour of the three coating colours will be different.

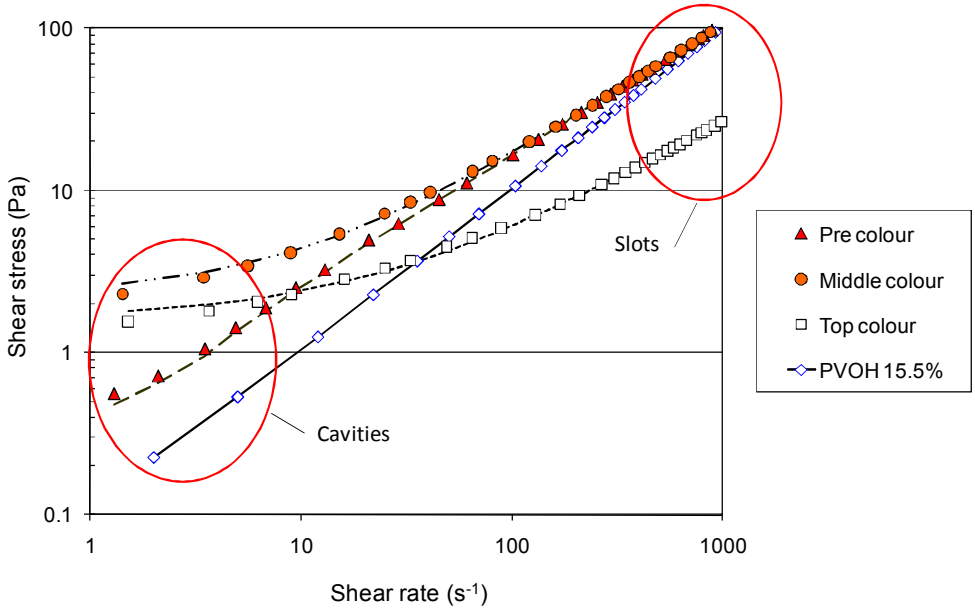

Figure 8 : Behaviour of the coating colours in the cavities and the slots.

Considering the shear rate range explored and the behaviour of the fluids:

- PVOH solutions were modelled as Newtonian fluids.
- The coating colours were modelled as Herschel-Bulkley fluids.

The rheological parameters of the models obtained by best fitting the experimental curves are gathered in Table 2. This table presents the properties of the model fluids.

Table 2: Physical properties of the real fluids used in the tests.

Fluids	Rheological parameters		
	Yield stress (Pa)	Consistency index / Viscosity ($Pa.s^n$)	Exponent
Pre–coating colour	0.27	0.38	0.82
Middle-coating colour	2.22	0.32	0.84
Top-coating colour	1.6	0.14	0.75
Carbopol 0.05%	1.25	0.33	0.65
Carbopol 0.1%	3.22	0.63	0.61
Carbopol 0.15%	4.78	1.97	0.50
PVOH (15-20%)	0	0.1 – 0.8	1
“Model” Herschel-Bulkley	0. 1 –-1.5	0. 1 –0.6	0.7 – 0.9
“Model” Power-law	0	0.1	0.7 – 0.9

It should be noted that the power-law model for a shear-thinning fluid and the Herschel-Bulkley model may cause problems in some cases with computational fluid flow simulation since the apparent viscosity is not defined when the shear rate tends towards zero. For instance, instead of the power-law model, the Carreau model is more appropriate for simulating the flow on the inclined plane. Indeed the viscosity remains finite as the shear rate approaches zero, which is no longer the case for the power-law model. The fluid has nearly Newtonian behaviour both at low and high shear rate whereas, in between, the behaviour is close to that of a power-law fluid. The model identification we made is sufficient for the simulations we performed in the present study, but the rheological study should be completed in the future. The same problem occurs for the simulation of flow in the slots and cavities with the CFD software used for fluids with a yield stress, but it can be overcome in a simple manner. The model is modified in order to have a Newtonian behaviour at very low shear rates until the value of the yield shear stress is reached and remains unchanged beyond this value.

4. Laboratory curtain coater

In this PhD work, we studied the flow in a laboratory curtain coater designed by TSE and delivered by Polytype. Its particularity concerns the inlet manifold where the radius of the cavity increases along the section but the length of the slot is constant (Figure 9) which is unusual. In order to manufacture a transparent coater and model the flow in the curtain coater, the geometry of the coating chamber must be known. The dimensions of the coater were determined with a Laser Triangulation Sensor developed in the CTP which has a very high accuracy. We used the coordinates of the points to compute the mathematical equations of some particular lines (edges) in order to design the transparent coater and create the geometry of the coater in the CFD software.

4.1. Main features of the pilot coater

The laboratory coater used has a variable semi-circular cross-section for its first cavity and a triangular shape with round ends for the second one. The inlet pipe is tangent to the manifold cross-section.

The geometric parameters of the laboratory coater are gathered in Table 3.

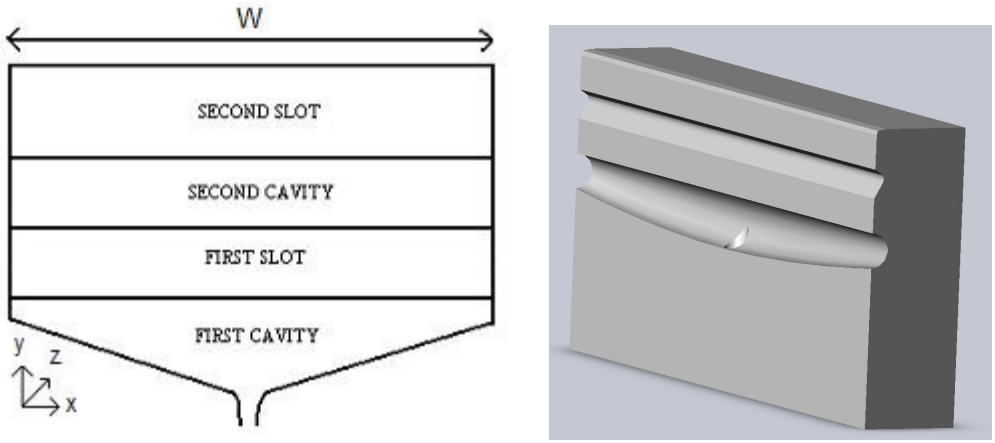

Figure 9: Design of the internal cavities of the pilot coater.

Table 3: Geometric parameters of the laboratory curtain coater.

Parameters	Dimensions	Parameters	Dimensions
Manifold width (L)	260 mm	First slot thickness	254 µm
Manifold diameter (side)	14 mm	Second slot thickness	500 µm
Manifold diameter (centre)	22 mm	Inclined plane tilt angle	30 °
Inlet pipe diameter	9.4 mm		

4.2. Description of the transparent coating experimental assembly

Since the pilot curtain coater is made of steel, it is not possible to observe the flow inside it. A transparent replica made of Plexiglas was therefore designed and manufactured in order to visualize the flow inside the manifold and validate CFD results (Figure 10). It is an exact replica of the pilot curtain coater.

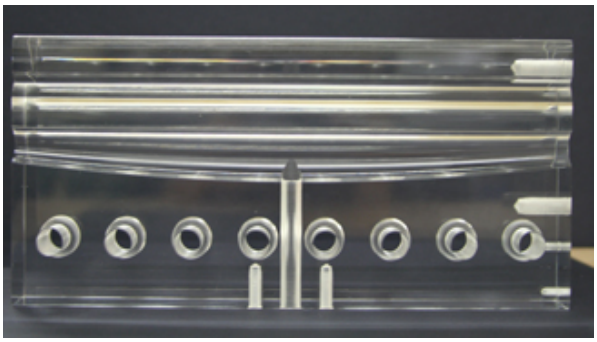

Figure 10: Transparent CTP laboratory curtain coater.

The curtain coater was fixed on two Plexiglas stands that were designed in order to have the same inclination angle as on the pilot. The system was fed with a pigtail pump and we ran all tests in a closed loop. A video camera was installed behind the coater in order to enable us to visualize the phenomena taking place in the manifold as shown on Figure 11.

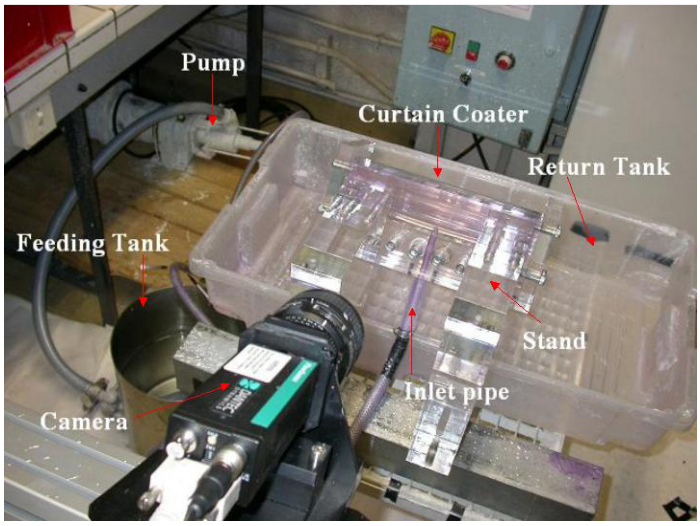

Figure 11: Coating experimental assembly.

5. Analysis of the flow in the coater

5.1. Flow visualisation with tracers

Tracers were used for the flow visualization. In the literature, a small amount of highly reflective aluminium particles is commonly added as a tracer. We preferred to inject dye solutions that have the same density as the cavity fluid. To do that we punctured the plastic pipe between the pump and the curtain coater with two syringes and maintained the two needles close to the inner wall in order to have the streamlines close to the wall at the junction between the inlet pipe and the manifold. Since the flow is laminar and injection is made with isokinetic condition, there is no mixing between dyes and the fluid studied. It will therefore be possible to follow streamlines.

The experimental assembly used with this method is presented on Figure 11. An example of the streamlines is shown on Figure 12. With this method, we cannot calculate the velocity field but it is not the point here. We check the presence or absence of vortex and its size in the considered area.

As already mentioned, we used Carbopol solutions at different concentrations instead of the coating colours in order to study the influence of the yield shear stress for the Non-Newtonian fluids.

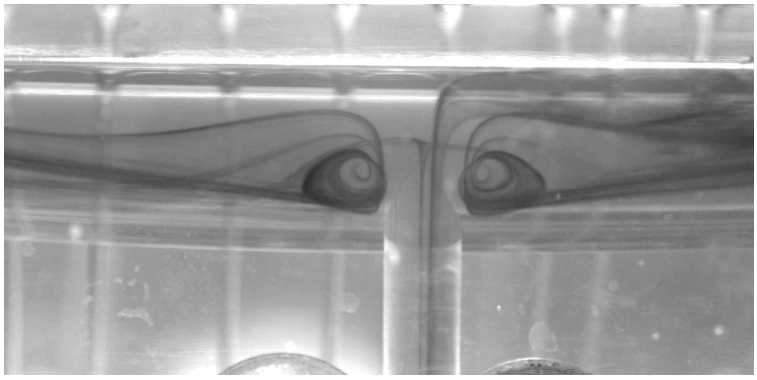

Figure 12 : An example of flow visualization with the tracer method.

5.2. Flow analysis with 2D PIV

Many areas of technical research and development require a measuring technique that can measure the flow velocity across a large domain of the flow field. This can be achieved by scanning the domain with a point velocity probe (such as a Pitot tube, which is an intrusive probe), but the procedure can be very time-consuming. Besides the qualitative flow visualization methods (direct injection), an optical non-intrusive quantitative technique has developed for the past 30 years. This method is called Particle Image Velocimetry (PIV). PIV is an optical technique to measure instantaneous 2D velocity fields. The 2D PIV data can also be used to compose a 3D volume. The main advantage of PIV compared to the traditional flow measurement techniques, is its capability to measure the entire 3D flow field at once with either two or three velocity components, providing the instantaneous velocity vectors. In our study, only 2D PIV will be used.

A PIV system typically consists of a laser with sheet optics, one or two digital cameras, and a computer with a timer unit to control the system and store the data. Velocity fields are

measured in a planar 2D domain. The measurement plane is cut in the flow by a laser sheet and the measurement area in this plane is cropped by the field of view of the camera(s). A schematic view of the apparatus and its typical layout is shown in Figure 13. The measurement frequency, *i.e.* the rate at which instantaneous velocity fields can be measured, depends on the hardware. Typically the measurement frequency is in the order of 10 Hz. With hardware able to do time-resolved PIV (TRPIV), several thousand velocity fields per second can be obtained.

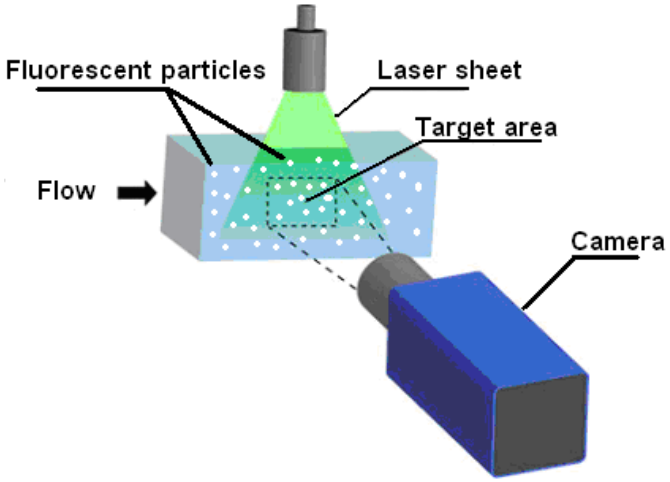

Figure 13 : Layout of the PIV equipment.

The 2D-PIV device used is a Dantec system. This device was lending by the LEMTA. It consists of:

- a Yag laser of 120 mJ pulsed at 10 ns,
- One 1024x1024 pixels CCD camera.

The PIV measurement principle is the following. Some fluorescent particles are added to the tested coating colour. The laser, put above the curtain coater, creates a straight line light. The camera, put in front of the curtain, receives only the light of the fluorescent particles of a plane thanks to a laser light filter (Figure 13 and Figure 14).

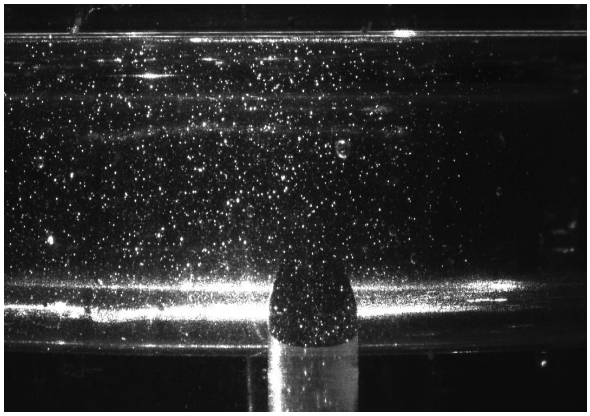

Figure 14: Fluorescent particles in the manifold with PVOH.

Two-dimensional displacement (ΔX, ΔY) is estimated. A 2D evaluation requires a numerical model, describing how objects in space are mapped onto the CCD-chip of the camera.

Parameters for the numerical model are determined through the camera calibration. It was done by recording images of a calibration target (Figure 15) that contains calibration markers in known positions. Thus, comparing known marker positions with corresponding marker positions on each camera image, model parameters are adjusted to give the best possible fit.

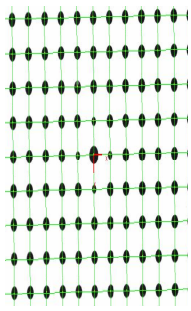

Figure 15: A calibration grid for 2D-PIV.

PIV is based on determining the movement of a group of particles seeded into the flow. The area of interest is illuminated by two consecutive short-duration light pulses produced by a laser. The duration of the light pulses and the time interval between the pulses are typically 10 nanoseconds and 10 to 100 microseconds, respectively. The light scattered from the seeding particles is acquired by a digital camera (a double-frame image) when the laser pulses and stored for subsequent analysis. The velocity of the particles can be estimated by finding the displacement of the particles between the laser pulses. Since the time separation between the pulses is known and the camera is calibrated to yield the displacement in the object plane, the flow velocity can be resolved. In practice, the image is divided into small sub-regions called interrogation areas and the local displacement of the particles is determined within each interrogation area. In this way, from one double-frame image, several thousand velocity vectors are computed, which are arranged to a rectangular grid. Figure 16 displays an example of a double-frame image exposed in the wake of a splitter plate.

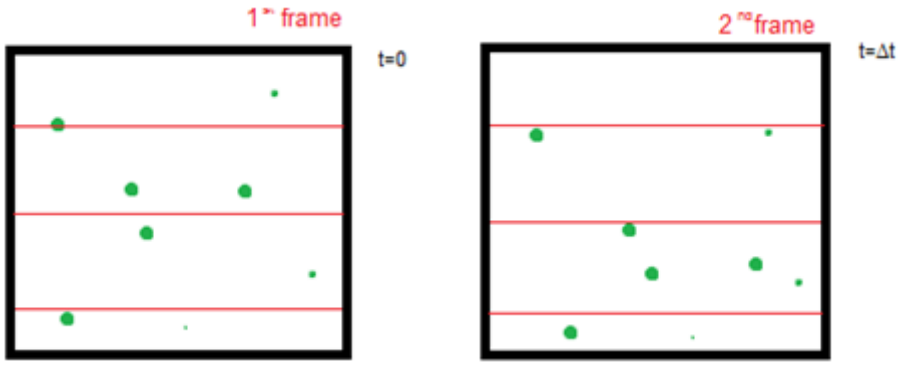

Figure 16: A double-frame image for PIV computation.

The basic principles of the method are summarized on Figure 17. An example of velocity field is presented in Figure 18 where two vortices can be observed in the centre zone, highlighted in the two red circles.

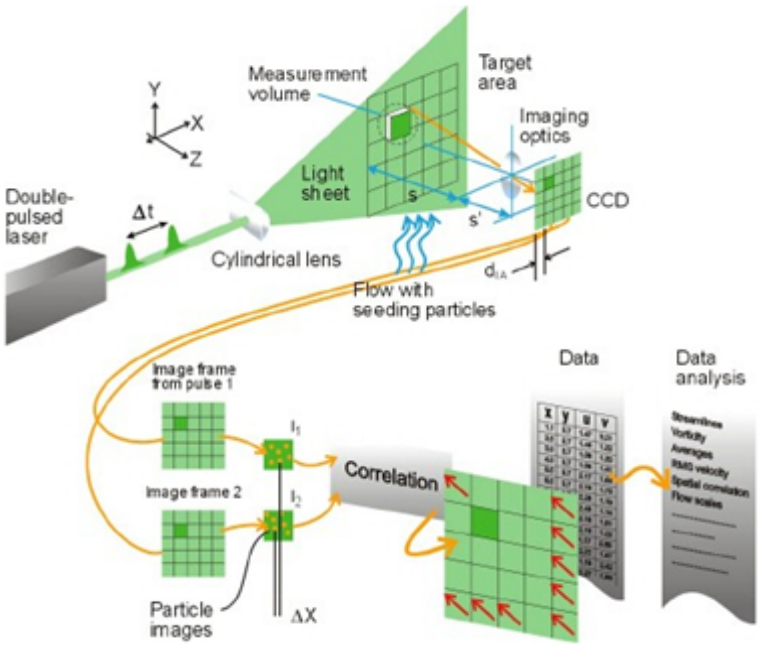

Figure 17: Summary of the 2D PIV method, from [60].

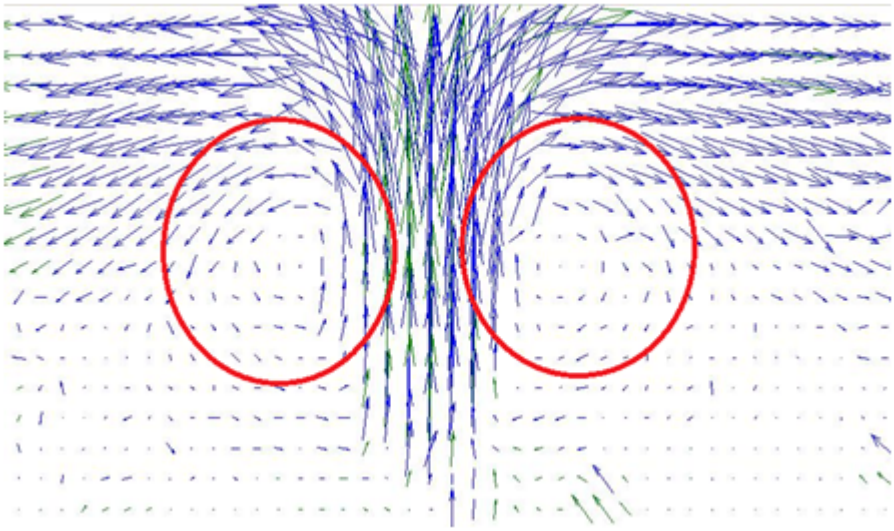

Figure 18: An example of the velocity field in the manifold with the 2D-PIV method.

5.3. CFD simulation

The partial differential equations that govern fluid flow and heat transfer are not usually amenable to analytical solutions, except for very simple cases. Therefore, in order to analyse fluid flows, flow domains are split into smaller subdomains (made up of geometric primitives like hexahedra and tetrahedra in 3D and quadrilaterals and triangles in 2D). The governing equations are then discretized and solved inside each of these subdomains. Typically, one of three methods is used to solve the approximate version of the system of equations: finite volumes, finite elements, or finite differences. Care must be taken to ensure proper continuity of solution across the common interfaces between two subdomains, so that the approximate solutions inside various portions can be put together to give a complete picture of fluid flow in

the entire domain. The subdomains are often called elements or cells, and the collection of all elements or cells is called a mesh or grid.

The fundamental method for creating a CFD model can be represented as a “pipeline” of six steps as illustrated in Figure 19 below. The process begins with the creation of an assembly of one or more parts (geometric shapes) that reflect the design under consideration. Because CFD deals with the flow through or around solid objects, the CFD model is built upon the inverse of the assembly and is referred to as the “Flow Volume Extract". This Flow Volume Extract is meshed with Gambit® and finally a simulation is performed with boundary conditions with Fluent® and the results of the simulation are analysed.

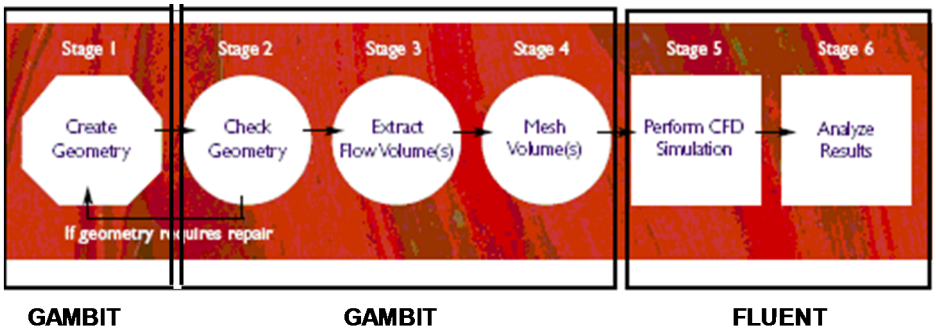

Figure 19: Fundamental method for creating a CFD model.

In order to simulate the flow in the manifold, we used the coordinates of specific points obtained with the laser triangulation sensor in order to create vertices, edges, faces and volumes to represent the geometry of the coater with Gambit. The same software was used to create the geometry of the external flow on the inclined plane.

Simulation software are based on two principle numerical methods – Finite Element Method (FEM) and Finite Volume Method (FVM). Both methods involve subdividing the flow domain into a large number of finite elements / control volumes and then solving the governing equations of fluid flow i.e. the 3-D Navier-Stokes equations. In the process a system of algebraic equations is formed and subsequently solved by an iterative method. The numerical methods differ in their derivation and definition of these algebraic equations. FVM provide discrete solutions, while FEM provides a continuous (up to a point) solution.

FEM use simple piecewise functions (e.g. linear or quadratic) to describe the local variations of unknown flow variables. The Navier-Stokes equations are precisely satisfied by the exact solution. If the piecewise approximating functions are substituted into the equation it will not hold exactly and a residual is defined to measure the errors. The residuals are next minimized in some sense by multiplying them by a set of weighing functions and integrating. As a result a set of algebraic equations for the unknown coefficients of the approximating functions is obtained.

For FVM, a formal integration of Navier-Stokes equations over all the control volumes of the solution domain is carried out. A variety of finite-difference-type approximations for the terms in the integrated equation representing flow processes such as convection, diffusion and sources are then applied. This converts the integral equations into a system of algebraic equations.

In our case, Fluent used the FVM which leads to less accurate solutions than FEM with lower order approximation within each cell but the accuracy is sufficient with an appropriate meshing. With this software, it is possible to simulate internal and external flows in 2 or 3 dimensions.

Experimental and simulation study of the flow in a pilot curtain coater

1. Introduction

This PhD study aims at getting a better understanding of the flow in curtain coating. It is commonly admitted that, in practical terms, know-how outperforms physical knowledge for the time being. We restricted the study to the flow inside the coater, *i.e.* in the manifold, second cavity and slots, and on the inclined plane. In Chapter 1, we presented a literature review on these topics and, in Chapter 2, we presented the properties of the different test fluids, with an accent on the characterisation of the coating colours, the coater and the various tools we would use in order to analyse the flow behaviour. The present chapter is focused on the analysis of the flow. It is divided into two parts that are independent of each other, firstly, the internal flow and, secondly, the external flow on the inclined plane. Conclusions will be drawn at the end of each part.

2. Study of the internal flow in a curtain coater

The purpose of the internal cavities of coating dies of all types is to distribute the coating liquid in a manner which, in conjunction with the rest of the coating process, produces a liquid film with uniform dimensions and properties. In the literature, the flow analysis of die manifolds mainly uses a combination of a one-dimensional flow model of viscous effects in the cavity and the slot to determine flow uniformity (Weinstein and Rushak, 1996, Winter and Fritz, 1986) [17, 18]. In addition, a number of papers specifically address the problem of using one-dimensional cavity flow models for the often encountered noncircular shapes (Miller, 1972, Liu and Hong, 1988) [19, 20]. Other authors, for instance Lee and Liu (1989, 1990) [24, 28] modelled the second cavity in two dimensions in order to find conditions of vortex formation for several fluids and geometrical conditions. Indeed, they used simpler shapes of manifold because of industrial interests or computation possibilities.

The internal flow in curtain coating is a three-dimensional problem, but little information about 3D simulations in the manifold is available in the literature. Some authors studied the flow uniformity on three dimensional simulations for extrusion dies but they neglected the inertial force since molten polymers have a high viscosity [31, 32]. Wen and Liu took into account the inertia force when they analyzed molten polymer flow in an extrusion die and after, they made a comparison with experimental observations [32, 33].

In the pilot curtain coater supplied by Polytype, the internal flow consists of the flow through the inlet pipe and then the two series of cavities followed by a slot (Figure 1).

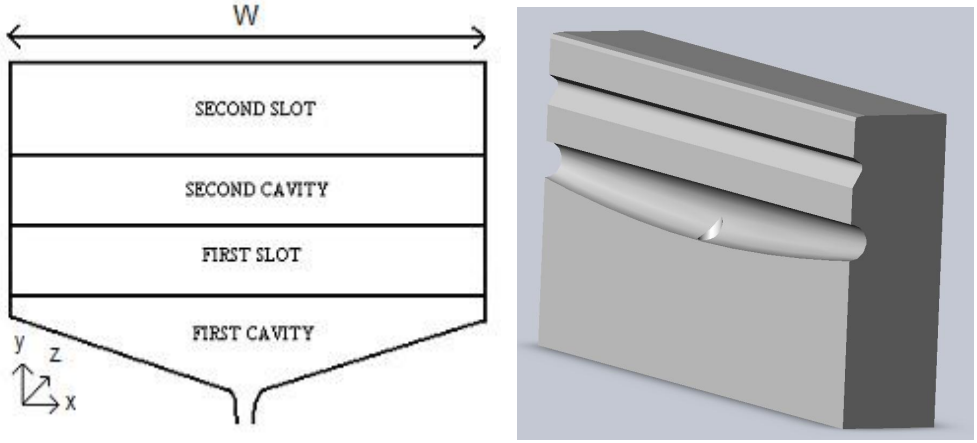

Figure 1: Design of the curtain coater.

In our pilot, we encountered some streaks on the final curtain coated paper and these defects are due to a non-uniform flow during the coating process (Figure 2). With our pilot made of steel, it is not possible to visualize the flow or measure some parameters inside the internal cavities. We can only observe some difference of opacity in the centre zone of the curtain (Figure 3). Thus CFD simulation was the best solution to determine the process limitations and try to find the origin of flow non-uniformity. Then, it will be possible to validate these results manufacturing a transparent replica of the curtain coater.

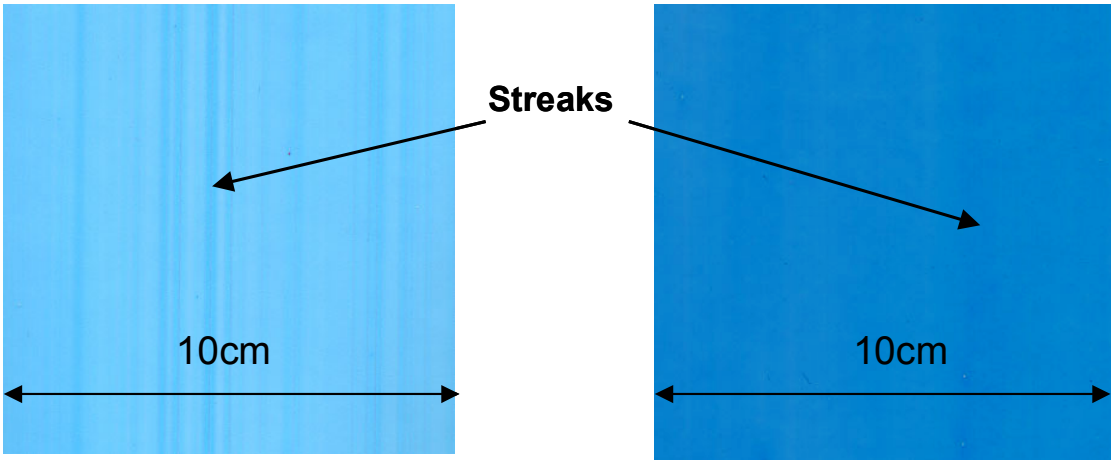

Figure 2 : Apparent defects on curtain coated paper.

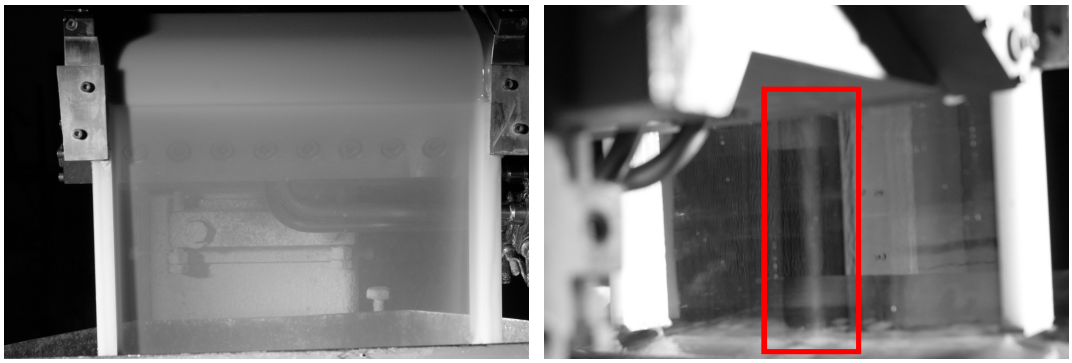

Figure 3: Pictures of the curtain with Xanthan at q=9.6L/m·min.

Preliminary tests, that will not be discussed here, showed us that the CFD study of the internal flow could be divided into two parts, simulation of the flow in the manifold and simulation of the flow in the second cavity. This is possible if we suppose that there is no defect in the die geometry. Simulation of the whole system would have required more computing resources and would have been much more time consuming. Therefore,

- Considering the geometry of the manifold, we performed 3D simulations of the flow in the inlet pipe and the first cavity of the pilot curtain coater, since the flow is transverse, in order to analyze the phenomena taking place in the manifold, find parameters that spark off eventual defects and then propose potential solutions. In addition, an experimental study has been performed to validate results using flow visualization technique with tracers and 2D-PIV in a transparent replica of the coater.

- Taking into account literature results (Lee *et al.* [28]), we performed 2D simulations of the flow in the second cavity in order to determine the conditions of vortex formation. Indeed a 3D simulation would not supply further information and the computing time would be increased.

In order to find which forces are predominant in the studied cases, we started this study with a dimensional analysis of the flow in the CTP pilot curtain coater.

2.1. Dimensional analysis of internal flow in the CTP pilot curtain coater

In order to better understand the role of viscous, inertial and gravitational forces in the CTP pilot curtain coater, a dimensional analysis is used, as described in Chapter 1. It enables us to have a better idea of the predominant forces in the coater. Three dimensionless numbers, namely the Viscous Number, N_v, for the viscous forces, the Momentum Number, N_m, which reflects the inertial forces and the Gravity Number, N_g, for the gravitational forces, were assessed.

The cavity shear rate and slot shear rate were assessed from equations 20 and 22 in Chapter 1. Then, the pressure drop due to the flow through the slot of the manifold was calculated from equations 19 and 20 for the first slot (between the manifold and the second cavity) and for the maximum and average flow rates used in the CTP pilot. All necessary data are gathered in Table 1 and results are presented in Table 2.

Table 1: Features of the curtain coater.

Parameters	Dimensions	Parameters	Dimensions
Manifold width (L)	260 mm	Inlet pipe diameter	9.4 mm
Manifold diameter (side)	14 mm	First slot length	1.32 cm
Manifold diameter (centre)	22 mm	First slot thickness	254 µm
Manifold mean hydraulic radius	2.95 mm	Second slot thickness	500 µm

Table 2: Example of shear rates in the first cavity and slot and pressure drops in the first slot from Eqs.19 and 20 for a Newtonian fluid with viscosity equal to 400 mPa.s.

		First cavity	Slot		
	Flow rate (L/min)	Shear rate (s^{-1})	Velocity (m/s)	Shear rate (s^{-1})	Pressure drop (Pa)
Maximum	3	9.6	0.76	18 000	$7.5 \cdot 10^5$
Average	1	3.2	0.25	6 000	$2.5 \cdot 10^5$

The dimensionless numbers, calculated for the CTP pilot case, and their ratios are given in Table 3. It should be noted that, as long as the rheological behaviour in the slot and the cavity is the same, the Viscous Number and so the relative flow resistance in the cavity and the slot is independent of the flow rate in the die. It depends only on its geometry. This is no longer the case if inertial forces are significant, which is measured by the Momentum Number. The Gravity number is equal to 0 because the curtain coater is horizontal in the x-

direction. The gravitational forces do not influence the flow in the die. In order to see if gravitational and inertial forces must be considered compared to viscous forces, ratios of these dimensionless numbers were calculated.

Table 3: Examples of dimensionless numbers for the flow in the first cavity for a Newtonian liquid with density equal to 1000 kg/m^3 and viscosity equal to 400 mPa.s, and a flow rate equal to 1 L/min.

N_v	N_m	N_g	N_m / N_v	N_g / N_v
$1.1 \cdot 10^{-2}$	$5.0 \cdot 10^{-5}$	0	$5.0 \cdot 10^{-3}$	0

- Influence of inertial forces

  The ratio of the momentum to viscous numbers reflects the relative importance of inertial and viscous forces in the cavity. The ratio is very low so inertial forces do not have a big impact on the flow in the manifold compared to viscous forces.

- Influence of gravitational forces

  The ratio of the gravity to viscous numbers reflects the role of gravitational forces in the cavity and it is closely associated to the Stokes Number which is the ratio of the solid particle inertia divided by the viscous forces.

  In the CTP pilot case, this ratio is equal to zero since the Gravity Number is equal to zero. The gravitational forces will not have any impact on the flow in the manifold compared to viscous forces.

2.2. CFD study of the flow in the manifold and experimental validation

2.2.1. Meshing of inlet and manifold in three dimensions

The manifold after the inlet pipe features a decreasing cavity size with cross-web distance from the feed location. We considered the inlet pipe, the manifold and also a piece of slot downstream in order to be able to evaluate velocity profiles. This system was meshed with Gambit® using T-grid mesh owing to the geometry of the die. T-grid is an unstructured grid consisting of triangular and tetrahedral cells. The internal volume was decomposed into several sub-volumes that were meshed successively.

Special attention was paid to meshing in order to minimise the computing time and enhance the precision. On the one hand, the meshing has to be refined to increase the precision of the results but, on the other hand, there is a threshold which is the capacity of the computer memory. That is why we have decided that only half of the internal flow would be simulated so the computing time and the memory used for the computation will be cut by half. To do that, we have checked by simulation that the flow is symmetrically distributed into the first cavity. Indeed, there is an elbow upstream of the inlet pipe, which might affect the flow at the inlet of the cavity.

The internal volume was meshed with about 1.2 million of elements (Figure 4). The average size of an element is $1.54 \cdot 10^{-2}$ mm^3, the maximum one is $6.19 \cdot 10^{-2}$ mm^3.

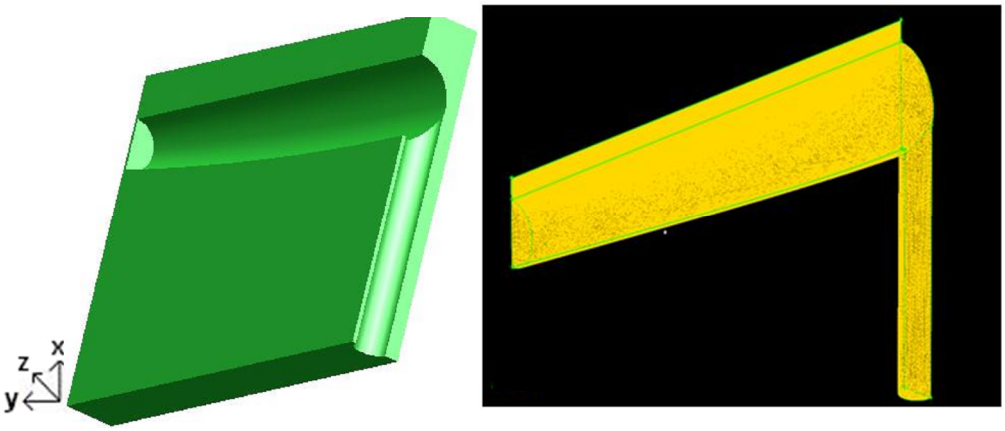

Figure 4: view (left) and meshing (right) of half 3-D manifold.

The quality of the resulting mesh was checked because it could greatly affect the accuracy of the CFD solution. We checked the skewness and it was noticed that there are a few "bad elements", but they only represent approx. 0.5% of the total number. Moreover, they are not aggregated in one location.

2.2.2. Fluent model solver with the boundaries conditions used for the manifold study

Several assumptions were made to solve it with the computational fluid dynamic software Fluent®. We considered a steady state, with isothermal and incompressible fluid. Considering the velocities and the viscosities of the fluids, the flow regime is laminar (Reynolds number much lower than $2 \cdot 10^3$) in the laboratory coater. The mathematical equations that describe the internal flow are based on Navier-Stokes equations and the continuity equation as found in the literature applied to our case.

It should be noted that in many articles, authors only used the x-component because the axial variation is usually dominant for flow in cavity, but it is not the case here.

We defined all the walls with the no slip-condition and specified the velocity at inlet and the pressure at the outlet of the piece of slot. It avoided altering the flow in the cavity by specifying a pressure value in a plane at the outlet of the cavity itself. Therefore the outlet pressure in the end of the slot was at the atmospheric pressure. Of course, in real conditions the pressure is higher because of the pressure drop in the second slot, but there will only be a shift in the pressures. Since we are working with incompressible fluids, it will not affect the results. Concerning the symmetry condition, which enabled us to reduce computing time, the conditions were a normal velocity and the gradient of all variables equal to zero on the symmetry plane.

We checked the convergence of the solution since it has a huge impact on the accuracy of the results. The solution may be converged when all discretized transport equations are obeyed to a specified tolerance defined by Fluent residuals or when the solution no longer changes with more iterations. Residuals permit to show which equations could have convergence problems and measure the imbalance on conservation equations. On Figure 5, it can be noticed that beyond 1000 iterations, the residuals of all the curves remain constant. It should be noticed that 5000 iterations require 20 hour computing time, that is why we allowed about 1000 iterations for all the following tests, which takes about 3 hours computing time with a Pentium 4 Workstation (Processor running at 3.0 GHz / 3 GB Memory).

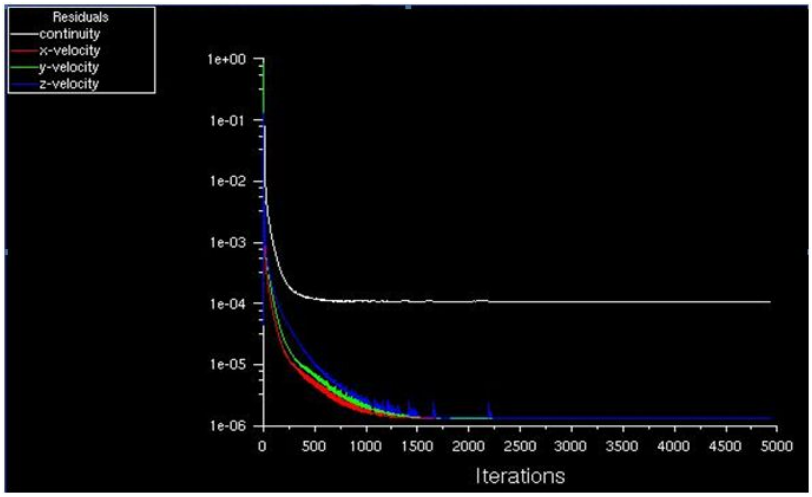

Figure 5: Convergence of velocities and continuity equations.

2.2.3. Simulation results and experimental validations

Our aim was to analyse the effect of rheological properties of fluids and geometrical parameters of the curtain coater. We ran simulations for Newtonian and non-Newtonian fluids and then experimentally validated some results.

In addition to the real fluids, model fluids following the power-law model were used in simulation:

- A PVOH solution at different concentrations was used as Newtonian liquid for experimental and simulation parts. It is a well-known synthetic binder in paper making and its particularity is a wide range of viscosity adjustable with the concentration.
- Three coating colours classically used in multilayer coating for Wood Free Coated paper (pre-coat, middle-coat and top-coat colours) were simulated. Their rheological behaviour was presented in the second chapter. They are shear-thinning and exhibit a yield stress.
- Three fluids following the power-law model, in order to analyse the influence of the power-law index. The value of the power-law index was kept in the range between 1 and 0.7 in order to have the Newtonian case and cases close to those of coating colours without yield shear stress.

Carbopol solutions were also used in experiments.

The properties of these fluids were presented in the previous Chapter and are reminded in *Table 4*.

Several flow rates ranging between 0.5 and 3 L/min (1.9 and 11.6 L/min·m) were tested. This range corresponds to coating weights between 5 and 25 g/m² at our pilot operating speed. Values for viscosities and flow rates are close to the values used with the curtain coater pilot. Some extreme values were added in order to analyse the behaviour of the flow in all these cases.

Table 4: Physical properties of the real fluids used in the tests.

Fluids	Density (kg/m^3)	Rheological parameters		
		Yield stress (Pa)	Consistency index / Viscosity ($Pa.s^n$)	Exponent
Pre–coating colour	1600	0.27	0.38	0.82
Middle-coating colour	1600	2.22	0.32	0.84
Top-coating colour	1600	1.6	0.14	0.75
Carbopol 0.05%	1000	1.25	0.33	0.65
Carbopol 0.1%	1000	3.22	0.63	0.61
Carbopol 0.15%	1000	4.78	1.97	0.50
PVOH (15-20%)	1200	0	0.1 – 0.8	1
"Model" Herschel-Bulkley	1600	0. 1 – 1.5	0. 1 – 0.6	0.7 – 0.9
"Model" Power-law	1200	0	0.1	0.7 – 0.9

Two possibilities are available for the simulation with the CFD software which are steady and unsteady flow. The question is what additional information or accuracy the unsteady flow could bring to us? It was decided to perform all our simulations with a steady flow since the flow rate is considered as constant over time. Indeed, computing time is deeply reduced when we simulate the internal flow using steady flow. We found that there is no difference between steady and unsteady flow whatever the operating conditions or kind of fluids used. Moreover, we are not interested here in the study of transient phenomena. Figure 6 highlights these results by plotting the streamlines.

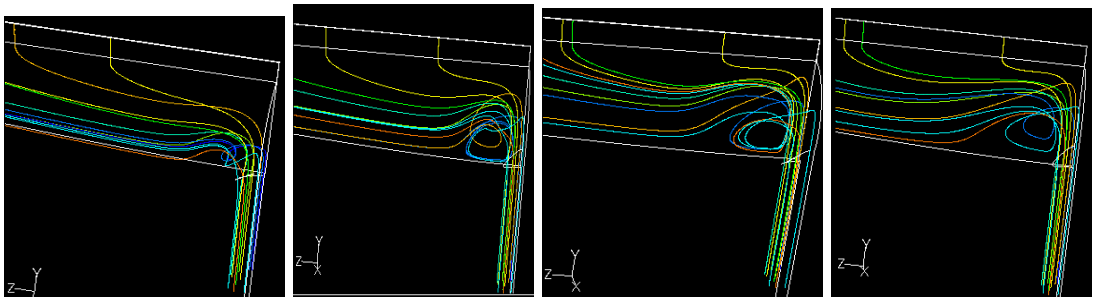

Unsteady flow, t=0.4s *Unsteady flow, t=1.2s* *Unsteady flow, t=3s* *Steady flow*

Figure 6: Evolution of streamlines for unsteady flow (Newtonian fluid, Q=4 L/min, q=15.4 L/m·min, μ=100 mPa·s).

We compare the shape of the streamlines of unsteady flows at several times (between 0.4 s and 3 s) to the one with a steady flow. It is obvious that after a short time (over 0.8 s), there is no difference on streamlines between steady and unsteady flows. Therefore, in order to reduce computing time, simulations of the internal flow will be carried out using the steady flow.

We focus now on the influence of several parameters of the fluids and the geometry on the uniformity of the flow in the manifold.

2.2.3.1. Influence of flow rate and rheological properties on the flow

We first studied the influence of flow rate and viscosity on the flow for fluids without yield shear stress. A first screening permitted to observe that the flow is uniform with fluids with high viscosity or low flow rates as described on Figure 7. Each line of colours represents a pathline, it means that we follow particles of the fluid one by one from the inlet pipe to the end of the slot.

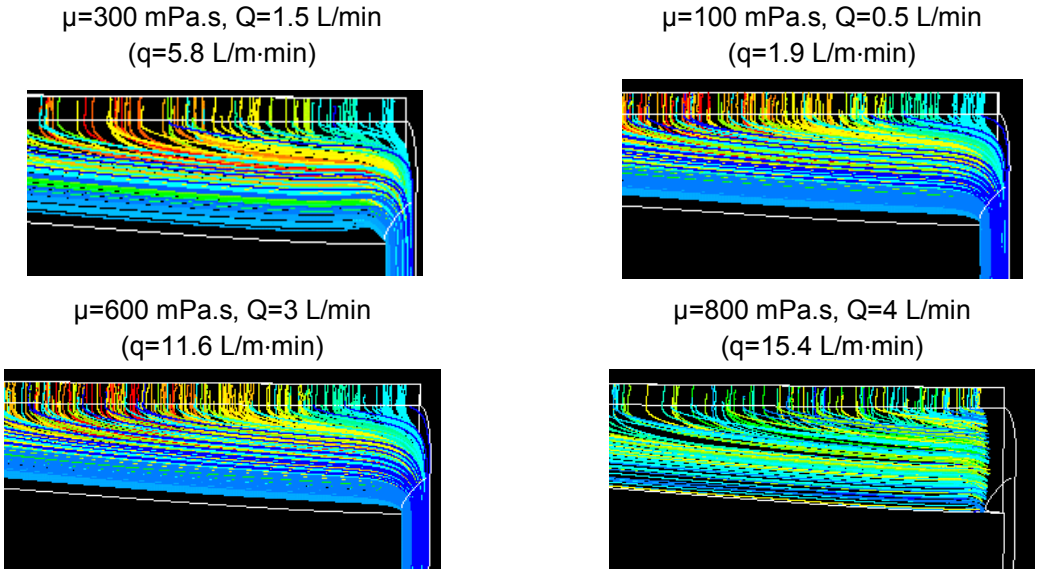

Figure 7 : Pathlines for a Newtonian fluid for high viscosities or low flow rates.

Then we simulated the flow with higher flow rates and lower viscosities for Newtonian fluids. Results for PVOH solutions depicted with streamlines on Figure 8 clearly showed that increasing the flow rate or decreasing the viscosity leads to significant disturbances. Indeed the simulation in the middle is vortex-free whereas for the two others, we can clearly observe a vortex close to the junction between the inlet pipe and the first cavity. For Newtonian fluids, the creation of vortex seems to be linked to the rheological parameter which is the viscosity and the operating condition, namely the flow rate.

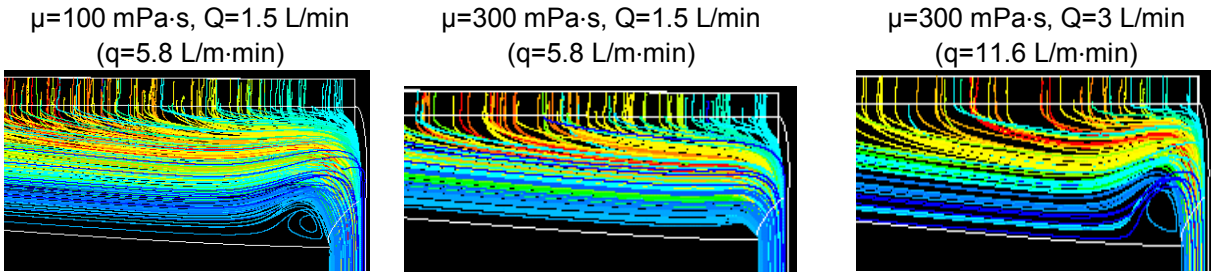

Figure 8: Influence of flow rate and viscosity on vortex formation for a Newtonian fluid.

The same result concerning the flow rate was found for power-law fluids for fixed power-law index and consistency index. Some results are presented on Figure 9 and all the tested cases with another power-law index or consistency index and their comments are gathered in Table 5.

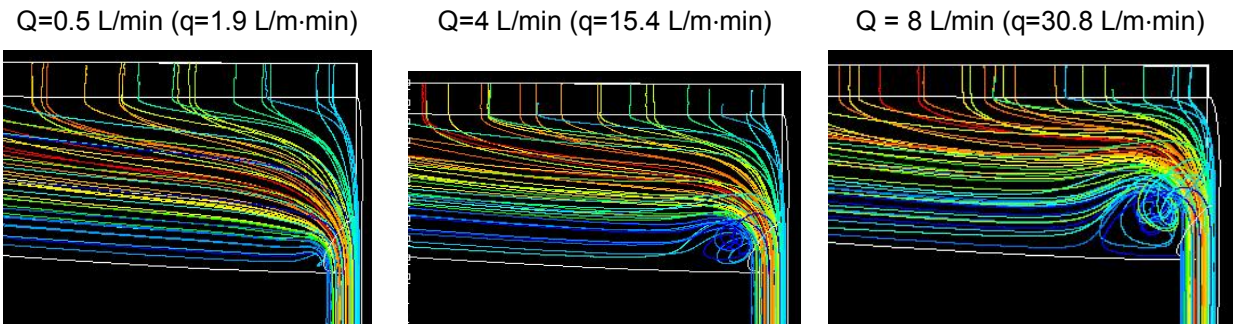

Figure 9: Influence of flow rate on vortex formation for a Power-law fluid with K=600mPa·s ^{n} and a power-law index n=0.8.

Table 5: Summary of all the simulations for Power-law fluids in the manifold.

Test number	Power-law index				Consistency index (mPa·s ^{n})				Flow Rate (L/min)					Comment
	0.7	0.8	0.9	1	100	300	600	800	0.5	1.5	3	4	8	
1	X				X				X					Increasing the flow rate leads to disturbances
2	X				X					X				
3	X				X						X			
4	X				X							X		
5	X				X								X	
6		X					X		X					Increasing the flow rate leads to disturbances Figure 14
7		X					X			X				
8		X					X				X			
9		X					X					X		
10		X					X						X	
11			X					X	X					Increasing the flow rate leads to disturbances
12			X					X		X				
13			X					X			X			
14			X					X				X		
15			X					X					X	
16				X		X			X					Increasing the flow rate leads to disturbances
17				X		X				X				
18				X		X					X			
19				X		X						X		
20				X		X							X	

Concerning non-Newtonian fluids, other rheological parameters may be considered for vortex formation, the power-law index and the yield shear stress:

- To study the influence of the yield-stress with coating colours, simulations were carried out with different values of this parameter close to the ones encountered with coating colours in multilayer curtain coating. Results are depicted on Figure 10 for fluids following the Herschel-Bulkley model.

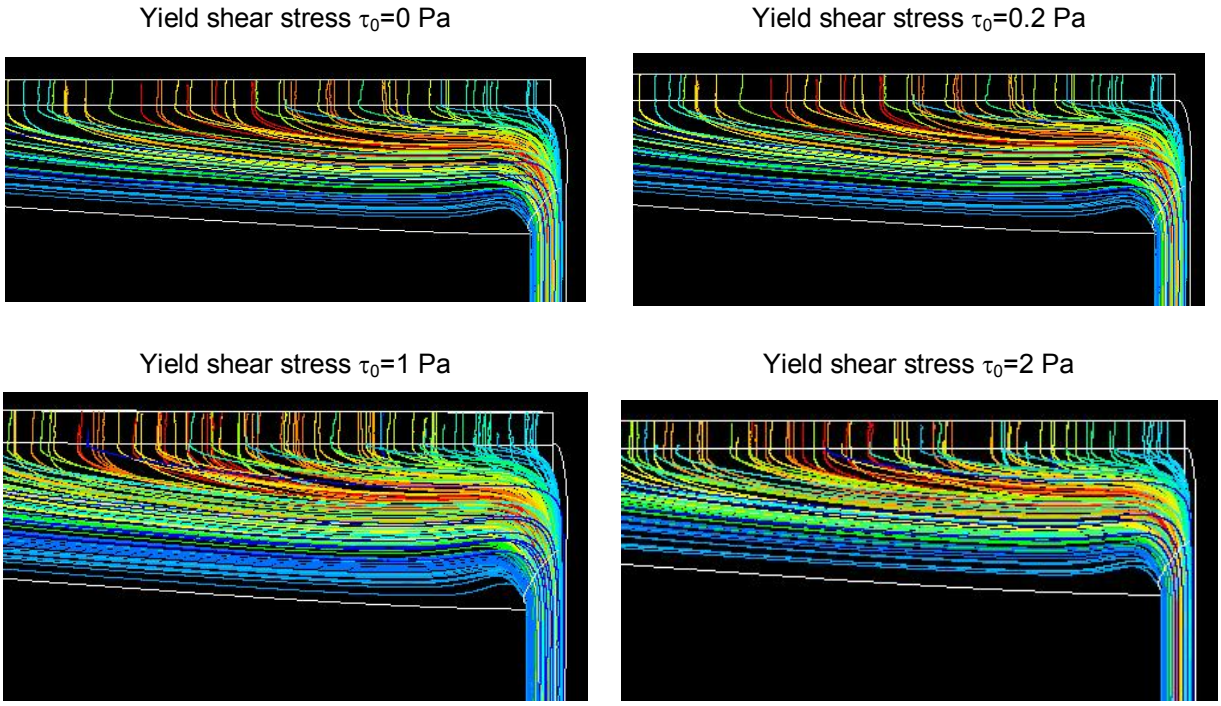

Figure 10 : Influence of yield shear stress for fluids following the Herschel-Bulkley model with a consistency index K=600mPa·s ^{n} and a power-law index n=0.8.

On this figure, streamlines are plotted and we are at the limit of vortex creation at the junction between the inlet pipe and the manifold. It appears clearly that the yield shear stress has no influence on vortex creation for the yield shear stresses tested, which are lower than 2 Pa in our case.

We explain the fact that the yield shear stress of non-Newtonian fluids has no influence on vortex creation in the range explored as follows: we found that the eddies are located close to the wall, so we can calculate the shear stress close to the wall for fluids following the Herschel-Bulkley model and compare this value to the yield shear stress. We know that [59]:

$$\frac{Q}{\pi R^3} = \frac{n}{3n+1}\left(\frac{\tau_w - \tau_0}{K}\right)^{1/n}\left[1 - \frac{1}{2n+1}\frac{\tau_0}{\tau_w} - \frac{2n}{(2n+1)(n+1)}\left(\frac{\tau_0}{\tau_w}\right)^2 - \frac{2n^2}{(2n+1)(n+1)}\left(\frac{\tau_0}{\tau_w}\right)^3\right] \quad (1)$$

where Q is the flow rate (m^3/s), R the inlet radius (m), τ_w is the wall shear stress (Pa), τ_0 the yield shear stress (Pa), K the consistency index (Pa.s^n) and n the power-law index.

In this non-linear equation, the yield shear stress is unknown but we can find its value with a simple solver. Values of the wall shear stress for several fluids following the Herschel-Bulkley model are gathered in Table 6. We fixed the consistency index and the

yield shear stress and we changed the flow rate (between 0.5 L/min and 3 L/min) and the power-law index (between 1 and 0.8). It is then possible to understand the influence of flow rate and power-law index on the wall shear stress and we are able to compare these values to the yield shear stress in order to see if this yield shear stress has an impact on the wall shear stress.

Moreover, by comparing results, it is possible to evaluate the influence of an increase in the consistency index (from 100 to 600 mPa.s^n) and of the yield shear stress (from 0.5 to 1.5 Pa).

Table 6: Wall shear stress in Pa for several fluids following the Herschel-Bulkley model.

Q (L/min)	τ_0 = 0.5 Pa·s K = 100 mPa·s^n			τ_0 = 1.5 Pa·s K = 100 mPa·s^n			τ_0 = 1.5 Pa·s K = 600 mPa·s^n		
	n=1	n=0.9	n=0.8	n=1	n=0.9	n=0.8	n=1	n=0.9	n=0.8
0.5	**11**	**7**	**5**	**11**	**8**	**7**	**71**	**42**	**25**
1.0	**21**	**13**	**8**	**22**	**14**	**9**	**132**	**74**	**44**
1.5	**31**	**19**	**11**	**33**	**20**	**12**	**194**	**107**	**62**
2.0	**41**	**24**	**13**	**43**	**25**	**15**	**255**	**142**	**78**
3.0	**62**	**34**	**18**	**64**	**36**	**20**	**377**	**202**	**108**

It is clear that using fluid with a lower power-law index leads to a lower wall shear stress since a lower power-law index means a higher shear-thinning behaviour. Moreover, whatever the fluid, increasing the flow rate will drastically increase the wall shear stress.

Concerning the influence of the consistency index, it appears that this parameter has a huge impact on the wall shear stress since values are 5-6 times higher when the consistency index is equal to 600 mPa.s^n. On the contrary, in the range explored (from 0.5 to 1.5 Pa), results are not really affected by the value of the yield shear stress. Table 6 enables us to conclude that whatever the other rheological parameters, the yield shear stress in the studied range has no influence on vortex formation at the manifold inlet for this geometry, which is close to a Tee-pipe, since its value is less than 5% compared to the wall shear stress in all the cases.

- To study the influence of power-law index, simulations with power-law fluids were run with values of the power-law index close to those of coating colours, *i.e.* between 1 and 0.7. At n=1, the fluid is Newtonian whereas it is non-Newtonian for the others. The lower the power-law index, the more shear-thinning the fluid will be. We have run several simulations keeping the flow rate and the consistency index constant, the only parameter that changes is the power-law index. The selected operating conditions give vortex-free condition for a Newtonian fluid.

  Results depicted with streamlines on Figure 11 clearly show that the power-law index has a huge impact on vortex formation. Indeed, decreasing the power-law index while keeping other parameters constant leads to bigger disturbances. Nevertheless, with real fluids, it is not possible to master this parameter contrary to flow rate or viscosity so in a practical way it is better to conclude that using fluids with decreasing power-law index may lead to higher instabilities.

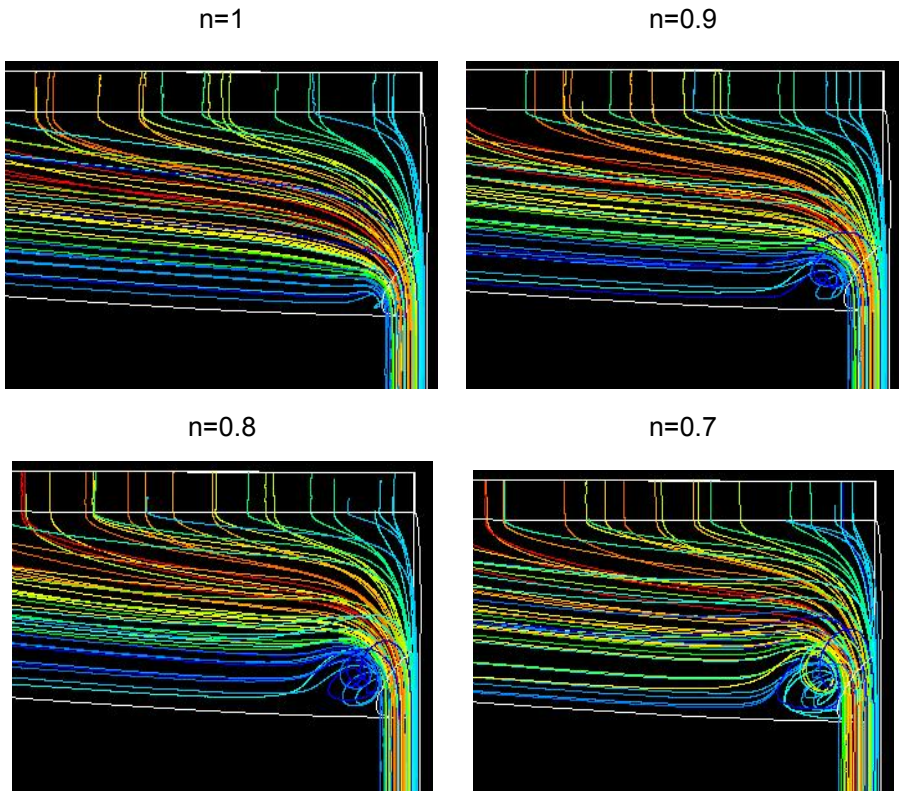

Figure 11: Influence of power-law index on vortex formation for a power-law fluid with a consistency index of 600mPa.s^n, for a constant value of the flow rate 4 L/min (15.4 L/m·min).

To understand the role of the power-law index, we calculate the apparent viscosity for fluids following the Herschel-Bulkley model once the wall shear rate is known. The equations to obtain the apparent viscosity are:

$$\tau_w = \tau_0 + K\dot{\gamma}_w^n \tag{2}$$

$$\mu_{app,w} = \frac{\tau_w}{\dot{\gamma}_w} = \frac{\tau_w}{\left((\tau_w - \tau_0)/K\right)^{1/n}} \tag{3}$$

Equations (2) and (3) permitted to calculate the apparent viscosity of the fluid at the wall of the inlet pipe, as vortices appear in the region at the junction between this pipe and the first cavity. The data are obtained for fluids with a consistency index of 600 mPa.s^n and several values of the power-law index and flow rates. Values are gathered in Table 7.

Table 7: Apparent viscosity at inlet pipe wall, in mPa.s, for fluids with a yield shear stress of 1.5 Pa and a consistency index K=600mPa.s^n.

Q (L/m.min)	n=1	n=0.9	n=0.8
1.9	**613**	**390**	**254**
3.9	**607**	**359**	**214**
5.8	**605**	**343**	**194**
7.7	**604**	**331**	**182**
11.6	**602**	**317**	**167**

These results show that for a given flow rate, fluids with a lower power-law index have a lower apparent viscosity close to the wall. This viscosity is nearly divided by three when the

power-law index varies from 1 to 0.8. As described above, decreasing the viscosity leads to instability and the use of fluids with lower power-law index involves having a lower apparent viscosity at the junction between the inlet pipe and the manifold in the area where vortex could appear.

2.2.3.2. Influence of the Reynolds number on the flow

The aim of this study was to check if it is the Reynolds number that controls the flow behaviour or if it is the flow rate, the viscosity or the power-law index that predominates for the creation of vortex. Taking into account some literature results (Wen and Liu, 1994 [32]), we may assume that it is the Reynolds number which in fact plays a role. We cannot define a Reynolds number in the manifold, so, similar to Wen and Liu, we will refer to the one in the inlet pipe. We will use the generalised Reynolds number. For a power-law fluid (and a Newtonian fluid, n=1), it is defined as:

$$Re = \frac{8\rho V^{2-n} D_h^n}{2^n \left(3 + \frac{1}{n}\right)^n K} \tag{4}$$

where ρ is the density of the fluid (kg/m^3), V the flow velocity (m/s), D_h the characteristic length (m), *i.e.* the pipe diameter here, K the consistency index of the fluid (Pa·s^n) and n the power-law index.

It is clear that increasing the Reynolds number will lead to flow perturbations since increasing the flow rate, *i.e.* flow velocity, or reducing the viscosity both lead to an increase of this dimensionless number and it was shown just previously than these two cases created perturbations in the cavity and sometimes a vortex. By increasing the Reynolds number, the inertial forces will be increased compared to the viscous forces.

We carried out a study with the previous power-law fluids at a constant Reynolds number where several simulations were performed changing the power-law index and adjusting the velocity. We have to notice that, in this study, the value of density was not varied, but we know that both viscosity and flow rate may vary in a much wider range than density. We wanted to be at the limit of vortex creation for the Newtonian fluid and observe the behaviour of the other fluids at the same Reynolds number. Using flow conditions at the limit of the vortex creation permitted to easily check if the streamlines are different in the manifold or not. Figure 12 shows that we are at the limit of vortex formation at constant Reynolds number whatever the power-law index. The same work was done with another consistency index (K =100 mPa·s^n) and the flow rate was changed in order to be at the limit of vortex creation and results reveal the same trend than those found with Figure 12.

The same work was done for Newtonian fluid with PVOH solutions where several simulations were performed changing the viscosity and adjusting the velocity. In this case a higher Reynolds number has been chosen in order to see if the vortex of the three fluids has the same shape. On Figure 13, streamlines were plotted and it is obvious that they are identical. We found a big vortex at the junction between the inlet pipe and the first cavity.

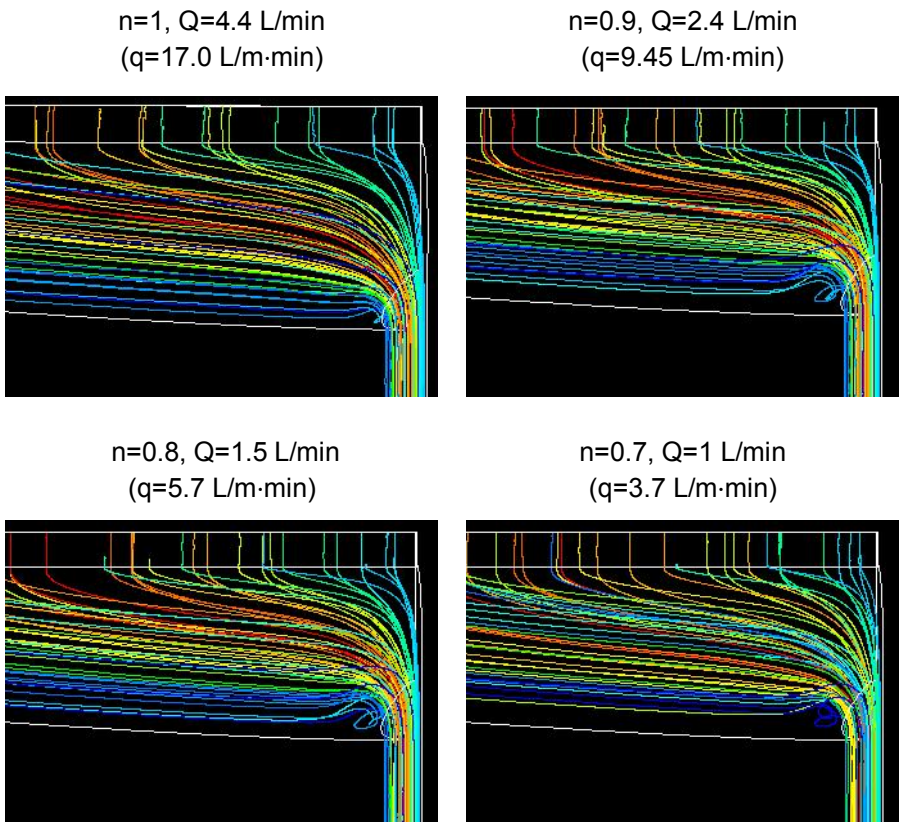

Figure 12: Influence of n and flow rate on vortex formation for a power-law fluid at a consistency index K=600mPa.s^n and Re=20.

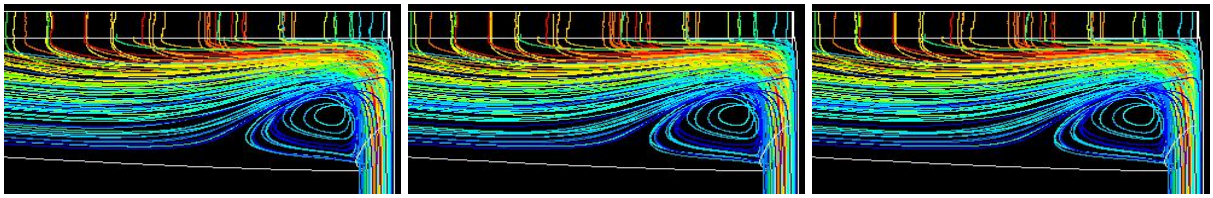

Figure 13: Influence of flow rate and viscosity on vortex formation at Re=110.

CFD simulations permitted to conclude that the Reynolds number is a relevant parameter for the internal flow whatever the fluid. As we have a fixed geometry, we cannot conclude on the influence of the angle of deviation but we know, from the literature review [33], that, this angle has an influence on the presence, the region and size of vortices. Moreover, trials permitted to find that there is a critical Reynolds number, Re_c, in order to avoid vortex creation. By comparing two different fluids at a same Reynolds number on Figure 14 below and beyond a certain value, it appears that the streamlines at the same Reynolds number are identical. The simulations on the left side are vortex-free and the Reynolds number is below the critical value whereas on the right side it is over this value and we can observe a vortex in the manifold. Therefore the critical Reynolds number is between 18 and 24 and it was found that the limit of vortex creation is equal to 20 with the studied geometry whatever the fluid (Newtonian or not). In this case, the critical Reynolds number is equal to 20. To maintain vortex-free operation, the Reynolds number at the inlet should not exceed this critical value. This value is specific of this special geometry. It means that if the geometry is different, the critical Reynolds number value will not be the same.

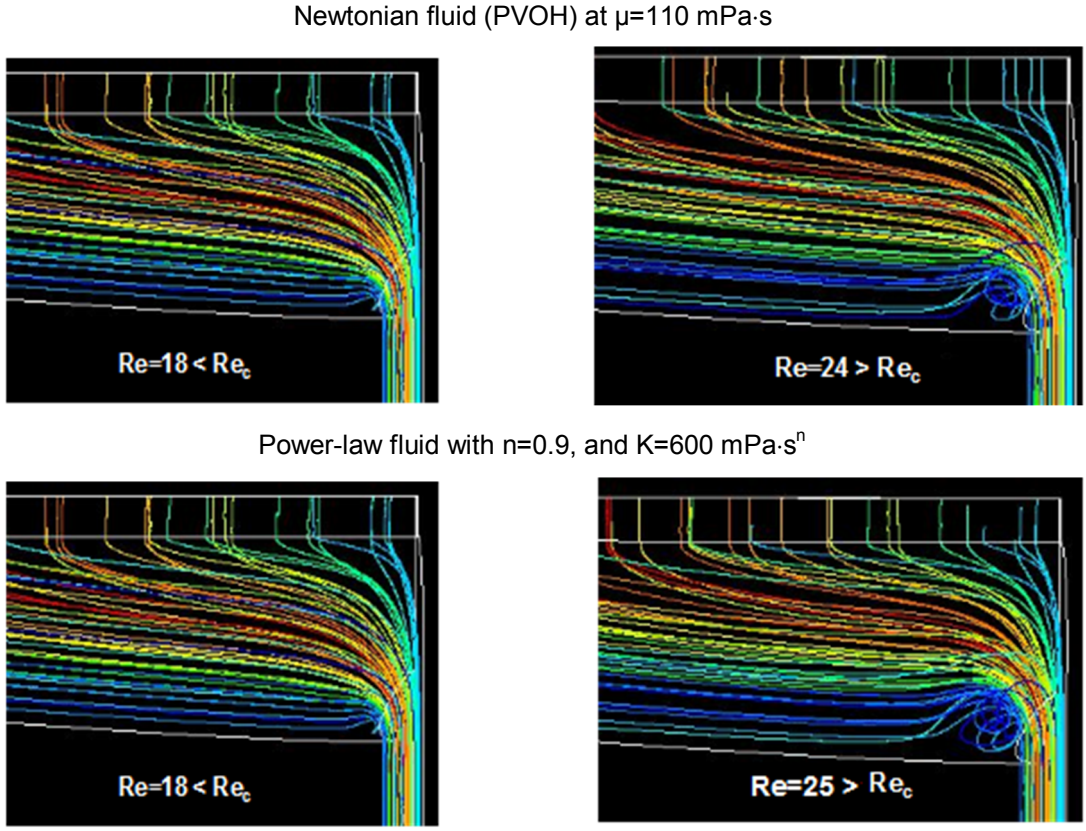

Figure 14: Illustration of the existence of a critical Reynolds number on vortex formation for Newtonian and non-Newtonian fluid.

Figure 15 summarizes results found on the existence of the critical Reynolds number. We plotted this critical value which is equal to 20 with the geometry used for the range of flow rates used on the pilot and several consistency indexes.

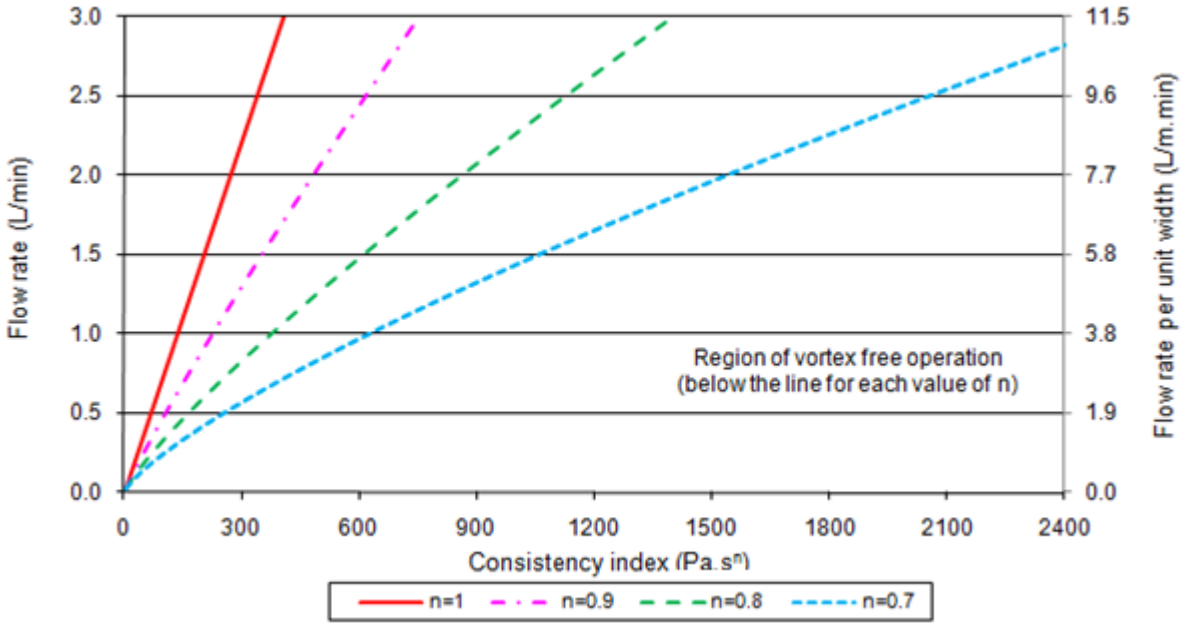

Figure 15 : Operating windows in curtain coating with our geometry for fluids with a density of 1200 kg/m^3.

For any value below the curve, the flow is vortex-free in the manifold whereas, above it, there is the creation of vortex which may lead to defects in the final coated paper.

These results point out that for a given geometry, decreasing the power-law index will drastically increase the consistency index available to be vortex free. Indeed the higher the flow rate is, the higher the difference of consistency index between fluids with different power-law indexes in order to have no perturbation will be. These results mean that it is better to have a fluid with a high power-law index to avoid flow perturbations for any value of flow rates and consistency index. Actually, it is not really possible to change independently the power-law index and the consistency index by adding rheological modifiers, and Figure 15 permits to know what the value of this parameter should be to be vortex-free.

To conclude with simulations in the first cavity, we found a relevant parameter both for Newtonian and non-Newtonian fluids to avoid flow disturbance which is the Reynolds number. We have shown that increasing the Reynolds number led to flow perturbations. To maintain vortex-free operation, a critical Reynolds number at the inlet exists. For the studied coater geometry, the knowledge of Reynolds number seems to be sufficient for Newtonian and non-Newtonian fluids with this shape of manifold. Now we have to validate all our results experimentally.

2.2.3.3. Experimental validations

We will focus in this part on the experimental validations of simulations in the internal flow done on a transparent replica of the coater. Two methods of measurements presented in Chapter 2 will be used, tracers and 2D-PIV, and, after that, we will compare these results to those found first with CFD.

Simulations showed that the main problem of the internal flow occurs at the junction between the inlet pipe and the/manifold. Here, depending on the value of the Reynolds number (calculated in the inlet pipe), a vortex is created or not. We aimed at validating the presence of vortex and the value of the critical Reynolds number for Newtonian and non-Newtonian fluids. The operating conditions were as follows:

- Flow rates: between Q=0.5 L/min and Q=3.0 L/min (q=1.9 L/m·min – 11.6 L/m·min)
- Newtonian fluids with 3 viscosities (PVOH): μ=110 mPa·s, μ=290 mPa·s, μ=580 mPa·s
- non-Newtonian fluids: Coating colours and Carbopol

a) Visualisation of streamlines with tracers

We used streamlines visualization with both Newtonian and non-Newtonian fluids.

Concerning Newtonian fluids, PVOH solutions at several viscosities close to those used with CFD were tested. Their viscosities are close but not exactly identical to those used for CFD because it is very difficult to obtain the exact desired viscosity at the right temperature in practice. Concerning coating colours, due to the opacity of such fluids, it is extremely difficult to clearly see the streamlines. That is why we will try to see vortex formation for these fluids with a 2D-PIV. Another solution to solve this problem and see streamlines with non-Newtonian fluid is to use Carbopol.

We focus first on the existence of the vortex in the area close to the junction between the inlet pipe and the manifold and the influence of flow rate and viscosity on the creation of vortex and compare these results to those obtained by simulation (Figure 16).

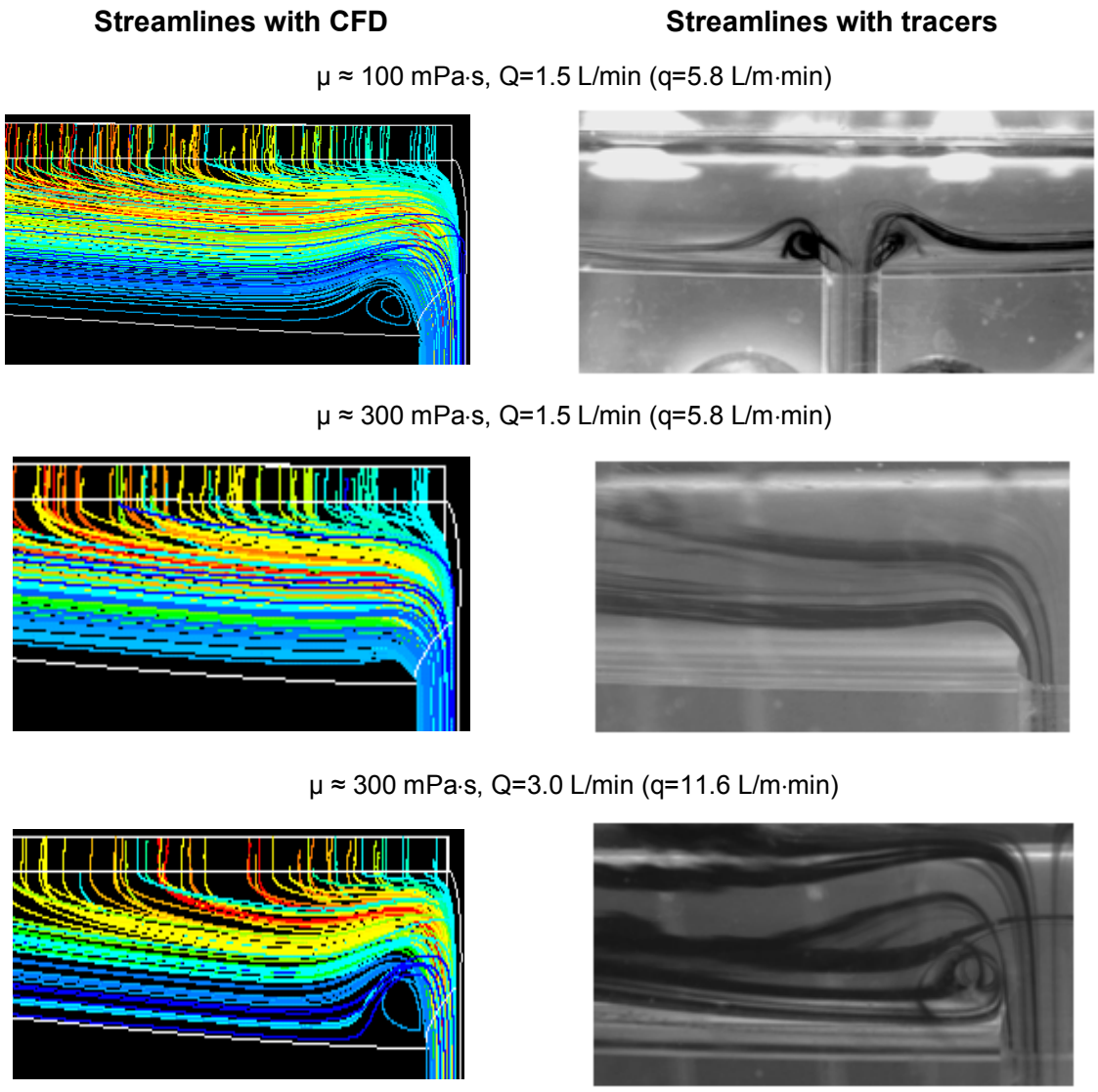

Figure 16: Comparison of PVOH streamlines in the manifold between CFD simulations and experiments (dye injection).

The first thing that we can notice is that, as expected, vortices really exist and they are located in the area found by simulation. Moreover, on Figure 16 it is clear that increasing the flow rate or decreasing the viscosity leads to significant disturbances of the flow, which implies that, as described in the previous part, vortices exist in the cavity under specific operating conditions. Streamlines from simulations and experiments are very similar, which means that our simulations with CFD are coherent with reality. Finally experiments validate that, as expected, the flow was symmetrically distributed into the first cavity since streamlines made by the dyes are symmetrical compared to the centreline of the inlet pipe. Simulations carried out on half of the manifold were appropriate. Moreover, the most important point found with CFD simulations for Newtonian and non-Newtonian fluids is that a relevant parameter for the absence or presence of vortex in the manifold is the critical Reynolds number, whose value (20) is specific of this geometry. Streamlines with tracers for PVOH solutions at several viscosities are depicted on Figure 17, Figure 18 and Figure 19. We focus here on the value of the Reynolds number in the inlet pipe, compare it to the critical Reynolds number found in simulations. We also try to check if the experimental critical Reynolds number is identical or, at least, has the same order of magnitude.

Q=0.8 L/min (q=3.0 L/m·min), *Re*=19 < Re_c

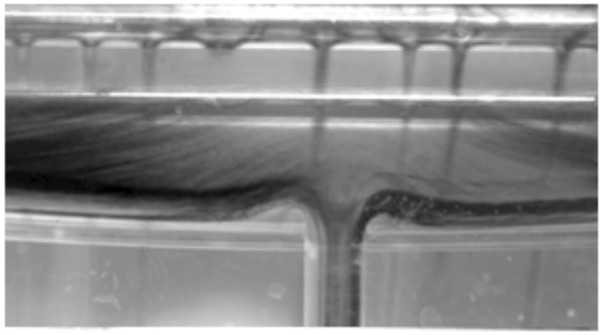

Q=1.0 L/min (q=3.9 L/m·min), *Re*=25 > Re_c

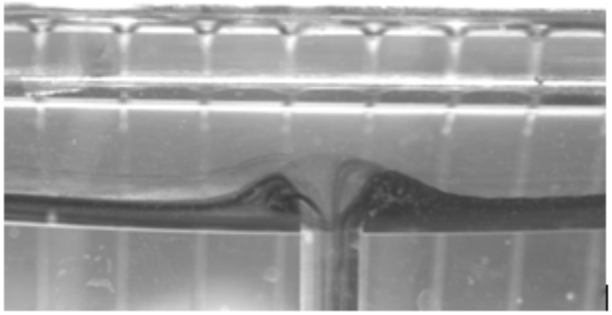

Q=1.5 L/min (q=5.8 L/m·min), *Re*=37 > Re_c

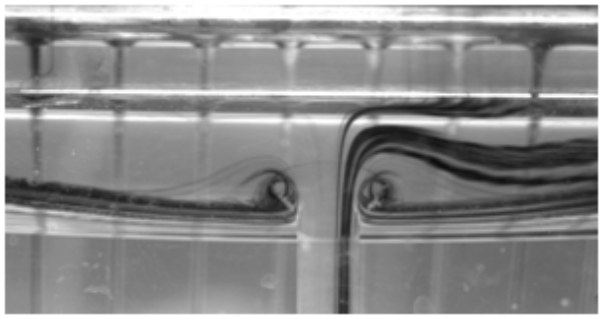

Q=3.0 L/min (q=11.6 L/m·min), *Re*=74 > Re_c

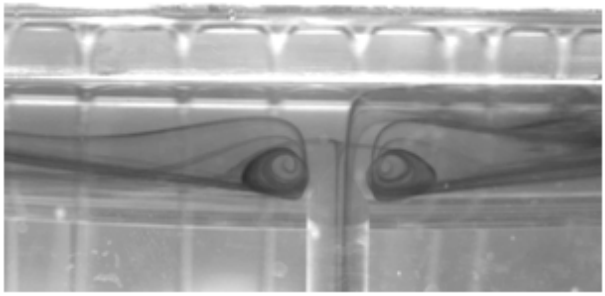

Figure 17: Influence of Reynolds number in the inlet pipe on vortex formation in the manifold for PVOH solution at μ=110 mPa·s highlighted with tracers.

Q=1.8 L/min (q=7.0 L/m·min), *Re*=17 < Re_c

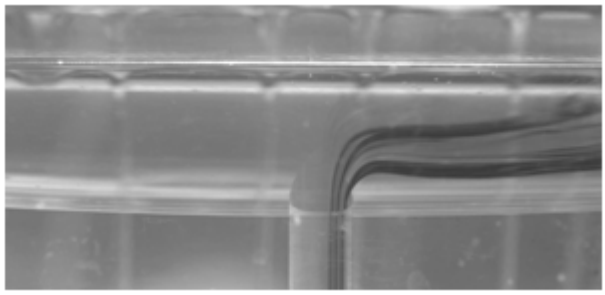

Q=2.2 L/min (q=8.5 L/m·min), *Re*=21 > Re_c

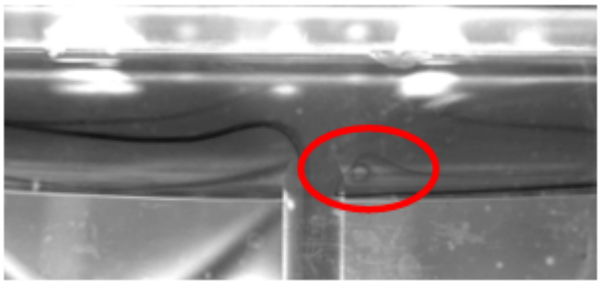

Q=3.0 L/min (q=11.6 L/m·min), *Re*=28 > Re_c

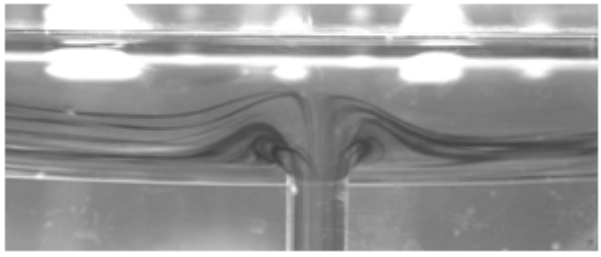

Figure 18: Influence of Reynolds number in the inlet pipe on vortex formation in the manifold for PVOH solution at μ=290 mPa·s highlighted with tracers.

Q=1.5 L/min (q=5.8 L/m·min), Re=7 < Re_c Q=30 L/min (q=11.6 L/m·min), Re=14 < Re_c

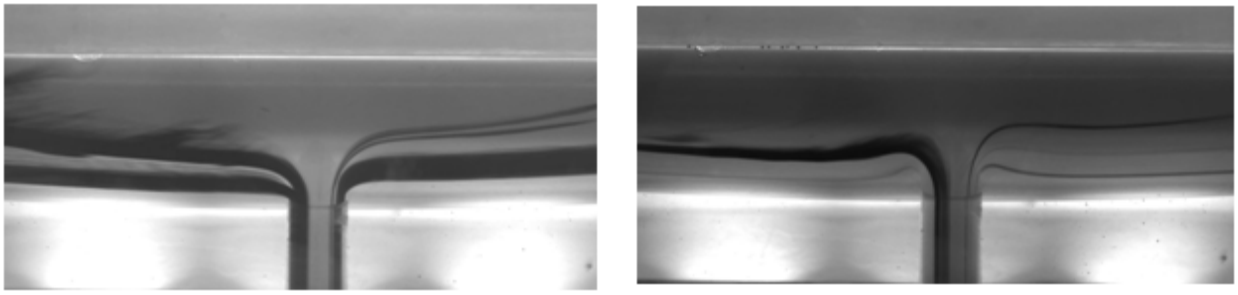

Figure 19: Influence of Reynolds number in the inlet pipe on vortex formation in the manifold for PVOH solution at μ=580mPa·s highlighted with tracers.

It is clear, from Figure 17 and Figure 18, that there is a critical value of the Reynolds number. Its value is independent of the viscosity for Newtonian fluids. Moreover, this critical Reynolds number is between 19 and 21, which validates the value of the critical Reynolds number found previously by simulations. On Figure 19, we are at the transition between vortex-free flow and the apparition of this vortex. A small loop can be observed which corresponds to the start of disturbances. Moreover, on Figure 17, it is obvious that increasing the Reynolds number leads to bigger disturbances as it was described with CFD simulations.

Results depicted on Figure 20 demonstrate that for a Newtonian fluid with a viscosity over 500 mPa.s, the flow is vortex-free in the manifold for the range of flow rates used on the pilot (below 3.0 L/min). So it means that for Newtonian fluids such as PVOH solutions, there is a range of viscosity for which the flow is vortex-free in the manifold whatever the flow rate.

In curtain coating, coating colours, which are non-Newtonian fluids, are used but it is not possible to use tracers because these fluids are opaque and it is very difficult to clearly see the streamlines. In order to highlight streamlines with tracers for non-Newtonian fluids, we used Carbopol solutions at very low concentrations.

Tests with the tracer method were carried out for three concentrations of Carbopol (0.05%, 0.1% and 0.15%) and the critical flow rates above which a vortex is created were found. Knowing the rheological parameters and the flow rate permitted to calculate the Reynolds number and to compare its value to the critical Reynolds number found in simulations as it was done with Newtonian fluids. Figure 20 shows the streamlines in the manifold for Carbopol at 0.05% for several flow rates. Here again we found that the critical Reynolds number is close to the one found previously by simulations. We found the same value of the critical Reynolds number for Carbopol at 0.1 and 0.15%, which permits to validate the simulation in the manifold for non-Newtonian fluids.

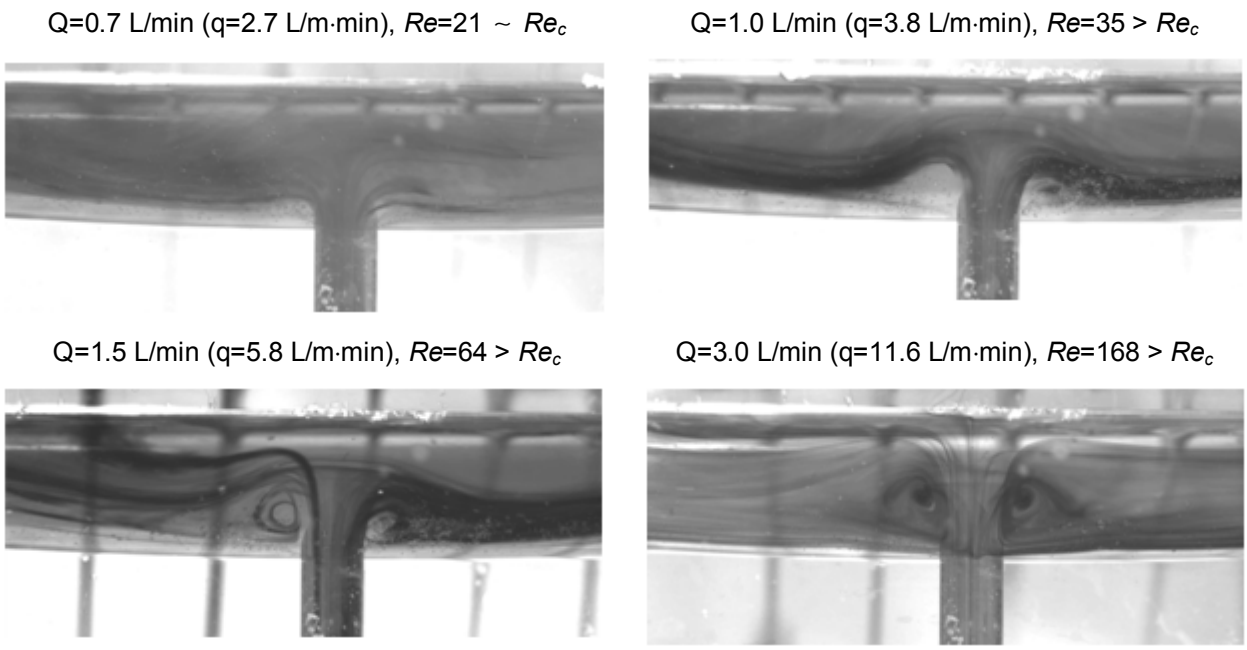

Figure 20: Influence of Reynolds number in the inlet pipe on vortex formation in the manifold for a Carbopol solution at 0.05% highlighted with tracers.

b) 2D-PIV for PVOH solutions

2D-PIV, which is another method of measurement presented in Chapter 2, was also used to compare results to those found first with CFD. We wanted to validate the results obtained by simulations on coating colours since it was not possible with the dye injection. 2D-PIV is an alternative to tracers in order to observe the flow behaviour of opaque fluids in the manifold. Before starting with coating colours, we verified that 2D-PIV and flow visualizations with tracers revealed the same trend. This comparison is depicted on Figure 21.

Figure 21 reveals that 2D-PIV and flow visualization with tracers give very close results since the shape of vortex is identical and the flow is vortex-free at Re =19 with both PIV and visualization with tracers. Other measurements with 2D-PIV for PVOH with other viscosities have been done; they are not presented here but results are identical whatever the method used.

c) 2D-PIV for coating colours

We first carried out tests with coating colours with the same configuration as with PVOH, which means that the laser was put above the curtain coater and thus created a straight line light. The camera, put in front of the manifold, should receive only the light of the fluorescent particles of a plane thanks to a laser light filter but this configuration does not work (Figure 22 a). Indeed whatever the coating colours, it is not possible to see fluorescent particles since the fluid is opaque and stops the laser on the inclined plane. Then we changed the configuration by putting the laser above the camera in front of the manifold (Figure 22 b).

PVOH at μ=110 mPa·s, Q=3.0 L/min (q=11.6 L/m·min). Re=74

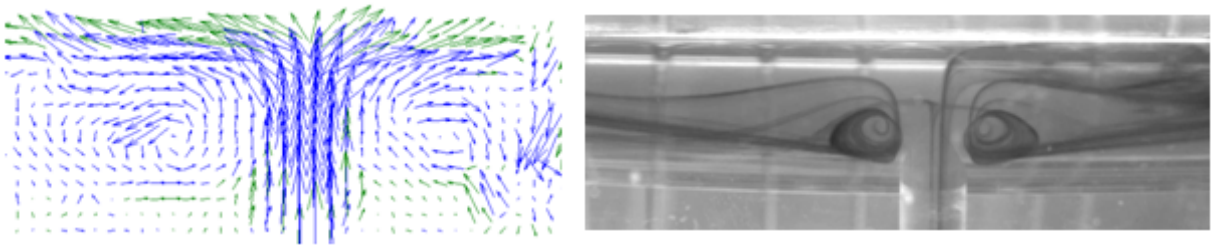

PVOH at μ=110 mPa·s, Q=0.8 L/min (q=3 L/m·min). Re=19

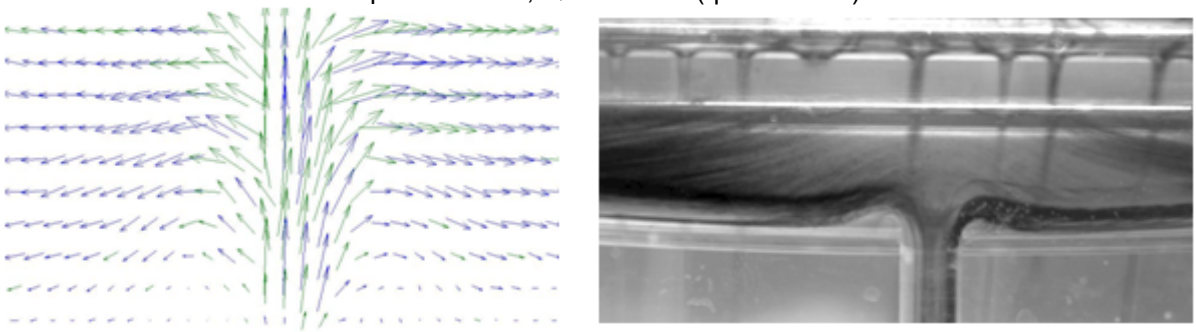

Figure 21: Comparison between flow visualization with tracers and 2D-PIV for a transparent fluid (PVOH).

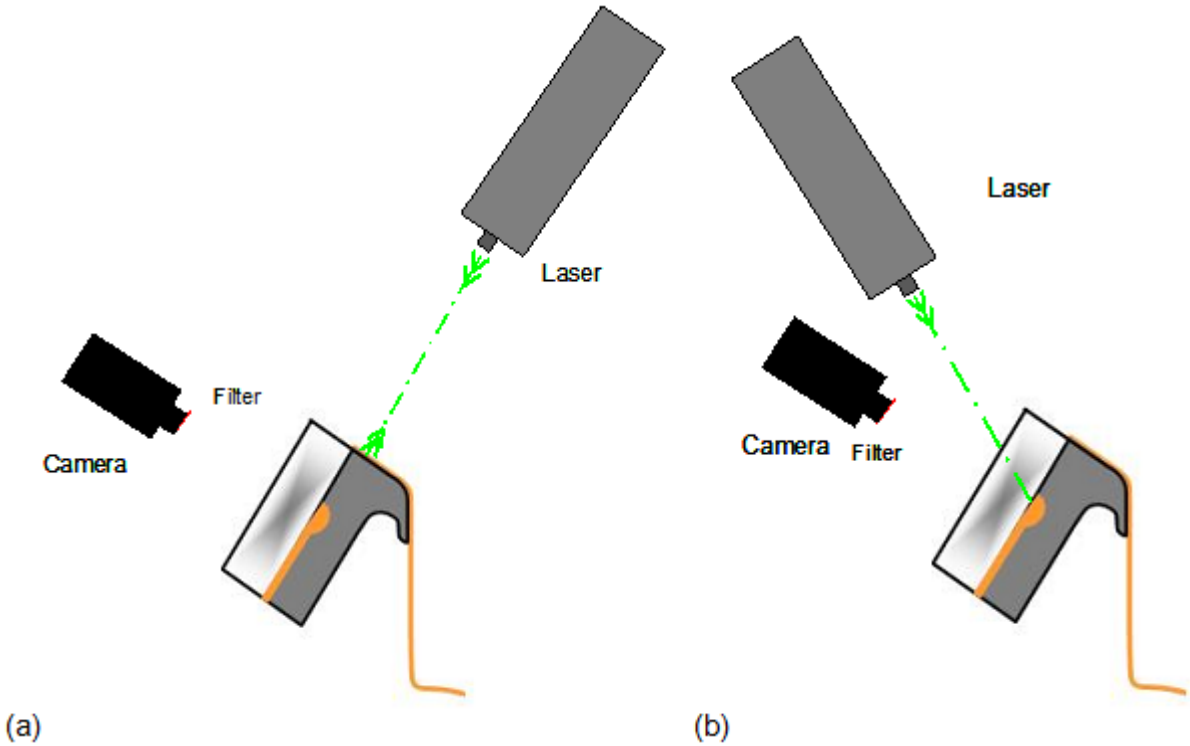

Figure 22: Schemes of different configurations of coating experimental assembly.

Figure 23 presents results obtained with the configuration b. It clearly shows that there are too few points available to make a calculation and give good results because of the opacity of this fluid. Moreover, the camera can only detect fluorescent particles close to the wall which are therefore immobile. The velocity field obtained in those cases does not mean anything as shown below. Indeed, in order to obtain the velocity field, a 2D displacement of particles is estimated by recording two photos at two very close moments and in those cases, particles do not move.

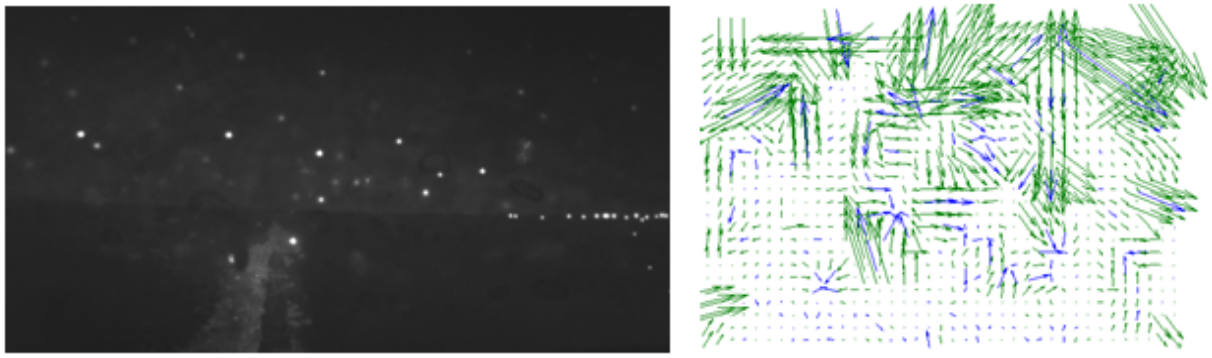

(a) (b)

Figure 23: Fluorescent particles in the manifold with top coat (a) and velocity vectors associated with 2D-PIV (b).

At this point, it is not possible to validate results obtained by simulation for coating colours with the 2D-PIV method. Here again, we will use Carbopol at a very low concentration.

Tests with 2D-PIV were carried out for Carbopol solutions at three different concentrations (0.05 %, 0.1 % and 0.15 %). Our aim was to compare results to those found with the dye injection method and simulations. Figure 24 and Figure 25 present a comparison between the velocity fields obtained with 2D-PIV and streamlines obtained with tracers and by CFD simulation, for two different concentrations of Carbopol and several flow rates,. The velocity field with the 2D-PIV also permitted to validate the presence of vortex in the considered area, *i.e.* close to the junction between the inlet pipe and the first cavity. We encountered the vortex at the same location for the three different methods and the size of the vortex is identical.

Finally the 2D-PIV seemed less accurate that the flow visualization with tracers for the distinction of the transition vortex-free/vortex creation since we observe the velocity field in a plane and not in a volume but with this method we can easily have the value of the velocity field in the manifold.

2D-PIV is not suitable for the determination of velocity fields inside the cavity for coating colours but permitted to validate results found with Newtonian and non-Newtonian fluids using transparent fluids (PVOH and Carbopol). This method, totally different from the dye injection method, also permitted to validate results found by CFD simulations such as the presence of a critical Reynolds number, equal to 20 in our case.

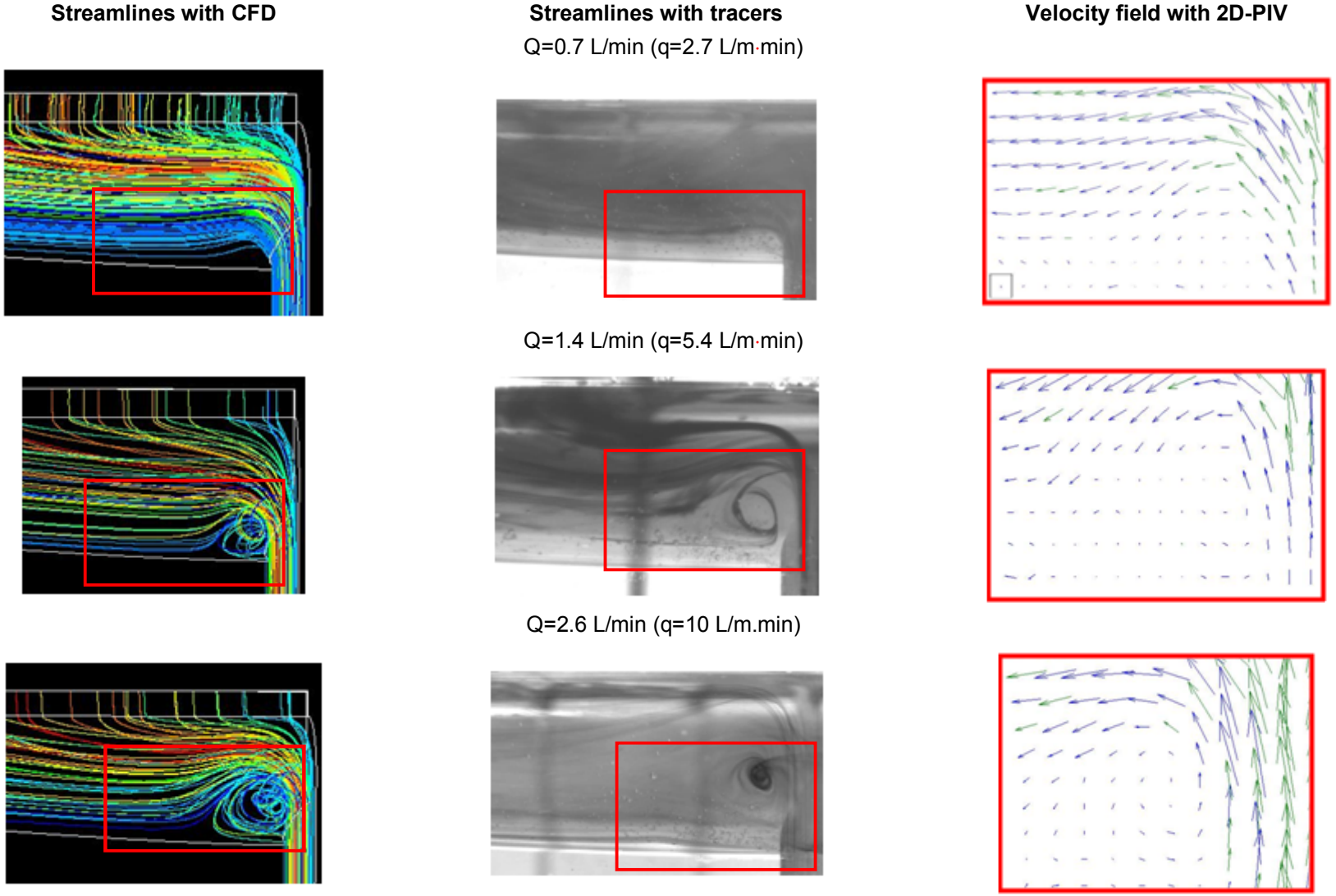

Figure 24: Comparison of flow visualization by simulation, with tracers and 2D-PIV for a non-Newtonian transparent fluid (Carbopol at 0.05 %).

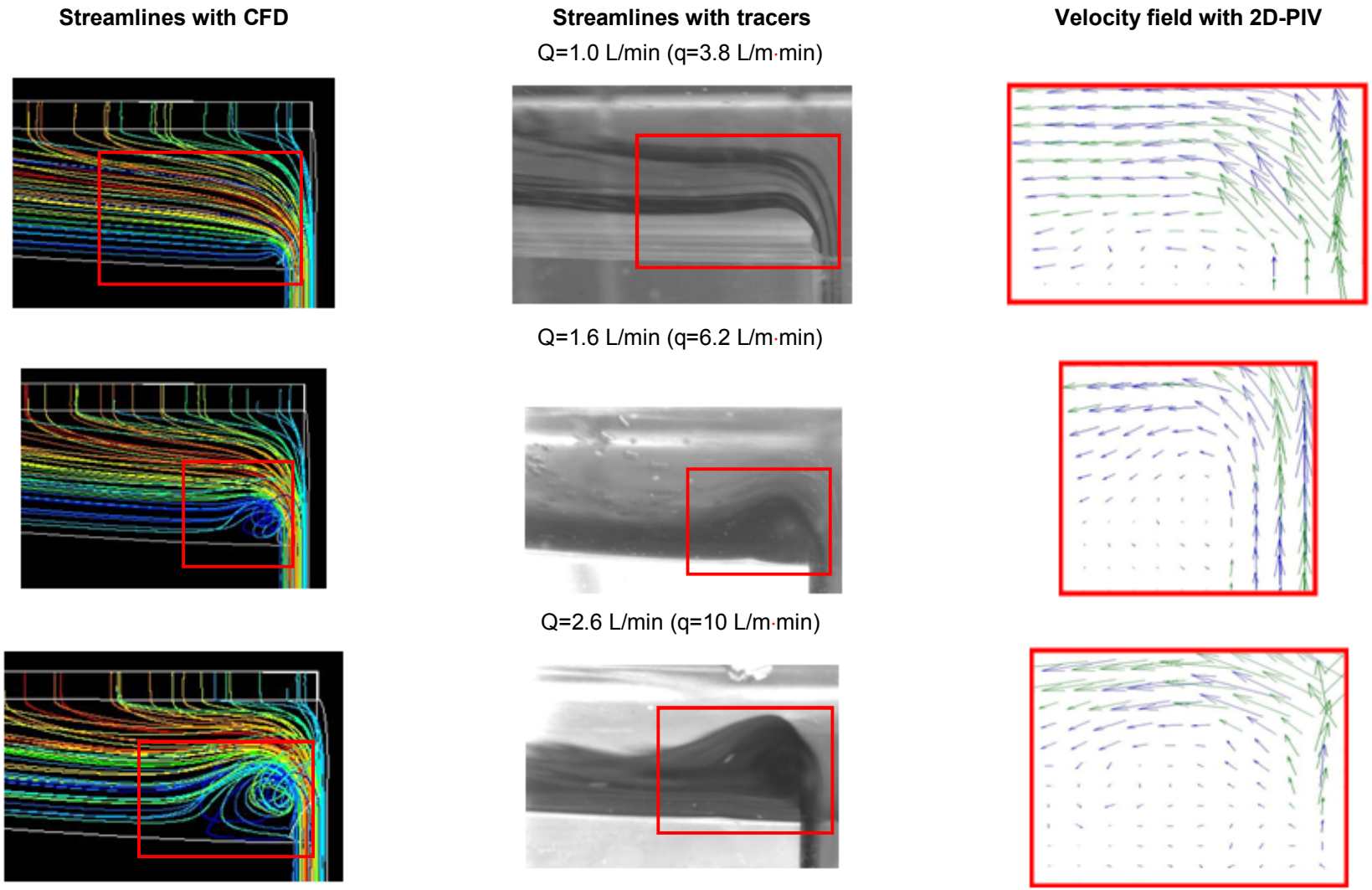

Figure 25: Comparison of flow visualization by simulation, with tracers and 2D-PIV for a non-Newtonian transparent fluid (Carbopol at 0.15 %).

2.2.3.4. Potential methods to reduce flow perturbations at the inlet of the first cavity

Conditions of vortex-free operation are now better known. We know that the inlet velocity is an important factor for the studied geometry. We also expect that the deviation angle is another one. It is now possible to propose some solutions to avoid vortex creation. We can modify the original geometry or propose a new geometry.

a) Increase of the inlet radius

The aim is here to reduce the Reynolds number in the inlet tube in order to be under the critical Reynolds number. Therefore it should be relevant to use fluids with a higher viscosity or adding a rheological modifier such as a thickener but in some cases we are forced to work with a very low viscosity fluid (around 100 mPa·s) or in other cases, depending on the power-law index for non-Newtonian fluid, the consistency index should be over 1000 mPa·s to be vortex-free, which leads to problems of runnability on the curtain itself and the impingement zone. So changing parameters on the curtain coater itself seems more appropriate because it will act in a similar way whatever the fluid.

We therefore increased the radius of the inlet pipe in order to reduce the inlet velocity keeping the same flow rate. Owing to the size of the first cavity, the maximum radius for the inlet pipe is 5.4 mm, the original value is 4.7 mm. Nevertheless, this increases the cross-section area of about 30 %. So, at constant flow rate, the velocity decreases by approx. 25 %.

At a constant flow rate, the Reynolds number (Eq. 5) varies just like the reciprocal of the diameter size for Newtonian fluids (n=1) and decreases more for shear thinning fluids since the power-law index, n, is below unity.

$$Re = \frac{8\rho V^{2-n} D_h^n}{2^n \left(3+\frac{1}{n}\right)^n K} = \frac{8 \cdot 4^{2-n} \rho Q^{2-n}}{2^n \pi^{2-n} \left(3+\frac{1}{n}\right)^n K D_h^{4-3n}} \quad (5)$$

As a result, the uniformity of the flow should be improved with this new geometry since the diameter has increased. Several tests were carried out under the same operating conditions as the previous tests but with the new geometry. We found that, as expected, there are fewer perturbations in the cavity when the inlet diameter is bigger. Figure 26 is an example of this result for the two different geometries for a coating colour. Thus, a solution to avoid vortex creation is to increase the diameter of the inlet pipe.

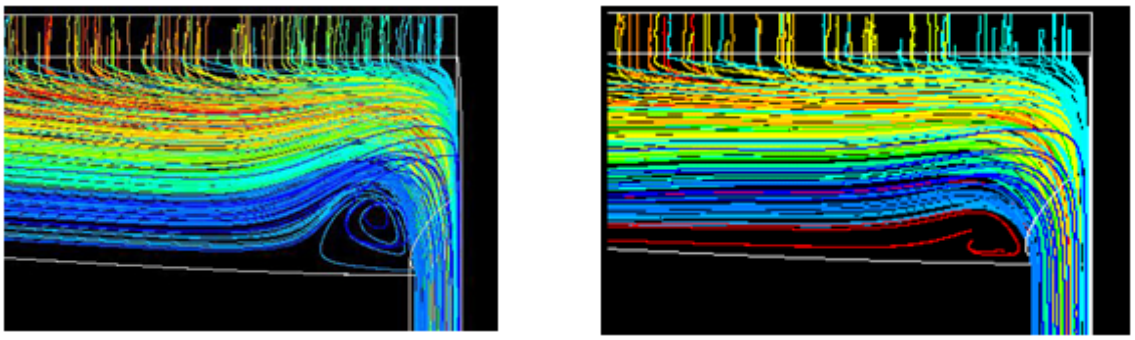

Inlet radius : 4.7 mm

Inlet radius : 5.4 mm

Figure 26: Influence of the size of the inlet pipe on vortex creation (middle colours, Q=1.5 L/min – q=5.8 L/m·min).

b) No deviation of the fluid at the inlet: an end-fed curtain coater

The problem of vortex creation comes from the junction between the inlet pipe and the manifold. It is similar to a problem of flow in a Tee. As a result, the behaviour of colours flowing into an end-fed cavity is studied to evaluate if this internal geometry could lead to better results. Indeed the angle of deviation between the inlet pipe and the manifold has a deep impact on vortex creation and we wanted to eliminate this change of direction.

To do so, half of the initial geometry was used where the inlet is located at the wider half cylinder (the centreline of our laboratory coater) as described on Figure 27. With these two geometries, we will be able to find the most appropriate geometry for our operating conditions.

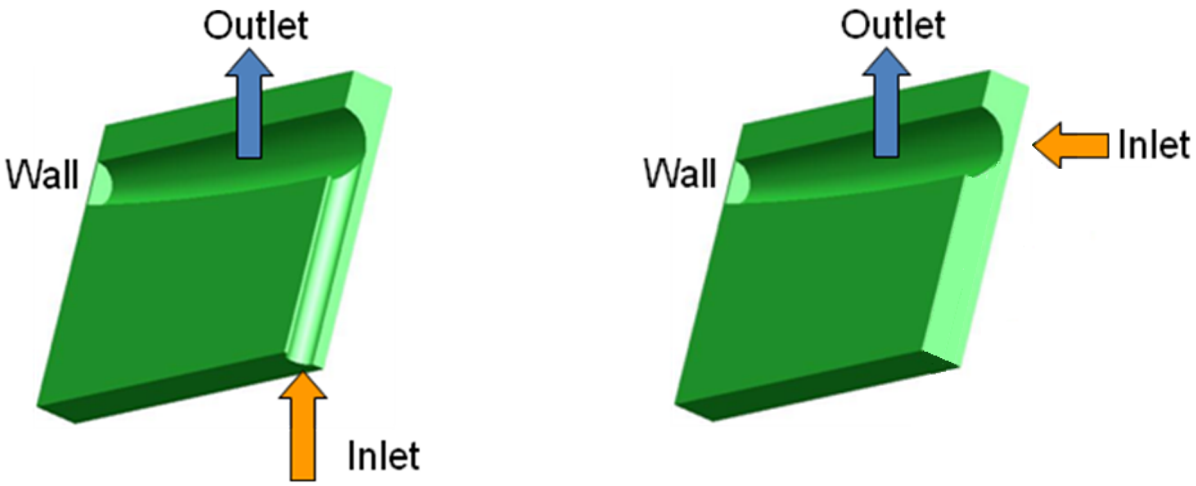

Half of the centre-fed system

End-fed system

Figure 27 : (left) and end-fed (right) curtain coater designs.

Several simulations were run at the four flow rates used with the previous geometry for Newtonians and non-Newtonians fluids. The operating conditions were as follows:

- 4 flow rates: Q=0.5, 1.5, 3.0, 4.0 L/min (q=1.9, 5.8, 11.6, 15.4 L/m·min)
- Newtonian fluids with 3 viscosities: μ=100, 300, 600 mPa·s

- Power-law fluids with 3 power-law index values n=0.7, 0.8, 0.9 and 2 consistency index values K=300 and 600 mPa·s^n

Before analysing these results, we can make a preliminary comment on the difference of the Reynolds number at the inlet for Newtonian and power-law fluids. If we compare the values of the Reynolds number in the inlet pipe for the two geometries (Eq. 6), keeping the same flow rate and properties of the fluid, we get:

$$\frac{Re_2}{Re_1} = 2^{2-n} \cdot \left(\frac{\pi}{\pi + 2} \right)^n \cdot \left(\frac{D_1}{D_2} \right)^{4-3n} \tag{6}$$

where Re_1 and Re_2 are the Reynolds numbers at the inlet pipes of the centre-fed and end-fed manifolds respectively and D_1 and D_2 the diameters of the pipes.

We found with equation 6 that the Reynolds number for the end-fed manifold will be at least twice as low as the one with the pilot configuration at the same flow rate ($Re_1/Re_2 \approx 2$ for $n=1$ and $Re_1/Re_2 \approx 3$ for $n=0.7$). Thus this security will lead to less instability. The streamlines were plotted in the manifold for all cases and results of simulation showed that we got a vortex-free flow whatever the operating conditions. Figure 28 presents streamlines for a Newtonian fluid at a Reynolds number (Re =25) over the critical Reynolds number found for the centre-fed configuration (Re_c =20) and there is no vortex in the manifold.

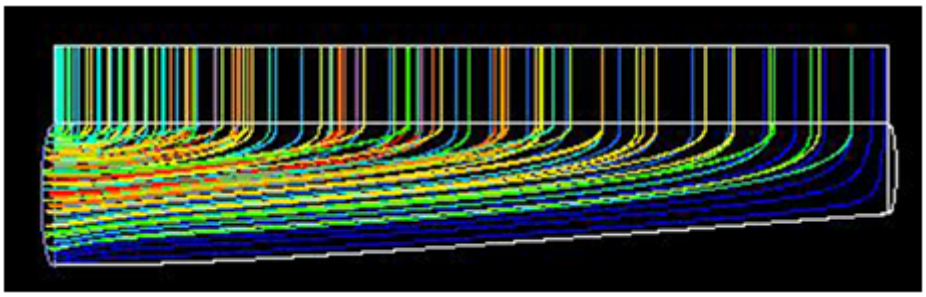

Figure 28 : Streamlines in the first cavity and slot of an end-fed curtain coater for a Newtonian fluid at Re =25.

Another important point is the absence of deviation of the flow at the inlet of the end-fed manifold compared to the case of the centre-fed manifold. In order to study the influence of the deviation of the flow on vortex creation, an extreme operating condition was tested and we observe that the flow is vortex-free (Figure 29). For this test, a very high flow rate was simulated (q=116 L/m·min which is 10 times the highest flow rate available with the pilot coater) and the Reynolds number is equal to 280. Here again, we could not find any vortex formation so a primary conclusion was that this new configuration seemed better than the centre-fed configuration. These results are consistent with those obtained by Wen and Liu, [32].

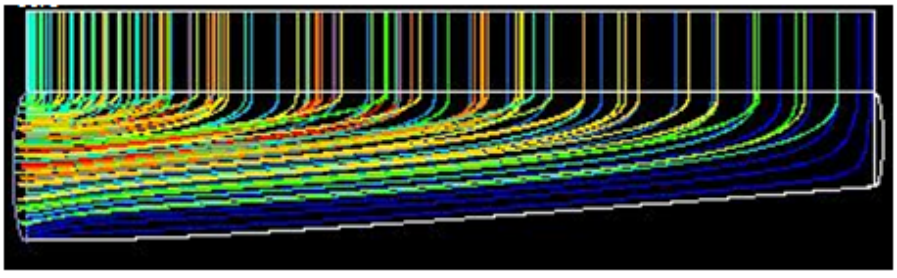

Figure 29: Streamlines in the first cavity and slot of an end-fed curtain coater with extreme operating conditions for a Newtonian fluid at Re =280.

It is well known that there may be some problems such as non-uniform distribution and residence time [32] with an end-fed manifold. With a proper geometry and eventually fluid recirculation, non-uniformity of the flow can be solved. We do not expect changes in fluid properties with variations of residence time. The only problem that could occur with this new geometry is the settling of particles of calcium carbonate present in coating colours. We calculated the settling velocity for particles of calcium carbonate for a wide range of viscosity and compared these values to those found by simulations close to the wall on the end of the centre-fed and end-fed curtain coater. The equation for the settling velocity of a particle in a Newtonian fluid is:

$$V_s = \frac{\left(\rho_p - \rho_f\right) g\, r^2}{4.5\mu} \tag{7}$$

where V_s is the settling velocity, ρ_p is the density of the particle (kg/m^3), ρ_f is the density of the fluid (kg/m^3), r is the radius of the particle and μ is the viscosity of the fluid (Pa.s) and g the gravitational acceleration.

Table 8 gathers the settling velocity of particles of calcium carbonate for several viscosities. The radius of the particles and their density were found on the data sheet of the dispersion of Carbital used for coating colours.

Table 8: Settling velocity for particles of calcium carbonate for several viscosities of the fluid (Particle radius: 1 µm, Solid density: 2830 kg/m^3, Fluid density: 1000 kg/m^3) .

Viscosity (mPa·s)	Settling Velocity (m/s)
100	$4.0 \cdot 10^{-8}$
300	$1.3 \cdot 10^{-8}$
600	$6.6 \cdot 10^{-9}$
800	$5.0 \cdot 10^{-9}$

In order to compare results of Table 8 to simulations, we plotted the y-velocity field in a plane close to the wall of the end of the new curtain coater for a low flow rate (Q=0.5 L/min – q=1.9 L/m·min) in order to compare the lowest value of the y-velocity in this plane with the settling velocity. Indeed, the velocity is equal to zero at the wall with the no-slip condition and when we increase the distance to this wall the velocity is higher. We wanted to observe the velocity in a plane close to the wall in order to find the size of the area when settling could appear and then conclude on this problem with the new geometry. On Figure 30, the plane is at 0.5 mm to the end of the new geometry of the curtain coater.

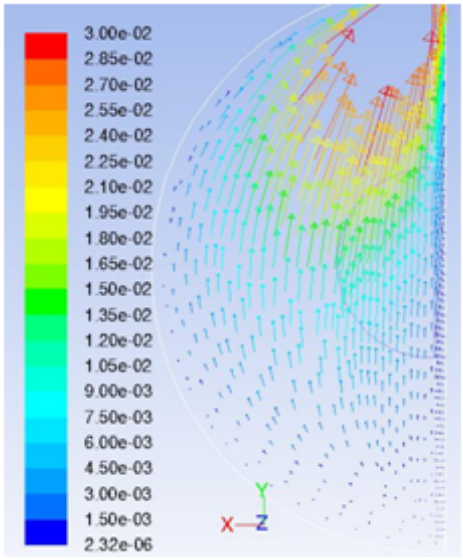

Figure 30: y-velocity vectors (m/s) in a plane at 0.5mm to the end wall for a Newtonian fluid with viscosity equal to 100 mPa·s at a flow rate of 0.5 L/min (1.9 L/m·min).

By comparing the settling velocity and the value of the lowest y-velocity in the plane at 0.5 mm to the wall in the end-fed curtain coater we can conclude that there will not have any settling with this new geometry at least in 99.96 % of the manifold since the particle settling velocity is at least 100 times lower than the minimum y-velocity of the fluid. The same simulation was run with the same inlet flow rate with the geometry of the CTP pilot and it was found, as expected, that the particles velocity is higher than the one of an end-fed curtain coater for several reasons: the inlet pipe is closer to the end of the manifold, the initial velocity is 2.7 times higher with the centre-fed geometry at the same flow rate since the inlet area is 2.7 times lower than in the centre-fed geometry..

So to conclude with this part, solutions to reduce vortex creation are:

- an increase of the diameter of the inlet pipe in order to reduce the Reynolds number
- or a new internal geometry (end-fed geometry) which will not create instabilities in the inlet area since for a given flow rate the Reynolds number is twice as low and there is no deviation of the flow. Nevertheless the critical point for an end-fed curtain coater is its practical making which is more difficult to achieve.

The main parameters in the manifold are the Reynolds number in the inlet pipe for a given geometry and the angle of deviation. That is why a centre-fed manifold with a more progressive inlet shape, *i.e.* a trumpet like pipe, should be efficient to avoid instabilities.

2.2.3.5. Influence of pump pressure pulsations

In order to totally close the study of the flow in the manifold, we will focus in this part on the influence of disturbances at the inlet caused by the pump on vortex formation. We demonstrated earlier that the Reynolds number is a relevant parameter to characterize the internal flow. On pilots, it is obvious that pumps can generate some disturbances at a certain frequency and we wanted to know if these disturbances were strong enough to create instabilities in the internal flow since it can increase or decrease the Reynolds number. The pumps of our pilot are Moineau progressing cavity pump from PCM (pigtail-like pump). This type of pump transfers fluid by means of the progress, through the pump, of a sequence of small, fixed shape, discrete cavities, as its rotor is turned (Figure 31). This leads to the volumetric flow rate being proportional to the rotation speed. Hence these pumps have

application in fluid metering and pumping of viscous or shear sensitive materials. Generally the flow rate fluctuation is very low and it was impossible to get relevant values from discussions with pump suppliers, so we will consider that the maximum fluctuation is ±10 % of the average flow rate, which is indeed much higher than the real value. We must also know the frequency of perturbations and we found in the data sheet of the PCM pump that frequencies of disturbances are between 1 and 5 Hz at the flow rates we used.

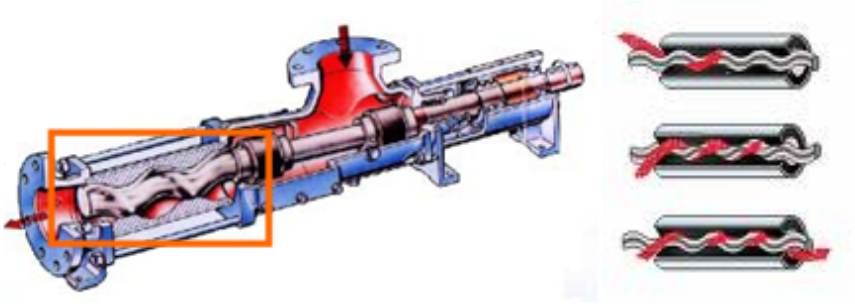

Figure 31: Progressing cavity Moineau pump.

In order to simulate a pulsation of the pump, a user defined function is required under Fluent, and we defined the equation of the velocity in the pump outlet as follows:

$$V(t) = V_0\left(1 + A\sin(\omega t)\right) \tag{8}$$

where $V(t)$ is the velocity at the time t, V_0 is the average velocity, A is the relative magnitude of the oscillation and ω is the pulsation.

The simulations were run with unsteady flow condition and values were recorded at the times when the maximum, average and minimum inlet velocities are reached.

We ran simulations for two Newtonian fluids at the same Reynolds number. This Reynolds number was chosen just above the value of vortex creation in order to see if it leads to strong disturbances or not. The operating conditions were the following:

- Simulation A: Q=2.0 L/min (q=7.6 L/m·min), μ=300 mPa·s and ρ=1200 kg/m^3
    - Frequency of the disturbances: 1 and 5 Hz
    - Magnitude of the oscillations: 1, 5 and 10 % of the average velocity
- Simulation B: Q=4.0 L/min (q=15.4 L/m·min), μ=600 mPa·s and ρ=1200 kg/m^3
    - Frequency of the disturbances: 1 and 5 Hz
    - Magnitude of the oscillations: 1, 5 and 10 % of the average velocity

Simulation results were compared and we concluded on the influence of the variation of the flow rate in the pump. It was found that the oscillation of the flow rate up to 5 % of the average value has no impact on vortex formation. Indeed, this perturbation is too small to lead to bigger disturbances in the cavity. Figure 32 is an example of the simulation results. Results for an oscillation of the flow rate up to 1% are not presented here but they reveal the same trend. We plotted on Figure 33 the streamlines for a higher magnitude of oscillations and even if it is possible to see a small difference between simulations with 10 % relative magnitude of oscillations, there is clearly no impact of pump disturbances on vortex formation in the laboratory coater.

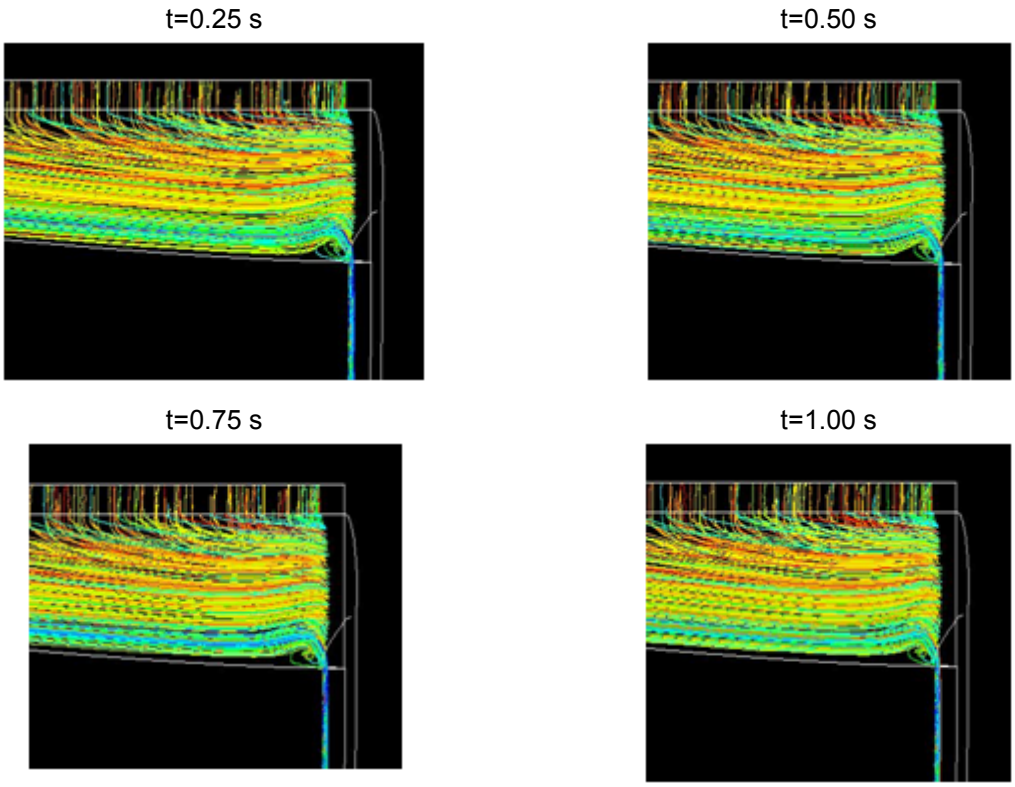

Figure 32 : Influence of oscillating flow rate on vortex formation for the fluid A Frequency of oscillations1 Hz and relative magnitude 5 % of the average velocity.

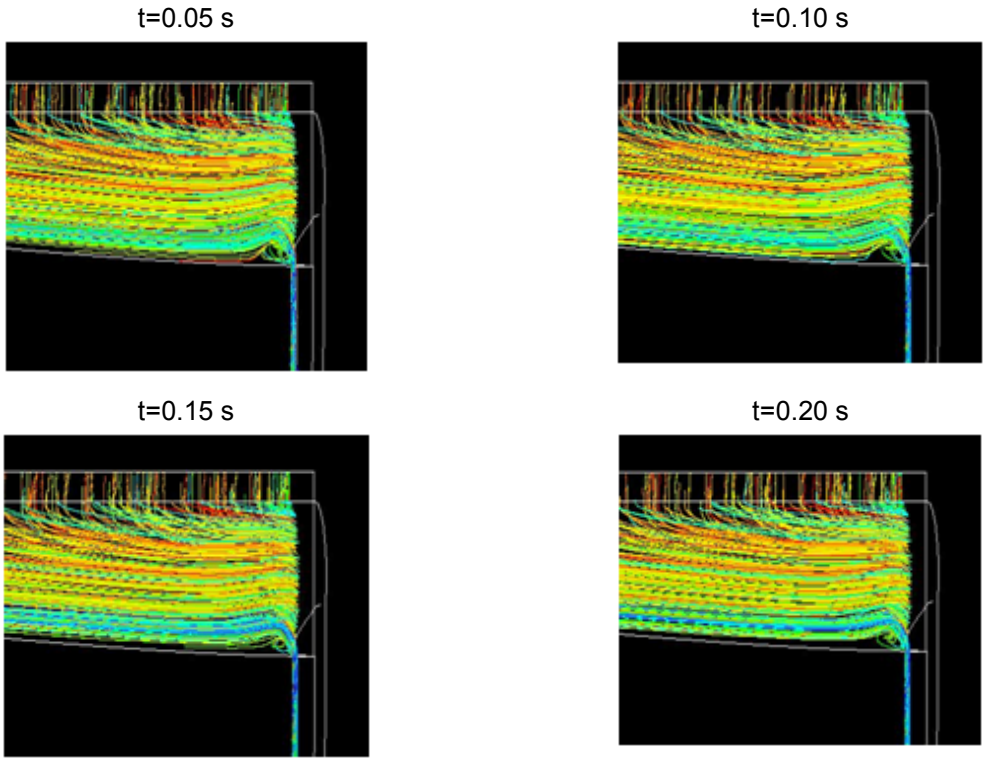

Figure 33: Influence of oscillating flow rate on vortex formation for the fluid B Frequency of oscillations 5 Hz and relative magnitude 10 % of the average velocity.

Finally, we compared results for different fluids and different frequencies at the maximum velocity in the oscillating flow. We wanted to validate the fact that the frequency has no influence on disturbances and that it is the Reynolds number in the inlet pipe which predominates. Figure 34 shows that streamlines are the same at a constant Reynolds number whatever the fluid or the frequency. So we can conclude here that the flow disturbance eventually caused by the pump will not have any influence on internal flow instabilities since the variation of flow rate is not so strong.

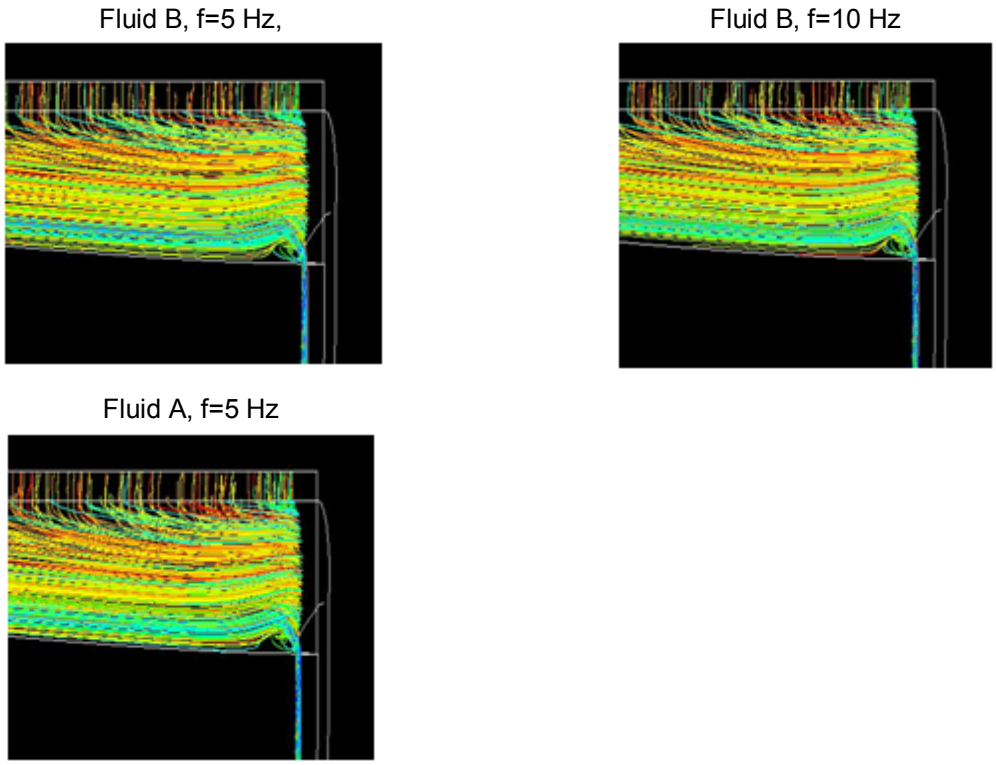

Figure 34: Influence of oscillating flow rate on vortex formation for different operating conditions (relative magnitude of oscillations 10 %, at maximum velocity).

2.2.4. Conclusions

A 3D-CFD simulation of the flow with experimental validations of the flow in a manifold of a curtain coater was presented in this part. We found relevant parameters both for Newtonian and non-Newtonian fluids on flow uniformity which are the Reynolds number in the inlet pipe and the deviation between the inlet pipe and the manifold. Moreover, simulation permitted to show that the yield shear stress has no influence on the behaviour of the flow in the manifold for the range studied (under 3 Pa).

We demonstrated that increasing the Reynolds number leads to flow perturbations. The power-law index has also a deep impact on flow uniformity since decreasing it leads to a lower apparent viscosity in the area of vortex formation but it is taken into account with the Reynolds number. To maintain vortex-free operation, the value of the Reynolds number at the manifold inlet must not exceed a critical value, which is equal to 20 with the geometry of the laboratory coater used.

Tests of flow visualization in the manifold on a replica in Plexiglas of our pilot curtain coater were carried out to clearly validate all these results. Two methods were used, one with tracers and the other one with a 2D-PIV. The flow visualization with tracers is very simple and well adapted to our study since it is possible to clearly see the transition between vortex-free flow and the vortex creation. Concerning the 2D-PIV, this technique is an alternative to tracers in order to quantify the velocity field and the velocity vectors of fluids in the whole manifold. Nevertheless it seems less accurate for the distinction of the transition vortex-free/vortex creation in the manifold. The simulation results are validated by the experimental study.

Finally we demonstrated that disturbances possibly caused by the pump had no impact on vortex formation.

We also proposed some solutions to improve flow uniformity such as increasing the radius of the inlet pipe or changing the internal geometry to an end-fed geometry. Indeed, our geometry which is a centre-fed curtain coater is not the most appropriate for the range of fluids used since flow simulations in an end-fed curtain coater with the same fluids proved to be better. Nevertheless, from a practical point of view, manufacturing the manifold of an end-fed curtain coater is harder and therefore more expensive.

2.3. CFD simulation of the flow in the second cavity

One option in the design of flow distribution manifolds is the inclusion of additional cavities in the slot region which is the case on our curtain coater. It provides another chance for flow across the die if a non-uniform distribution resulted from the flow out of original cavity [16, 24, 25, 28, 34]. Nevertheless Lee and Liu [24] had shown that it could lead to the formation of a vortex which can cause polymer degradation, deteriorate product quality and generate sedimentation, notably when the Reynolds number increases. There are many articles dealing with this problem in two dimensions for rectangular cavities which is a similar problem. As it was done in the manifold, we will simulate the flow in the second cavity with Newtonian and non-Newtonian fluids and analyse the influence of rheological parameters of the fluid and geometrical parameters of the cavity on the flow.

2.3.1. Meshing of the second cavity meshing in two dimensions

The second cavity has been meshed with Gambit® but in two dimensions since its shape is constant widthwise. The fact that the simulations will be in two dimensions will greatly reduce the computing time since there are only a few thousand elements. The Copper meshing algorithm is used here to automatically create an unstructured, hexahedral mesh and is presented on Figure 35. The skewness of the meshing was checked and was good.

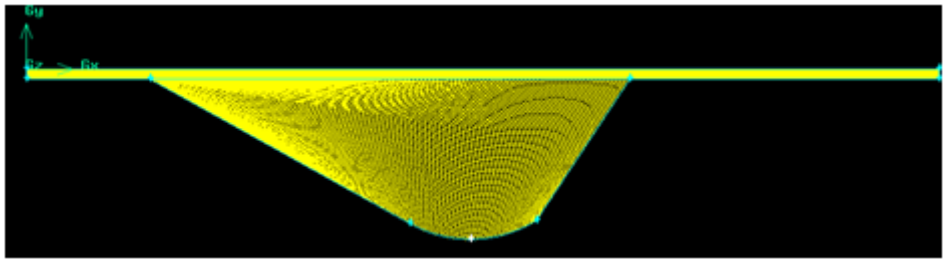

Figure 35 : Meshing of the area of the second cavity.

2.3.2. CFD simulation results of the flow in the second cavity

2.3.2.1. Influence of the divergent angle of the cavity and of the power-law index of the rheological properties of the fluid on the flow

The second cavity is depicted in Figure 36 where the thickness of the slot is in the z-direction. The first angle is called the divergent angle (30° in our case) and the second one is the convergent angle.

The mainstream of liquid in the inner cavity is in the y-direction. However, as the fluid moves toward the outer cavity, it gradually reduces to nearly 2 dimensional flow (*i.e.* the x-component of the fluid velocity is small). Moreover, the shape of the cavity is the same along the width of the coater. Therefore the flow field in the outer cavity can be approximated by a two-dimensional flow model as shown on Figure 36, if our aim is not to analyse the effect of transverse defects of the die.

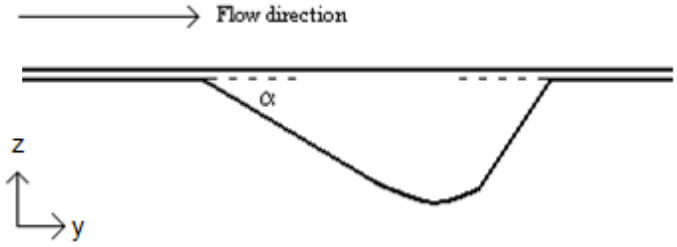

Figure 36 : Shape of the laboratory outer cavity.

The meshing was presented earlier on Figure 35 and the downstream slot length was selected long enough to ensure that the fluid flow had fully developed profiles.

Five different divergent angles between 15° and 90° (round shape) were tested for power-law fluids with a power-law index between 0.7 and 1, which are values close to those of coating colours.

Similarly to Lee and Liu, we take the inlet Reynolds number as reference in order to specify the flow rate in simulations. The mathematical expression of the generalized Reynolds number for the case of power-law fluids flowing between two planes is [63]:

$$Re = \frac{12\rho V^{2-n} D_h^n}{4^n \left(2+\frac{1}{n}\right)^n K} = \frac{12\rho V^{2-n} H^n}{2^n \left(2+\frac{1}{n}\right)^n K} \tag{9}$$

where ρ is the density of the fluid, V the flow velocity, D_h characteristic length which is here two times the slot gap (H), K the consistency index of the fluid and n the power-law index.

All the tested configurations are gathered on Table 9: Summary of the simulation cases for power-law fluids in the second cavity. in which the values of the divergent angles, power-law indexes (the same used for the manifold), the operating conditions. In this table, we also add on a comment on simulation results, *i.e.* the eventual presence of a vortex in the second cavity and its size.

Table 9: Summary of the simulation cases for power-law fluids in the second cavity.

Test number	Divergent angle			Power-law index				Operating conditions	Presence of a vortex and size
	30°	60°	90°	0.7	0.8	0.9	1		
1	X						X	Re=10	No
2		X					X		No
3			X				X		No
4	X						X	Re=45	No
5		X					X		Yes, a small one
6			X				X		Yes a third of the cavity
7	X						X	Re=110	Yes, a small one
8		X					X		Yes, half of the cavity
9			X				X		Yes, in all the cavity
10	X			X				24 L/m·min	Yes, half of the cavity
11	X				X				Yes, quarter of the cavity
12	X					X			Yes, a small one
13	X						X		No
14-33	X			X	X	X	X	Several Re in order to find the Re_c	No, below the Re_c and Yes over the Re_c
34-53		X		X	X	X	X		
54-73			X	X	X	X	X		

The flow patterns for a Newtonian fluid with several divergent angles and different Reynolds number are shown on Figure 37. It is clear that, whatever the divergent angle, as the Reynolds Number increases, a vortex that is indicated by closed streamlines starts to appear and grows in size. Moreover, at constant Reynolds number, we can observe that the vortex is bigger for a cavity with a higher divergent angle.

The effect of the power-law index on vortex formation for a power-law fluid passing the second cavity is shown in Figure 38 at a constant flow rate. As it was found with the manifold in 3 dimensions, decreasing the power-law index while keeping constant the flow rate, leads to a bigger vortex. It appears that increasing the Reynolds number leads to a bigger vortex and it centre moves to the left of the cavity.

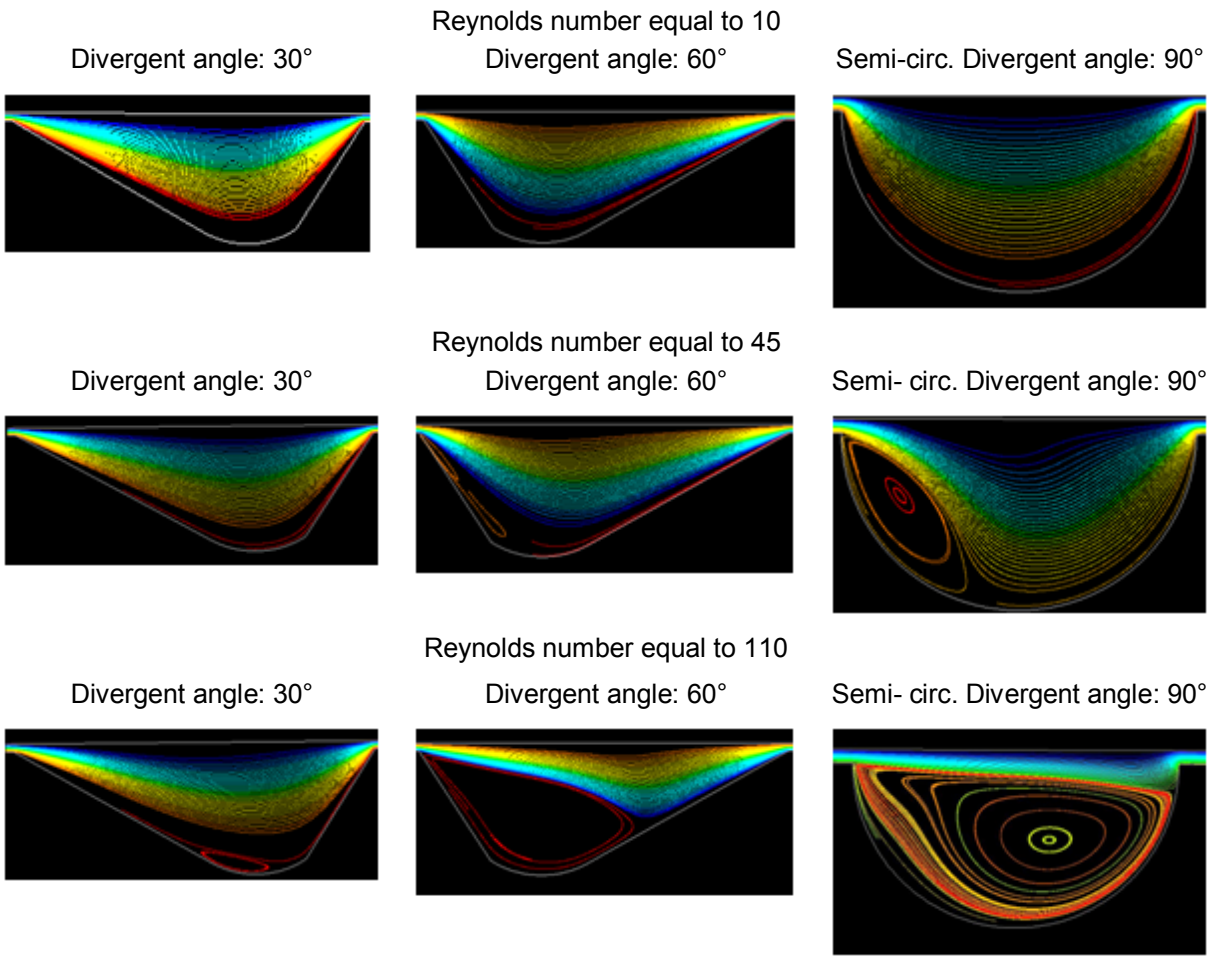

Figure 37 : Streamlines for a Newtonian fluid in different cavities and several values of the Reynolds number.

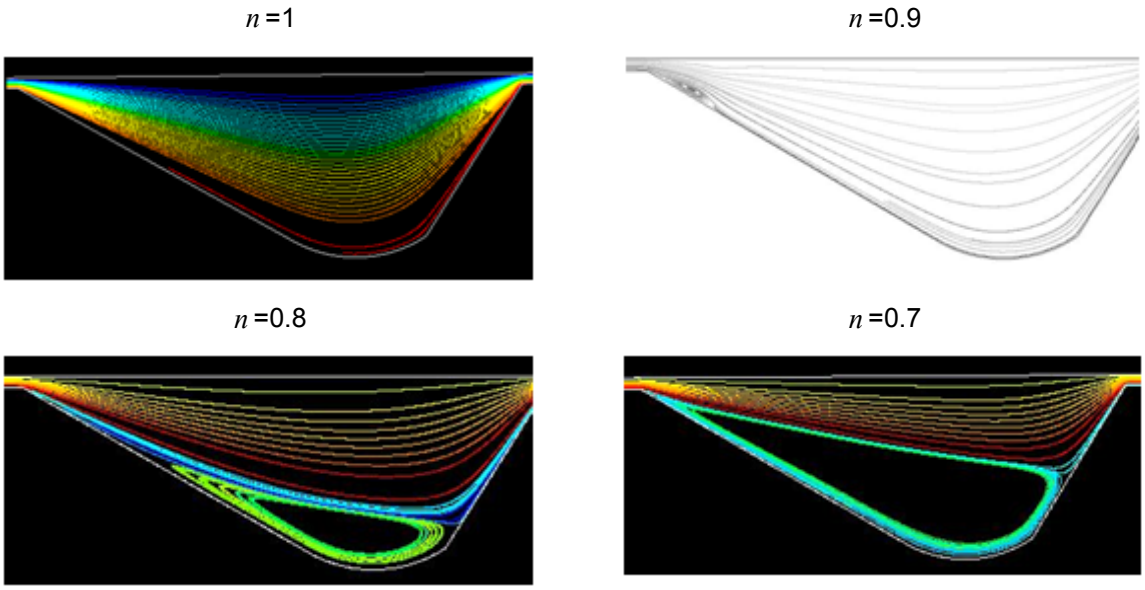

Figure 38 : Influence of power-law index on vortex formation at q=24 L/m·min.

2.3.2.2. Influence of the Reynolds number on the flow

Similar to the case of the flow in the manifold, it appears that there is a critical value of the Reynolds number, above which a vortex appears in the outer cavity whatever the fluid. For each divergent angle, we simulated the flow of power-law fluids with a power-law index ranging between 0.7 to 1 in order to determine the value of the critical Reynolds number. The solution process started from a very low velocity and then successive simulations were run by incrementing the velocity until we found the creation of vortex as depicted on Figure 39. The estimated precision on the critical Reynolds number is better than 1%.

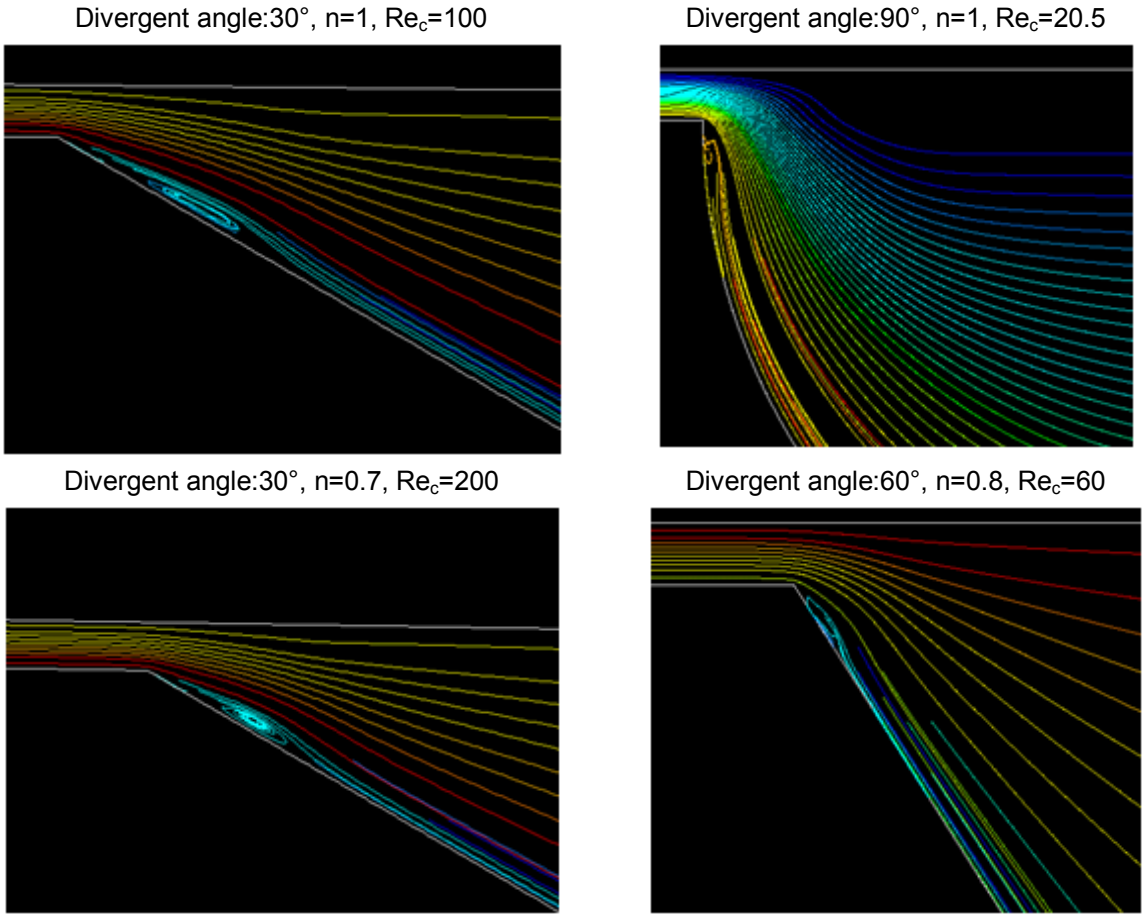

Figure 39 : Critical Reynolds number for non-Newtonian fluids at a consistency index of 100 mPa·s^n for different cavity geometries.

It is clear that the divergent angle and the power-law index have a huge impact on the value of the critical Reynolds number for the second cavity. All our results are displayed on Figure 40 in terms of critical Reynolds number, and in terms of critical flow rate on Figure 41. Indeed, thinking in terms of flow rate could be more convenient for industrials but these values have to be calculated for a given consistency (K =100 mPa·s^n in this case). Nevertheless, the tendency will remain the same whatever the consistency index; there will only have a shift. On Figure 40, where the value of the critical Reynolds number is plotted as a function of the power-law index, for several values of the divergent angle, the region below each curve corresponds to vortex-free conditions for the considered angle. The same type of result is shown on Figure 41, but here in terms of flow rate.

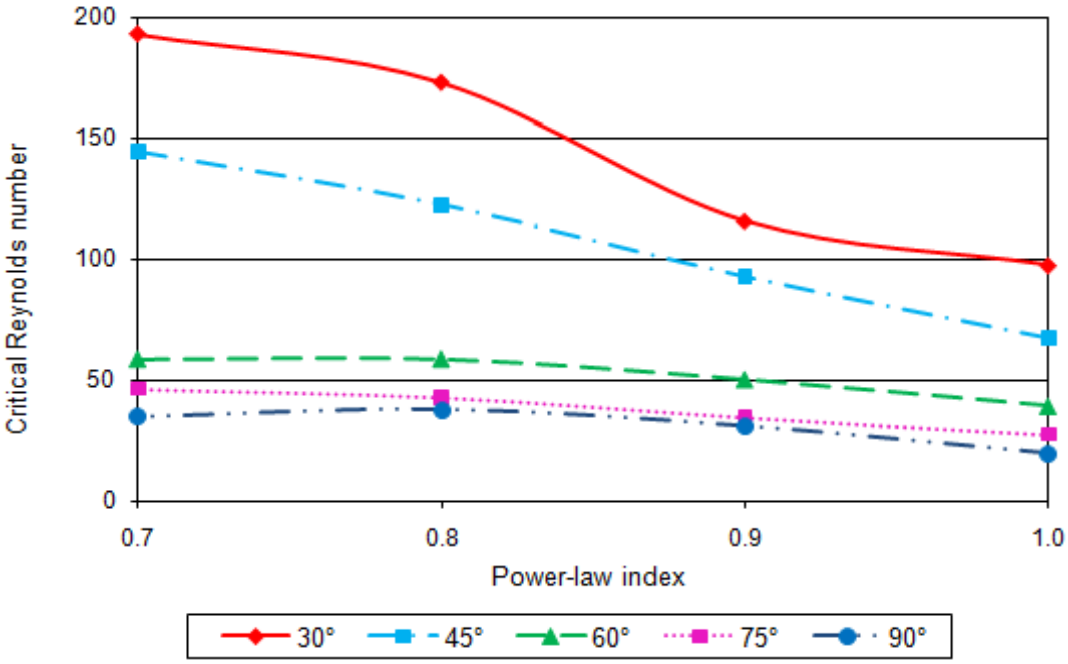

Figure 40 : Critical Reynolds number as a function of fluid power-law index and cavity divergent angle.

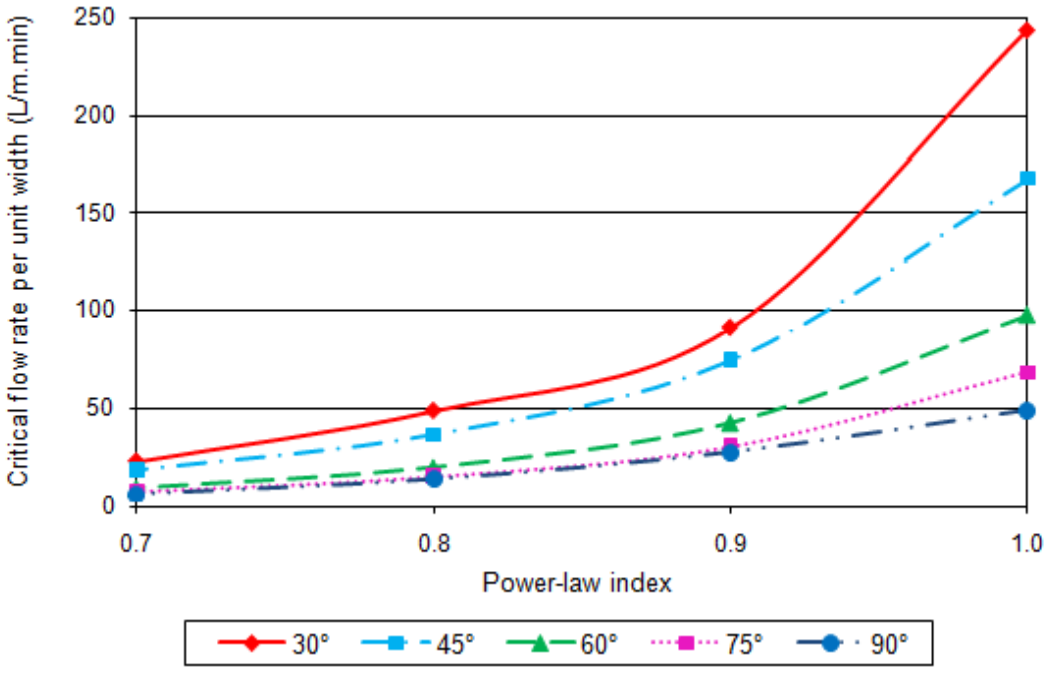

Figure 41 : Critical flow rate as a function of fluid power-law index and cavity divergent angle at K=100 mPa·s^n.

These results point out that, for any value of the power-law index, the critical Reynolds number (and the flow rate) is higher when the divergent angle is low. So to avoid vortex, a low divergent angle is recommended and that is the case with the pilot curtain coater where the divergent angle is equal to 30°.

Concerning the influence of the power-law index, we can notice that for a given geometry, decreasing the power-law index will increase the critical Reynolds number but reduce the critical flow rate (for a given consistency index). Indeed, the difference of critical flow rates between a Newtonian fluid and a fluid with a power-law index of 0.9 is really significant. These results show that it is better to have a fluid with a high power-law index to avoid flow perturbations. Moreover if the fluid with the lowest power-law index is tested and a vortex-free flow is observed, shear-thinning fluids with a higher power-law index will flow without disturbance problem in the second cavity with the same operating conditions.

These results foreground the results obtained by Leonard [23], concerning the usefulness of the second cavity. Indeed, for very strong shear-thinning fluids, a second cavity could be useless since the critical flow rates are very low. It would not provide another chance for flow to be more uniform but it would create more instabilities whereas for Newtonian fluids or fluids with a high power-law index (over 0.8), a second cavity is useful since it will not create any disturbances, and instabilities coming from the first cavity will be filtered.

Figure 42 displays the values of the critical Reynolds number as function of the power-law index for several values of the divergent angle. In this figure, we compared some of our results to those published by Lee *et al*. [28]. There is a huge difference between the values found by Lee and those obtained in the present work but results reveal the same trend. Indeed, for a given divergent angle, decreasing the power-law index leads to a higher critical Reynolds number and for a given power-law index, increasing the divergent angle decreases the critical Reynolds number.

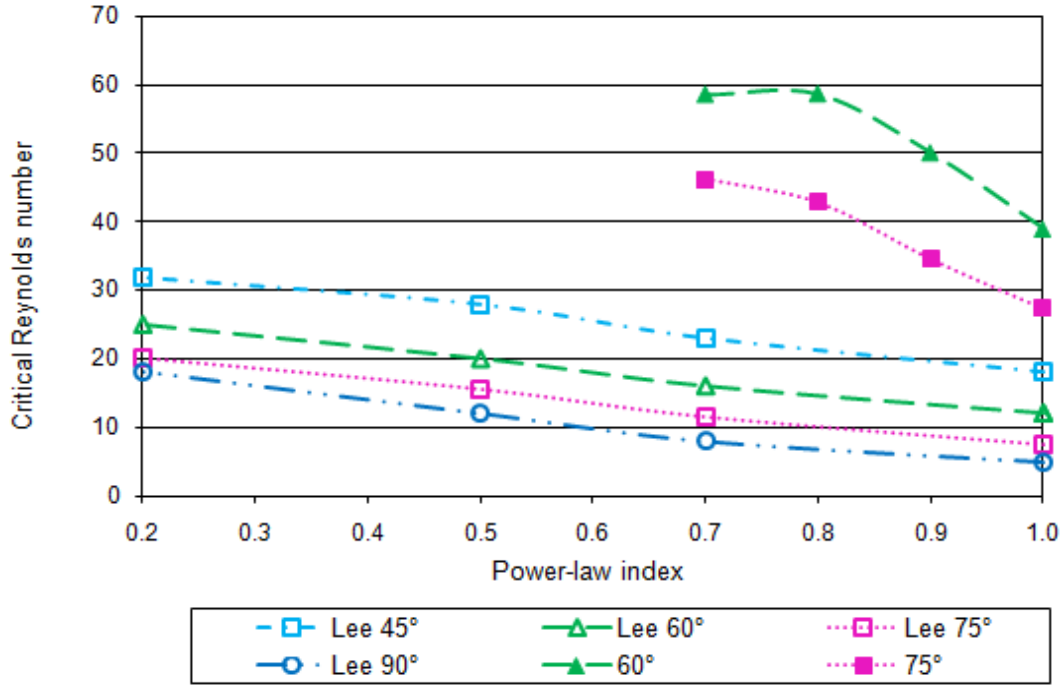

Figure 42 : Comparison of critical Reynolds number values for several values of the power-law index and cavity divergent angle at K=100mPa·s^n.

The difference partly comes from the definition of the Reynolds number. In fact, Lee did not use the generalized Reynolds number but a different expression of the Reynolds number:

$$Re = \frac{\rho V^{2-n} H^n}{K} \tag{10}$$

where ρ is the density of the fluid (kg/m^3), V the flow velocity (m/s), H the slot gap (m), K the consistency index of the fluid (Pa.s^n) and n the power-law index. The ratio of these two expressions of the Reynolds number, κ , is a function of the power-law index:

$$\kappa = \frac{\left[2 \cdot (1+2n)\right]^n}{12} \tag{11}$$

It is equal to 0.5 when the power-law index is equal to unity and 0.25 when the power-law index is equal to 0.7.

Using the same definition of the Reynolds number, for instance the generalized Reynolds number, then we can compare the results of the present study to those obtained by Lee and Liu, as shown on Figure 43. The shift observed on Figure 42 is reduced but there still remain some differences that we cannot explain. Yet, for a given power-law index, increasing the divergent angle decreases the critical Reynolds number.

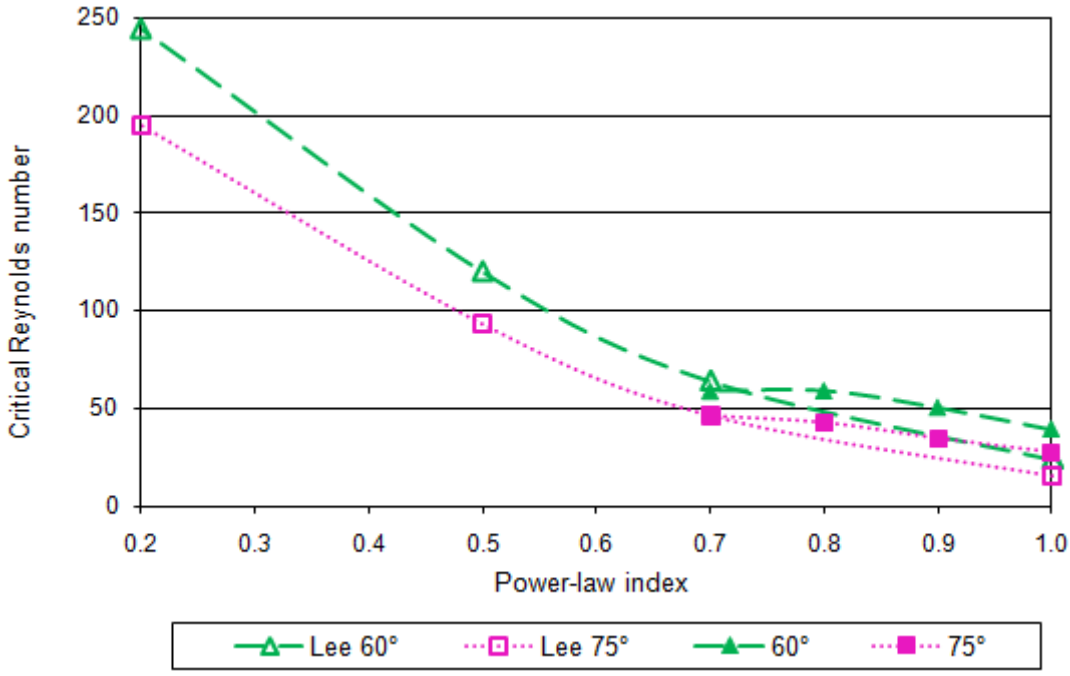

Figure 43 : Comparison of critical Reynolds number values with the same Reynolds number equation for several values of the power-law index and cavity divergent angle, at K=100 mPa·s^n.

We finally compared the values of the flow rate when the critical conditions are reached either in the manifold or in the second cavity, in order to conclude on the usefulness of this second cavity for the pilot curtain coater. In the manifold we found that the critical Reynolds number is equal to 20 whatever the rheological parameters of the non-Newtonian fluids whereas in the second cavity, it varies with the power-law index of the fluid and the divergent angle of the cavity. From the results plotted on Figure 42, the worst case is when the cavity divergent angle is equal to 90° and the fluid has a power-law index equal to 0.7. In this case,

the critical conditions are reached for a flow rate equal to 1.6 L/min. Then, the Reynolds number in the inlet pipe would be 225, which is much higher than the critical Reynolds number at the manifold inlet. Therefore, it means that if the fluid enters the manifold without any perturbations, then it will pass through the second cavity without any problems.

2.3.3. Conclusions

Results generated by the two-dimensional simulation of the second cavity indicate that a vortex can appear close to the entrance of this cavity, in the divergent region. A decrease of the angle could prevent any vortex creation. We also found that the power-law index has a deep impact on flow uniformity, indeed fluids with a very strong shear thinning behaviour will create vortex in the second cavity. This result was in accordance with what Leonard found on the usefulness of the second cavity [23].

It should be noticed that no experimental validation had been done owing to the shape and size of the cavity in the pilot but we compared our results of critical Reynolds number to others found in literature. We noted that they revealed the same trend, but it required using the same definition of the Reynolds number which was not originally the case.

The last point studied is the usefulness of the second cavity on a curtain coater with a centre-fed curtain coater (with the geometry of the studied pilot). We demonstrated that, whatever the operating conditions and the values of the rheological parameters of the fluids tested, the critical flow rate is higher in the second cavity, which means that, in our case, the second cavity will not create any disturbances and can act as a filter to reduce non uniformity of the flow coming from the manifold.

2.4. Conclusions on the study of the internal flow

In this part, our objective was to study the flow inside the coater. In order to do that we divided the problem of the internal flow into two parts which are the flow in the inlet pipe with the manifold and the one in the second cavity with the first and second slot. Indeed the geometries of these two parts are totally different and that is why we performed 3D- CFD simulations for the manifold and 2D-CFD simulations for the second cavity since its shape is constant widthwise. Concerning the manifold, we carried out experiments on a replica of the curtain coater made of Plexiglas which was especially designed and manufactured for this study, and then we compared these simulations to results. Two methods of measurements were used, namely the use of tracers to observe streamlines and detect vortex creation and 2D-PIV in order to have the velocity fields inside the manifold. For the second cavity, it was not possible to carry out experiments and thus validate simulation results but a comparison to the literature was done.

From the CFD simulations in the manifold, we found a relevant parameter both for Newtonian and non-Newtonian fluids on flow uniformity: it is the Reynolds number. We demonstrated that increasing the Reynolds number led to flow perturbations at the junction between the inlet pipe and the manifold. For non-Newtonian fluids, the power-law index has also a deep impact on flow uniformity since decreasing it, leads to a lower apparent viscosity in the area of vortex formation but it is taken into account with the Reynolds number.

Moreover, simulation permitted to show that the yield shear stress has no influence on the behaviour of the flow in the manifold for the range studied (under 3 Pa). This was confirmed by calculating the wall shear stress for several Newtonian and non-Newtonian fluids and comparing it to the yield shear stress, indeed the values are less than 5 % compared to the

wall shear stress in all the studied cases. We found that there is a critical Reynolds number at the inlet which is equal to 20 for the studied geometry. To maintain vortex-free operation, the Reynolds number at the inlet should not exceed this critical value. This value is specific of this special geometry. It means that if the geometry were different, the critical Reynolds number would not be the same.

Experiments were carried out on a transparent replica of the pilot coater in order to validate the simulation results. For the first method, we injected dye tracers at the wall of the inlet pipe and visualized the streamlines in the manifold. This simple method led to satisfactory results. It is indeed possible to clearly see the transition between vortex-free flow and the vortex creation. We validated the fact that vortices exist and are located in the area found by simulation and also as expected that the flow was symmetrically distributed at the junction of the inlet pipe with the manifold since vortices are symmetrical in the manifold. Moreover, we recover a critical Reynolds number between 19 and 21, whatever the rheological behaviour of Newtonian and non-Newtonian fluids, which is close to the value found previously by simulations. Concerning the 2D-PIV, this technique is an alternative to tracers in order to see the rheological behaviour of fluids in the manifold, moreover it is possible to obtain the velocity field and have numerical values of this field. The 2D-PIV is not suitable for visualization of velocity fields on the internal flow for coating colours since they are opaque. However, it permitted to add another validation of results found with Newtonian and non-Newtonian fluids using transparent fluids (PVOH and Carbopol solutions). Results found with this method are very close to those found by CFD simulations and with the tracer injection method since the shape of vortex is identical and the value of the critical Reynolds number is close to 20. Nevertheless, it seems somewhat less accurate for the distinction of the transition vortex-free/vortex creation in the manifold. Finally CFD simulation results are in accordance with those of the experimental part.

We demonstrated with the CFD software that disturbances eventually caused by the pump had no impact on vortex formation whatever the frequency of the perturbation and proposed some solutions to improve flow uniformity such as increasing the radius of the inlet pipe or changing the internal geometry to an end-fed geometry. Indeed, at constant flow rate, the Reynolds number varies in the same way as the reciprocal of the diameter size for a Newtonian fluid, therefore increasing the radius of the inlet pipe improves the uniformity of the flow by reducing the Reynolds number. The second solution proposed was to totally change all the geometry of the curtain coater to an end-fed curtain coater. This geometry permitted to eliminate the angle of deviation between the inlet pipe and the manifold which has a deep impact on vortex creation. Simulations showed that the geometry of the curtain coater pilot used is not the most appropriate for the range of fluids used since there is no vortex in the manifold whatever the operating conditions. The only problem that could occur with this new geometry is the settling of particles of calcium carbonate present in coating colours. In order to evaluate this impact on flow uniformity, we calculated the settling velocity for particles of carbonate for a wide range of viscosity and found that they were at least one hundred times lower than the lowest vertical velocity in the end-fed curtain coater found by simulations. The main drawback in this case is its manufacturing which is not easy to implement.

The second cavity in the internal flow could provide another chance for flow across the die if a non-uniform distribution resulted from the flow out of the original cavity. Results generated by the two-dimensional CFD simulation of the second cavity indicate that a vortex can appear just after the first slot and a decrease of the divergent angle could prevent a vortex creation. We also found that the power-law index has a deep impact on flow uniformity,

indeed fluids with a very strong shear thinning behaviour will create a vortex in the second cavity for a given geometry. In order to validate our simulations, we compared our results of critical Reynolds number to others found in literature and found that they revealed the same trend. A difference of these values can be observed because of the definition of a different Reynolds number.

The last point studied is the usefulness of the second cavity on the studied pilot curtain coater. We demonstrated that whatever the operating conditions and the rheological parameters of all the fluids the critical flow rate is higher in the second cavity than in the manifold, which means that there is a window of Reynolds number where a vortex is present in the manifold and not in the second cavity, therefore in this case it can act as a filter to reduce non uniformity of the flow coming from the manifold. Moreover, if the fluid passes through the manifold without any perturbations, then it will pass through the second cavity without any problems.

These results permit to increase fundamental knowledge of key parameters governing the curtain coater process and could be applied industrially to reduce streaks on the final coated paper after a rheological characterization of coating colours.

We can now focus on the next part of this PhD work, which is the simulation of the flow of liquid films down an inclined plane.

3. Study of liquid film flow down the inclined plane

In the curtain coating process, the inclined plane itself provides a means by which individual layers can be stacked on top of another one; at the end of the plane and after the curtain, these layers are deposited simultaneously on a moving substrate. But it is well-known that the flow down the inclined plane can be very unstable. Literature showed us that it could create waves on fluid interfaces called barring that can be translated onto the substrate and lead to coating defaults such as periodic coverage variations contrary to defects into the internal cavities which bring about streaks on the final product. These waves occur also in geophysical phenomena such as on glaciers (Figure 44). That is why the knowledge of the conditions under which these waves can develop is an important point. Indeed it is interesting to understand how these instabilities occur and propagate to avoid a spoiling of the final product.

Figure 44: Apparent waves on the Leschaux glacier (Mont-Blanc massif).

Literature shows that the influence of several parameters changes depending on long or short wavelength conditions and in interface or surface mode. Regarding the CTP pilot case, we can approximate the wavenumber and the wavelength in order to see if we should find small or long waves in curtain coating. The thickness of the film is about 1mm and we found in the data sheet of the CTP pilot pump that frequencies of disturbances are between 1 and 5 Hz. We know that the wave velocity is two times greater than that of the fluid. If we calculate the velocity for a flow rate Q=1.9 L/m·min, which is the minimum flow rate acceptable on the CTP pilot, and approximate that the depth of the film is 1mm, then we get:

$$\alpha = \frac{2\pi d}{\lambda} = \frac{2\pi df}{v_w} \approx \frac{2\pi \times 10^{-3} \times 5}{0.033 \times 2} \approx 0.5 \qquad (12)$$

Thus, we will focus here only on cases of long wavelength and both interface and surface modes for Newtonian fluids since single or multi-layer curtain coating is used.

The extensive literature review on the stability of Newtonian flow down an inclined plane in multi-layers provided us with some practical parameters to reduce or avoid instabilities. It was found that the best configuration is an increase of depth and viscosity from the bottom to the upper layer. A low viscosity middle-layer configuration has to be avoided because it is the

worst configuration. Nevertheless there is still a lack of knowledge on non-Newtonian stability, especially for multi-layer systems of only shear-thinning fluids.

All analyses were restricted to two-dimensional wave disturbances in the vertical plane since it was pointed out in the literature that each three-dimensional disturbance is governed by the same equations of a two-dimensional disturbance in a similar flow at a low Reynolds number. This simplification is therefore completely adequate if only the stability of the flow is questioned and the computing time will be greatly reduced.

In this study, we performed 2D-CFD simulations of the flow down the inclined plane in order to understand the conditions of the development of waves for three layers with several operating conditions. We first carried out a short parametric study in order to validate the model used and then performed a comparison between simulations and bibliographic results for the case of three Newtonian fluids flowing down the inclined plane of the curtain coater with the influence of viscosity and depth stratifications. After that a focus on what really happens for the range of operating conditions used was done in order to quantify the influence of the flow down the inclined plane on the overall stability.

3.1. Simulation of the flow on the inclined plane

On the CTP pilot coater, the inclined plane is composed of three straight sections that are 3.95 cm long followed by a curved one that is about 3.5 cm long. A coating layer is delivered just upstream of a straight section. The curtain is delivered at the tip of the curved section.

3.1.1. Meshing geometry

In order to simulate the flow on the inclined plane, the geometry of the system had to be drawn and then meshed. Similar to the study of internal flow, we determined the geometry of the device, including the regions downstream of the outer slots where the fluids are delivered onto the inclined plane, with a Laser Triangulation Sensor developed in the CTP. We measured the coordinates of some points and then the inclined plane with its three inlets (outlets of the die outer slots) was drawn and meshed in two-dimensions with Gambit using PAVED and MAPPED meshes.

Before meshing the inclined plane and the area over it where the three fluids and a layer of air are simulated, the distance between two nodes on the thickness had to be calculated. Indeed, the evolution of the waves on fluid interfaces is the subject of this study and the meshing could act as a filter of these waves if the amplitude of the oscillation of the fluid is lower than the distance between two nodes. In order to integrate this recommendation, the mathematical equation that describes the thickness of a layer of fluid as function of rheological and geometrical parameters and operating conditions was used.

We consider a fully-developed liquid film flow down an inclined plane (Figure 45) with a laminar and steady state.

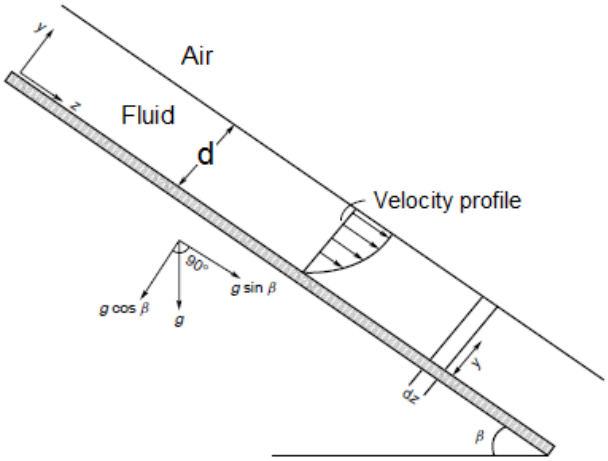

Figure 45: Fluid flow on an inclined plane.

The mathematical equation that describes the flow down an inclined plane is based on the momentum conservation applied to our case. At the free surface, the shear stress is null and, at the interface with the inclined plane, the velocity of fluid is null (no-slip condition). An explicit relationship linking the flow rate per unit width and the thickness of the film is obtained by integration of the velocity profile over the thickness of the film:

$$q = \frac{1}{3\mu}\rho g \sin(\beta) d^3 \qquad \text{or} \qquad d = \left(\frac{3q\mu}{\rho g \sin(\beta)} \right)^{1/3} \tag{13}$$

where q is the volumetric flow rate per unit width, d the thickness of the film, ρ the density of the fluid, μ its viscosity and β the tilt angle of the inclined plane.

The thickness of a layer of Newtonian fluid can easily be calculated knowing the flow rate and the angle (30° in our case). From equation 13, we know that the film thickness variations related to the flow rate fluctuations are:

$$\Delta d = \frac{1}{3}\frac{\Delta q}{q}\left(\frac{3q\mu}{\rho g \sin(\beta)} \right)^{1/3} \tag{14}$$

Equation 14 shows that, for a constant value of relative flow rate fluctuations, the smallest variations in film thickness will be obtained for a low flow rate or a low viscosity, considering the other parameters constant. Assuming relative flow rate fluctuations of about 5 %, it is then possible to calculate the difference in thickness for a layer with and without perturbation for a given flow rate and viscosity in order to be able to choose an accurate meshing. On the pilot, the flow rate is ranging between 1.9 and 4.2 L/m·min. Thus, we calculated the thickness variations for the lowest flow rate. Results are presented in Table 10 for several values of the viscosity and two values of the density.

Table 10 : Influence of an increase of flow rate on the layer thickness for several values of the viscosity and two values of the density (q=1.9 L/m.min).

Density (kg/m^3)	1200	1200	1200	1600	1600	1600
Viscosity (mPa·s)	50	600	1500	50	600	1500
Layer thickness at q (µm)	931	2133	2892	845	1937	2628
Layer thickness at q + 5 % (µm)	946	2166	2940	859	1968	2671
Variation in layer thickness (µm)	15	33	48	14	31	43

The lowest difference is about 15 µm. Therefore, the distance between two nodes must be below 10 micrometres in the y-direction in the region where fluid interfaces are present.

In addition, we must take into account that the layer thickness depends on the flow rate. From equation 13, we know for instance that the thickness is increased by nearly 50 % when the flow rate is multiplied by 3.

The inclined plane was therefore meshed with about 0.5 million of elements (Figure 46). It should be noted that one simulation took about 3 hours computing time with a Quad core Xeon processor running at 3.2 GHz and 16 GB memory.

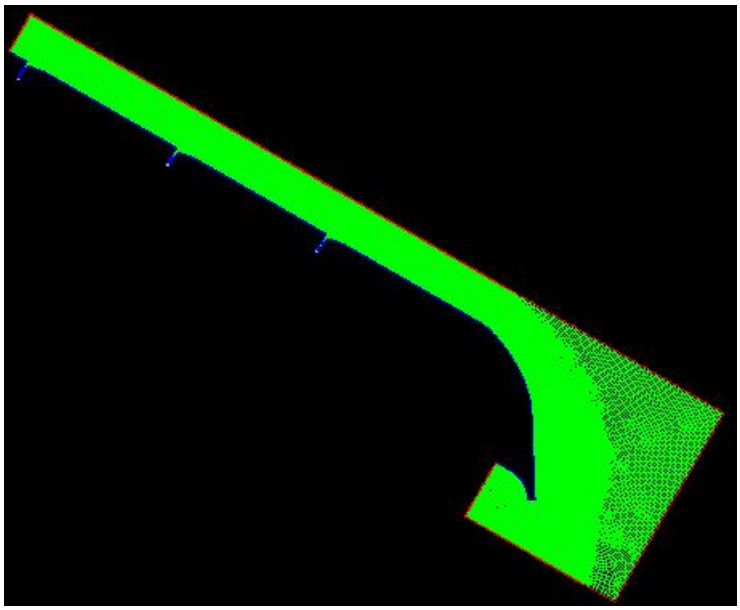

Figure 46 : Meshing of the inclined plane in two-dimensions.

3.1.2. Fluent model solver with boundaries conditions used

Contrary to the internal flow in curtain coating which is a three-dimensional problem, the flow down an inclined plane is a two-dimensional problem. Several assumptions were made to solve it with the computational fluid dynamic software Fluent®. We consider an unsteady state, with isothermal and incompressible fluids. Considering the velocities and the viscosities of the fluids, the flow is laminar in our laboratory coater. In this case, a multiphase model called Volume Of Fluid (VOF), which is appropriate for free-surface flows, is used.

The VOF model is a surface-tracking technique applied to a fixed Eulerian mesh. It is designed for two or more immiscible fluids where the position of the interface between the

fluids is of interest. In our case, up to four fluids will be simulated (3 coating colours and the ambient air). In the VOF model, a single set of momentum equations is shared by the fluids, and the volume fraction of each of the fluids in each computational cell is tracked throughout the domain.

The VOF formulation relies on the fact that two or more fluids (or phases) are not interpenetrating. For each additional phase added to the model, a variable is introduced: the volume fraction of the phase in the computational cell. In each control volume, the volume fractions of all phases sum to unity. The fields for all variables and properties are shared by the phases and represent volume-averaged values, as long as the volume fraction of each of the phases is known at each location. Thus the variables and properties in any given cell are either purely representative of one of the phases, or representative of a mixture of the phases, depending upon the volume fraction values.

The appropriate properties and variables will be assigned to each control volume within the domain.

The mathematical equations that describe the flow on the inclined plane are based on the equation of a continuity for the volume fraction of one (or more) of the phases, the Navier-Stokes equation and the continuity equation applied to our case with specific simplifications.

In order to define a problem with a unique solution, we have to specify the information of all the variables at the domain boundaries. To do that, we have to identify all the boundaries with their nature (inlets, pressure outlet, wall) and give information on them. Boundaries conditions have a huge impact on the accuracy of the results. So we defined all the walls with the no slip-condition and specified the velocity inlet with the volume fraction of each phase and the pressure outlet. The surface tension must be specified. It was decided to keep it constant along the inclined plane since it does not have a big impact on wave formation even if this surface tension is in reality a dynamic surface tension. A default value would be 0.072 N/m but in the case of coating colours, the value is closer to 0.04 N/m.

The process of solving a multiphase system is inherently difficult and some stability or convergence problems could be encountered. Because of a time-dependent problem a small time step is recommended, at least an order of magnitude smaller than the characteristic time of the flow. In our case, a time step between 10^{-5} and 10^{-6} s with 10 iterations per time step is used.

3.1.3. Preliminary simulation study

The objective of this parametric study is to evaluate the performance of the model of VOF used for the studied cases with Fluent. A short time-step can improve the accuracy of the analysis; it was thus decided to have a time-step of 10^{-6} s for this parametric study. Several simulations were performed with three layers in order to reduce the number of simulations and the thickness of each layer was calculated and compared to the prediction for a Newtonian fluid (Eq. 13).

In this short study, the variables are the flow rate and the viscosity values which were varied in order to have significant variations of the thickness of the film. Table 11 summarizes the cases performed in the parametric study. In each case, only one parameter is changed to clearly demonstrate the influence of each parameter. The simulations were stopped before the junction of two layers and, thanks to the meshing, the thicknesses were measured. An example is exposed on Figure 47 where three Newtonian fluids are flowing down the inclined plane and each colour represents a viscosity (case 1).

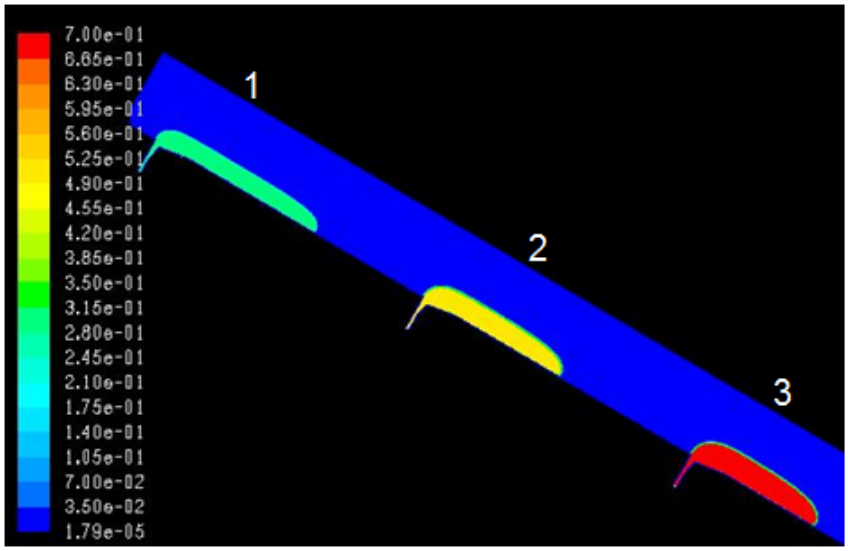

Figure 47: Example of a simulation for the parametric study (case 1), the scale is for the viscosity.

Results are reported in Table 11 which permitted to compare the thickness layer obtained from Eq. 13 and by simulations in order to add a validation of the simulation technique. It appears that values are very close, whatever the fluid viscosity and the operating conditions. Therefore, simulation results are satisfactory.

Table 11: Variable parameter values used in the parametric study for a Newtonian fluid with density 1200 kg/m^3 – the tilt angle of the inclined plane is 30°.

Case		Flow rate (L/m·min)	Viscosity (mPa·s)	Thickness (mm)	
				Simulation	Prediction
1	1.1	1.9	300	1.65	1.69
	1.2		500	1.99	2.01
	1.3		700	2.20	2.24
2	2.1	1.9	100	1.15	1.17
	2.2		800	2.38	2.35
	2.3		1500	2.93	2.89
3	3.1	1.9	300	1.65	1.69
	3.2	3.0		2.00	1.97
	3.3	4.2		2.17	2.20
4	4.1	1.9	600	2.10	2.13
	4.2	3.0		2.55	2.48
	4.3	4.2		2.84	2.78

3.2. Simulation results

We ran simulations for Newtonian fluids. In this part, only real fluids were used in simulation. All simulations were carried out with 3 layers in order to compare these results to the ones encountered in the bibliographic part. A PVOH solution at different concentrations, and thus

different viscosities, was used as Newtonian liquid and the same three coating colours classically used for the simulation in the manifold.

Several flow rates ranging between 1.9 and 6.2 L/m·min were tested. These values are close to the values when a three-layer curtain coating is running on the pilot.

In all these cases, we will examine the superposition of the three fluids (Figure 48) in order to see the evolution and the propagation of instabilities. Indeed, the perturbations can grow and affect the final product or decay. The layers are coloured by the viscosity of each fluid.

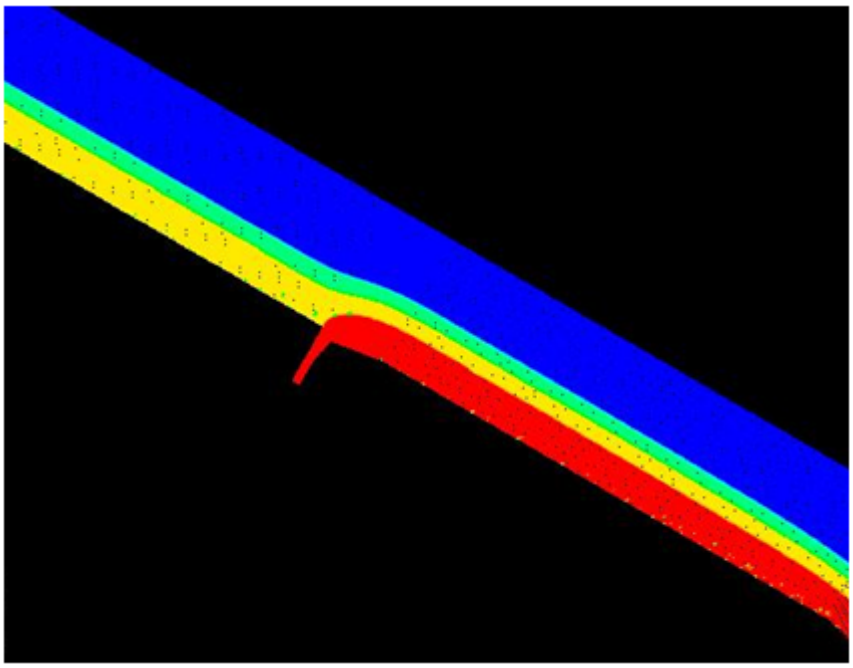

Figure 48: Example of the superposition of three layers flowing down an inclined plane.

Only one layer is disturbed at each simulation with fluctuation between ±30 and ±70 % of the average flow rate at a frequency of 10Hz. In reality, we found that perturbation on the fluid interfaces coming from a pressure pulsation creates a flow rate variation at a frequency between 1 and 5 Hz and the maximum fluctuation is about ±5 % but the aim of this part is to compare our simulations to what can be found in literature by analyzing the influence of rheological parameters and operating conditions which is made easier with huge disturbances at high frequencies.

In order to simulate a pulsation of the pump, the same user defined function detailed in the previous chapter is required under Fluent with an unsteady flow.

All the preliminary tests having been carried out, we can now focus on the influence of several parameters on the uniformity of a three-layer flow on the inclined plane.

3.2.1. Comparison of literature and CFD simulation results for Newtonian fluids

Before starting the comparison, simulations without added perturbations were carried out, and it was observed that no disturbance is created on the inclined plane whatever the configuration and the operating conditions, each interface remains stable as shown on Figure

49. The influence of viscosity stratifications and depth ratios on the flow was then studied for three-layer curtain coating.

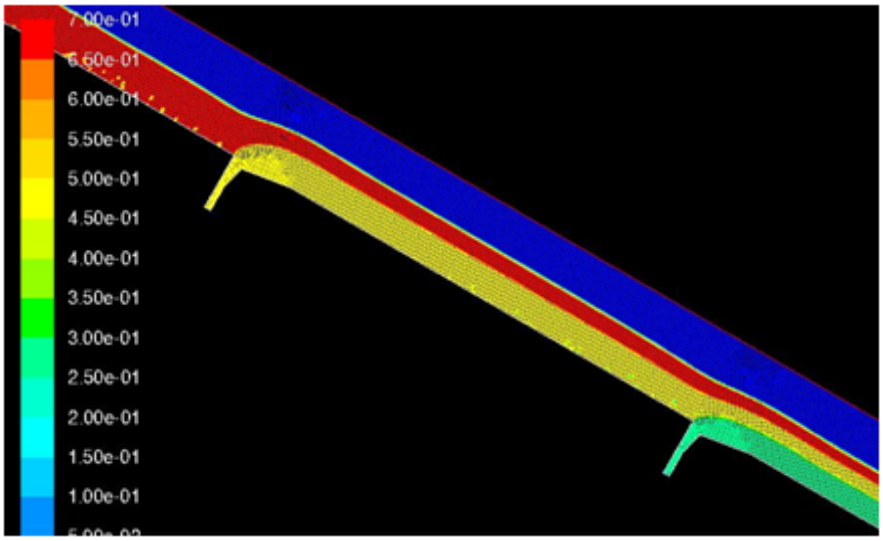

Figure 49: Flow without any perturbations.

3.2.1.1. Influence of viscosity stratifications on the flow

The influence of viscosity stratifications on the flow for Newtonian fluids with the geometry of the curtain coater pilot was first studied. Several arrangements can occur and three of them will be studied, that were found as critical with the same flow rate for the three layers, 6.2 L/m·min: an increase of the viscosity from the bottom to the upper layer, the opposite configuration and a case with the lower viscosity for the middle-layer.

We observed that, in the case of a perturbation on the top layer, the wave decays before the junction of the top layer with the middle layer as described on Figure 50 and Figure 51. In the literature, a critical Reynolds number was found by Benjamin [36] and Yih [37] for long waves (compared with the thickness d , i.e. about 10 times d which is our case) above which some disturbances will appear or be amplified. This critical Reynolds number is a function of the angle of inclination of the plane β :

$$Re_c = \frac{5}{6}\cot(\beta) \qquad (15)$$

Since the angle of inclination is equal to 30° in our case, the critical Reynolds number on the inclined plane of the pilot should be 1.4 which was not validated by simulations. Indeed the Reynolds number is equal to 3.7 in the case presented on the Figure 51 and perturbations are damped. In all the other simulations carried out, the Reynolds number is lower, therefore whatever the perturbation and the operating conditions, the wave for the top layer disappears before reaching the middle layer.

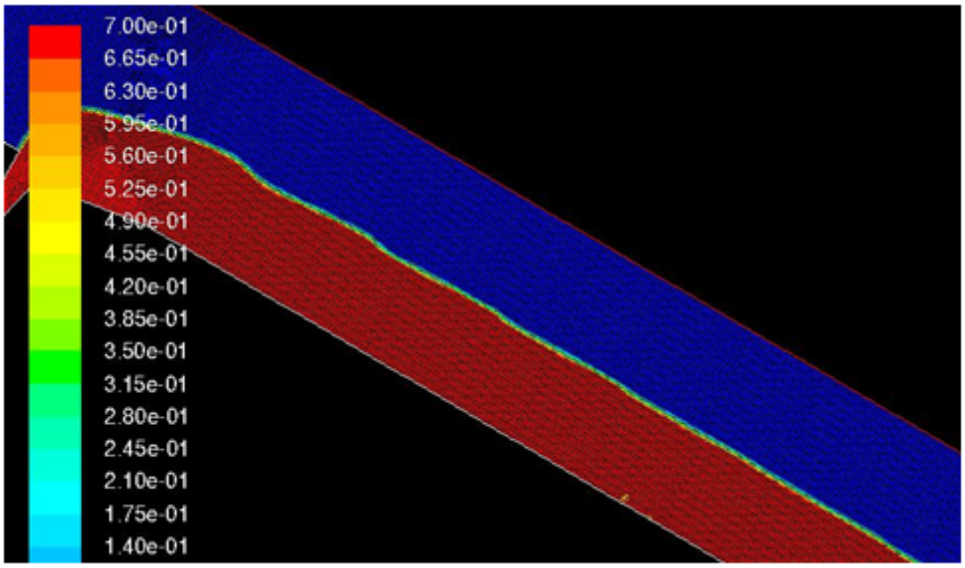

Figure 50: Damping of the oscillations (30 % of the average velocity) on the top layer at Q=1.9 L/m·min with a viscosity of 700 mPa·s.

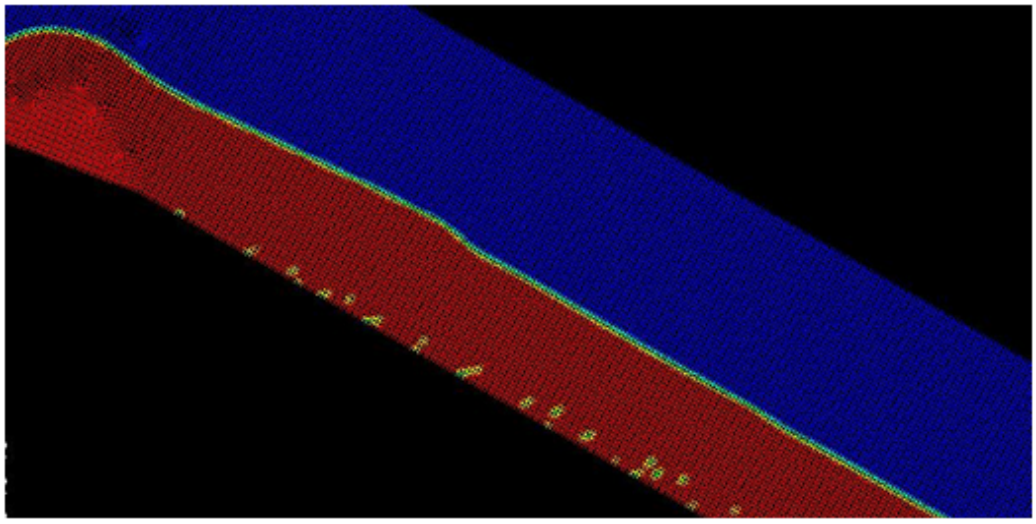

Figure 51: Damping of the oscillations (30 % of the average velocity) on the top layer at Q=3.1 L/m·min with a viscosity of 150 mPa·s.

Then we simulated the flow for Newtonian fluids with perturbations on the middle or pre layer. Results for viscosity stratifications with an increase from the bottom to the top layer are depicted on Figure 52 with two fluctuations on the pre-coating. This figure clearly shows that the perturbations are damped at the end of the inclined plane. Simulations with perturbations on the middle-coating are not presented here but revealed the same trend. In fact the three layers at the beginning of the curtain are stable.

The same simulations were carried out with a decrease of viscosity from the bottom to the top layer and Figure 53 present some of these results which permitted to conclude that, even for huge instabilities in the middle-coating, the waves did not propagate and did not affect the other layers at the end of the inclined plane. The same results were found with fluctuations of the flow rate in the pre-coating.

Pulse Pre-Coating: frequency 10 Hz, fluctuation ±30 %

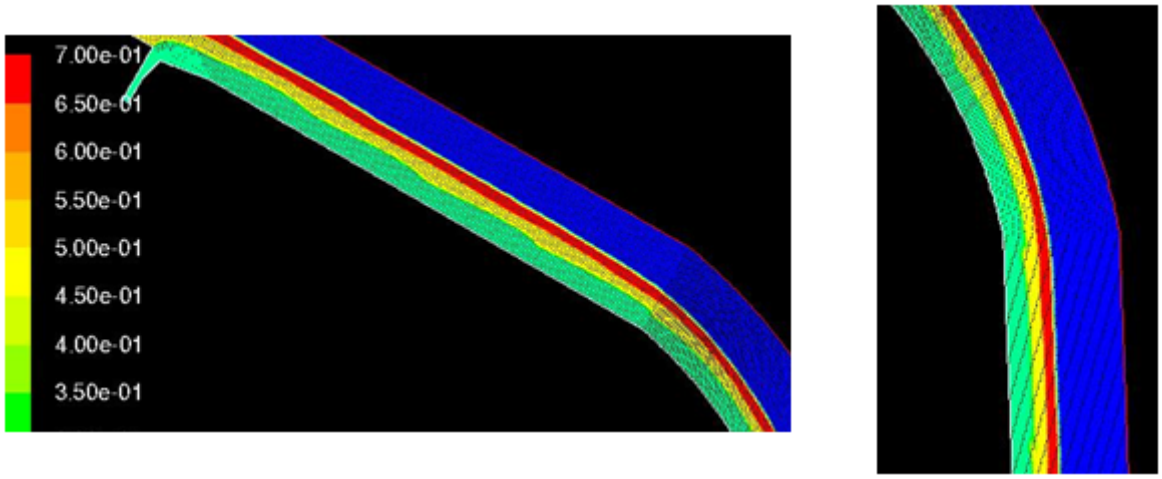

Pulse Pre-Coating: frequency 10 Hz, fluctuation ±70 %

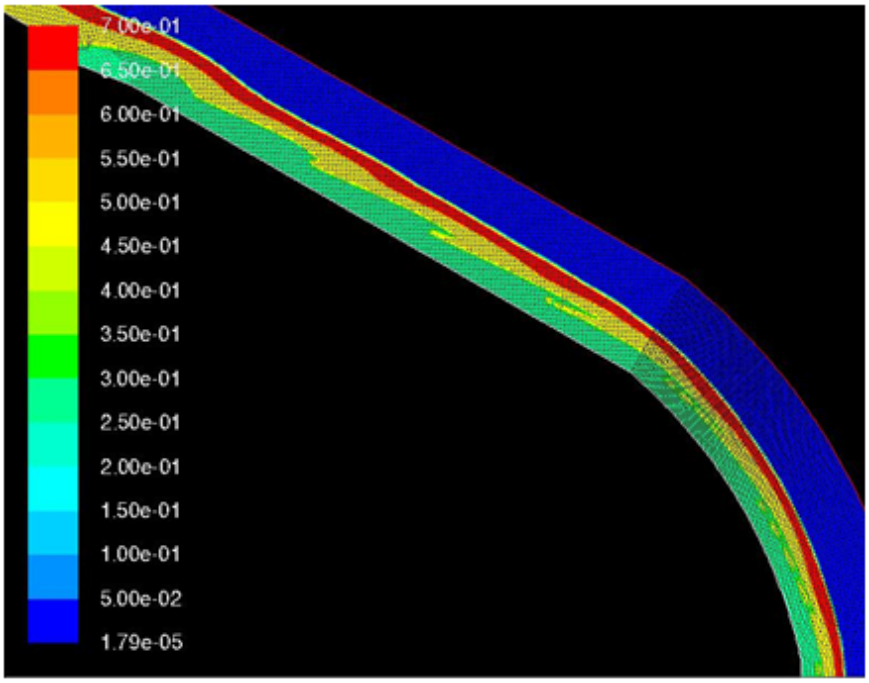

Figure 52: Influence of an increase of the viscosity from the bottom to the top layer on the propagation of waves.

Pulse Middle-Coating: frequency 10 Hz, fluctuation ±70 %

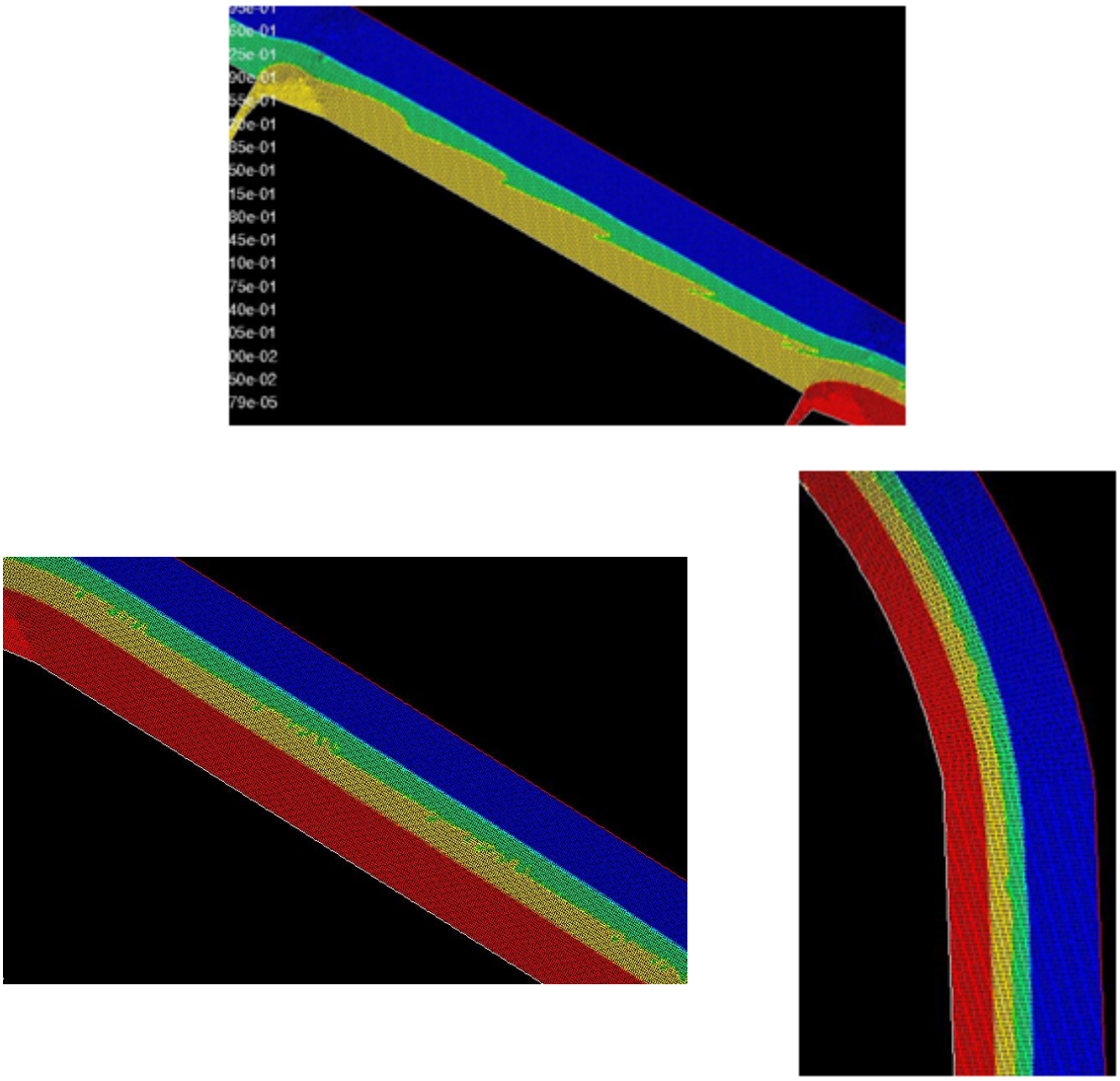

Figure 53: Influence of a decrease of the viscosity from the bottom to the top layer on the propagation of waves.

At constant flow rate, these two configurations led to flow stability on the inclined plane whatever the localization, the frequency and the intensity of the perturbation. The last viscosity stratification studied is the one with the lowest viscosity middle-layer configuration which was found as the worst configuration in the literature.

Several simulations were carried out with this configuration and results are presented on Figure 54. It is apparent that when the middle layer viscosity is smaller than those of the two adjacent layers, instabilities arise and are reflected at each interface. The three layers were therefore destabilized all the way to the lip where the curtain is formed. These perturbations can affect the final product by producing a difference of coat-weight in the machine direction (barring). This configuration has to be avoided on the inclined plane of the curtain coater in order to have a uniform flow along it.

Pulse Pre-Coating: frequency 10 Hz, fluctuation ±30%

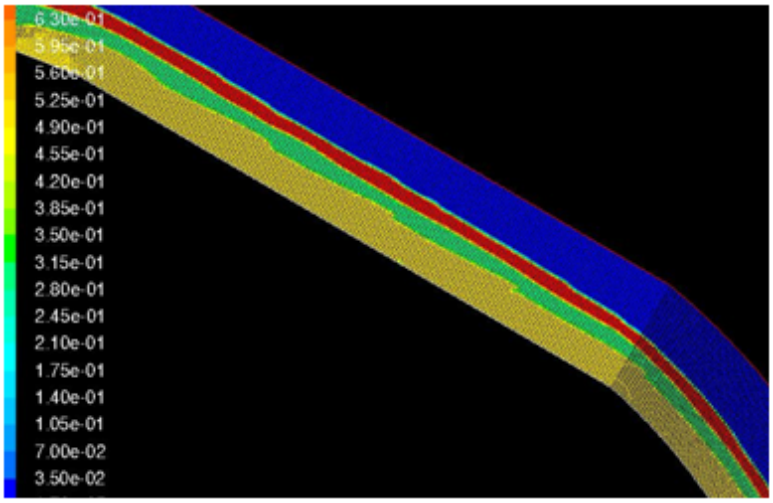

Pulse Pre-Coating: frequency 10 Hz, fluctuation ±70 %

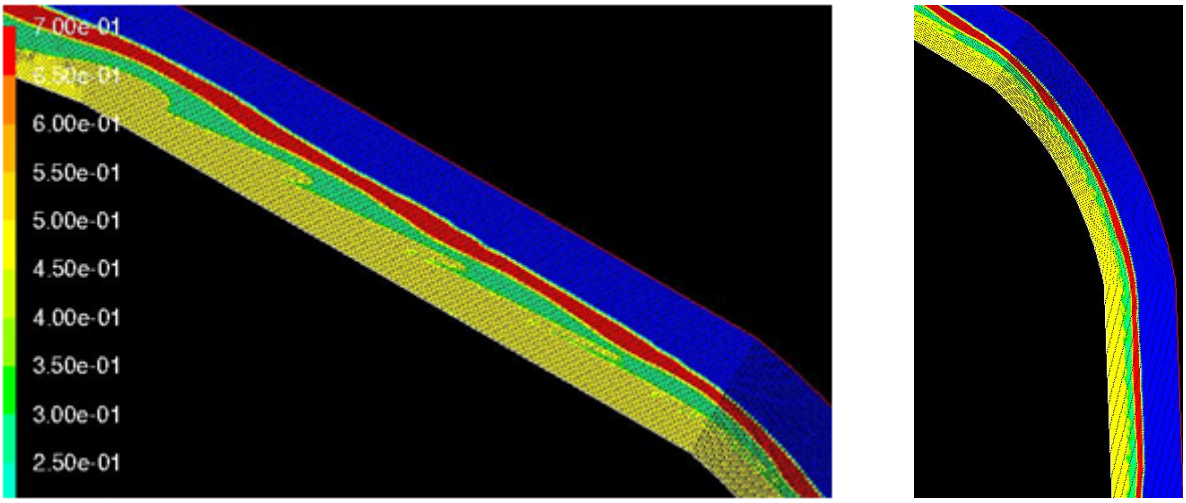

Pulse Middle-Coating: frequency 10 Hz, fluctuation ±70 %

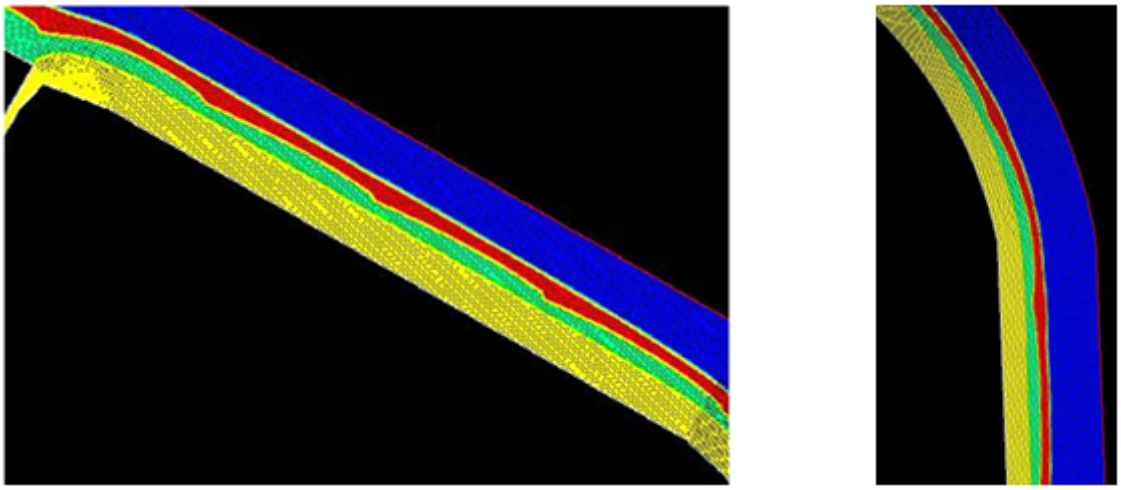

Figure 54: Influence of a smaller middle layer viscosity on the propagation of waves.

It was demonstrated that the viscosity stratification has a huge impact on wave propagation. Having a monotonically increasing or decreasing viscosity configurations permitted to damp the perturbations before entering the curtain itself. Moreover, the case where the middle-layer has the lowest viscosity leads to unstable flow, the disturbance extends all the way. These first conclusions corroborate what was found in the literature when authors studied the stability of three layers flowing down an inclined plane with a negligible surface tension.

Nevertheless, other operating conditions were considered for the stability of a Newtonian three-layer flow flowing down the inclined plane, which are the flow rate and the depth stratification. We will focus on the depth stratification since authors found that it has a huge impact on wave propagation.

3.2.1.2. Influence of the depth ratio on the flow

We studied here the influence of the depth ration on wave propagation for Newtonian fluids flowing down an inclined plane. In most of the previous simulations carried out, the three fluids had the same flow rate and therefore the depth ratio did not change. Of course it did not mean that the thickness of the three fluids was the same since their viscosities were different and two of them flowed on a liquid surface with a certain velocity. Three different depth stratifications were simulated in this part.

Since one of the goal of using curtain coating is to reduce the cost of coating without changing the properties, the idea is to add a thin bottom layer able to create a good adhesion between the substrate and the coating colours, a thick middle layer to add thickness and to cover the fibres and finally a thin top layer in order to add good properties of printability (by adding OBA for the brightening which is quite expensive) as shown on Figure 55. Indeed some references used with the CTP's pilot coater in the project Curtain II of WFC paper with the associated coat weight are detailed in Table 12 in order to have an idea of the depth stratification used in curtain coating. In this study, the main target was to define the optimal ratio of each layer and the best combination of products.

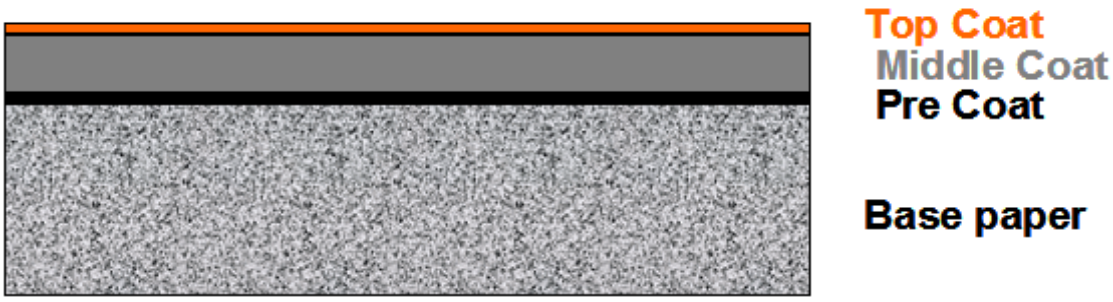

Figure 55: An example of the depth ratio used in curtain coating for WFC paper.

Therefore three different depth stratifications are simulated in the worst case concerning the viscosity stratification: One with the same flow rate for the three layers, one with a thick middle-coating and a thin pre-coating which is the target of the depth stratification in curtain coating and one with a thick pre-coating and a thin middle-coating. In all these simulations, the total flow rate was kept constant and some results are gathered on Figure 56. They highlighted the fact that, as the bottom layer becomes thinner, the region of instability decreases in size whereas a thick pre-coat leads to huge instabilities up to the mixing of layers. Thus the best depth ratio to avoid the wave propagation is in the agreement with the economic issue of the curtain coating. Concerning the depth ratio, it was found in the literature that a very thin bottom-layer (under 22% of the total thickness) and a thick middle-

layer (over 18% of the total thickness) is recommended and these simulations are in agreement with this advice.

Table 12 : Coating weights used in the tests.

Trial reference		A	B	C	D
Pre-coating	Coat weight (g/m²)	2	6	2	6
	Remark	Red dye		Red dye	
Middle-coating	Coat weight (g/m²)	17	13	17	13
	Remark			0.40 pph of CMC FF5	
Top-coating	Coat weight (g/m²)	7	7	7	7
	Remark	Blue dye		Blue dye	
				0.35 pph of CMC FF5	

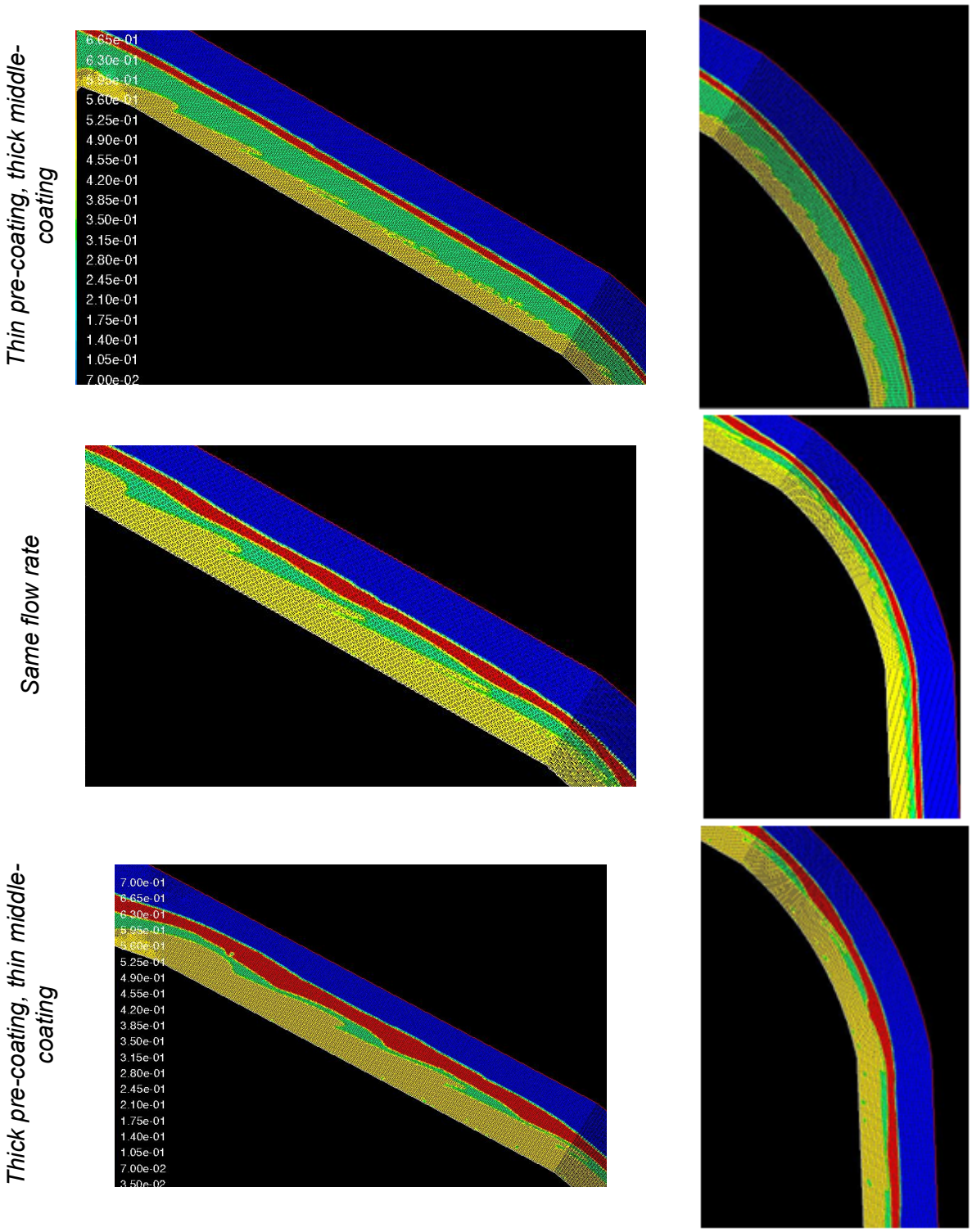

Figure 56 : Influence of Depth stratification for a Pulse in the Middle-Coating frequency 10 Hz, fluctuation ±70 %.

3.2.1.3. Conclusions

A two-dimensional flow modelling of three layers on the inclined plane of a curtain coater was presented in this part in order to compare what can be found in literature to results with the geometry of the curtain coater pilot. We validated the fact that for Newtonian fluids, depth and viscosity ratio were relevant parameters to predict the stability of a 3 layer-flow.

All the simulations carried out permitted to conclude that the viscosity stratification has the biggest impact on the propagation of waves; indeed having a monotonically increase or decrease viscosity configurations permitted to damp the perturbations before entering the curtain itself with better results for an increase. Moreover, having a low viscosity middle-layer configuration has to be avoided since perturbations grow along the inclined plane and can create some defects on the final coated paper. Finally, the depth ratio also influences the flow, indeed, as the bottom layer becomes thinner, the region of instability decreases in size whereas a thick pre-coat leads to huge instabilities up to the mixing of layers.

Simulations of three Newtonian layers flowing down the inclined plane of the curtain coater pilot are totally in agreement with what can be found in the literature. The best solution should be to use a monotonically increase of the viscosity from the bottom layer to the top layer with a thin pre-coat and a thick middle-coat which is in agreement with what was done in practice for economic reasons.

3.2.2. Operating conditions encountered on the CTP curtain coater pilot

The comparison between literature results and CFD with our geometry for Newtonian fluids flowing down the inclined plane is now achieved. We can now focus on what really happens on the inclined plane of a curtain coater with the appropriated operating conditions.

A thorough study was carried out for the Newtonian fluids with the influence of several rheological and operating parameters. To conclude on the influence of all these parameters on the propagation of waves, the perturbations on the inclined plane were voluntary overestimated: a layer was disturbed with fluctuation between ±30 and ±70 % of the average flow rate at a frequency of 10 Hz which is no longer the case in reality with a curtain coater pilot.

Since the aim of this study is to understand the various phenomena taking place in the curtain coater and find parameters that spark off defects, we will analyse whether the propagation of waves on the inclined plane is an encountered problem or not in curtain coating, especially for a three-layer or fewer-layer curtain coating for the range of fluids and operating conditions used.

On the pilot, the curtain coater is assembled on silent blocks which are designed for damping the vibrations of the machine that could spark off the perturbations. Thus it is obvious that only pumps can generate some disturbances at a certain frequency that are able to create instabilities on the inclined plane. The pumps used in our pilot are Moineau progressing cavity pump from PCM (pigtail-like pump). This type of pump transfers fluid by means of the progress, through the pump, of a sequence of small, fixed shape, discrete cavities, as its rotor is turned. This leads to the volumetric flow rate being proportional to the rotation. Hence these pumps have application in fluid metering and pumping of viscous or shear sensitive materials. Generally the flow rate fluctuation is very low and it was impossible to get relevant values from discussions with pump suppliers, who said that the fluctuations are below ± 4 % of the average flow rate. Moreover, it was found in the data sheet of the PCM pump that frequencies of disturbances were close to 1 or 5 Hz at our flow rates.

- Concerning the frequency of the eventual perturbations: the length of the inclined plane is about 20 cm and the average velocity is close to 0.4 m/s since it was found thanks to the bibliographic results that the velocity of the perturbation is twice higher than the flow, as a result, only very few periods of the perturbation can propagate along the plane and they cannot grow. Of course in other applications with a longer plane such as the case of glaciers, waves will have enough time to propagate and grow.
- Concerning the amplitude of the fluctuations: it was previously found that for fluctuations of ±70 %, instabilities can affect the three layers and spoil the final product. It is already harder to clearly observe the evolution of waves along the inclined plane when it is ±30 %. This is no longer the case for fluctuations below ±4 % which is what really happens on our pilot since the waves did not affect the overall stability of the multi-layer curtain coating.

As a result, it is possible to conclude that the problem of liquid films flowing down the inclined plane of the curtain coater is not a real problem since the frequency and the amplitude of the perturbations are too low to enable their propagation and spoil the final product.

3.3. Conclusions

In this part, we demonstrated first the coherence of the model used thanks to a parametric study. It was found that the thickness of a layer of Newtonian fluid on the inclined plane depends on the flow rate, the angle of inclination of the plane and the viscosity of the fluid.

A comparison between literature results and CFD simulations were carried out. It was found that the most relevant parameters for the evolution of waves at the interfaces of liquids along the inclined plane are the viscosity and density stratifications. Indeed a monotonically increase or decrease of the viscosity permitted to damp the perturbations before entering the curtain itself whereas a low viscosity middle-layer configuration has to be avoided since perturbations grow along the inclined plane and can spoil the final coated paper. Moreover, as the bottom layer becomes thinner, the region of instability decreases in size whereas a thick pre-coat leads to huge instabilities up to the mixing of layers. All these results are in agreement with bibliographic results.

Fortunately, in practice a thin pre-coating and top-coating (the most expensive) were used for binding and optical properties whereas a thick middle coating is used to cover the fibres, physic is here in agreement with the use.

Nevertheless, all these results permit to conclude that the problem of liquid films flowing down the inclined plane of the curtain coater is not in fact a real problem since the frequency and the amplitude of the perturbations are too low to enable their propagation and finally to spoil the final product.

The only problem that may occur could come from the perturbations in the manifold which generate concentration gradient along the width of the curtain coater with a lower concentration in the middle and could be recovered on the final coated paper.

Conclusions - Perspectives

Conclusions and perspectives

This work aimed at increasing fundamental knowledge of key parameters governing the curtain coating process by characterising the internal flow in a pilot curtain coater and the flow down the inclined plane. The main objective was to help understand the main criteria for a successful multi-layer curtain application on a pilot curtain coater and subsequently permit to develop coating colours adapted to the curtain coating process for WFC papers thanks to their rheological parameters.

The first chapter is a literature review and presents an overview of the coating defects that can occur in the curtain coating process, researches on the internal flow and finally those on liquid films flowing down an inclined plane. It was found that some simplifications were used in studies of the internal flow according to the complexity of the geometry of the cavities and the different domains where it is encountered. That is why, in this thesis, we developed a study with the operating conditions used for curtain coating in paper industry for WFC. Concerning the flow down an inclined plane, the CFD study had apparently not been done before.

The second chapter presented the types of fluids used (Newtonian and Non-Newtonian), their composition and their rheological properties in relation with the coating process. Three coating colours classically used in multilayer coating for Wood Free Coated paper were tested in addition with Newtonian fluids and model shear-thinning fluids. Then the experimental device was described; it is a transparent replica of the CTP pilot curtain coater made of Plexiglas designed and manufactured in order to visualize the flow inside the manifold and validate CFD results. Two methods of measurements for experimental validations were used in this study, the tracer method and 2D Particle Imaging Velocimetry.

The third chapter was devoted to the analysis of the flow in the pilot curtain coater with CFD simulations and experimental validations. We first performed CFD simulations of the internal flow both for Newtonian and Non-Newtonian fluids by dividing the problem into two parts: the flow in the manifold of the laboratory curtain coater which was simulated in three dimensions and a two dimensional simulation of the flow in the second cavity since its shape is constant along the width of the coater. In addition, an experimental study was performed to validate the CFD results in the manifold using a flow visualization technique with tracers and 2D-PIV in a laboratory setup with transparent parts. Finally 2D CFD simulations on the inclined plane were carried out in order to understand the conditions of the development of waves for three layers with several operating conditions for the range of those used on the pilot curtain coater.

From the CFD simulations in the manifold, relevant parameters for Newtonian and non-Newtonian fluids on flow uniformity were highlighted: the inlet Reynolds number and the angle of deviation between the inlet pipe and the manifold. It was demonstrated that increasing the Reynolds number led to flow perturbations at the junction between the inlet pipe and the manifold. For Non-Newtonian fluids, the power-law index also affects flow uniformity, because its decrease leads to a lower apparent viscosity in the area of vortex formation but it is taken into account with the Reynolds number. In the operating conditions of this study, the apparent viscosity is divided by up to three when the power-law index varies from 1 to 0.8. Moreover, simulation permitted to show that the yield shear stress does not affect the behaviour of the flow in the manifold for the range studied (under 3Pa). This was confirmed by calculating the wall shear stress for several Newtonian and Non-Newtonian fluids and comparing it to the yield shear stress, indeed the values are less than 5% compared to the wall shear stress in all the studied cases. We found that there is a critical

Reynolds number at the inlet in order to avoid vortex creation and it is equal to 20. To maintain vortex-free operation, the Reynolds number at the inlet should not exceed this critical value. This value is specific of this special geometry; it means that if we had a different geometry, the critical Reynolds number would not be the same. Flow visualization tests in the manifold of a replica in Plexiglas of the pilot coater were performed in order to validate the simulation results. For the tracers method, we injected dye tracers at the wall of the inlet pipe and visualized the streamlines in the manifold. This simple method led to satisfactory results; indeed it is possible to clearly see the transition between vortex-free flow and the vortex creation. We validated the fact that vortices exist and are located in the area found by simulation. Moreover, we recovered the same value of the critical Reynolds number and identical vortex sizes whatever the rheological behaviour of Newtonian and Non-Newtonian fluids. Concerning the 2D-PIV, this technique is an alternative to tracers in order to see the rheological behaviour of fluids in the manifold, moreover it is possible to obtain the velocity field and have numerical values of this field. The 2D-PIV was not suitable for visualization of velocity fields on the internal flow for coating colours since they are opaque but permitted to add another validation of results found with Newtonian and Non-Newtonian fluids using transparent fluids (PVOH and Carbopol). Results found with this method were very close to those found by simulations and with the tracer method. Finally simulations done on a CFD were in accordance with the experimental part. We then demonstrated with the CFD software that disturbances eventually caused by the pump had no impact on vortex formation whatever the frequency of the perturbation and proposed some solutions to improve flow uniformity such as increasing the radius of the inlet pipe or changing the internal geometry to an end-fed geometry. Indeed, at constant flow rate, the Reynolds number varies in the same way as the reciprocal of the diameter size for a Newtonian fluid, therefore increasing the radius of the inlet pipe improves the uniformity of the flow by reducing the Reynolds number. The second solution proposed was to totally change all the geometry of the curtain coater to an end-fed curtain coater. This geometry permitted to eliminate the angle of deviation between the inlet pipe and the manifold, which has a deep impact on vortex creation. Simulations showed that the geometry of the curtain coater pilot used is not the most appropriate for the range of fluids used since there is no vortex in the manifold whatever the operating conditions. The only problem that could occur with this new geometry is the settling of particles of carbonate present in coating colours. In order to evaluate this impact on flow uniformity, we calculated the settling velocity for particles of carbonate for a wide range of viscosity and found that they were at least one hundred times lower than the lowest Y velocity in the end-fed curtain coater found by simulations. The main drawback in this case is its manufacturing which is not easy to implement.

CFD simulations in the second cavity permitted to conclude that it could provide another chance for flow across the die if a non-uniform distribution resulted from the flow out of the original cavity. Results indicate that a vortex can appear just after the first slot and a that decrease of the divergent angle could prevent a vortex creation. We also found that the power-law index has a deep impact on flow uniformity, indeed fluids with a very strong shear thinning behaviour will create vortex in the second cavity for a given geometry. As validation of simulations, the critical Reynolds number encountered was compared to others found in literature and it was found that they revealed the same trend. A difference of these values can be observed because of the definition of a different Reynolds number. Concerning the usefulness of the second cavity on the studied pilot curtain coater, we demonstrated that whatever the operating conditions and the rheological parameters of all the fluids, the critical Reynolds number is higher in the second cavity than in the manifold, which means that there is a window of Reynolds number where a vortex is present in the manifold and not in the second cavity; therefore in this case it can act as a filter to reduce non uniformity of the flow coming from the manifold. Moreover, if the fluid passes through the manifold without any perturbations, then it will pass through the second cavity without any problems.

A two-dimensional flow modelling of three layers on the inclined plane of a curtain coater was thereafter presented in order to compare what can be found in literature with the results provided with the geometry of the curtain coater pilot. We validated the fact that for Newtonian fluids, depth and viscosity ratio were relevant parameters to predict the stability of a 3-layer-flow. All the simulations carried out permitted to conclude that the viscosity stratification has the biggest impact on the propagation of waves; indeed having a monotonically increase or decrease viscosity configurations permitted to damp the perturbations before entering the curtain itself with better results for an increase. Moreover, having a low viscosity middle-layer configuration has to be avoided since perturbations grow along the inclined plane and can create some defects on the final coated paper. Finally, the depth ratio also influences the flow; indeed, as the bottom layer becomes thinner, the region of instability decreases in size whereas a thick pre-coat leads to huge instabilities up to the mixing of layers. Simulations of three Newtonian layers flowing down the inclined plane of the curtain coater pilot were in agreement with what can be found in the literature. The best solution should be to use a monotonically increase of the viscosity from the bottom layer to the top layer with a thin pre-coat and a thick middle-coat which is in agreement with what was done in practice for economic reasons. A thin pre-coat and top-coat (the most expensive) is used for binding and optical properties whereas a thick middle coat is used to cover the fibres, Physics is therefore in agreement with what can be found in paper industry. Nevertheless, all these results permitted to conclude that the problem of liquid films flowing down the inclined plane of the curtain coater does not actually pose a problem since the frequency and the amplitude of the perturbations are too low to enable their propagation and finally to spoil the final product.

All these results permitted to increase fundamental knowledge of key parameters governing the curtain coater process and could be applied industrially to reduce defects on the final coated paper. Even though much progress has been done, several questions must be answered and additional simulations must be performed. We have first studied the internal flow and several phenomena were observed thanks to CFD and to an experimental work performed with our laboratory setup. It could be interesting to perform CFD simulations of fluids with local gradients of viscosity that could be encountered by adding rheological modifiers into the coating colours in order the increase the viscosity. Moreover in all the studied cases, homogeneous fluids were used but a model with particle of pigments into a matrix of fluid (composed of binders and water) could be considered in order to see how vortices impact on the flow. Concerning the flow down an inclined plane, additional 2D CFD could be performed by adding a defect on the coater such as an asperity or a stripe on the slot. In addition, it should be worth considering 3D CFD simulations in order to take into account the edge effect and consider concentration gradient along the width of the curtain coater with a lower concentration in the middle due to perturbations in the manifold and observe their behaviour on the inclined plane. It should be noticed that 3D CFD using VOF in unsteady state will require extended computational resources. Finally this work has to be continued by simulating the flow on the curtain itself and on the impingement zone which had not been done yet in 3D. Experimental validations on the curtain should be carried out by using 3D PIV, which technique has been used in the research program at the CTP and has worked very well.

Literature cited

[1] Helmer, K., Karppinen, T., and Lindqvist, B. 2005. “Curtain vs. blade coating: Experience in board application.” *Pap. Technol* , 46(6): 37-42.

[2] Salminen, P., Yang, A., and Kritzinger, J., *et al.* 2010. “The Influence of Application System on the Structure of Coating Layer.” *PaperCon, Proc.,* TAPPI PRESS, Conf. CD.

[3] Endres, I., and Tietz, M. 2007. “Blade, film, and curtain coating techniques and their influence on paper surface characteristics.” *TAPPI J.* 6(11): 24-32.

[4] Weinstein, S.J., and Ruschak, K.J. 2004. “Coating flows.” *Annu. Rev. Fluid Mech.* 36: 29-53.

[5] Tripathi, P., Joyce, M., Fleming, P.D., and Sugihara, M. 2009. “A statistical study of process variables to optimize a high speed curtain coater- Part I.” *TAPPI J.* 8(1): 20-26.

[6] Triantafillopoulos, N.G., Grön, J., and Luostarinen, I., *et al.* 2004. “Operational issues in high-speed curtain coating of paper, Part 2: Curtain coating of lightweight coated paper.” *TAPPI J.* 3(12): 11-16.

[7] Black, T.D., Clarke, A., and Ruschak, K.J. 1994. “Hydrodynamic assist of dynamic wetting.” *AIChE J.* 40(2): 229-242.

[8] Shikhmurzaev, Y.D. 1996. “Dynamic contact angles and flow in vicinity of moving contact line.” *AIChE J.* 42(3): 601-612.

[9] Tripathi, P., Joyce, M., Fleming, P.D., and Sugihara, M. 2009. “A statistical study of process variables to optimize a high speed curtain coater- Part II.” *TAPPI J.* 8(1): 29-32.

[10] “Advances in coating and drying of thin films”. 1999. Proceedings of the 3rd European Coating Symposium (ECS ’99). University of Erlangen-Nürnberg. September 7-10, 1999. F. Durst and H. Raszillier editors.

[11] Kistler, S. E, and Scriven, L. E., 1982 "Finite element analysis of dynamic wetting for curtain coating at high capillary numbers." presented at AIChE Spring Meeting, Orlando, FL, March 1982.

[12] Miyamoto, K., and Katagari Y., "Premetered coating processes: Curtain coating" in *Liquid Film Coating* (S.F. Kistler and P.M. Schweizer, Eds), Chapman & Hall, London. 363-395.

[13] Christodoulou, K. N., 1990. “Computational physics of slide coating flow.” PhD thesis, University of Minnesota Published by University Microfilms International, Ann Arbor, MI.

[14] Tjiptowidjojo, K., 2009. “Flow limits in slide coating.” PhD thesis, University of Minnesota, Ann Arbor, MI.

[15] Gutoff, E. and Cohen, E. 1995. “Problems in slot, extrusion, slide and curtain coating” in *Coating and Drying Defects: troubleshooting operating problems*. John Wiley and Sons, 97-142.

[16] Kistler S.F. and Schweizer P.M. 1997. “Liquid film coating", Chapman & Hall, London.

[17] Weinstein, S.J., and Ruschak, K.J. 1996. “One-dimensional equations governing single-cavity die design.” *AIChE J.* 42(9): 2401-2414.

[18] Winter, H. H., and Fritz, H.G. 1986. “Design of dies for the extrusion of sheets and annular parisons: the distributions problem.” *Polym. Eng. Sci.* 26(8): 543-553.

[19] Miller, C. 1972. “Predicting non-Newtonian flow behaviour in ducts of unusual cross section.” *Ind. Eng. Chem. Fundam*. 11(4): 524-528.

[20] Liu, T., and Hong, C. 1988. “The pressure drop/flow rate equation for non-Newtonian flow in channel or irregular cross-section.” *Polym. Eng. Sci.* 28(23): 1559-1564.

[21] Booy, M.L. 1982. “A network flow analysis of extrusion dies and other flow systems.” *Polym. Eng. Sci.* 22(7): 432-437.

[22] Matsubara, Y. 1983. “Residence time distribution of polymer melts in the linearly tapered coat-hanger die.” *Polym. Eng. Sci.* 23(1): 17-19.

[23] Leonard, W.K. 1985. “Inertia and gravitational effects in extrusion dies for non-Newtonian fluids.” *Polym. Eng. Sci.* 25(9): 570-576.

[24] Lee, K., and Liu, T. 1989. “Design and analysis of a dual-cavity coat-hanger die.” *Polym. Eng. Sci.* 29(15): 1066-1075.

[25] Secor, R.B. 1997. “Analysis and design of internal coating die cavities.” in *Liquid Film Coating* (SF Kistler and PM Schweizer, Eds), Chapman & Hall, London. 369-398.

[26] Boger, D.V. 1987. “Viscoelastic flows through contractions.” *Ann. Rev. Fluid Mech*. 19:157-182.

[27] Acrivos, A., Babcock, B.D., and Pigford, R.L. 1959. “Flow distribution in manifolds.” *Chem. Eng. Sci.* 10:112-124.

[28] Lee, K., Wen, S., and Liu, T. 1990 “Vortex formation in a dual-cavity coat-hanger die.” *Polym. Eng. Sci.* 30(19): 1220-1227.

[29] Vrahopoulou, E.P., 1991. “A model for fluid flow in dies.” *Chem. Eng. Sci.* 46(2): 629-636

[30] Dooley J., 1990. “Simulating the flow in a film die using finite element analysis.” *TAPPI Polym., Laminations Coat. Conf.,* TAPPI PRESS. 957-964.

[31] Na, S.Y., and Kim, D.Y. 1995. “ Three-dimensional modelling of non-Newtonian fluid flow in a coat-hanger die.” *Korean J. of Chem. Eng*. 12(2): 236-243.

[32] Wen, S.H., and Liu, T. 1994. “Three-dimensional finite element analysis of polymeric fluid flow in an Extrusion Die. Part I: Entrance effect.” *Polym. Eng. Sci*. 34(10): 827-834.

[33] Chang, Y.H., Wen, S.H., and Liu, T. 1996. “Experimental observation on entrance flow inside extrusion dies.” *Polym. Eng. Sci*. 36(21): 2663-2675.

[34] Leonard, W.K. 1985. “Effects of secondary cavities, inertia and gravity on extrusion.” *ANTEC ’85* 144-148.

[35] Millet, S. 2007. “Stabilité de l'écoulement multicouche de films non newtoniens sur un plan incliné.“ PhD Thesis, Institut National des Sciences Appliquées, Lyon – France.

[36] Benjamin, T. 1957. “Wave formation in laminar flow down an inclined plane.” *J. Fluid. Mech. 2(6): 554-574*.

[37] Yih, C.S. 1963. “Stability of liquid flow down an inclined plane.” *Phys. Fluids*, 6(3): 321-334.

[38] DeBruin, G.J. 1974. “Stability of a layer of liquid flowing down an inclined plane.” *J. Eng. Math.* 8(3): 259-270.

[39] Floryan, J.M., Davies, S.H., and Kelly, R.E. 1987. “Instabilities of a liquid flowing down a slightly inclined plane.” *Phys. Fluids*. 30(4): 983-989.

[40] Kao, T.W. 1965. “Role of the interface in the stability of stratified flow down an inclined plane.” *Phys. Fluids*. 8(12): 2190-2194.

[41] Kao, T.W. 1968. “Role of viscosity stratification in the stability of two-layer flow down an incline.” *J. Fluid. Mech.* 33(3): 561-572.

[42] Loewenherz, D.S., and Lawrence, C.J. 1989. “The effect of viscosity stratification of a free surface flow at low Reynolds number.” *Phys. Fluids*. 1(10): 1686-1693.

[43] Yih, C.S. 1967. “Instability due to viscosity stratification.” *J. Fluid. Mech*. 27(2): 337-352.

[44] Hooper, A.P., and Boyd, W.G.C. 1987. “Shear-flow instability due to a wall and a viscosity discontinuity at the interface.” *J. Fluid. Mech*. 179: 201-225.

[45] Hooper, A.P. 1985. “Long-wave instability at the interface between two viscous fluids: thin layer effects.” *Phys. Fluids*. 28(66): 1613-1618.

[46] Chen, K.P. 1993. “Wave formation in the gravity-driven low-Reynolds number flow of two liquid films down an inclined plane.” *Phys. Fluids*. 5(12): 3038-3048.

[47] Wang, C.K., Seaborg, J.J., and Lin, S.P. 1978. “Instability of multi-layered liquid films.” *Phys. Fluids*. 21(10): 1669-1673.

[48] Weinstein, S.J., and Kurz, M.R. 1991. “Long-wavelength instabilities in the three-layer flow down an incline.” *Phys. Fluids* 3(11): 2680-2687.

[49] Weinstein, S.J., and Chen, K.P. 1999. “Large growth rate instabilities in the three-layer flow down an incline in the limit of zero Reynolds number.” *Phys. Fluids*. 11(11): 3270-3282.

[50] Yih, C.S. 1965. “Stability of a non-Newtonian liquid film flowing down an inclined plane.” *Phys. Fluids*, 8(7): 1257-1262.

[51] Hwang, C-C., Chen, J-L., Wang, J-S., *et al.* 1994. “Linear stability of power-law liquid film flows down an inclined plane.” *J. Phys.* 27(11): 2297-2301.

[52] Rousset, F., Millet, S., Botton, V., *et al.*2007. “Temporal stability of Carreau fluid flow down an incline.” *J. Fluid. Eng.* 129: 913-920.

[53] Weinstein, S.J. 1990. “Wave propagation in the flow of shear-thinning fluids down an incline.” *AIChE J.* 36(12): 1873-1889.

[54] Millet, S., Rousset, F., Botton, V., *et al.* 2008. “Stabilité de l’écoulement à deux couches de films non-newtoniens sur un plan incliné.” *C.R. Mecanique*. 336: 313-319.

[55] Millet, S., Rousset, F., Botton, V., *et al.* 2009. “Stability analysis of stratified coating flow of shear-thinning fluids” *Eur. Phys. J. Spec.Topics*. 166(1): 143-146.

[56] Triantafillopoulos, N. G. and Farrington Jr,. T.E. 1988. “Flash X-Ray Radiography techniques for visualizing coating flows.” *IPC Technical Papers Series* 274.

[57] AR-1000 manual (TA instruments).

[58] Midoux, N. 1999. “Mécanique et rhéologie des fluides en génie chimique.” Tech & Doc Lavoisier.

[59] Chhabra, R.P. and Richarson, J.F. 1999. “Non-Newtonian flow in the process industries: Fundamentals and engineering applications”. Butterworth Heinemann.

[60] http://www.dantecdynamics.com/Default.aspx?ID=1049

[61] Gambit manual.

[62] Fluent manuals.

[63] Delplace, F. and Leuliet, J.C. 1995.“Generalized Reynolds number for the flow of power law fluids in cylindrical ducts of arbitrary cross-section.” *Chem. Eng. J. and Biochem. Eng. J.* 56 (2): 33-37.

Annexe
Coating colour formulations

The coating colours were defined according to past work done on CTP's coater. It was not necessary to add extensional viscosity modifier since during CTP's coating trials, the speed was low. However this additive is mandatory for higher speeds in the industry and we used the one from BASF (DF 3X).

Table 1: Pre-coat colour formulation.

Product	Reference	Supplier	Formulation
GCC	Carbital 60	Imerys	100 parts
Starch	Stabilys A030	Roquette	10 parts
Latex	L0607	EOC polymers	6 parts
Surfactant	Surfynol 420	Air products	0.6 %
Solid content 62%			

Table 2: Middle-coat colour formulation.

Product	Reference	Supplier	Formulation
GCC	Carbital 60	Imerys	100 parts
Starch	Stabilys A030	Roquette	6 parts
Latex	L0607	EOC polymers	8 parts
Surfactant	Surfynol 420	Air products	0.8 %
Solid content 66%			

Table 3: Top-coat colour formulation.

Product	Reference	Supplier	Formulation
GCC	Carbital 90	Imerys	100 parts
Latex	L7032	EOC polymers	11 parts
OBA	Blankophor NC extra liquid	Kemira	0.6 part
Surfactant	Surfynol 420	Air Products	0.8%
Solid content 64%			

GCC: ground calcium carbonate

OBA: optical brightening agent

Résumé étendu

1. Introduction

L'objectif du couchage est de modifier les propriétés de surface dans le but d'améliorer l'imprimabilité du papier, son aspect ou ses propriétés barrières. Le couchage rideau est un procédé d'enduction sans contact qui est utilisé depuis une quarantaine d'années pour les industries photographiques et alimentaires. De nos jours, on l'utilise aussi pour la fabrication de papiers spéciaux tels que les papiers thermiques et les papiers jet d'encre. Récemment, de nouvelles possibilités de marchés sont apparues, notamment pour les cartons et les papiers graphiques. On compte actuellement une trentaine de machines industrielles installées dans le monde.

Cette technologie sans contact offre de nombreux avantages comparée à des méthodes de couchage plus traditionnelles telles que le couchage à lame ou l'enduction par « metering size press ». En effet, elle permet d'augmenter la productivité notamment en minimisant le risque de casse papier et donne la meilleure uniformité en termes d'épaisseur de couche. De plus, le couchage rideau permet de déposer plusieurs couches simultanément (jusqu'à 10 couches en un seul passage pour les papiers photographiques) comme le montre la Figure 1. Cela signifie que plusieurs couches ayant chacune ses propriétés spécifiques peuvent être déposées sur le papier en une fois tandis qu'avec les autres systèmes traditionnels plusieurs opérations de séchage et de couchage consécutives sont nécessaires.

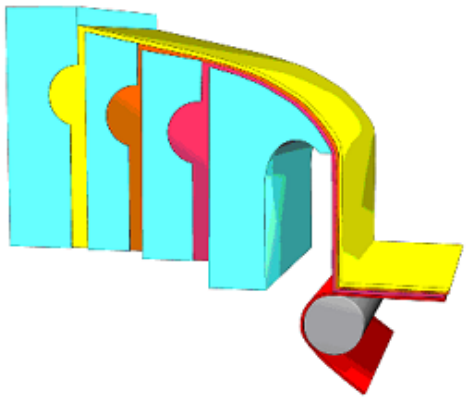

Figure 1 : Schéma d'une coucheuse rideau multicouches

Néanmoins, ce procédé présente de très fortes contraintes et ses exigences diffèrent de celles des procédés de couchage traditionnels concernant la composition et la préparation des sauces de couchage. Différents fluides peuvent être déposés selon les propriétés finales du papier recherchées : pour améliorer l'imprimabilité, des sauces à base de pigments seront utilisées tandis que, pour obtenir des propriétés barrière (aux graisses, à l'humidité, à l'oxygène ...), des sauces à base de polymères telles que du PVA ou de l'amidon seront appliquées. Ces fluides ont des comportements rhéologiques très différents, ce qui influe sur l'écoulement. En effet, certains sont newtoniens, ce qui signifie que leur viscosité sont

indépendantes du taux de cisaillement et d'autres sont rhéofluidifiants (leur viscosité diminue lorsque le taux de cisaillement augmente) ; leur viscosité n'est pas constante lors du process lorsque le taux de cisaillement varie significativement. La qualité du couchage dépend donc directement du comportement rhéologique du fluide utilisé mais aussi de sa tension superficielle, de la géométrie interne et externe de la coucheuse et des conditions opératoires.

Il existe néanmoins aujourd'hui un écart important entre la stabilité théorique du rideau et les observations faites lors de travaux expérimentaux. C'est pourquoi il est essentiel de mieux comprendre les paramètres clés qui gouvernent le couchage rideau. Face à la complexité de cette thématique, nous nous sommes intéressés dans cette thèse à l'écoulement interne et à celui le long du plan incliné dans la coucheuse pilote du CTP. En effet, de nombreuses publications font état de problèmes directement liés à la ligne de contact dynamique et des moyens pour diminuer ces perturbations.

Cette thèse fait partie intégrante d'un projet international de recherche au CTP (Curtain II) dont le but est de développer le couchage rideau pour des papiers couchés sans bois (WFC). Son principal objectif est de comprendre les principaux critères permettant d'avoir un couchage multicouche sans défaut et donc de permettre le développement de sauces de couchage adaptées pour les papiers WFC en fonction de leurs paramètres rhéologiques. Cette thèse est basée sur la modélisation d'écoulement avec une partie expérimentale permettant de valider les résultats obtenus par simulation.

Ce mémoire est structuré en trois chapitres. Le premier est une étude de la littérature existante portant sur les défauts que l'on peut rencontrer lors du couchage rideau, l'écoulement interne et l'écoulement le long d'un plan incliné. Le second chapitre porte sur la description du matériel expérimental et des méthodes utilisées dans ce travail ainsi que des types de fluides utilisés, leur composition et leurs propriétés rhéologiques en relation avec le couchage rideau. Enfin le dernier chapitre est le cœur de ce travail portant sur l'analyse de l'écoulement dans le pilote de couchage rideau. Nous avons donc analysé par CFD l'écoulement interne dans un dispositif de couchage avec différents fluides newtoniens et non-newtoniens en divisant le problème en deux parties : l'écoulement dans la première cavité qui a été simulé en trois dimensions et l'écoulement dans le seconde cavité en deux dimensions dans le but de déterminer l'utilité de cette dernière cavité pour les fluides et les conditions opératoires utilisés. Les résultats obtenus par simulation ont par la suite été validés expérimentalement sur la réplique en Plexiglas. Enfin, une étude par CFD en deux dimensions de l'écoulement externe sur le plan incliné de l'appareil a été faite pour comprendre dans quelles conditions des perturbations sous formes d'ondes pouvaient se

développer pour un système de trois couches sur notre pilote dans les conditions opératoires utilisées lors d'essais réels.

2. Matériels et méthodes

Nous présentons dans ce chapitre les types de fluides utilisés, leurs compositions et leurs propriétés rhéologiques en lien avec le couchage rideau. L'étude rhéologique s'est limitée aux gradients de cisaillement rencontrés dans les cavités et sur le plan incliné. Ensuite le montage expérimental est décrit ainsi que les différentes techniques de mesure employées.

Trois sauces de couchage classiquement utilisées lors d'essais multicouches sur une coucheuse rideau pour des papiers WFC ont été testées ainsi que des solutions de carbopol à différentes concentrations (fluide rhéofluidifiant transparent) et quelques fluides newtoniens et des fluides modèles rhéofluidifiants. De plus, l'ensemble des fluides réels ont été caractérisés à l'aide d'un rhéomètre cône-plan pour trouver par la suite les modèles rhéologiques se représentant correctement le comportement de ces fluides. Les résultats sont présentés sur la Figure 2 où les points représentent les valeurs expérimentales et les lignes représentent les modèles les plus adaptés.

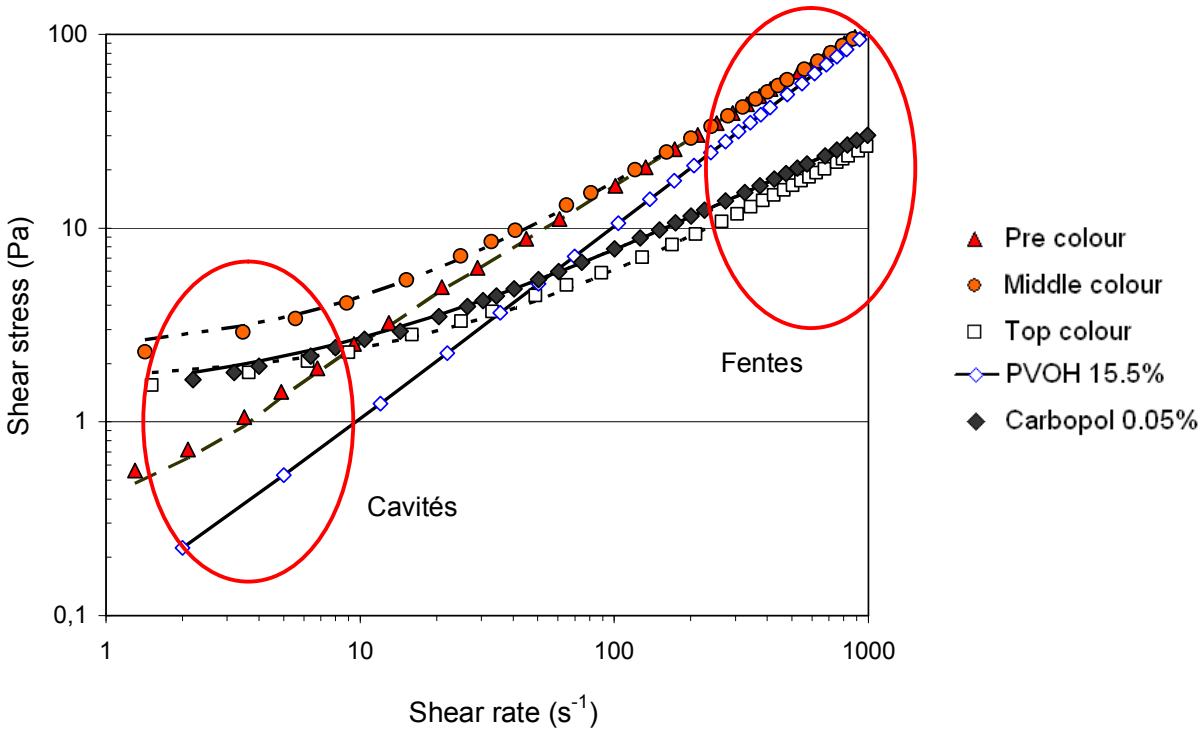

Figure 2: Comportement rhéologique des fluides réels testés avec un rhéomètre cône-plan.

Cette étude rhéologique nous a permis de trouver que la solution de PVOH est bien un fluide newtonien et que les sauces de couchages et le carbopol suivent un modèle rhéologique

d'Herschel-Bulkley ($\tau = \tau_0 + K \cdot \dot{\gamma}^n$). L'ensemble des coefficients des modèles rhéologiques est présenté dans le tableau suivant.

Tableau 1 : Propriétés rhéologiques des fluides testés

Fluids	Rheological parameters		
	τ_0 Yield stress (Pa)	K Consistency index / Viscosity (Pa.s^n)	n Exponent
Pre–coating colour	0.27	0.38	0.82
Middle-coating colour	2.22	0.32	0.84
Top-coating colour	1.6	0.14	0.75
Carbopol 0.05%	1.25	0.33	0.65
PVOH (15-20%)	0	0.1 – 0.8	1
"Model" Herschel-Bulkley	0. 1 –-1.5	0. 1 – 0.6	0.7 – 0.9
"Model" Power-law	0	0.1 – 0.6	0.7 – 0.9

Nous avons ensuite étudié l'écoulement des fluides dans la coucheuse rideau pilote du CTP. Celle-ci présente 2 cavités et 2 fentes (1 fente après chaque cavité). Sa particularité est que la première chambre a un rayon qui augmente lorsque l'on se rapproche de son centre, tout en étant suivie par une fente de taille constante. La figure ci-dessous présente la coucheuse rideau utilisée avec ses dimensions caractéristiques.

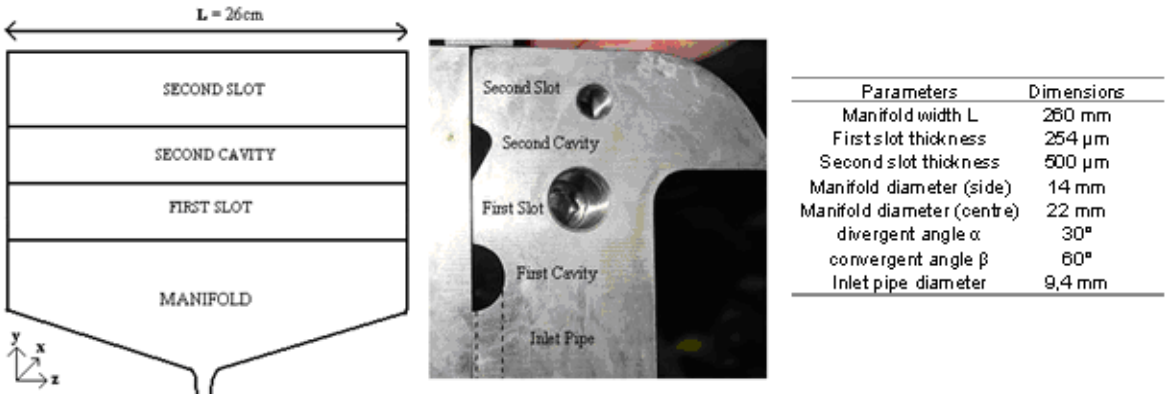

Figure 3: Vue de l'intérieur et de côté de la coucheuse rideau avec ses principales caractéristiques.

Une réplique exacte en Plexiglas a été fabriquée dans le but de visualiser l'écoulement interne et de valider les résultats obtenus par simulation. Le montage expérimental est décrit dans la figure ci-dessous.

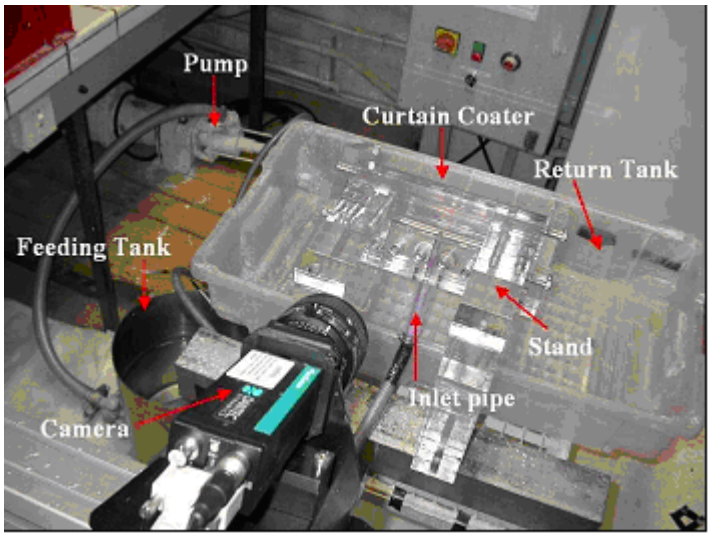

Figure 4 : Montage expérimental pour valider les simulations.

Concernant la partie expérimentale, deux méthodes ont été testées : une méthode de visualisation à l'aide de traceurs et une méthode utilisant la PIV en deux dimensions.

- Pour la méthode utilisant des traceurs, nous injectons des colorants à l'aide de deux seringues proche de la paroi dans le but de voir des lignes de courant à la jonction entre le tube d'entrée et la première cavité. Pour éviter tout mélange avec le fluide observé, le colorant est introduit de façon laminaire dans des conditions les plus iso-cinétiques possibles. Cette méthode est une méthode qualitative.
- La méthode de la PIV 2D (Vélocimétrie par images de particules) est une technique optique non intrusive qui permet d'avoir des données quantitatives sur les différents champs de vitesse, les tailles de vortex dans un plan en 2 dimensions. Le principe est résumé dans la Figure 5.

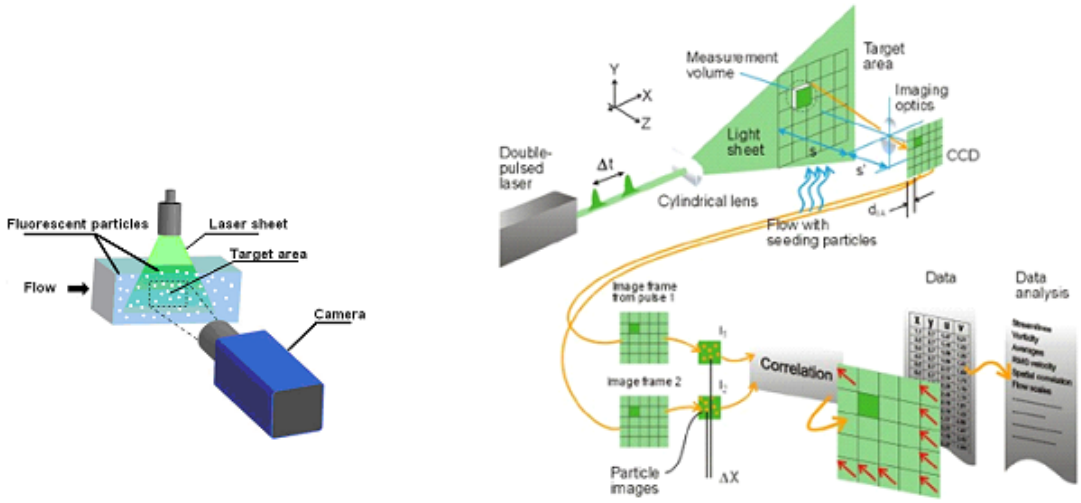

Figure 5: Schéma de principe de la PIV 2D.

3. Etude expérimentale et simulation de l'écoulement dans une coucheuse rideau pilote

3.1. Etude de l'écoulement interne

Cette étude est découpée en deux parties bien distinctes : une étude portant sur l'écoulement dans la première cavité avec des simulations en trois dimensions suivie d'une validation expérimentale et une étude de l'écoulement dans la deuxième cavité en deux dimensions.

3.1.1. Ecoulement dans la première cavité

L'étude des articles de la littérature montrent que l'écoulement dans un manifold est principalement analysé en une ou deux dimensions avec des formes simples, principalement pour des questions de capacité de calcul. Les seuls articles traitant d'une étude en trois dimensions concernent des cas rencontrés dans des extrudeuses de polymères. Les auteurs négligent alors les forces inertielles puisque la viscosité est très élevée. Ils trouvent qu'augmenter le nombre de Reynolds entraîne la création de vortex à l'intersection entre le tube d'entrée et la cavité comme le montre la figure suivante.

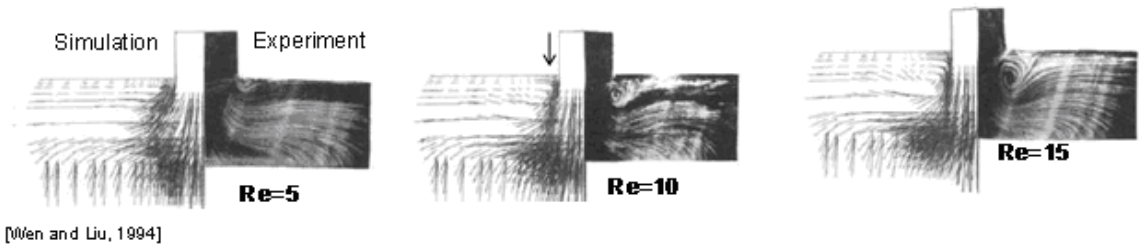

Figure 6: Evolution de l'écoulement en fonction du nombre de Reynolds.

Nous avons simulé l'écoulement de fluides newtoniens et non-newtoniens et étudié l'impact des propriétés rhéologiques et des conditions opératoires sur les phénomènes dans la première cavité. Nous avons montré que le nombre de Reynolds généralisé et l'angle de déviation entre le tube d'entrée et la cavité sont les paramètres ayant le plus d'influence sur l'écoulement et notamment la création de vortex. En effet nous avons trouvé que, pour avoir un écoulement sans perturbation, ce nombre de Reynolds ne doit pas excéder une valeur critique, qui est égale à 20 pour la géométrie étudiée, et ce quelles que soient les propriétés rhéologiques du fluide (Figure 7). En effet, pour une géométrie différente il faudra trouver par simulation la valeur du nombre de Reynolds critique.

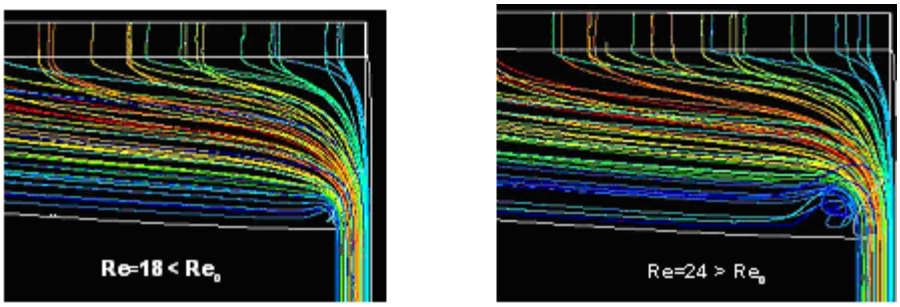

Figure 7: Lignes de courant mettant en évidence d'un nombre de Reynolds critique à l'entrée de la première cavité.

Ces résultats ont été corroborés par une étude expérimentale sur la réplique en Plexiglas de la coucheuse avec les 2 méthodes décrites plus tôt. Il apparaît que la technique de visualisation avec des traceurs est plus facile à mettre en œuvre et semble très bien adaptée pour cette étude puisque l'on peut clairement voir la transition entre l'absence et l'apparition du vortex. La PIV 2D semble moins précise même si on déterminer les champs de vitesse ainsi que les vecteurs vitesses du fluide à l'intérieur de toute la cavité.

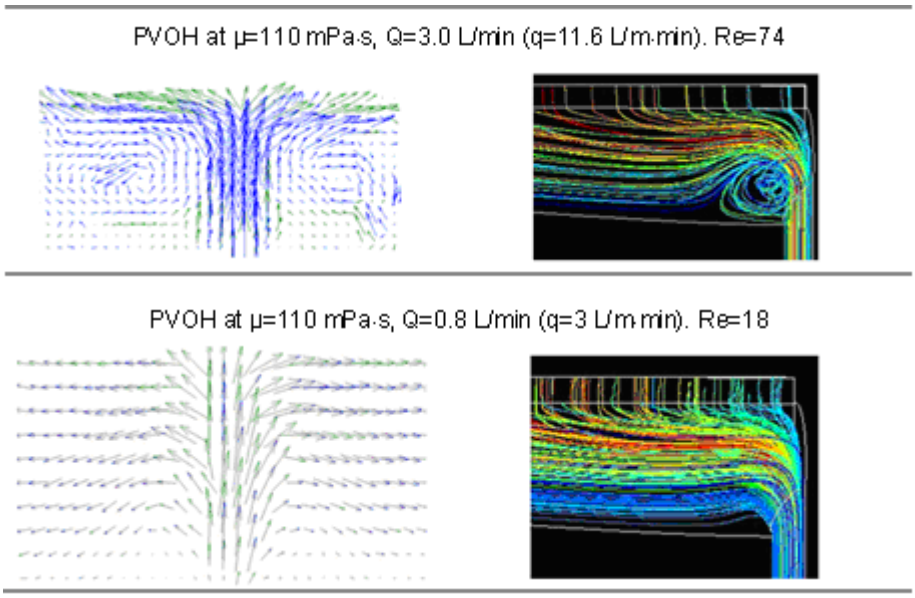

Figure 8: Comparaison entre les simulations et la PIV 2D pour un fluide Newtonien.

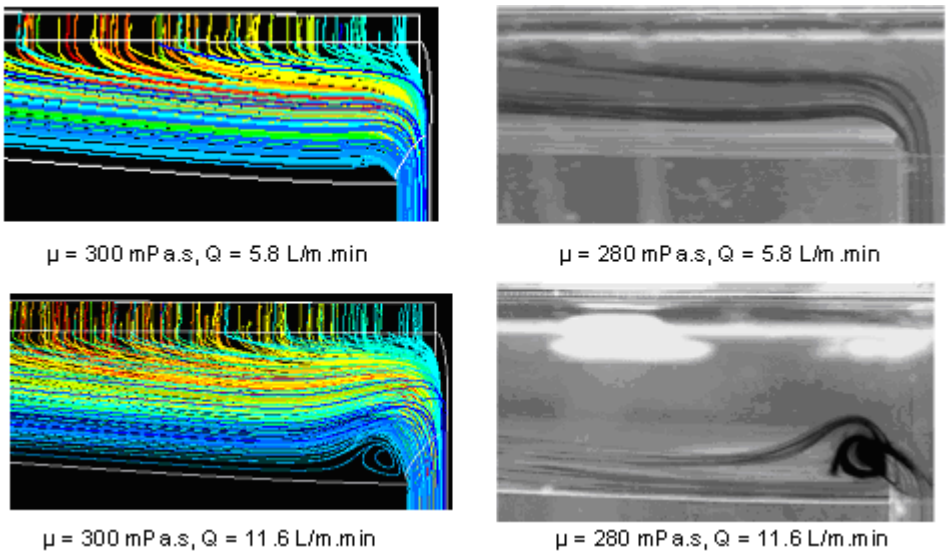

Figure 9: Comparaisons entre les simulations et la méthode par injection de traceur pour un fluide newtonien.

Plusieurs solutions ont été proposées dans le but de réduire ces perturbations : augmentation du rayon du tube d'entrée pour réduire la vitesse ou changement de géométrie de la coucheuse en passant d'une entrée centrale à une entrée latérale. En effet, cela a permis de montrer que la géométrie de la coucheuse rideau pilote du CTP n'est pas la plus appropriée pour la gamme de fluides et de conditions opératoires utilisés dans cette étude. La Figure 10 montre que, pour des conditions opératoires identiques, il n'y a pas de recirculation avec la nouvelle géométrie.

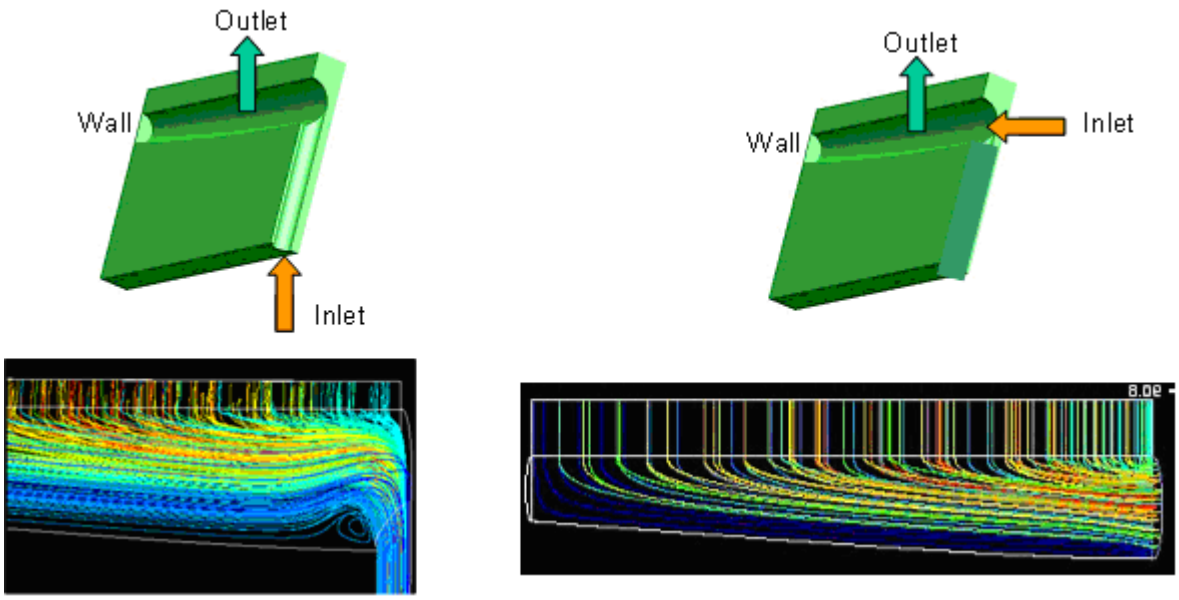

Figure 10: Comparaison des écoulements avec une entrée centrale et une entrée latérale (tracé des lignes de courant).

3.1.2. Ecoulement dans la seconde cavité

Les articles dans la littérature portant sur des écoulements dans une deuxième cavité montrent que celle-ci peut dans certain cas améliorer l'uniformité de l'écoulement. Ainsi Léonard a comparé l'effet d'une addition de volume similaire dans la première ou la seconde cavité sur la réduction de défauts d'écoulement et l'on peut voir sur la Figure 11 que dans notre cas, quel que soit le fluide utilisé, la seconde cavité devrait réduire les perturbations.

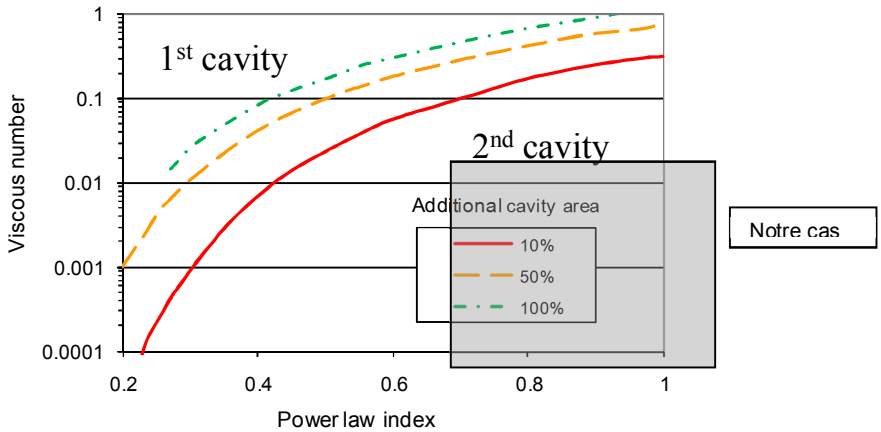

Figure 11: Comparaison de différentes additions de volume dans la première ou la seconde cavité sur l'uniformité de l'écoulement.

D'autres chercheurs ont trouvé que, comme pour l'écoulement dans la première cavité, augmenter le nombre de Reynolds pouvait entraîner l'apparition de vortex (Figure 12, gauche). De plus, diminuer l'angle divergent permet de réduire les perturbations éventuelles (Figure 12, droite).

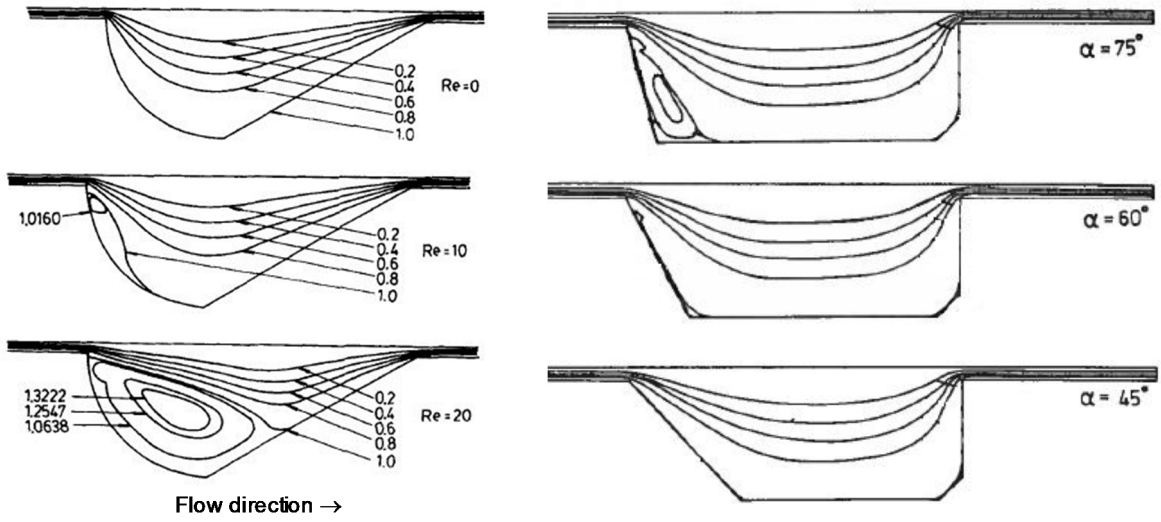

Figure 12 : Influence du nombre de Reynolds dans la fente d'entrée (gauche) et de l'angle divergent (droite) sur l'écoulement dans une seconde cavité.

Les résultats des simulations en 2D ont permis de montrer qu'un vortex peut apparaître dans la cavité, à proximité de l'entrée. Une diminution de l'angle divergent ou l'utilisation d'un fluide peu rhéofluidifiant peut éviter la présence du vortex comme nous le montre le graphique suivant obtenu grâce à un grand nombre simulations où nous avons fait varier la vitesse du fluide toutes conditions égales par ailleurs, jusqu'à détecter un vortex. En effet, pour un fluide donné, diminuer l'angle va augmenter le nombre de Reynolds critique au-delà duquel un vortex se formera. De plus, concernant l'exposant de la loi rhéologique, augmenter celui-ci va diminuer la valeur du nombre de Reynolds critique mais d'un point de vue pratique cela va augmenter la valeur du débit critique. Pour les fluides dont le modèle rhéologique est une loi puissance, nous utiliserons la définition suivante pour calculer le nombre de Reynolds généralisé :

$$Re = \frac{12\rho V^{2-n} D_h^n}{4^n \left(2+\frac{1}{n}\right)^n K} = \frac{12\rho V^{2-n} H^n}{2^n \left(2+\frac{1}{n}\right)^n K}$$

où ρ est la masse volumique du fluide, V la vitesse moyenne du fluide dans la fente, D_h la longueur caractéristique donc ici le double de l'épaisseur de la fente (H), K l'indice de consistance et n l'exposant de la loi rhéologique.

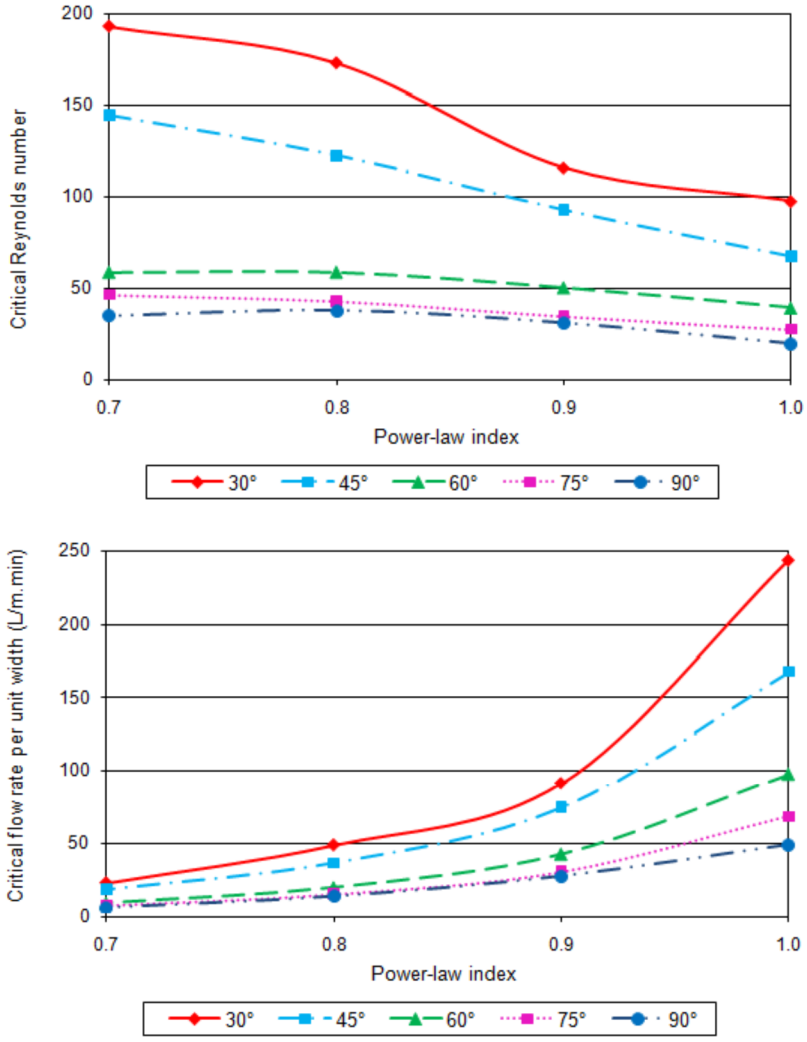

Figure 13 : Influence de l'exposant du modèle rhéologique sur les valeurs du nombre de Reynolds et du débit critiques pour K = 100 mPa.s^n.

Nous considérons les valeurs de nombre de Reynolds critique pour un angle de 30° dans la deuxième cavité (qui correspond à celui de la coucheuse rideau pilote), pour les différents fluides, et calculons le débit correspondant dans la coucheuse et le nombre de Reynolds dans le tube à l'entrée de la première cavité. Nous trouvons que, pour que des vortex apparaissent dans la seconde cavité, il faudrait que le nombre de Reynolds généralisé à l'entrée de la première cavité dépasse 1300 pour des fluides dont l'exposant de la loi rhéologique (loi puissance) est supérieur à 0.7. Ce cas n'est pas possible pour le système étudié, le débit étant bien trop élevé.

Nous avons aussi comparé nos résultats aux résultats de la littérature en termes de nombre de Reynolds critique, après avoir éventuellement recalculé la valeur du nombre de Reynolds afin d'utiliser toujours la même définition. Les résultats, bien qu'un peu différents, révèlent la même tendance. La seconde cavité doit bien servir à filtrer les perturbations pour des fluides peu rhéofluidifiants, ce qui est le cas des sauces de couchages pour des papiers WFC.

L'ensemble des résultats obtenus sur l'écoulement interne a permis d'augmenter les connaissances fondamentales sur des paramètres clés du procédé de couchage rideau et peuvent être appliquées industriellement pour réduire les défauts sur le papier couché :

- pour une géométrie de manifold donnée (première chambre), il ne faut pas dépasser un certain débit, de manière à ce que le nombre de Reynolds à l'entrée reste en dessous d'une valeur critique qui dépend de la géométrie.
- Pour une géométrie de deuxième cavité donnée, de même il ne faut pas dépasser un certain débit, de manière à ce que le nombre de Reynolds à l'entrée reste en dessous d'une valeur critique qui dépend de la géométrie. Cependant, pour des fluides peu rhéofluidifiants, le risque d'apparition d'un vortex dans la deuxième cavité est faible, le débit à l'entrée de la première cavité étant limitant ou bien la valeur de débit trop élevée pour être réelle.

3.2. Etude de l'écoulement sur le plan incliné

Dans le couchage rideau, le plan incliné permet de mettre différentes couches les unes sur les autres pour qu'elles se déposent simultanément après le rideau sur le papier. Mais la littérature nous dit que l'écoulement sur celui-ci peut être très instable. En effet, cela peut créer des vagues au niveau des interfaces qui peuvent être reportées sur le substrat et créer des défauts au niveau de l'homogénéité de la dépose dans la largeur (« ribbing » ou cordon) ou dans le sens marche (« barring »). Ces défauts se retrouvent aussi bien dans les industries papetière ou alimentaire mais aussi dans des phénomènes géophysiques tels que des glaciers comme le montre la Figure 14.

Le but de cette étude est donc de comprendre dans quelles conditions ces perturbations peuvent se produire et se propager sur le produit final. Dans cette étude, nous nous sommes uniquement intéressés au problème de « barring » puisque les simulations ont été effectuées en deux dimensions.

Figure 14: Différents défauts pouvant apparaître sur un plan incliné (« barring » à gauche et « ribbing » à droite).

Une étude de la littérature nous a permis de résumer l'influence de différents paramètres physiques et géométriques sur l'écoulement de fluides newtoniens et rhéofluidifiants sur un plan incliné avec de une à trois couches (Tableau 2).

Tableau 2 : Influence des paramètres physiques et géométriques sur la stabilité de l'écoulement sur un plan incliné.

Fluid behaviour	Number of layers	Influence of an increase of					
		Surface tension parameter	Angle of inclination	Reynolds number	Density ratio	Viscosity ratio	Depth ratio
Newtonian	1	+	--	--			
	2	+	--	--	-	-	-
	3	+	--	--	-	++	++
Non-Newtonian	1	+	--	--			
	2 or 3	+	--	--	=	++	

++ : forte stabilisation, + légère stabilisation, = effet négligeable, - légère déstabilisation, -- forte déstabilisation.

De nombreuses simulations ont été faites en utilisant un modèle multiphasique en régime transitoire (VOF). Les simulations ont porté sur un écoulement de trois couches de fluides newtoniens avec différents rapports de viscosité entre les couches et une tension de surface constante ; une perturbation de débit était apportée sur l'une des couches avec des fluctuations de ±30 et ±70% à une fréquence de 10 Hz. Ces valeurs ont volontairement été exagérées pour observer plus facilement les phénomènes sur le plan incliné. Nous avons trouvé qu'une augmentation de la viscosité de la pré-couche vers la top-couche permettait d'atténuer les perturbations tandis qu'une configuration avec une couche centrale ayant la plus faible viscosité doit être évitée. Ces résultats sont présentés dans la Figure 15.

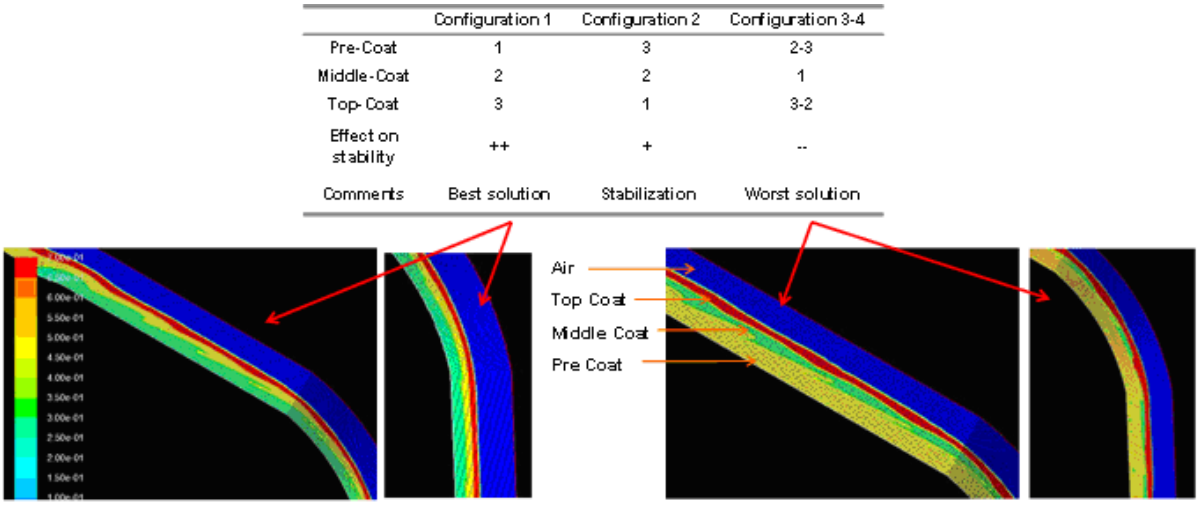

Figure 15 : Influence de la répartition des viscosités sur la stabilité de l'écoulement sur le plan incliné (dans le tableau 1 correspond à la viscosité la plus faible et 3 la plus forte).

En prenant en compte les paramètres réels rencontrés lors d'essais sur le pilote de couchage rideau (fluctuations maximum de ±4% et fréquences de défaut maximum de 5 Hz sur un plan incliné de longueur 20 cm), les simulations ont permis de montrer que les instabilités ne se développent pas sur le plan incliné. L'utilisation de la CFD nous a donc permis de conclure que pour les dispositifs de couchage utilisés et les conditions opératoires de nos industries, les phénomènes de « barring » que l'on retrouve dans la littérature ne devraient pas exister. Seuls des problèmes de gradient de concentration dans la largeur issus d'une perturbation de l'écoulement interne pourraient générer des défauts qui se transmettraient au final sur le papier, mais cela requiert une étude de ces phénomènes en 3D.

4. Conclusions

Le but de cette thèse était d'améliorer les connaissances des paramètres fondamentaux qui gouvernent le procédé de couchage rideau en caractérisant à la fois l'écoulement interne dans la coucheuse pilote du CTP et celui sur le plan incliné. Le principal objectif était d'aider à mieux comprendre les critères permettant d'avoir un couchage rideau sans défaut et de développer des sauces de couchage adaptées à ce procédé pour des papiers LWC.

L'étude de l'écoulement interne par CFD a permis de faire ressortir la cause de vortex pouvant apparaître dans le dispositif. Pour avoir un écoulement sans vortex, le nombre de Reynolds à l'entrée doit être inférieur à une valeur critique égale à 20 pour la géométrie étudiée quel que soit le fluide utilisé. De plus la présence d'une seconde cavité permet de filtrer les perturbations pour des fluides peu rhéofluidifiants, ce qui est le cas des sauces de couchages pour des papiers WFC. Ces résultats de simulation ont été validés expérimentalement par injection de traceur et par PIV 2D, en utilisant une réplique exacte en Plexiglas de la coucheuse rideau.

Enfin, en ce qui concerne l'étude de l'écoulement externe sur le plan incliné, les paramètres pertinents sont les ratios de viscosités et d'épaisseurs des couches. Le cas avec une viscosité très faible dans la couche centrale et une faible épaisseur est à proscrire. De plus, l'utilisation de la CFD a permis de conclure que, pour les dispositifs de couchage utilisés et les conditions opératoires de nos industries, le problème de « barring » présenté dans la littérature ne devrait pas exister.

Ce travail peut permettre à des industriels de prédire la présence ou non de défauts dans leur coucheuse rideau selon leurs propres conditions d'essais et les fluides utilisés. De plus,

des optimisations en termes de design pour des coucheuses rideau ont été démontrées pour réduire les défauts éventuels dus aux écoulements dans les cavités.

Publications and presentations

Peer-reviewed journal

Martinez, P., Rueff, M., Guérin, D., and Morin, V. 2010. “Experimental and theoretical study of the manifold flow in a curtain coater.” TAPPI J. 15(11): 15-21.

International conferences

Martinez, P., Rueff, M., Guérin, D., and Morin, V. 2011. “CFD simulation and experimental study of the flow in the cavities of a slide die curtain coater.” Extended abstract proceedings of the European Coating Symposium (ECS ’11) Turku (Finland) - 4p. - and oral presentation. June 2011.

Martinez, P., Rueff, M., Guérin, D., and Morin, V. 2010. “Experimental and theoretical study of the flow in the manifold of a curtain coater.” Proceedings of the 2010 TAPPI Advanced Coating Fundamentals Symposium. Munich (Germany) - 19p. - and oral presentation. October 2010.

National conference

Martinez, P., Rueff, M., Guérin, D., and Morin, V. 2009. “Study of the internal flow in a curtain coater.” Octobre 2009. Récents Progrès en Génie des Procédés, number 98, 2-910239-72-1, Ed. SFGP, Paris, France. Proceedings of the « XIIe congrès de la SFGP » Marseille (France) - 6p. - and poster presentation. October 2009.

Étude expérimentale et simulation d'écoulements de fluides modèles et de dispersions pigmentaires dans une coucheuse rideau

Résumé

Le couchage rideau est un procédé d'enduction sans contact qui permet un couchage « contour » d'une feuille de papier dont le point clé est la stabilité du rideau. Ce procédé semble devoir se développer dans les années à venir pour la production de papiers impression-écriture et de papiers et cartons d'emballages. Néanmoins, il existe aujourd'hui un écart important entre la stabilité théorique du rideau et les observations. Nous avons donc analysé par CFD l'écoulement interne dans un dispositif de couchage pilote avec différents fluides Newtoniens et Non-Newtoniens ainsi que l'écoulement externe sur le plan incliné de l'appareil. L'étude de l'écoulement interne par CFD a permis de faire ressortir la cause de vortex pouvant apparaître dans le dispositif. Pour avoir un écoulement sans vortex, le nombre de Reynolds à l'entrée doit être inférieur à une valeur critique égale à 20 pour la géométrie étudiée quel que soit le fluide utilisé. De plus la présence d'une seconde cavité permet de filtrer les perturbations pour des fluides peu rhéofluidifiants, ce qui est le cas des sauces de couchages pour des papiers WFC. Ces résultats ont été validés expérimentalement à l'aide de traceurs et de PIV en utilisant une réplique exacte en Plexiglas de la coucheuse rideau. Enfin en ce qui concerne l'étude de l'écoulement externe sur le plan incliné, l'utilisation de la CFD a permis de conclure que, pour les dispositifs de couchage utilisés et les conditions opératoires de nos industries, certains problèmes présentés dans la littérature ne devraient pas exister.

Mots clés : Couchage rideau, CFD simulation, Fluides non Newtoniens

Experimental study and CFD simulation of the flow of model fluids and coating colours in a slide die curtain coater

Abstract

Curtain coating is a contactless coating process which permits a contour coating of the paper and the key parameter of this process is a perfect stable curtain. This technology is expected to spread widely for graphic paper grades and boards in the next few years. Nevertheless, many experimental works revealed some differences between stability theory and results observed on the curtain. In this work, we performed CFD simulations both for Newtonian and Non-Newtonian fluids on the internal flow in a pilot curtain coater and on the flow down the inclined plane. The CFD study of the internal flow revealed the cause of vortex creation into the coater. To maintain vortex-free operation, the Reynolds number at the inlet must remain below a critical value whatever the fluid, which is equal to 20 with the studied geometry whatever the studied fluid. Moreover, a second cavity is useful since instabilities coming from the first cavity could be filtered for low shear-thinning fluids, which is the case of the WFC coating colours. These simulation results were validated thanks to flow visualization experiments with tracers and PIV using a transparent replica of the coater. Finally CFD simulations on the inclined plane were carried out and permitted to conclude that for the range of operating conditions used on the pilot curtain coater, some issues presented in literature should not exist industrially.

K**eywords:** Curtain coating, CFD simulation, Non-Newtonian fluids